



**A University of Sussex PhD thesis**

Available online via Sussex Research Online:

<http://sro.sussex.ac.uk/>

This thesis is protected by copyright which belongs to the author.

This thesis cannot be reproduced or quoted extensively from without first obtaining permission in writing from the Author

The content must not be changed in any way or sold commercially in any format or medium without the formal permission of the Author

When referring to this work, full bibliographic details including the author, title, awarding institution and date of the thesis must be given

Please visit Sussex Research Online for more information and further details

# Investigating the Scope of the Pentafluorosulfanyl Group in Medicinal Chemistry



**Arathy Jose**  
**Supervisor: Prof John Spencer**

Submitted to the University of Sussex in part fulfilment of the requirements of the  
degree of Doctor of Philosophy

May 2021

## **Declaration**

I hereby declare that this thesis is my own work and effort and that it has not been submitted anywhere for any award of another degree. I also undertake that any quotation or paraphrase from the published work of other people has been acknowledged. This work was supervised by Prof John Spencer.

Arathy Jose

## Acknowledgements

I have been fortunate enough to receive a great deal of support throughout my PhD. First and foremost, I would like to thank my supervisor Prof. John Spencer for directing, encouraging, and inspiring me from start to finish.

I would like to thank my co-supervisors Prof. Mark Bagley and Dr Barnaby Greenland for their expertise and guidance in formulating this thesis.

This project would not have been possible without the funding from the European Regional Development Fund (ERDF) via the Interreg France (Channel) England program, and I would like to acknowledge them at this occasion.

I would like to thank Dr Alaa Abdul-Sada at the University of Sussex for carrying out all the mass spectrometry, Dr Edward Wright and Dr Mariliza Derveni for performing biological studies mentioned in Chapter 2, the National Crystallography Service (NCS) at the University of Southampton for carrying out the X-Ray crystallographic measurements, Dr Stephen Boyer (London metropolitan university) for the elemental analysis service and Dr Remi Legay (Université de Caen, Normandie) for NMR studies.

I would like to acknowledge all my lab colleagues Andy, Storm, Dan, Ant, Asma, and Joy as well as team LabFact for their company and kindness. Special thanks to my friends Raysa, Sergi, Hugo, Jerome and Ajesh for making my PhD life all the brighter.

And finally, I would like to thank my parents, sister, and brother in law for believing in me and cheering me on, all the way.

## Abstract

This thesis focuses on developing SF<sub>5</sub>-substituted biologically active compounds or building blocks, often using microwave synthesis. SF<sub>5</sub> is a fluorine containing functional group that has only recently been explored in medicinal chemistry due to lack of commercially available building blocks. Exploring its biological activities as well as expanding the repertoire of SF<sub>5</sub> chemistry appeared necessary.

Chapter 2 explores the scope of SF<sub>5</sub> in medicinal chemistry by incorporating it into known drugs, triflunomide and leflunomide, HDHODH inhibitors. Affinity of the SF<sub>5</sub> analogues towards HDHODH will be discussed and compared with the parent drugs' affinity. In addition their potential as SARS-CoV-2 antivirals will be presented.

Chapter 3 contains a brief description of the development of a small library consisting of 3 and 4-SF<sub>5</sub>-substituted phenyl rings that are bonded to heterocycles including morpholine, piperidine, piperazine, and pyridine via an amide bond. Small libraries of novel compounds consisting of SF<sub>5</sub>, which is a bioisostere of the familiar trifluoromethyl group (CF<sub>3</sub>) and halogens, have been developed to improve commercial availability of SF<sub>5</sub>-containing building blocks. SF<sub>5</sub> is often compared to the trifluoromethyl group and even dubbed as a 'super trifluoromethyl group' due to its superior lipophilicity, bulkiness, electronegativity, electron withdrawing properties, etc. A few compounds from this library have been contributed to the COVID Moonshot program, which is an initiative to accelerate the development of a COVID antiviral.

Chapter 4 describes the synthesis of a series of SF<sub>5</sub> substituted oxindoles. Included in the series are two SF<sub>5</sub> cognates of Semaxanib. Using molecular modelling and a radioactive kinase assay we compared activities of Semaxanib and its SF<sub>5</sub> counterparts in the VEGFR2 binding site.

Chapter 5 explores SF<sub>5</sub> as a bioisostere in 1,4 diazepines. We synthesised and compared bioisoteres of SF<sub>5</sub>- and the known Cl-analogues of diazepam and nordiazepam.

Chapter 6 concludes the thesis and describes future directions.

## List of abbreviations

Å	Angstrom
AAA	ATPase Associated with diverse cellular Activities
ACE2	angiotensin-converting enzyme 2
Ala	alanine
AMPA	$\alpha$ -amino-3-hydroxy-5-methyl-4-isoxazolepropionic acid
AngII	angiotensin II
ARDS	acute lung respiratory damage
Arg	arginine
Asp	aspartic acid
ATP	adenosine triphosphate
B cells	bone marrow cells
Boc	<i>tert</i> -butyloxycarbonyl
BSA	broad spectrum antivirals
BZDs	benzodiazepine/1, 4-diazepine
CCK receptor	cholecystokinin receptor
CNS	central nervous system
<i>coenzyme Q</i>	ubiquinone
CTP	cytidine triphosphate
Cys	cysteine
d	doublet
DCM	dichloromethane
DHO	dihydroorotic acid
DHODH	dihydroorotate dehydrogenase
DMARD	disease modifying antirheumatic drug
DMSO	dimethyl sulfoxide
DNA	deoxyribonucleic acid
DYRK	dual-specificity tyrosine phosphorylation-regulated kinases
EGFR	epidermal growth factor receptor
FA	fluoroacetate
FGFR	fibroblast growth factor receptor
FMN	flavin mononucleotide
FMNH <sub>2</sub>	dihydroflavin mononucleotide
GABA	$\gamma$ -aminobutyric acid
Gln	glutamine
Glu	glutamic acid

Gly	glycine
GTP	guanosine triphosphate
HATU	hexafluorophosphate azabenzotriazole tetramethyl uronium
Hie	histidine on Schrodinger
His	histidine
HRMS	high resolution mass spectra
HTAs	host targeting antivirals
Hz	hertz
IGFR	insulin receptor, and insulin like growth factor receptor
IPA	isopropyl alcohol
IR	infrared
LAG	liquid assisted grinding
LCD	liquid crystal displays
Leu	leucine
Lys	lysine
m	multiplet
Met	methionine
MHz	megahertz
mg	milligram
mL	millilitre
M <sup>pro</sup>	main protease
MM	mixer mill
mmol	milli-mole
NHE	Na <sup>+</sup> /H <sup>+</sup> exchanger
NGFR	nerve growth factor receptor
nM	nanomolar
NMR	nuclear magnetic resonance
OAc	acetate
p	pentet
PAM	positive allosteric modulators
PDB	Protein Data Bank
PDGFR	platelet-derived growth factor receptor
<i>Pf</i> DHODH	<i>Plasmodium falciparum</i> dihydroorotate dehydrogenase
P-gp	P-glycoprotein
Phe	phenylalanine
PM	planetary mill
pp	polyproteins

ppm	parts per million
Pro	proline
Pt	platinum
PTB	phosphotyrosine-binding domain
Py	pyridine
q	quartet
QSAR	quantitative structure activity relationship
RA	rheumatoid arthritis
RdRp	RNA-dependent RNA polymerase
RNA	ribonucleic acid
rt	room temperature
RTK	receptor tyrosine kinase
s	singlet
SAR	structure activity relationship
SH2	Src homology-2
S <sub>w</sub>	water solubility
SSRI	selective serotonin reuptake inhibitor
STK	serine/threonine kinases
T	thymus cells
t	triplet
TCICA	trichloroisocyanuric acid
THF	tetrahydrofuran
TFA	trifluoroacetic acid
Thr	threonine
TK	tyrosine kinases
TLC	thin layer chromatography
TR	trypanothione reductase
t <sub>R</sub>	retention times
TRI	trypanothione reductase inhibitors
Tyr	tyrosine
UMP	uridine monophosphate
UMPS	uridine monophosphate synthase
UTP	uridine-5'-triphosphate
VBM	vibratory ball mill
Val	valine
VEGFR	vascular endothelial growth factor receptor
W	watt



$\sigma_m$	Hammett substituent constant, <i>meta</i>
$\sigma_p$	Hammett substituent constant, <i>para</i>
$\sigma_I$	Hammett substituent constant, inductive effect
$\sigma_R$	Hammett substituent constant, resonance effect
$\pi$	Hansch hydrophobicity constant
$\mu\text{M}$	micromolar
$\mu\text{W}$	microwave

## Table of Contents

<b>Chapter 1.0 Introduction</b> .....	<b>1</b>
<b>1.1 LabFact</b> .....	<b>1</b>
<b>1.2 Fluorination in medicinal chemistry</b> .....	<b>1</b>
<b>1.3 The pentafluorosulfanyl (SF<sub>5</sub>) group</b> .....	<b>3</b>
<b>1.4 Synthesis of aryl pentafluorosulfanyls</b> .....	<b>8</b>
<b>1.5 SF<sub>5</sub> as a bioisosteric replacement</b> .....	<b>11</b>
<b>1.5.1 Replacing the CF<sub>3</sub> group</b> .....	<b>11</b>
<b>1.5.2 Replacing the nitro group</b> .....	<b>14</b>
<b>1.5.3 Replacing halogens</b> .....	<b>15</b>
<b>1.6 Other interesting examples of SF<sub>5</sub> in medicinal chemistry</b> .....	<b>15</b>
<b>1.7 SF<sub>5</sub> in materials science</b> .....	<b>17</b>
<b>1.8 SF<sub>5</sub> in agricultural chemistry</b> .....	<b>18</b>
<b>1.9 Microwave Chemistry</b> .....	<b>18</b>
<b>1.10 Mechanochemistry</b> .....	<b>21</b>
<b>1.11 Thesis aims</b> .....	<b>23</b>
<b>Chapter 2.0 SF<sub>5</sub> as a Bioisosteric Replacement of CF<sub>3</sub> in Leflunomide and Teriflunomide</b> .....	<b>25</b>
<b>2.1 Introduction</b> .....	<b>25</b>
<b>2.1.1 Leflunomide and teriflunomide against SARS-CoV-2</b> .....	<b>29</b>
<b>2.2 Results and Discussion</b> .....	<b>34</b>
<b>2.2.1 Comparing HDHODH inhibiting potency of SF<sub>5</sub>-containing analogues against known DHODH inhibitors</b> .....	<b>34</b>
<b>2.2.2 Identifying a SARS-CoV-2 M<sup>pro</sup> inhibitor</b> .....	<b>47</b>
<b>2.3 Conclusion</b> .....	<b>53</b>
<b>2.4 Experimental</b> .....	<b>53</b>
<b>2.4.1 Chemistry</b> .....	<b>53</b>
<b>2.4.2 Toxicity assay and SARS-CoV-2 infection inhibition assay</b> .....	<b>55</b>
<b>Chapter 3.0 A Library of SF<sub>5</sub> Containing Small molecules</b> .....	<b>56</b>
<b>3.1 Introduction</b> .....	<b>56</b>
<b>3.2 Results and Discussion</b> .....	<b>59</b>
<b>3.2.1 Synthesis</b> .....	<b>59</b>
<b>3.2.2 Modelling</b> .....	<b>66</b>
<b>3.3 Conclusion</b> .....	<b>71</b>
<b>3.4 Experimental</b> .....	<b>72</b>
<b>Chapter 4.0 SF<sub>5</sub>-Substituted Oxindole Scaffolds as Kinase Inhibitors</b> .....	<b>82</b>
<b>4.1 Introduction</b> .....	<b>82</b>
<b>4.2 Results and discussion</b> .....	<b>87</b>
<b>4.2.1 Synthesis</b> .....	<b>87</b>
<b>4.2.2 Modelling (performed using Schrodinger Maestro Version 12.6.144)</b> .....	<b>94</b>
<b>4.2.3 <i>In Vitro</i> Analysis</b> .....	<b>99</b>

<b>4.3 Conclusion</b> .....	<b>99</b>
<b>4.4 Experimental</b> .....	<b>99</b>
<b>Chapter 5.0 Synthesis and Biological Evaluation of SF<sub>5</sub>-Containing Diazepines.</b>	<b>105</b>
<b>5.1 Introduction</b> .....	<b>105</b>
<b>5.2 Results and Discussion</b> .....	<b>110</b>
<b>5.2.1 Synthesis</b> .....	<b>110</b>
<b>5.2.2 Modelling</b> .....	<b>126</b>
<b>5.3 Conclusion</b> .....	<b>131</b>
<b>5.4 Experimental</b> .....	<b>132</b>
<b>5.4.1 Organic Chemistry</b> .....	<b>132</b>
<b>5.4.2 Computational ligand docking</b> .....	<b>135</b>
<b>5.4.3 Cell culture and recombinant GABA<sub>A</sub>R expression</b> .....	<b>135</b>
<b>5.4.4 Electrophysiology experiments</b> .....	<b>135</b>
<b>Chapter 6.0 Conclusion, Future Directions and Thesis Outcome</b> .....	<b>137</b>
<b>6.1 Thesis outcomes</b> .....	<b>141</b>
<b>6.2 References</b> .....	<b>142</b>

## Chapter 1.0 Introduction

### 1.1 LabFact

LabFact is a project that involves 6 institutes within the France (Channel) England (FCE) region, (Universities of Sussex, Southampton, Rouen, Caen, ENSICAEN and CNRS) and an industrial partner (Pareon Chemicals) that brings together expertise in environmentally friendly chemistry. LabFact aims to bridge the gap between laboratories and factories by training small and medium enterprises in the Channel region to use environmentally friendly techniques to develop fine chemicals. A major goal of LabFact is to produce 1000 novel scaffolds between the institutes using non-conventional techniques such as flow, microwave, mechanochemistry, etc., to reduce the amount of waste generated. All novel scaffolds are acquired by the industry partner, Pareon Chemicals, to be commercialised. These scaffolds are hoped to act as building blocks or biologically active molecules and accelerate the production of next generation medicines and agrochemicals.<sup>1,2</sup>

This thesis commenced under project LabFact and focused on developing pentafluorosulfanyl (SF<sub>5</sub>) containing biologically active compounds and building blocks while using microwave and mechanochemistry as the environmentally friendly alternatives whenever possible.

### 1.2 Fluorination in medicinal chemistry

Traditional medicinal chemistry depended on natural products or related derivatives to develop drugs. Therefore, fluorinated compounds in medicinal chemistry remained under-developed until the 1950s as organofluorine compounds are almost absent in natural compounds.<sup>3,4</sup> An example of organofluorine in natural compounds is Fluoroacetate (FA). FA refers to a series of compounds with the general formula CH<sub>2</sub>FCOOR. It is found in a range of plant species such as *Dichapetalum*, *Gastrolobium*, *Oxylobium*, *Acacia*, and *Palicourea*, and are highly toxic towards humans and other mammals upon ingestion.<sup>5</sup>

In 1954, initial work carried out by Fried and Sabo on fluorinated cortisone and hydrocortisone derivatives revealed enhancement of biological property of the parent drug following fluorination.<sup>6</sup> Since the synthesis and evaluation of the antimetabolite drug, 5-fluorouracil in 1957<sup>7</sup>, fluorine substitution became a common practice in contemporary medicinal chemistry to improve metabolic stability, bioavailability, enable antimetabolite use and for protein-ligand interactions.<sup>4</sup> Fluorine can provide unique protein-ligand interactions as the highly electronegative fluorine atom allows C-F bonds to form dipolar and multipolar interactions with protein backbone or side-chain amide groups.<sup>3</sup> One of the major effects of fluorination is the modulation of acidity and basicity of a parent compound leading to a strong influence on binding affinity, pharmacokinetic properties, and bioavailability of a given drug candidate.<sup>8</sup> Introducing a fluorine or a fluorine-containing compound

such as trifluoromethyl group ( $\text{CF}_3$ ), trifluoromethoxy group ( $\text{OCF}_3$ ) or trifluoromethylthio group ( $\text{SCF}_3$ ) can modulate the lipophilicity of a compound.<sup>9,10</sup> Lipophilic compounds are more susceptible to oxidative metabolic degradation by the enzyme cytochrome P450 monooxygenase. Introducing a fluorine atom can slow down drug metabolism by altering the rate, route or extent of metabolism. Moreover, a C-F bond is less susceptible to attack by cytochrome P450 due to the enhanced polarity. Replacing a hydrogen for fluorine brings only minor steric alterations.<sup>11</sup>

New fluorinating reagents and fluorination processes have increased the range of synthetic fluorinated building blocks. The success of fluorine substitution in drug design is portrayed by the production of some of the key drugs available on the market.<sup>12</sup>

Approximately one third of the top-performing drugs in the market contain fluorine atoms in their structure. For example, Lipitor (Atorvastatin), used for the treatment of high cholesterol and triglyceride levels and prevention of heart attacks and strokes was registered as the best-selling drug globally in 2008, Lansoprazole, a gastric acid secretion regulating drug, and Prozac, an antidepressant, are a few of the drugs that make the list of top-selling fluorinated drugs (Figure 1.1).<sup>11</sup>

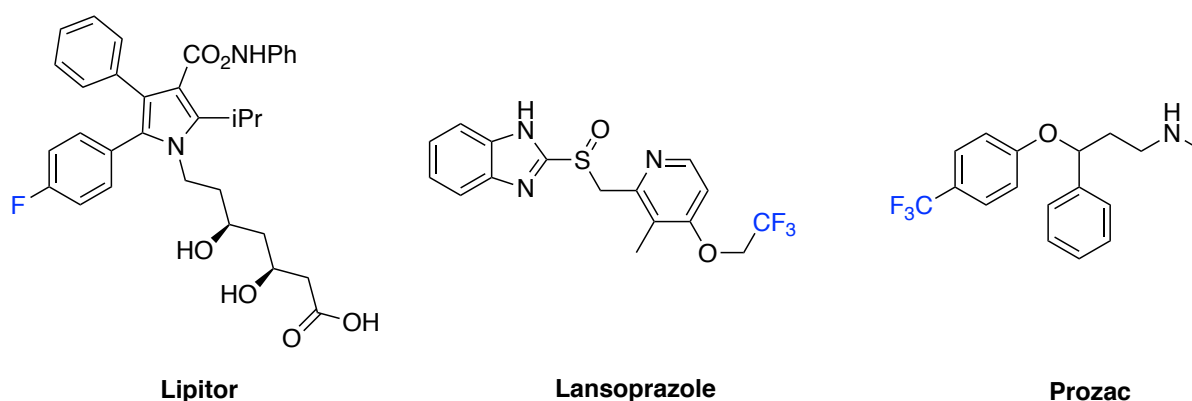


Figure 1.1 Top selling fluorinated drugs

The incorporation of fluorine into organic molecules is commonly done by direct fluorination, using fluorinating reagents or by adding fluorinated functional groups on both aromatic rings and aliphatic chains. The latter is generally achieved using a  $\text{CF}_3$  group and it is one of the most accustomed fluorine moieties to be explored in medicinal chemistry.<sup>13</sup> Selective incorporation of a  $\text{CF}_3$  group in a compound of pharmacological relevance usually results in significant enhancement of its lipophilicity, binding selectivity, and metabolic stability.<sup>14</sup>

As the role of fluorine is very valuable in medicinal chemistry, the search for new fluorine containing functional groups is all the more important.

In recent years, agrochemical, materials science and pharmaceutical industries have been investigating the potential benefits of highly fluorinated, yet rigid pentafluorosulfanyl ( $\text{SF}_5$ ) derivatives.  $\text{SF}_5$  containing compounds have been known for more than half a century, though they

remain an underdeveloped class of compounds despite possessing a combination of interesting properties.

### 1.3 The pentafluorosulfanyl (SF<sub>5</sub>) group

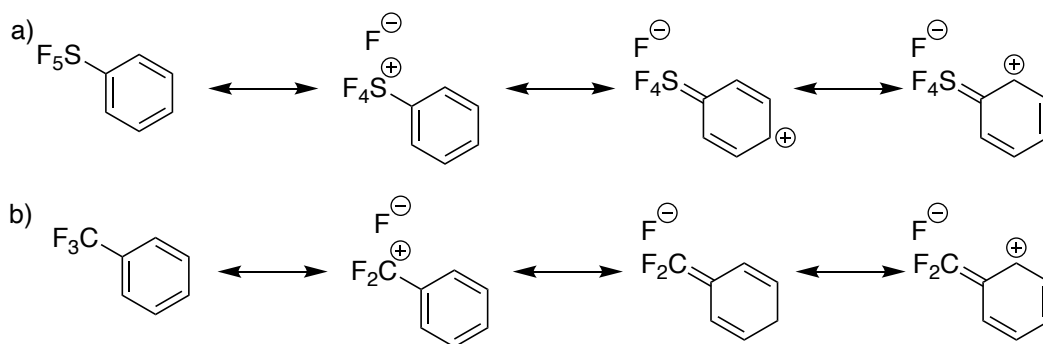
Synthesis of aryl pentafluorosulfanyl compounds and their unique physiochemical properties were first reported in 1960 by W.A. Sheppard.<sup>15</sup> The synthesis required hazardous reagents and specialised equipment such as Teflon containers. Hence, SF<sub>5</sub> chemistry was not explored adequately until after 40 years of its discovery.

Sheppard reported the SF<sub>5</sub> group to be highly electronegative as well as *meta* directing towards electrophilic aromatic substitutions. By virtue of having two extra fluorine atoms, larger size, higher hydrolytic stability, enhanced lipophilicity and electronegativity, the SF<sub>5</sub> group is superior to the CF<sub>3</sub> group. The electronegativity of SF<sub>5</sub> is estimated to be approximately 3.65, versus 3.36 for CF<sub>3</sub>. The Hammett substituent constants ( $\sigma_p$  and  $\sigma_m$ , Table 1.1) are also a reflection of the SF<sub>5</sub> moiety's enhanced electronegativity.<sup>16</sup> The Hammett substituent constant,  $\sigma$ , represents the relative strength of a substituted benzoic acid compared to a non-substituted benzoic acid, by measuring the rate at which they dissociate in water at 25 °C.  $\sigma$  is therefore dependant on the nature and position of the substituent.  $\sigma$  value of benzoic acid is 0. More electron withdrawing a substituent is, the greater the  $\sigma$  value. Electron donating groups give negative  $\sigma$  values meaning they are acid weakening.  $\sigma_m$  and  $\sigma_p$  represent resonance effect of the substituent at *meta* and *para* positions while  $\sigma_i$  represents the inductive effect. Using the Hammett free-energy relationship, the resonance and inductive parameters of SF<sub>5</sub> substituted benzoic acids were calculated and compared with the parameters of CF<sub>3</sub> group by Sheppard (Table 1.1).<sup>17</sup>

Hammett parameters	SF <sub>5</sub>	CF <sub>3</sub>
$\sigma_I$	0.55	0.39
$\sigma_R$	0.11	0.12
$\sigma_p$	0.68	0.53
$\sigma_m$	0.61	0.41

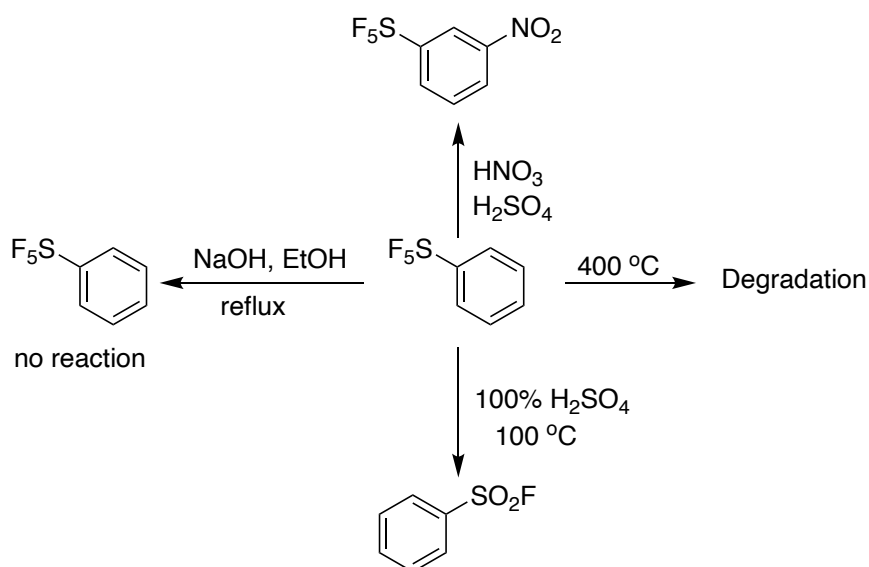
Table 1.1: Comparison of  $\sigma$ -parameters of SF<sub>5</sub> and CF<sub>3</sub> groups

The data demonstrate the strong inductive effect exerted by SF<sub>5</sub> ( $\sigma_I = 0.55$ ) in comparison to CF<sub>3</sub> ( $\sigma_I = 0.39$ ) as well as a similar resonance influence of SF<sub>5</sub> ( $\sigma_R = 0.11$ ) and CF<sub>3</sub> ( $\sigma_R = 0.12$ ) groups. Scheme 1.1 shows that resonance effects are possible with SF<sub>5</sub> and CF<sub>3</sub> groups due to negative hyperconjugation and their ability to adopt “no-bond resonance” forms.<sup>12</sup> The scheme also portrays the *meta* directing characteristic of CF<sub>3</sub> and SF<sub>5</sub> groups, to electrophilic aromatic substitutions. Electron attracting effect of SF<sub>5</sub> on the *para* position is enhanced by resonance interaction.<sup>17</sup>

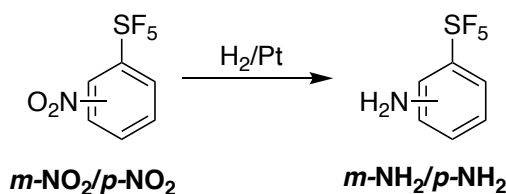


Scheme 1.1: "No-bond" resonance in a)  $CF_3$  & b)  $SF_5$ -substituted arenes

$SF_5$ 's peculiar and superior physicochemical properties, in comparison to the  $CF_3$  group, were also reported by Sheppard in a separate paper.<sup>18</sup> Upon analysing (pentafluoro- $\lambda^6$ -sulfanyl)benzene, Sheppard reported it to be a colourless liquid with a pleasant aromatic odour, unlike other aromatic sulfur compounds. He stated that the compound is chemically and thermally stable compared to trifluoromethyl benzene. When refluxed in a solution of sodium hydroxide in aqueous ethanol, (pentafluoro- $\lambda^6$ -sulfanyl)benzene was recovered unchanged. It was also inert to concentrated sulfuric acid at moderate temperature but was hydrolysed to phenylsulfonyl fluoride when heated at 100 °C in 100% sulfuric acid; whereas, trifluoromethylbenzene degrades at 90 °C under the same conditions. Only a small amount of degradation occurs to the (pentafluoro- $\lambda^6$ -sulfanyl)benzene, when heated at 400 °C for several hours in a sealed glass tube (Scheme 1.2).<sup>18</sup> Catalytic hydrogenation of *meta*- and *para*- nitrophenyl(pentafluorosulfanyl)benzene afforded the corresponding aminophenyl(pentafluorosulfanyl)benzene in over 90% yield (Scheme 1.3). This is a further demonstration of the stability of the  $SF_5$  group. Pentafluorosulfanyl groups are however, sensitive towards strong Lewis acids, alkali metals and organolithiums.<sup>18</sup>



Scheme 1.2: Reactions of (pentafluoro- $\lambda^6$ -sulfanyl)benzene



*Scheme 1.3: Hydrogenation of meta- and para- nitrophenyl(pentafluorosulfanyl)benzene*

Infrared examination of SF<sub>5</sub>-arenes showed very strong absorption in the 820 to 880 cm<sup>-1</sup> region.<sup>20</sup> However, many substituted aromatic compounds possess strong absorption in this region due to C-H deformation.

The water solubilities of SF<sub>5</sub> and CF<sub>3</sub> compounds were analysed by Jackson and Mabury.<sup>15</sup> Analyses were performed on SF<sub>5</sub> and CF<sub>3</sub> substituted *meta*- and *p*-anilines, *p*-benzoic acids, and *p*-phenols at 24 °C. Due to their bulky nature, SF<sub>5</sub> substituted compounds were hypothesised to be less water soluble than their CF<sub>3</sub> substituted analogues. Although, SF<sub>5</sub> compounds are predicted to be less favourable to dissolve in water due to the larger entropic costs, C-F bonds are shorter and less polarizable than SF<sub>5</sub> and so enthalpic costs maybe low for SF<sub>5</sub> compounds. The water solubility (S<sub>w</sub>) values of SF<sub>5</sub> compounds were much lower than their CF<sub>3</sub> counterparts which proves the concept that steric effects play a bigger role than polarizability in determining water solubility.

Fluorine (<sup>19</sup>F) NMR of SF<sub>5</sub> is highly characteristic (Figure 1.2).<sup>16</sup> The chemical shifts of SF<sub>5</sub>-compounds appear in the positive region indicating downfield shifts compared to the CF<sub>3</sub> group's chemical shifts which appear in the negative region (Figure 1.3).<sup>17</sup> SF<sub>5</sub> fluorine atoms appear typically in the range of δ = 55 – 90 ppm while the CF<sub>3</sub> fluorine atoms appear in the range of δ = -60 to -80 ppm. As the SF<sub>5</sub> group contains fluorine atoms in two different magnetic environments, one axial fluorine and four equatorial fluorine atoms, it is represented by a doublet (d) integrating to four fluorine atoms and a pentet/quintet (p) integrating to one fluorine atom. The pentet is usually observed downfield to the doublet in SF<sub>5</sub>-arenes. The two-bond, F-F coupling constant in the SF<sub>5</sub> group is between *J* = 140 and 160 Hz.<sup>18</sup>



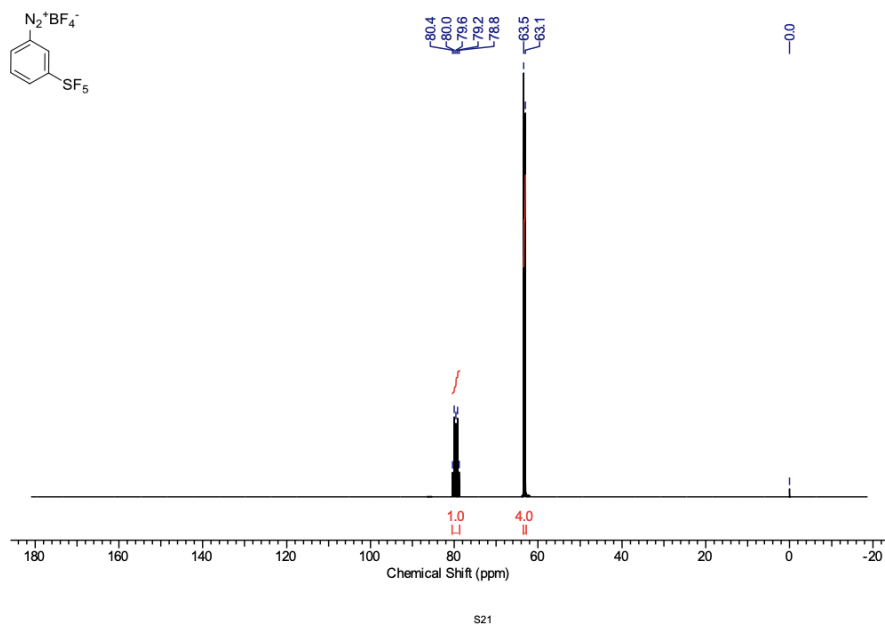


Figure 1.2:  $^{19}\text{F}$  NMR of  $\text{SF}_5$ -substituted arene<sup>16</sup>

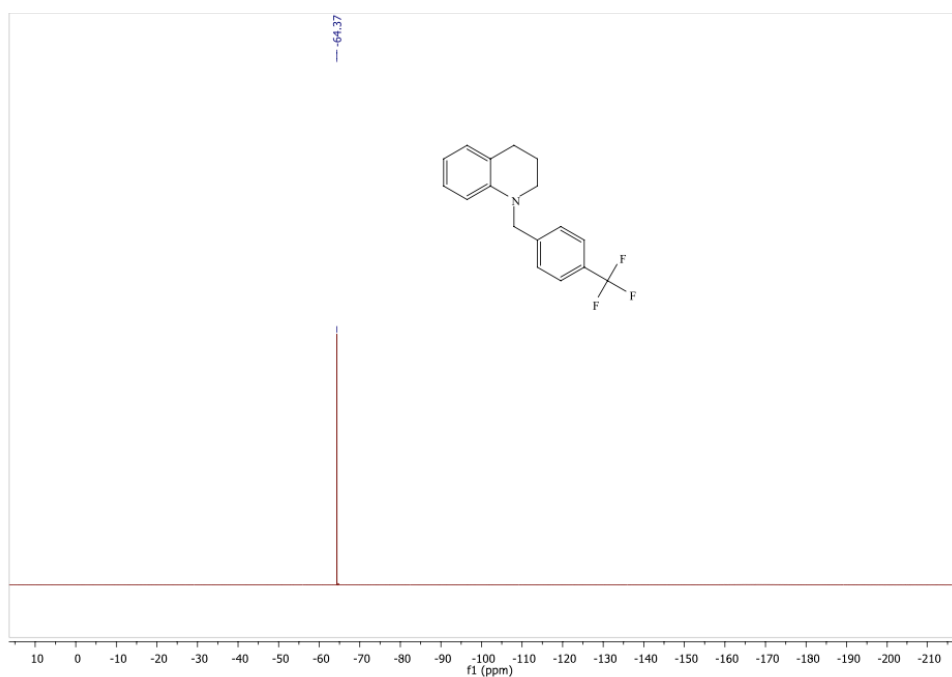


Figure 1.3:  $^{19}\text{F}$  NMR of  $\text{CF}_3$ -substituted arene

The  $^{13}\text{C}$  NMR spectra of  $\text{SF}_5$ -arenes are distinguishable like the  $^{13}\text{C}$  NMR of  $\text{CF}_3$ -arenes. Figure 1.4 shows an example of the  $^{13}\text{C}$  carbon of an  $\text{SF}_5$ -arene (structure shown in the figure). The carbon bearing the  $\text{SF}_5$  group appears as a pentet (p) between  $\delta = 161.3$  and  $162.2$  ppm with a coupling constant,  $^2J_{\text{FC}} = 17.7$  Hz and the two allylic carbons appear as a multiplet between  $\delta = 130.6$  and  $134.9$  ppm with a coupling constant  $^3J_{\text{FC}} = 4.6$  Hz. The appearance of these peaks can differ depending on the concentration of the NMR sample. Concentrated samples often show these peaks as pentets. Unlike the carbon signals stemmed from the  $\text{CF}_3$  group,  $\text{SF}_5$  derived carbon signals are easy to spot.  $^{13}\text{C}$  chemical shifts of  $\text{CF}_3$  groups appear in the range,  $\delta = 107$ -  $128$  ppm. The

trifluoromethyl carbon as well as other neighbouring carbons in vicinity are all split into quartets by the fluorine atoms.  $^1J_{FC}$  splits in the range of 275 – 285 Hz,  $^2J_{FC}$  usually split in the range of  $^2J_{FC} = 25 – 35$  Hz, while three bond ( $^3J_{FC}$ ) couplings are observed with values in the range of 2 – 3 Hz.<sup>18</sup> A combination of weak signal and multiple couplings make these carbon signals difficult to be identified. The quartets with large coupling constants appear as individual singlets whereas the quartets that splits in the  $J = 2 – 3$  Hz range can be very small and difficult to spot.<sup>18</sup>

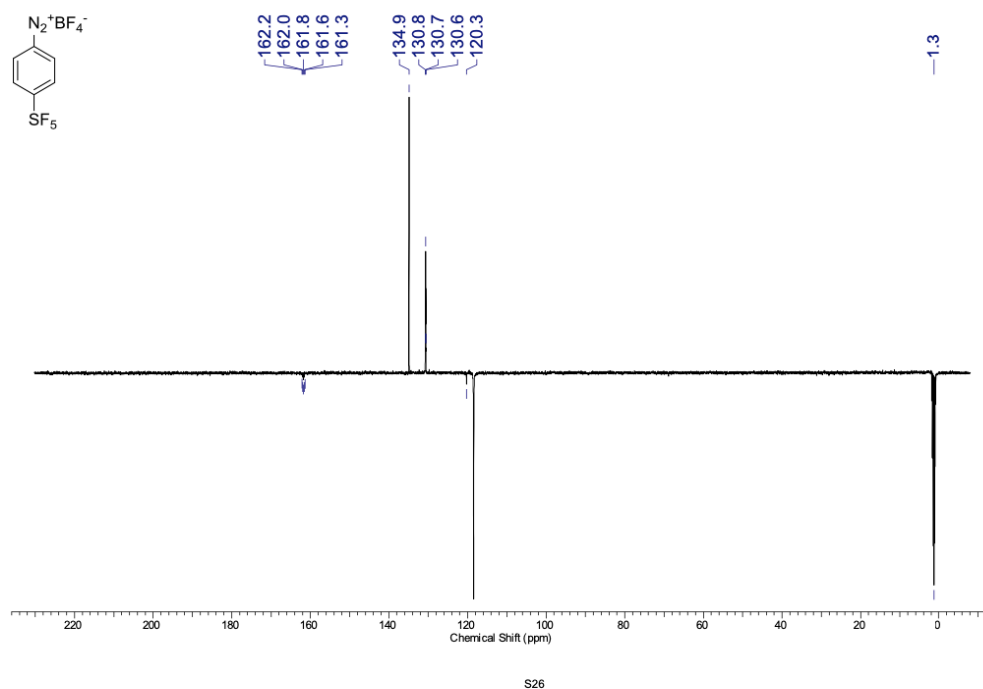
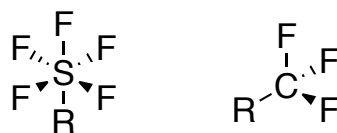


Figure 1.4:  $^{13}C$  NMR of an  $SF_5$ -arene<sup>16</sup>

Other properties that outline the superiority of  $SF_5$  in comparison to  $CF_3$  are enhanced lipophilicity demonstrated by Hansch hydrophobicity constants,  $\pi = 1.51$  for  $SF_5$  and  $\pi = 1.09$  for  $CF_3$ .<sup>19</sup>  $SF_5$  group has an octahedral geometry while  $CF_3$  has a tetrahedral geometry (Figure 1.5). The 4 equatorial fluorine atoms and 1 axial fluorine result in a square pyramidal array of fluorine atoms. This in effect achieves a reduced barrier of rotation giving  $SF_5$  the ability to optimize receptor interactions effectively. Steric hindrance of  $SF_5$  can be compared and contrasted with both tert-butyl group and the  $CF_3$  group. A tert-butyl group is often substituted in drugs due to its large volume, providing steric hindrance although, it is prone to oxidative metabolism.<sup>20</sup>  $SF_5$  has a slightly smaller volume than the tert-butyl group but much bigger than the  $CF_3$  group.<sup>21</sup>



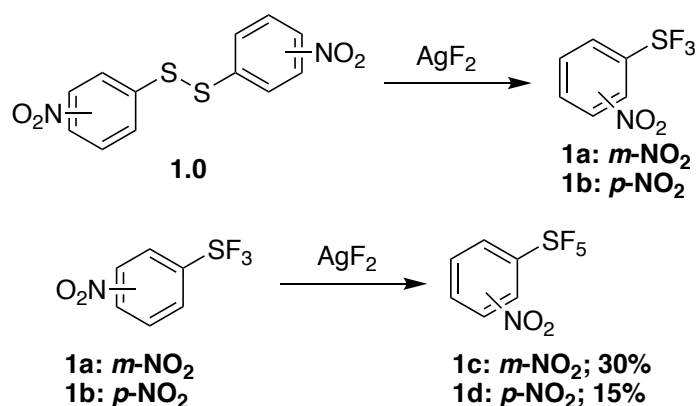
R = alkyl or aryl

Figure 1.5 SF<sub>5</sub> and CF<sub>3</sub> geometry

All these superior characteristics earned SF<sub>5</sub> its nickname, “super-trifluoromethyl group”. Their thermal and chemical stability along with high electronegativity and remarkable lipophilicity make them an attractive moiety for drug design and development.<sup>22</sup> Other than in medicinal chemistry, SF<sub>5</sub> is of interest in the agrochemical industry and new materials chemistry.

## 1.4 Synthesis of aryl pentafluorosulfanyls

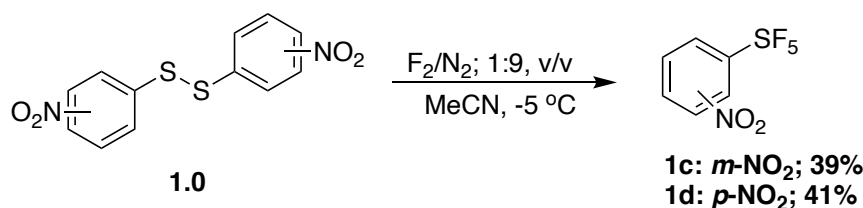
As mentioned before, large scale synthesis of aryl-SF<sub>5</sub> compounds requires dangerous and expensive reagents. Consequently, there is a lack of commercially available pentafluorosulfanyl benzenes that can be used as building blocks while available SF<sub>5</sub>-arenes are high-priced. The initial synthesis of pentafluorosulfanyl benzenes were accomplished by reacting aryl disulfides or arylsulfur trifluorides with silver fluoride at 120 °C for several hours in a copper autoclave to afford meta- and para-nitrophenyl(pentafluorosulfanyl)benzene in moderate yields (Scheme 1.4). This procedure was futureless due to low yield and unreliable reproducibility.



Scheme 1.4: First synthesis of arylsulfur pentafluorides

In 1997, a reliable synthetic protocol was developed by F<sub>2</sub> Chemicals Ltd leading to the commercial development of *p*- and *m*-nitrophenyl(pentafluorosulfanyl)benzenes. Direct fluorination of bis(nitrophenyl)disulfides enabled multigram production of nitrophenyl(pentafluorosulfanyl)benzenes in moderate yields (Scheme 1.5). This method can only be employed to make pentafluorosulfanyl benzenes with an electron withdrawing substituent.<sup>23</sup> Strongly electron withdrawing groups on the aromatic ring are necessary to avoid ring fluorination. Attempted synthesis of *o*-nitrophenyl(pentafluorosulfanyl)benzene using this method failed due to the formation of an unstable arylsulfur trifluoride which impeded the progress of the reaction.<sup>24</sup> In addition,

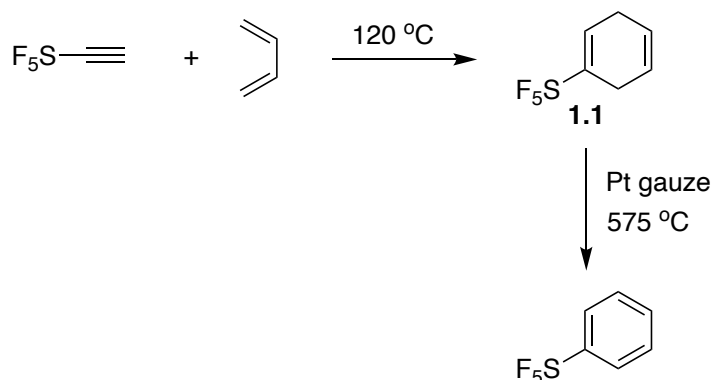
specialised equipment like Teflon is required as molecular fluorine reacts with glass. Most other commercially available SF<sub>5</sub>-aromatics and heteroaromatics are derived from nitro(pentafluorosulfanyl)benzenes.<sup>25,26</sup>



Scheme 1.5: Industrial synthesis of nitrophenyl(pentafluorosulfanyl)benzenes

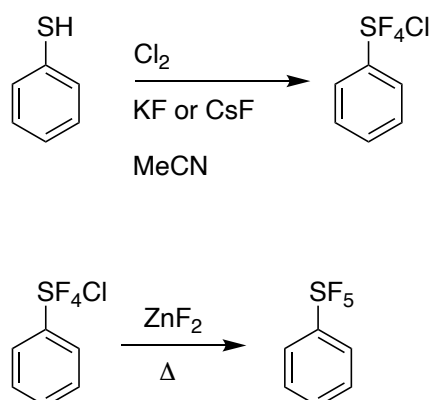
Not long after Sheppard's and F<sub>2</sub> Chemicals Ltd's publications, Janzen *et al.* introduced a method which replaced silver (II) fluoride (AgF<sub>2</sub>) with Xenon difluoride (XeF<sub>2</sub>) and tetraethyl ammonium chloride to convert phenyl disulfides to ArSF<sub>5</sub> via ArSF<sub>3</sub> as an intermediate.<sup>27</sup> Limitations of this protocol include poor yields (ca. 25%) as well as the use of an expensive reagent, XeF<sub>2</sub>.

An alternative route to aromatic SF<sub>5</sub> compounds was via cycloaddition of pentafluorosulfanylacetylene to butadiene to form an intermediate (**1.1**) that can be aromatized under extreme temperatures to afford the desired product (Scheme 1.6).<sup>28</sup>



Scheme 1.6: SF<sub>5</sub>-arene via cycloaddition

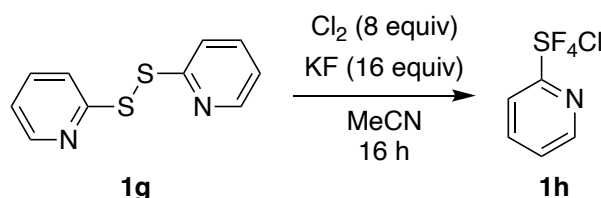
In 2008, Umemoto *et al.* published and patented a new synthetic pathway to SF<sub>5</sub>-arenes.<sup>29</sup> The method converts thiols to SF<sub>5</sub> via a tetrafluoro-λ<sup>6</sup>-sulfanyl chloride (-SF<sub>4</sub>Cl) intermediate (Scheme 1.7). Initially, an aromatic thiol (ArSH) is treated with potassium fluoride (KF) and chlorine gas to give ArSF<sub>4</sub>Cl. In the next step, ArSF<sub>4</sub>Cl undergoes Cl-F exchange in the presence of ZnF<sub>2</sub> to yield ArSF<sub>5</sub>.



Scheme 1.7: Umemoto's route to ArSF<sub>5</sub>

Using this method, Umemoto was successful in producing non-substituted and substituted SF<sub>5</sub>-arenes. Few examples include F at *para* and *ortho* positions, Br at *para* and *meta* positions, Cl at *para* position, CH<sub>3</sub> at *para* position and NO<sub>2</sub> at *para* position in excellent yields. For example, the *p*-nitro(pentafluorosulfanyl)benzene was synthesised at 89% yield. Numerous SF<sub>5</sub>-containing building blocks have been developed and commercialised since this method was published. A downside of this route is the use of elemental chlorine gas that is hazardous. Although, recent developments in ArSF<sub>5</sub> synthesis revealed Cl<sub>2</sub> gas can be substituted with trichloroisocyanuric acid.<sup>30,31</sup>

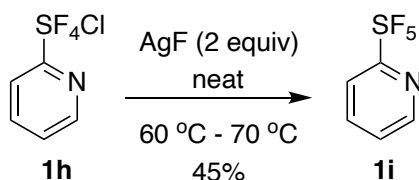
Kanishchev and Dolbier Jr. took advantage of Umemoto's method to synthesise a series of 2-SF<sub>5</sub>-pyridine derivatives. Treating 2,2'-dipyridyl disulfide which is a relatively inexpensive and readily available starting material, in the same manner as the thiol in Scheme 1.7, they obtained 2-pyridylsulfur chlorotetrafluoride (Scheme 1.8).<sup>25</sup>



Scheme 1.8: Synthesis of 2-pyridylsulfur chlorotetrafluoride

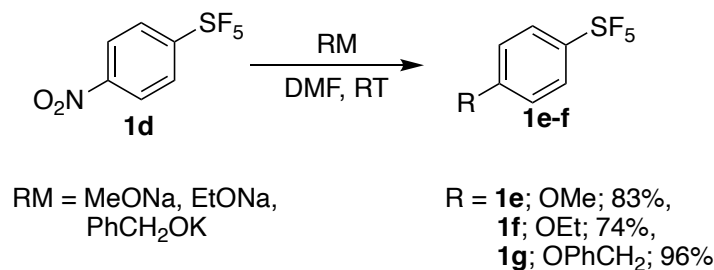
Product **1h** was reported to be a viscous liquid that is extremely sensitive to moisture, fuming in the presence of air and extremely reactive with water. It also reacts with glass particularly at high temperatures.

**1h** was fluorinated using 2 equivalence of silver (I) fluoride (AgF) without any solvent under inert atmosphere in a closed flat bottomed PFA vial to obtain the product 2-SF<sub>5</sub> pyridine in 45% yield (Scheme 1.9).<sup>25</sup>



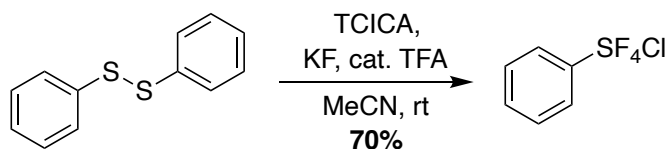
Scheme 1.9 Synthesis of 2-SF<sub>5</sub> pyridine

Functionalisation of pentafluorosulfanyl arenes can be achieved by S<sub>N</sub>Ar reactions where the arene nucleus is activated by the SF<sub>5</sub> group. For example, *m*- and *p*-nitro-(pentafluorosulfanyl)benzenes when treated with alkoxides generate a range of 3- and 4-(pentafluorosulfanyl) benzenes in a single step reaction. Scheme 1.10 shows *p*-nitro-(pentafluorosulfanyl)benzene reacting with alkoxides at room temperature to afford the respective ethers.



Scheme 1.10: *S<sub>N</sub>Ar* reaction of SF<sub>5</sub> arenes

As the synthesis of aryl-SF<sub>5</sub> compounds progresses mostly via aryl-SF<sub>4</sub>Cl intermediates, Togni *et al.* recently published a gas-free method towards their synthesis. Trichloroisocyanuric acid (TCICA), which is an inexpensive, and bench-stable solid was reacted with potassium fluoride as well as catalytic amount of acid under inert conditions to form the desired intermediates (eg: Scheme 1.11).<sup>31</sup>



Scheme 1.11: Aryl-SF<sub>4</sub>Cl synthesis

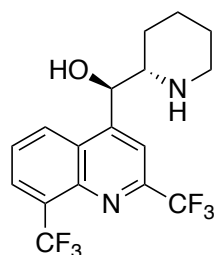
On account of these constructive developments, diverse SF<sub>5</sub>-containing building blocks are becoming more and more commercialised. Tokyo Chemical Industry, SpiroChem, and Fluorochem Ltd are a few providers of SF<sub>5</sub>-containing building blocks. Increased availability of SF<sub>5</sub>-compounds has seen a surge in research involving SF<sub>5</sub>-chemistry.<sup>32</sup>

## 1.5 SF<sub>5</sub> as a bioisosteric replacement

### 1.5.1 Replacing the CF<sub>3</sub> group

The unique properties of SF<sub>5</sub> make it an attractive substituent in medicinal chemistry. Recent years have seen applications of pentafluorosulfanylated compounds in known drugs with the aim of studying the effect of SF<sub>5</sub> on drug activity. Such studies commonly substitute antecedent functional groups like CF<sub>3</sub>, NO<sub>2</sub> or halogen atoms with SF<sub>5</sub> as a bioisostere.

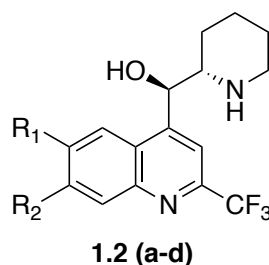
Mefloquine (Figure 1.6) is an active antimalarial drug as well as a prophylaxis with long half-life (2-3 weeks). It is associated with serious side effects including dizziness, diarrhoea, anxiety, depression, and central nervous system problems, among others.<sup>33</sup> Mefloquine's ability to inhibit P-glycoprotein and cross the blood-brain barrier has been suggested as a possible explanation to the neurological side effects.

**Mefloquine***Figure 1.6: Antimalarial drug, mefloquine*

With the aim of reducing Mefloquine's drawbacks, Wipf and co-workers re-engineered its structure by replacing  $\text{CF}_3$  groups with  $\text{SF}_5$  to "probe slight perturbations of the electron density" of the molecule.<sup>34</sup> Their new compound was hoped to exhibit fewer neurological effects while retaining its antimalarial efficacy.<sup>34</sup>

Initially Wipf *et al.* were unable to substitute position 8 of mefloquine with  $\text{SF}_5$ , as the building block required (*ortho*- $\text{SF}_5$  aniline) was not readily accessible. Functionalising positions 6 and 7 with  $\text{SF}_5$  was accomplished by using *meta* and *para*- $\text{SF}_5$  anilines as starting materials.

$\text{SF}_5$  and  $\text{CF}_3$  mefloquine analogues were synthesised and evaluated for their antimalarial activity (Figure 1.7 & Scheme 1.12). Compounds **1.2(a-d)** were compared to mefloquine against four drug resistant strains of the parasite *Plasmodium falciparum* (Table 1.2).  $\text{SF}_5$  substituted compounds **1.2a** and **1.2c** exhibited similar inhibitory activities to compounds **1.2b**, **1.2d** and mefloquine. Compound **1.2a** was however slightly more active than its  $\text{CF}_3$  congener, **1.2b**, against all strains.

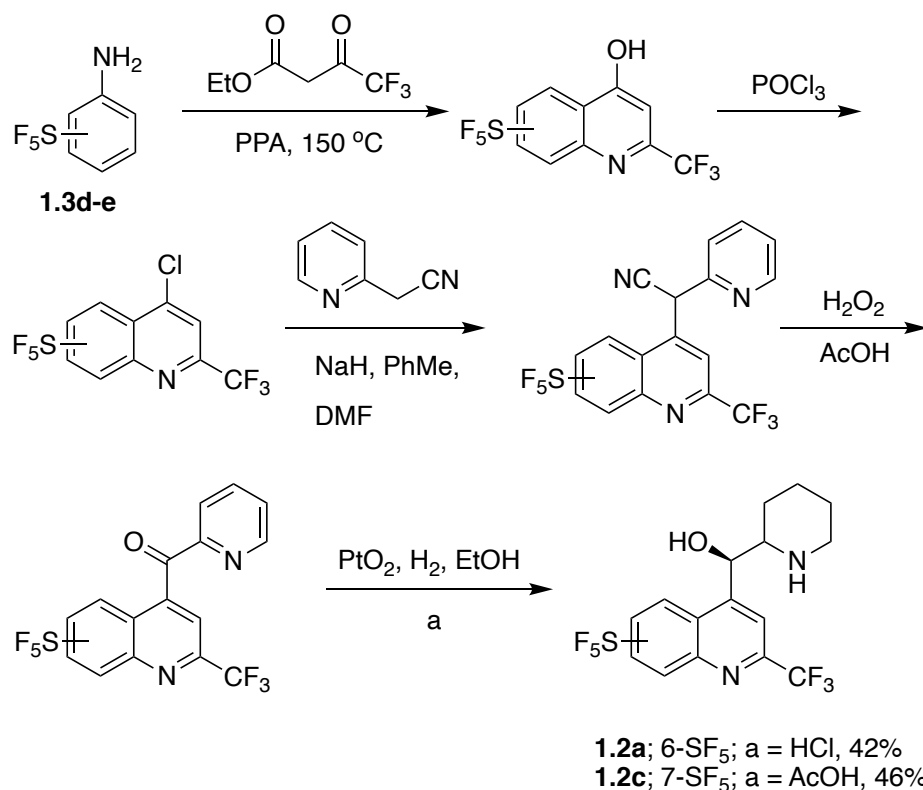


- a)  $\text{R}_1 = \text{SF}_5$ ;  $\text{R}_2 = \text{H}$
- b)  $\text{R}_1 = \text{CF}_3$ ;  $\text{R}_2 = \text{H}$
- c)  $\text{R}_1 = \text{H}$ ;  $\text{R}_2 = \text{SF}_5$
- d)  $\text{R}_1 = \text{H}$ ;  $\text{R}_2 = \text{CF}_3$

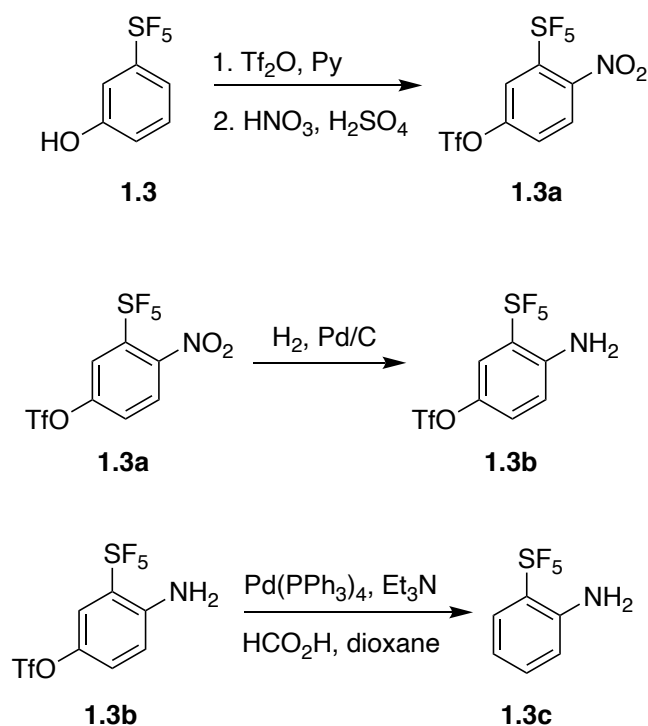
*Figure 1.7: SF<sub>5</sub> and CF<sub>3</sub> analogues of Mefloquine*

Analogue	Pf W2	Pf D6	Pf C235	Pf C2A
<b>Mefloquine</b>	2.5	8.0	18	22
<b>1.2a</b>	3.3	9.2	9.8	14
<b>1.2b</b>	5.0	17	53	21
<b>1.2c</b>	3.3	12	10	16
<b>1.2d</b>	3.0	12	30	13

*Table 1.2: Antimalarial activity of Mefloquine and its analogues*

Scheme 1.12: SF<sub>5</sub>-Mefloquine synthesis

A year later, in 2010, Wipf and co-workers published the preparation of novel *ortho*-SF<sub>5</sub> aniline from commercially available 3-SF<sub>5</sub> phenol (**1.3**, Scheme 1.13).<sup>35</sup> Compound **1.3** led to the synthesis of SF<sub>5</sub>-mefloquine where position 8 is substituted with the SF<sub>5</sub> group. Although, its activity with respect to Mefloquine was not reported.

Scheme 1.13: Synthesis of *ortho*-SF<sub>5</sub> aniline

Fluoxetine or Prozac (Figure 1.8) was the first selective serotonin reuptake inhibitor (SSRI) to be approved by the FDA as an antidepressant. It has the highest potency for 5-HT<sub>2c</sub> receptors. However,



inhibition of 5-HT<sub>2c</sub> receptors results in activation syndrome and weight loss. Welch and Lim were interested to see the effect of SF<sub>5</sub> group on 5-HT receptor binding by substitution of the CF<sub>3</sub> group (Scheme 1.14).

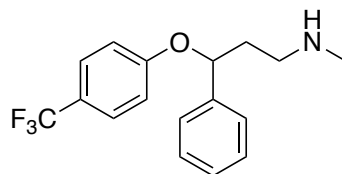
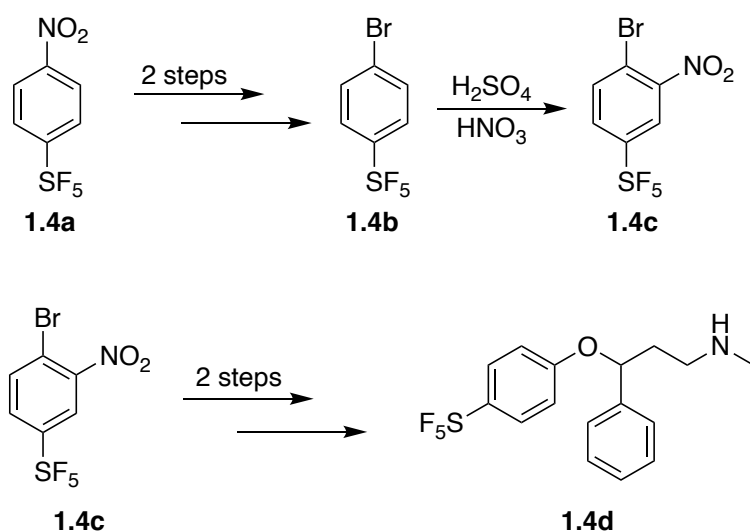


Figure 1.8: Fluoxetine or Prozac



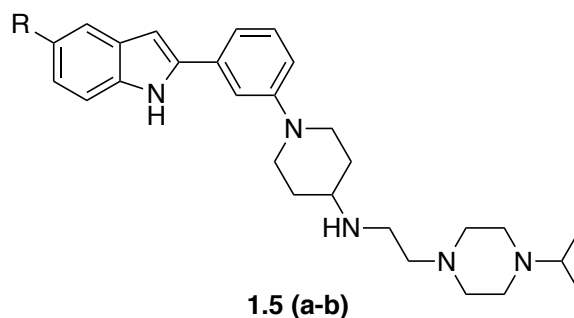
Scheme 1.14: Synthesis of SF<sub>5</sub>-Prozac

The pentafluorosulfanyl analogue selectively inhibited binding of the 5-HT receptors. At 10  $\mu$ M concentration, 97.3% of 5-HT<sub>2a</sub>, 75.8% of 5-HT<sub>2c</sub> and 77.8% of 5-HT<sub>1e</sub> were inhibited. However, in contrast to the Mefloquine study, this example shows a reduction in affinity for 5-HT receptors by compound **1.4d** compared to Prozac.<sup>36</sup>

### 1.5.2 Replacing the nitro group

The nitro group which is significantly smaller in size in relation to the SF<sub>5</sub> group has an electronegativity of 3.4 and a similar electronic effect. Plenty of examples on the bioisosteric replacement of CF<sub>3</sub> with SF<sub>5</sub> can be found in the literature. However, there are only a handful examples studying the replacement of the NO<sub>2</sub> group with SF<sub>5</sub>.

Wipf and colleagues investigated the effect of SF<sub>5</sub>-indole inhibitors on the AAA ATPase p97 while comparing it to its nitro analogue. p97 is an ATPase of the AAA family (ATPases associated with diverse cellular activities) which is involved in homotopic membrane fusion. The ATPase (AAA) p97 is essential to regulate processes including endoplasmic reticulum associated degradation, mitochondrial associated degradation, autophagy, etc.<sup>37</sup> Interchanging the C5 nitro on the indole with SF<sub>5</sub> reduced its potency (Figure 1.9). Even though, SF<sub>5</sub> and NO<sub>2</sub> are similar electronically, SF<sub>5</sub>'s large size resulted in diminished P97 inhibition of the indole.<sup>38</sup>



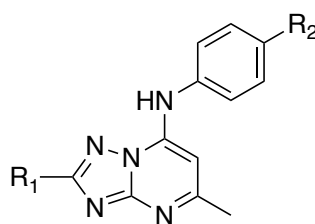
- a) R = NO<sub>2</sub>; IC<sub>50</sub> = 0.05 μM  
 b) R = SF<sub>5</sub>; IC<sub>50</sub> = 21.5 μM

Figure 1.9: SF<sub>5</sub> and NO<sub>2</sub> AAA ATPase p97 inhibitors

### 1.5.3 Replacing halogens

Halogens have been used commonly in drug design to block metabolic sites, alter electronic and lipophilic properties as well as steric interactions. The SF<sub>5</sub> group possesses a bulky steric volume and demonstrates greater hydrophobicity and electronegativity. Due to these differences, SF<sub>5</sub> is regarded as a viable alternative to halogens. Much like the nitro group, only a few comparisons between halogens and SF<sub>5</sub> have been reported.

The parasite *Plasmodium falciparum* possess *Plasmodium falciparum* dihydroorotate dehydrogenase (*PfDHODH*) enzyme in its de novo pyrimidine biosynthetic pathway. Inhibition of *PfDHODH* blocks the parasite's pyrimidine nucleotide synthesis. Hence, *PfDHODH* is an ideal target for antimalarial treatment. A lead-optimisation study by Coteron *et al*, on triazolopyrimidine based SF<sub>5</sub>, CF<sub>3</sub>, and Cl derivatives as *PfDHODH* inhibitors demonstrate similar potency for all the analogues (Figure 1.10).<sup>39</sup>



- 1.6a**; R<sub>1</sub> = CF<sub>2</sub>CH<sub>3</sub>; R<sub>2</sub> = Cl; IC<sub>50</sub> = 38 nM  
**1.6b**; R<sub>1</sub> = CF<sub>2</sub>CH<sub>3</sub>; R<sub>2</sub> = SF<sub>5</sub>; IC<sub>50</sub> = 33 nM  
**1.6c**; R<sub>1</sub> = CF<sub>2</sub>CH<sub>3</sub>; R<sub>2</sub> = CF<sub>3</sub>; IC<sub>50</sub> = 38 nM

Figure 1.10: SF<sub>5</sub>, CF<sub>3</sub>, & Cl based *PfDHODH* inhibitors

More than 100 triazolopyrimidine analogues were evaluated and the SF<sub>5</sub> derivative (**1.6b**) was chosen to be carried forward into clinical studies because of its oral bioavailability, metabolic stability and in vivo efficacy.

## 1.6 Other interesting examples of SF<sub>5</sub> in medicinal chemistry

Benzoyl guanidine **HOE 694** is a  $\text{Na}^+/\text{H}^+$  exchanger inhibitor (Figure 1.11).  $\text{Na}^+/\text{H}^+$  exchanger inhibitors protect the cardiac tissue during heart attack, chemotherapy, and organ transplant.<sup>40</sup> Structure-activity studies revealed that insertion of lipophilic and bulky groups at the 4-position of the benzene ring of **HOE 694** could enhance its activity. Inserting  $\text{SF}_5$  at position 4 resulted in a first-generation derivative (**HOE 694-a**) that showed an improved  $\text{Na}^+/\text{H}^+$  exchanger inhibition activity. By increasing the bulk at position 4, a second generation of compounds were developed, of which **HOE 694-b** had 7-fold more potency than **HOE 694-a**. In both generations, insertion of an  $\text{SF}_5$  group increased the NHE inhibition activity, improved bioavailability and *in vivo* half-life.<sup>41</sup>

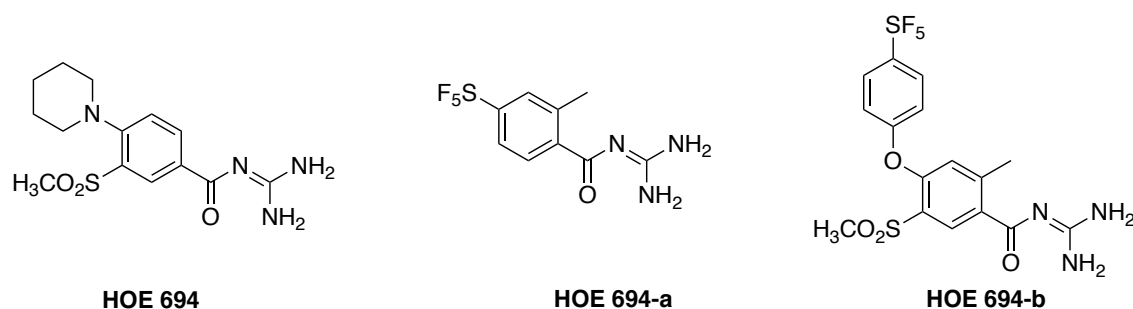


Figure 1.11: NHE inhibitors

Parasites of the family trypanosomatid are responsible for three human diseases; sleeping sickness, Chagas' disease, and leishmaniasis.<sup>42</sup> These parasites use trypanothione for the maintenance of their thiol-redox potential to protect them from oxidative and chemical stress. Function of trypanothione is regulated by two enzymes; trypanothione reductase (TR) and trypanothione peroxidase.<sup>43</sup> TR has become a popular target for the treatment of diseases caused by trypanosomatidae.

Stump *et al.* synthesised a series of TR inhibitors (TRI), bearing either a  $\text{SF}_5$ ,  $\text{CF}_3$ , or *tert*-butyl group ( $\text{C}(\text{CH}_3)_3$ ) targeting the parasite *T. cruzi* that is responsible for Chagas' disease (Figure 1.12).<sup>44</sup> Compounds **TRI(a-c)** were screened against *T. cruzi* TR. The  $\text{SF}_5$  derivative, **TRIf** ( $K_{\text{ic}} = 28 \mu\text{M}$ ), competitively inhibited *T. cruzi* TR similar to the  $\text{CF}_3$  compound, **TRIfa** ( $K_{\text{ic}} = 24 \mu\text{M}$ ), and illustrated threefold improvement compared to **TRIfc** ( $K_{\text{ic}} = 84 \mu\text{M}$ ) (Figure 1.12).

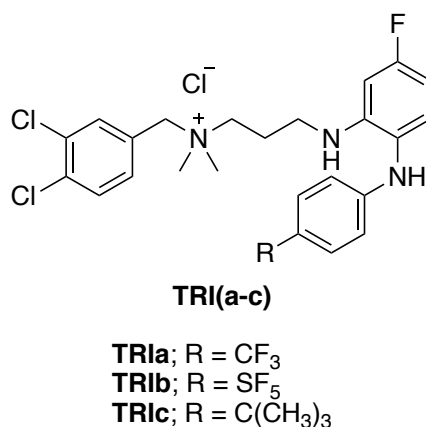


Figure 1.12: TR inhibitors

Inhibition mode of compounds **TRI(a-c)** were analysed through molecular modelling studies which revealed that the changes in binding affinity are a consequence of different steric and electronic properties of the groups  $\text{CF}_3$ ,  $\text{SF}_5$ , and  $\text{C}(\text{CH}_3)_3$ . Bulkiness of the *tert*-butyl group leads to loss of important interactions as **TR1c** is unable to efficiently occupy the binding site. Although, the size of  $\text{SF}_5$  is relatively large, **TR1b** showed a similar binding affinity to its  $\text{CF}_3$  counterpart due to the strong electron-withdrawing nature of the  $\text{SF}_5$  group, that may strengthen the interaction of **TR1b** with the electron-rich residues of the TR active site.

## 1.7 $\text{SF}_5$ in materials science

In material chemistry,  $\text{SF}_5$  was first employed by Kirsch and co-workers in the synthesis of liquid crystal displays (LCD) in 1999.<sup>45</sup> The late 90s saw the rapid growth of LCDs towards becoming the major technology for flat panel displays. Available LCD technology predominantly depended on the electrical and optical properties of nematic liquid crystalline molecules. Design of nematic liquid crystals has been based on cyanated biphenyls and phenylcyclohexane derivatives. A disadvantage of nitrile based liquid crystals are that they mobilise and solvate ionic impurities in devices resulting in a low voltage holding ratio. Another popular choice in liquid crystal design is the use of fluorinated aromatic rings primarily due to the unusual combination of high polarity and low polarizability imparted on the molecule by the fluorine atom (Figure 1.13).<sup>32</sup>

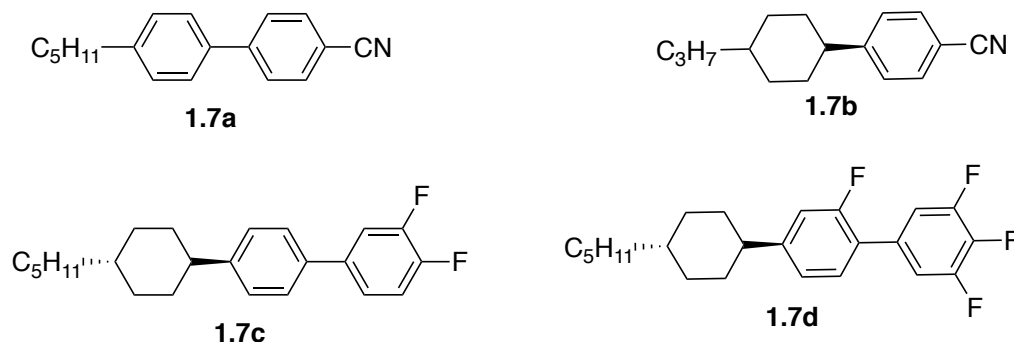


Figure 1.13: Cyano- and fluoro-substituted nematic liquid crystal molecules

The high demand for display panels led to mass production. In order to reduce the cost, the driving voltage of the active matrix LCD was lowered. This meant nematic liquid crystals with a higher dielectric anisotropy were required to obtain an electro-optical response. The most efficient way to increase dielectric anisotropy when designing a liquid crystal is to use a polar terminal group with the maximum possible dipole moment. Unfortunately, the overall molecular dipole moments provided by the fluorinated molecules were insufficient for certain LCD applications. Kirsch's search for a new and more polar terminal group that would bring about an acceptably high dielectric anisotropy led him to the discovery of  $\text{SF}_5$  group. They synthesised a series of  $\text{SF}_5$  based liquid crystal molecules that exhibited high dielectric anisotropy (Figure 1.14).

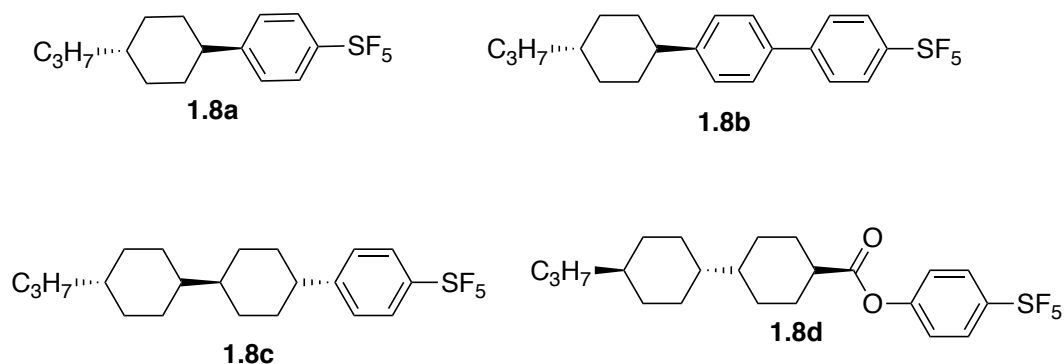


Figure 1.14: SF<sub>5</sub>-substituted nematic liquid crystal molecules.

Liquid crystals are merely one example where SF<sub>5</sub> was found to be applicable in material science. Others include molecular superconductors, triboluminescent materials, luminescent transition metal complexes etc., among others.

## 1.8 SF<sub>5</sub> in agricultural chemistry

An initial utility of SF<sub>5</sub> in life sciences was chiefly as pesticides in the form of herbicides, fungicides, parasiticides, and insecticides. Trifluralin is an exemplar pesticide where the herbicidal activities of SF<sub>5</sub> and CF<sub>3</sub> congeners were compared (Figure 1.15).

Trifluralin is a dinitroaniline herbicide used to control pre-emergence of annual grasses and some dicotyledon weeds in cotton, soybean, wheat and oilseed crops.

To compare the relative efficacy of CF<sub>3</sub> and SF<sub>5</sub> in dinitroaniline herbicides, Lim *et al.*<sup>46</sup> prepared the SF<sub>5</sub> analogue of trifluralin and tested it alongside the parent compound.

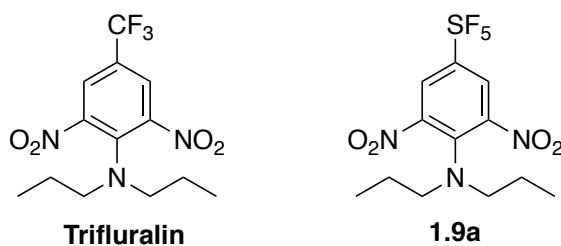


Figure 1.15: Trifluralin & its SF<sub>5</sub> analogue

Application of **1.9a** in place of trifluralin did not show any advantage in post-emergence applications. However, when used in pre-emergence applications, **1.9a** proved to be a superior herbicide than trifluralin as assessed by visual injury estimation. In pre-emergence applications, crop injury and growth inhibition were relatively low for **1.9a** as opposed to trifluralin meaning that the crops are more tolerant to **1.9a** than trifluralin.

## 1.9 Microwave Chemistry

Towards the end of World War-II, in 1946, Percy LeBaron Spencer discovered the use of low-density microwave energy as a method of heating while making magnetrons. Spencer noticed the melted candy bar in his pocket after standing in front of an active radar that produces microwave radio

signals.<sup>47</sup> Led by his curiosity, he tested other food items like popcorn and egg and observed fast cooking of these items. In 1947, Raytheon Corporation where Spencer was an engineer, built first commercially available microwave oven costing approximately US \$5000 each.<sup>48</sup> It wasn't until the late 70s, the first microwave laboratory instrument was developed by CEM Corporation to analyse moisture in solids. Towards mid 80s, microwave energy saw its use in chemical synthesis, explored by Gedye *et al.* who published papers relating to microwave mediated reactions.<sup>49</sup> Since then microwave has been used widely in synthetic chemistry to reduce reaction time and increase product yield. A number of microwave reactor models of different specifications have been available in the market since 2000. Major producers of microwave technology include CEM, Biotage, Anton Paar etc.<sup>50</sup>

Microwaves are electromagnetic waves in the frequency range of 0.3 to 300 GHz. All microwave reactors operate at a frequency of 2.45 GHz to avoid interference with telecommunication and mobile phone frequencies. At this frequency, microwave photons, on their own, are not capable of inducing chemical reactions. The dielectric properties of a material govern its heating characteristics under microwave irradiation conditions. The ability of a specific substance to convert electromagnetic energy into heat at a given frequency and temperature is determined by a parameter called loss tangent,  $\tan \delta$ .

Microwaves consist of an electric and a magnetic field component. The electric component is responsible for the heating of the material. Two main mechanisms involved in heating are dipolar polarization and ionic conduction.<sup>51,52</sup>

To generate heat, the substance being irradiated with microwaves must possess a dipole moment that aligns in the applied electric field. The dielectric constant describes the ability of molecules to be polarized by the electric field. Oscillation of the applied field causes the dipole of the sample to realign with the alternating electric field.<sup>51</sup> Energy is lost in the form of heat during the process. The amount of heat generated is directly linked to the ability of the matrix to align itself with the frequency of the applied field. In essence, field energy is transferred to the medium and electric energy is converted into either kinetic or thermal energy and eventually into heat energy. Reaction mediums with high loss tangent ( $\tan \delta$ ) are required for efficient absorption of microwave energy and for rapid heating. High microwave absorbing solvents have a  $\tan \delta > 0.5$  and when  $\tan \delta < 0.1$ , the solvent is classed as low absorbing. The  $\tan \delta$  for ethanol = 0.941 in comparison to water,  $\tan \delta = 0.123$ . Examples of poor microwave absorbing solvents are hexane ( $\tan \delta = 0.020$ ), toluene ( $\tan \delta = 0.040$ ), dichloromethane ( $\tan \delta = 0.042$ ), etc.

Ionic conduction occurs when ions in the sample oscillate back and forth under the influence of microwave field and collide with the neighbouring atoms. The collision generates heat.<sup>53</sup>

Traditional conductive heating makes use of external heating sources like a heating mantle or oil bath to perform synthesis. These methods depend on thermal energy and convection current to transfer

heat energy to the matrix, hence, are inefficient and comparatively slow. Moreover, temperature of the reaction vessels is higher than that of the reaction. And occasionally local overheating of the reaction mixture can develop which may result in degradation of reactants as well as product. Microwave irradiation on the other hand can produce efficient and uniform heating by direct coupling of microwave energy with the matrix. Figure 1.16 illustrates the difference in heating profiles of microwave vs conventional heating method. Microwave irradiation (left) raises the temperature of the whole volume simultaneously, while in the oil-heated tube (right), the contents next to the vessel are heated first.

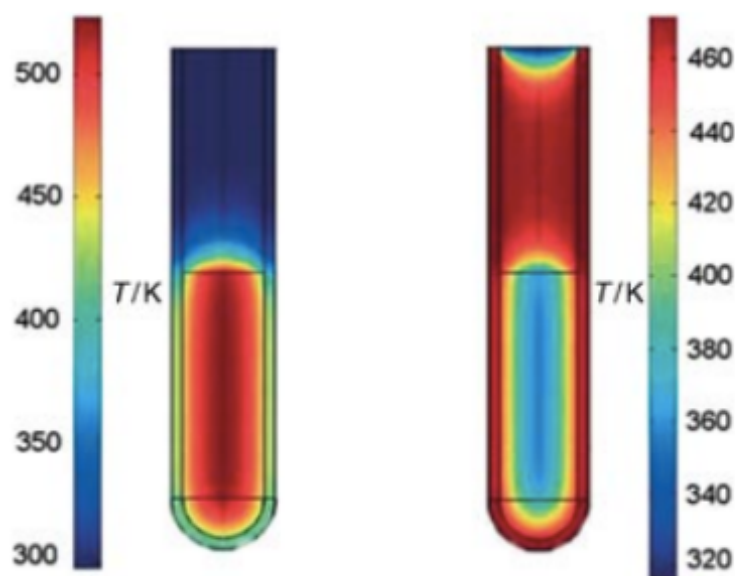


Figure 1.16 Inverted temperature gradients of Microwave (left) versus oil-bath heating (right) after 60 seconds of heating<sup>57</sup>

Advantages of microwave irradiation over thermal include efficient and rapid heating, increased rate of reactions, higher yields, and environmentally friendly reactions. In organic synthesis the use of water as an environmentally benign, cheap, and readily available solvent is appealing. Due to water's ability to polarize, it makes an excellent choice of solvent in microwave mediated synthesis, providing it solubilises the reagents.

The Suzuki reaction is one of the most used and versatile C-C coupling reactions in organic synthesis.<sup>53</sup> Carrying out high-speed microwave mediated Suzuki reactions has become a regular practice. A significant advancement in Suzuki chemistry has been the ability to use water as a solvent in microwave facilitated synthesis. Leadbeater and Marco described a very rapid, ligand-free palladium-catalysed aqueous Suzuki coupling of aryl halides with aryl boronic acids in the microwave. A series of biphenyls were synthesised in the microwave at temperatures between 150-175 °C for 5 minutes, affording yields between 45-95%, with only 0.4 mol% of Pd(OAc)<sub>2</sub> as catalyst. Scheme 1.15 shows microwave mediated coupling of bromobenzene and phenylboronic acid, affording the product in 84% yield.<sup>55</sup>





A major disadvantage related to ball millers is lack of control of temperature. The temperature of a reaction run in a mixer mill will only incidentally rise due to the frictional forces experienced during the milling process. On the other hand, planetary ball milling can result in the temperature exceeding 200 °C. Scalability is another concern related to mixer mill, especially in an industrial setting. The mixer miller can achieve gram scales which is sufficient for laboratory investigations.

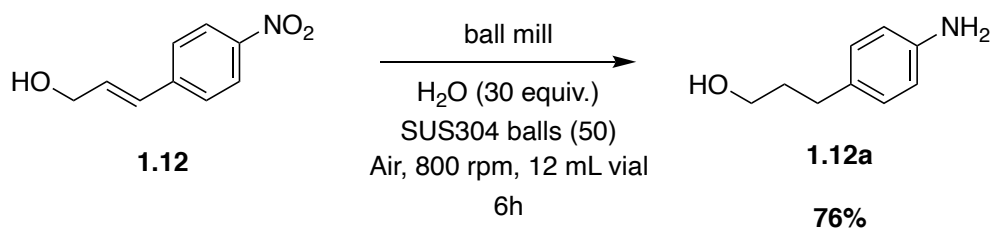


Figure 1.17: Retsch MM400 mixer mill and different types of jars and balls used for milling<sup>62</sup>



Figure 1.18: Retsch PM 100 planetary ball mill<sup>63</sup>

Traditionally, catalytic hydrogenation is performed in either the gas or liquid phase. Liquid phase hydrogenation is more commonly used for small-scale synthesis where, a slurry containing a catalyst and a substrate is contacted with gaseous hydrogen.<sup>64</sup> Gaseous hydrogen can be generated in situ, e.g. by transfer hydrogenation,<sup>65</sup> or a balloon filled with hydrogen gas is fed into the reaction. In a recent study, it was reported that the hydrogenation of olefins could be accomplished using water as a hydrogen source, mediated by mechanochemical energy and stainless steel (SUS304) in a planetary ball mill. The study was commenced after observing generation of H<sub>2</sub> gas when moistened stainless-steel balls were exposed to friction. Scheme 1.16 shows hydrogenation of an alkene as well as a nitro group in the planetary ball mill.<sup>66</sup>



*Scheme 1.16: Hydrogenation mediated by mechanochemistry*

## 1.11 Thesis aims

The increased availability of SF<sub>5</sub> containing reagents has promoted the growth of the SF<sub>5</sub> group in medicinal chemistry. Nevertheless, compared to CF<sub>3</sub> in medicinal chemistry, SF<sub>5</sub>'s presence is only imperceptible. Therefore, it is imperative to develop and investigate novel biologically active SF<sub>5</sub> containing compounds. This project aims to explore the effect of SF<sub>5</sub> in known drugs (Figure 1.19) while comparing it to other functional groups such as halogens, NO<sub>2</sub> and CF<sub>3</sub>. In doing so, the project would expand the repertoire of SF<sub>5</sub> in medicinal chemistry. In addition, we intended to develop a range of SF<sub>5</sub> containing building blocks that can be commercialised. For biological studies, pentafluorosulfanyl containing compounds such as oxindoles and benzophenones were purchased and modified into analogues of known drugs like diazepam. To develop chemicals in an eco-friendly manner, we took advantage of microwave and mechanochemistry whenever possible (Scheme 1.17).

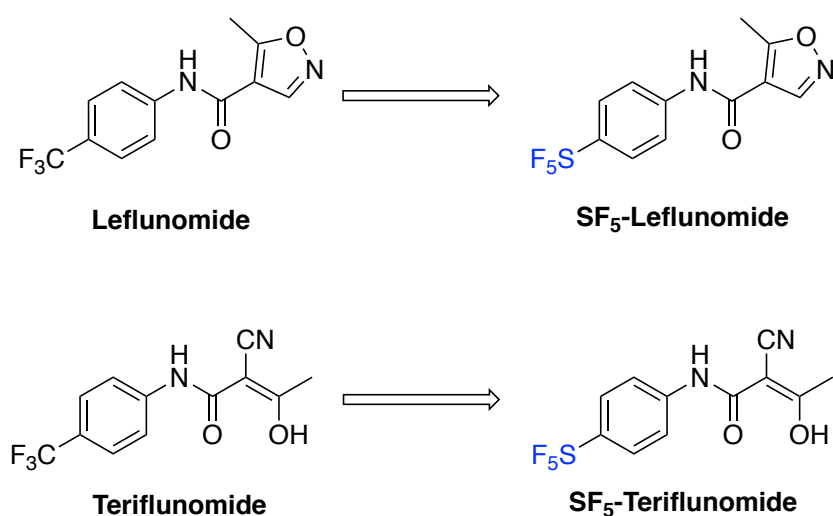
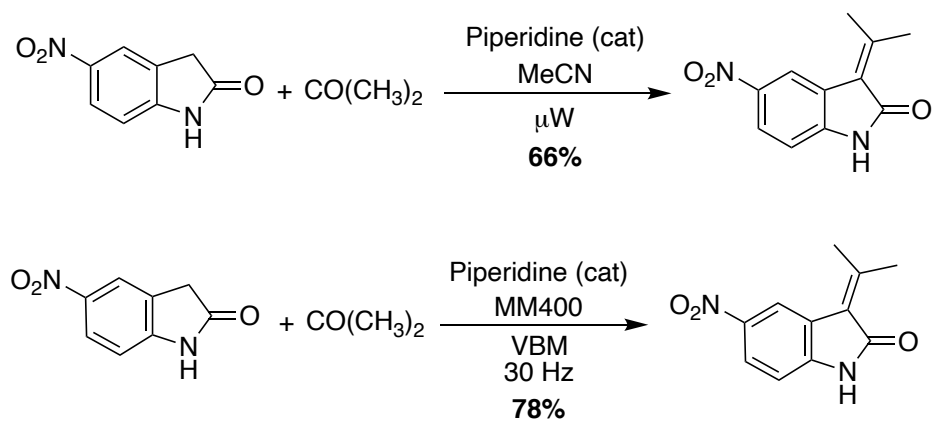


*Figure 1.19: Bio-isosteric replacement of CF<sub>3</sub> in two known drugs, leflunomide and teriflunomide*



*Scheme 1.17:  $\mu\text{W}$  vs mechano-mediated Knoevenagel condensation*

## Chapter 2.0 SF<sub>5</sub> as a Bioisosteric Replacement of CF<sub>3</sub> in Leflunomide and Teriflunomide

### 2.1 Introduction

Purine and pyrimidine nucleotides are the fundamental building blocks of DNA and RNA.<sup>63</sup> Additionally, they play a critical role in membrane lipid biosynthesis and protein glycosylation. Biosynthesis of RNA requires two pyrimidine nucleoside triphosphates; uridine-5'-triphosphate (UTP) and cytidine triphosphate (CTP), and two purine nucleoside triphosphates; adenosine triphosphate (ATP) and guanosine triphosphate (GTP). The nucleosides are generated either via *de novo* synthesis or through utilization of a salvage pathway.<sup>64</sup> The *de novo* biosynthetic pathway for the synthesis of UTP and CTP involves five phases and begins with the assembly of the pyrimidine ring using simple precursors. At the third phase, dihydroorotic acid (DHO), a precursor for the synthesis of pyrimidine, is formed. In phase four, dihydroorotase (DHODH), the only mitochondrial enzyme in pyrimidine biosynthesis catalyses the oxidation of DHO to orotic acid via a 'ping-pong' mechanism. It is the only enzyme capable of performing this conversion making it essential for the cell's ability to produce uridine monophosphate. Orotic acid is then converted to uridine monophosphate (UMP) in two enzymatic steps. Firstly, ribose-5'-phosphate is transferred to orotic acid followed by decarboxylation resulting in UMP. Uridine monophosphate synthase (UMPS); a bifunctional enzyme consisting of orotate phosphoribosyltransferase and orotidine-5-monophosphate decarboxylase catalyses the synthesis (Figure 2.1).<sup>65</sup> In eukaryotes, DHODH is a ubiquitous enzyme located in the inner mitochondrial membrane with ubiquinone as the proximal electron acceptor for DHO's oxidation to orotic acid.<sup>66</sup>

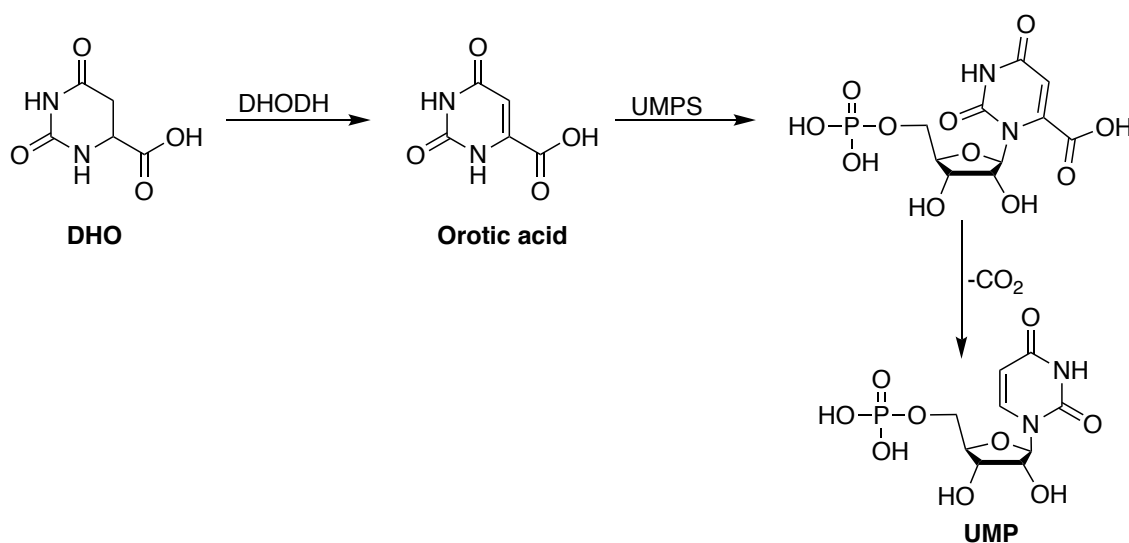


Figure 2.1: Phase 4 of *de novo* pyrimidine synthesis<sup>67</sup>

Lymphocytes are white blood cells that consist of T, B and natural killer cells. B lymphocytes make antibodies while T lymphocytes help kill tumour cells and control immune response. Purine and pyrimidine are necessary for the development and survival of mature T lymphocytes.<sup>68</sup> Lymphocytes require eightfold more pyrimidine during proliferation.<sup>69</sup> This demand can only be met by using both salvage and *de novo* synthesis pathways. Thus, inhibition of DHODH prevents lymphocytes from accumulating sufficient pyrimidines to support DNA synthesis. Pyrimidines are also needed for glycosylation of lipids and proteins. DHODH inhibitors therefore demonstrate immunosuppressant and anti-inflammatory properties and are effective treatment option for diseases such as multiple sclerosis<sup>70</sup>, rheumatoid arthritis (RA) and cancer.<sup>71</sup>

In the above oxidation process, there is obviously an accompanying reduction process (Figure 2.2). Human DHODH (HDHODH) belongs to the class 2 DHODH family with flavin mononucleotide (FMN) as its redox cofactor. DHODH has two binding sites. DHO binds to the first site and is oxidised to orotic acid. Initially electrons from DHO are transferred to FMN as part of the redox reaction generating dihydroflavin mononucleotide (FMNH<sub>2</sub>) and orotic acid. After the dissociation of orotic acid from the enzyme, FMNH<sub>2</sub> is oxidised back to FMN by a second cofactor, called *coenzyme* Q (ubiquinone) that binds to the second site. Ubiquinone is also found in the inner mitochondrial membrane.

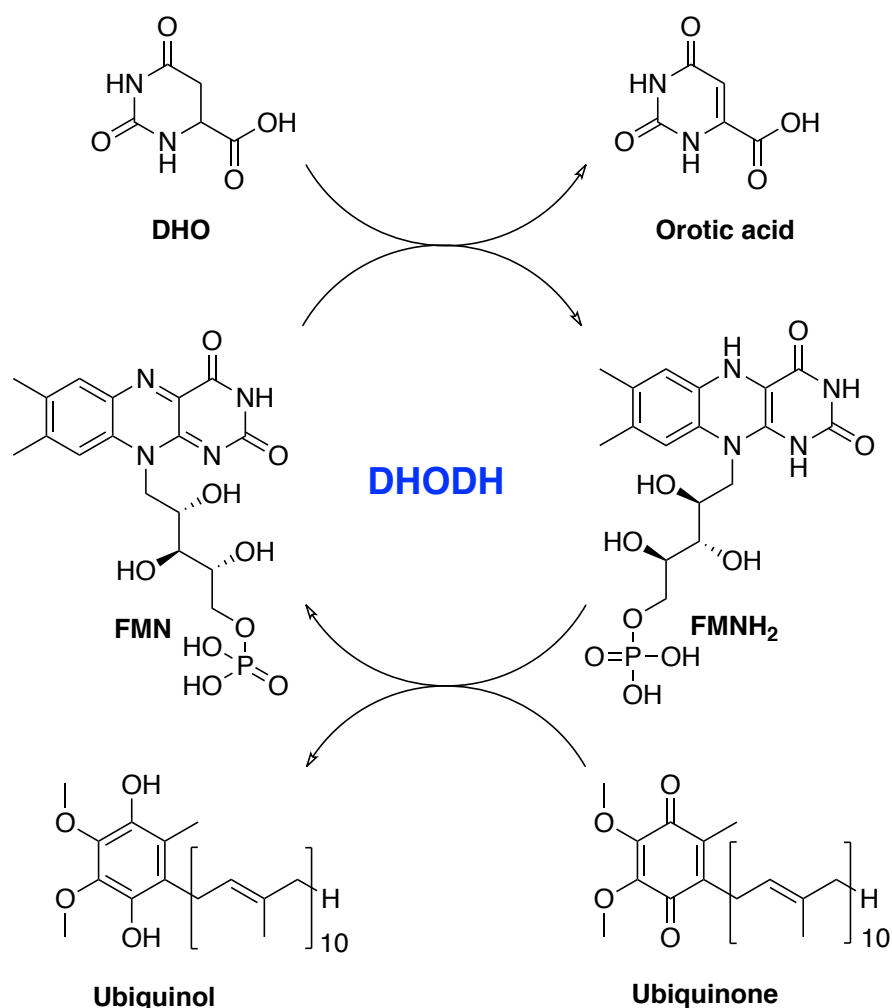


Figure 2.2: Ping-pong redox reactions catalysed by DHODH<sup>2</sup>

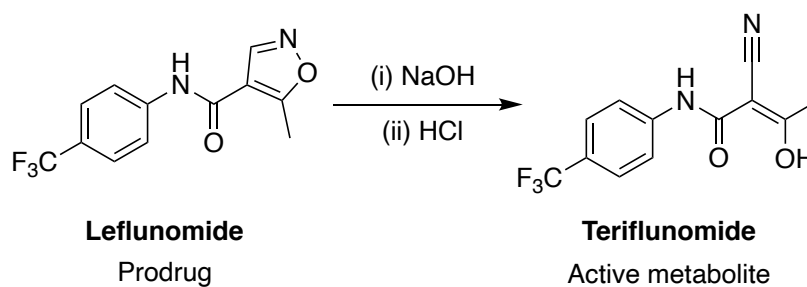
Full length HDHODH has 396 amino acid residues. A high-resolution crystal structure (PDB ID: 1D3H; Figure 2.3) of HDHODH, in complex with teriflunomide (Scheme 2.1), revealed that the long N-terminal extension of the enzyme folds into a helical domain that forms the entrance of a tunnel leading to the active site. The helical domain is responsible for the membrane interaction of HDHODH. The N-terminal extension contains a small domain that consists of two  $\alpha$  helices:  $\alpha 1$  and  $\alpha 2$  and a loop connecting it to the large C-terminal domain. The small N-terminal domain is amphipathic i.e. with both hydrophobic and hydrophilic parts. All of the charged and most of the polar amino acid residues orient towards the large domain while the hydrophobic side chains project away from the large domain. The hydrophobic side chains form a large hydrophobic protruding patch. The structure of the small domain provides information about membrane association of the enzyme. The hydrophobic patch is able to push into the hydrophobic interior of the membrane while the polar and positively charged border interacts with the negatively charged phospholipid head groups. An ideal HDHODH inhibitor should address both polar and lipophilic characteristics of the binding pocket. The space between the  $\alpha 1$  and  $\alpha 2$  helices forms a slot in the hydrophobic patch. The hydrophobic tunnel leads to the redox site containing the flavin molecule. Several charged or polar side chains (Gln47, His56, Tyr356, Thr360 and Arg136) are located at the narrow end of the channel.

Ubiquinone that can easily diffuse in the mitochondrial inner membrane uses this channel to approach the FMNH<sub>2</sub> for a redox reaction.<sup>73</sup>

Leflunomide (Arava®) is a disease modifying antirheumatic drug (DMARD) with immunomodulatory properties. It has been approved for the treatment of rheumatoid arthritis since 1998 (USA) and 1999 (EU).<sup>74,75</sup> However, leflunomide is a prodrug with little or no immunomodulatory activity until it is rapidly converted to its active form, teriflunomide, in the gastrointestinal tract and plasma (Scheme 2.1). In plasma it is highly protein-bound, >99%, and as a consequence, its plasma half-life is approximately 15 days. This can be reduced to 1-2 days by the use of cholestyramine, an ion exchange resin, or an activated charcoal washout. The long half-life implies significant enterohepatic recirculation. The latter refers to the process by which a drug or its metastable metabolite in the liver is secreted into the bile, followed by release into the small intestine from where it can be reabsorbed back into circulation and subsequently returned to the liver. This can result in significant plasma levels being maintained for up to two years after stopping the treatment. In the event of pregnancy, female users of teriflunomide must undergo accelerated elimination of teriflunomide until the concentration in plasma falls below 0.02 mg/L which is the value predicted to have minimal risk to the foetus, based on animal studies.<sup>76</sup> Teriflunomide is contraindicated in pregnant women or women planning on getting pregnant as teratogenicity and embryo-lethality in the off-spring of teriflunomide treated rats and rabbits are observed. *In vitro* and *in vivo* studies proved teriflunomide as not mutagenic and clastogenic. Clastogen is a mutagenic substance with the ability to alter the structure and number of chromosomes and chromatids.

Rheumatoid arthritis is an autoimmune and inflammatory disease, where in, the immune system attacks healthy cells causing inflammation. B-cells, T-cells and macrophages play important roles in RA pathogenesis. B-cells secrete proteins that promote RA such as rheumatoid factor and pro-inflammatory cytokines. The main function of T-cells in RA is to activate macrophages and fibroblasts and transform them into tissue-destructive cells.<sup>77</sup> The principal mechanism of action of teriflunomide is the inhibition of DHODH. This leads to depletion of ribonucleotide precursors in lymphocytes reducing DNA and RNA synthesis and resulting in the arrest of cell proliferation in the G1 phase of the cell cycle.<sup>78</sup>

Teriflunomide (Aubagio®) is one of the FDA approved treatments for multiple sclerosis, a chronic inflammatory disease. It is able to inhibit human DHODH in the low  $\mu\text{M}$  range and it binds in the same region of the tunnel which is a narrow cleft near the flavin molecule (Figure 2.3).<sup>73</sup> As it shares affinity for the binding site with ubiquinone,<sup>79</sup> it is dubbed as a redox silent coenzyme Q antagonist of DHODH.<sup>80</sup> Teriflunomide has a polar head consisting of one hydrogen bond donor; enol and two hydrogen bond acceptors, a nitrile and a carbonyl group, while the tail of teriflunomide, which occupies the entrance of the tunnel, is hydrophobic.



*Scheme 2.1: Isoxazole ring opening under basic conditions*

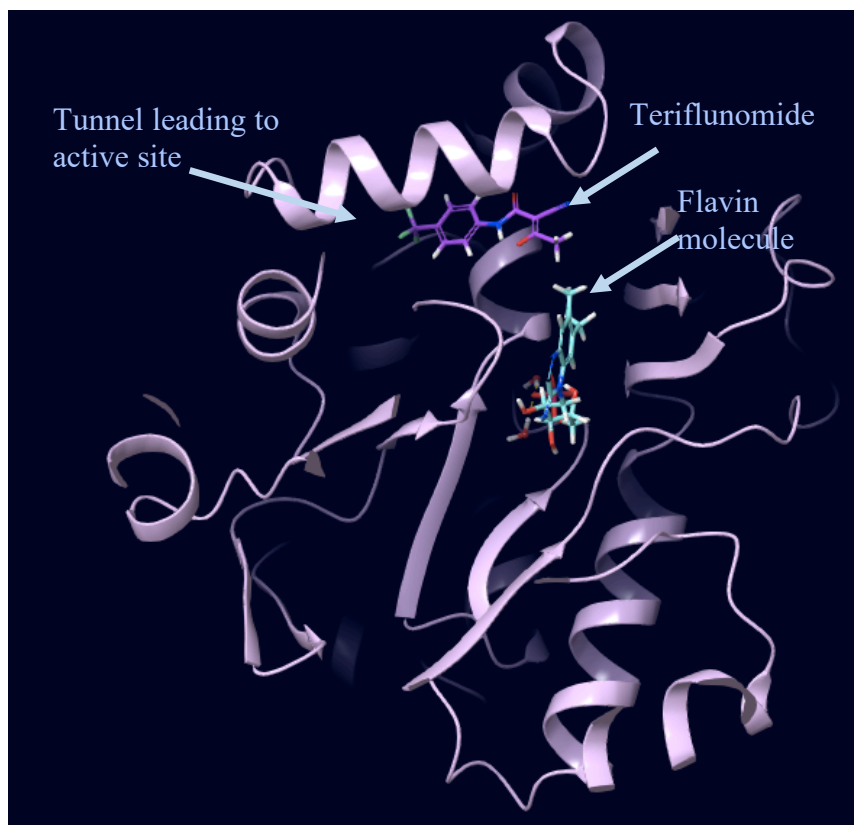


*Figure 2.3: Teriflunomide and FMN in complex with HDHODH. PDB ID: 1D3H. FMN: Teal, Teriflunomide: Purple*

### 2.1.1 Leflunomide and teriflunomide against SARS-CoV-2.

Viral infections can be addressed as a global crisis endangering our existence on this planet. Hundreds of viruses are known to us as pathogenic but fewer than 10 of them can be treated using clinically available anti-virals.<sup>81</sup> The increasing number of viral infections such as influenza virus, SARS-CoV, MERS-CoV, Ebola virus, Zika virus and the very recent SARS-CoV-2, are probably lasting global threats. Developing broad spectrum antivirals (BSA) is one way to tackle this issue. BSA work by either inhibiting the viral proteins, known as direct-acting antiviral agents (DAA) or by targeting the host proteins and processes that facilitate viral replication, known as host targeting antivirals (HTAs).<sup>81</sup>

A new initiative focused on developing therapeutics for the new coronavirus, identified COVID-19 virus main protease (M<sup>Pro</sup>) as a potential target. The genome of COVID-19 comprises approximately 30,000 nucleotides. Its replicase gene encodes two overlapping polyproteins, pp1a and pp1ab, which



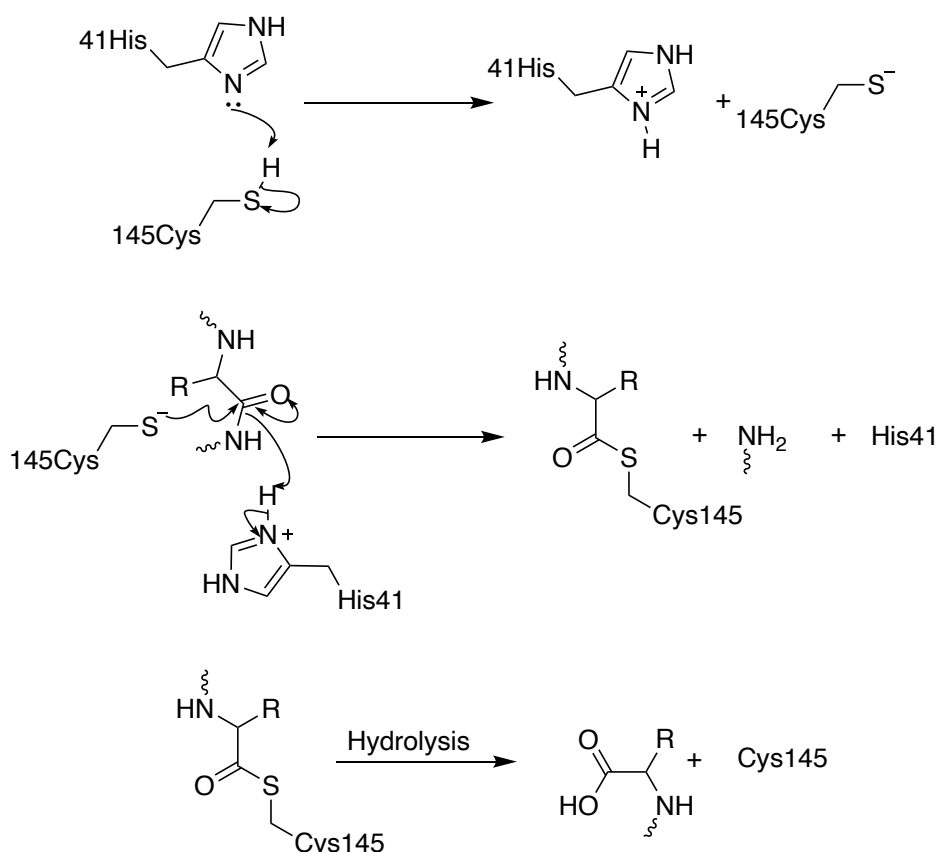
are required for viral replication and transcription.  $M^{\text{pro}}$  is a key enzyme in coronaviruses, which is crucial in mediating viral replication and transcription. X-ray crystal structures of the main proteases of SARS-CoV-2, SARS-CoV and MERS-CoV revealed high degree of structural similarities and conservation of the active site.<sup>82</sup> Inhibitors for SARS-CoV-2  $M^{\text{pro}}$  could be adapted from previously identified compounds targeting SARS-CoV or MERS-CoV main proteases.

$M^{\text{pro}}$  releases the functional polypeptides from the polyproteins by extensive proteolytic processing. It digests the polyproteins at no less than 11 cleavage sites, starting with autolytic cleavage<sup>83</sup> and exclusively cleaves polypeptides after a glutamine residue. No human host-cell proteases are known to possess this substrate specificity.<sup>84</sup>

Its functional importance and the absence of closely related homologues in humans, render  $M^{\text{pro}}$  as an attractive target for antiviral drug design as an example of a DAA.

$M^{\text{pro}}$  is a cysteine protease with a catalytic dyad; cysteine (Cys145) and histidine (His41), in its active centre. Cysteine proteases commonly contain a catalytic triad.  $M^{\text{pro}}$  contains a buried water molecule in its active site instead of the third catalytic residue.

The proteolytic process is believed to proceed with extraction of a proton on the cysteine side chain (S-H) by the histidine's imidazole side chain, followed by nucleophilic attack at the amide bond of the substrate by the thiolate forming thioester. The *N*-terminal peptide product is released by proton abstraction from histidine before the hydrolysis of thioester to release the C-terminal product and regenerate the catalytic dyad (Scheme 2.2).



Scheme 2.2: Proteolytic cleavage aided by cysteine protease with a catalytic dyad

Inhibitors of SARS-CoV-2<sup>85</sup> and MERS-CoV<sup>86</sup> have been reviewed comprehensively, reporting peptidomimetics and small molecules with affinities in the micro molar to nanomolar range. These inhibitors were designed based on a warhead design strategy. Warheads such as Michael acceptors, aldehydes, epoxy ketones and other ketones were employed to undergo covalent attack by the catalytic cysteine residue.

Previous studies had identified N3 (Figure 2.4, a), a Michael acceptor inhibitor (Figure 2.4, b), to inhibit multiple CoVM<sup>pro</sup>s, including those from SARS-CoV and MERS-CoV.<sup>87</sup> N3 irreversibly modifies Cys145. Molecular docking analysis of N3 (Figure 2.5) in COVID-19 M<sup>pro</sup> showed that it could fit inside the substrate-binding pocket and a kinetic analysis demonstrated a two-step irreversible inactivation of the enzyme. In Vero cells, N3 exhibited anti-SARS-CoV-2 activity. The inhibitor initially associates with the enzyme followed by the formation of a stable covalent bond between N3 and M<sup>pro</sup>.<sup>87, 88</sup>

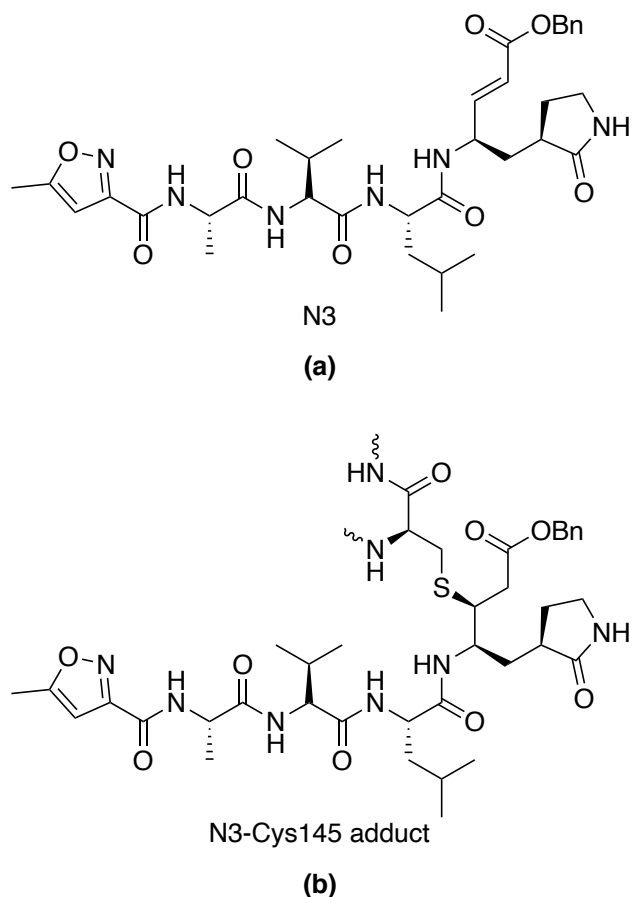


Figure 2.4: Potent COVID-19 M<sup>pro</sup> inhibitor. (a), structure of N3. (b), N3-Cys 145 adduct

Figure 2.5 shows M<sup>pro</sup> in complex with N3. In addition to several non-covalent bonds, a covalent bond, Michael addition, between Cys145 and the alpha-beta unsaturated ketone can be seen. The structure of SARS-CoV-2 M<sup>pro</sup> in complex with N3 was a useful model to identify lead inhibitors to target SARS-CoV-2 M<sup>pro</sup>.

Teriflunomide possesses a Michael acceptor warhead capable of covalently binding with M<sup>pro</sup>. Therefore, teriflunomide and its analogues were hypothesised to make potential inhibitors of SARS-CoV-2 M<sup>pro</sup>.

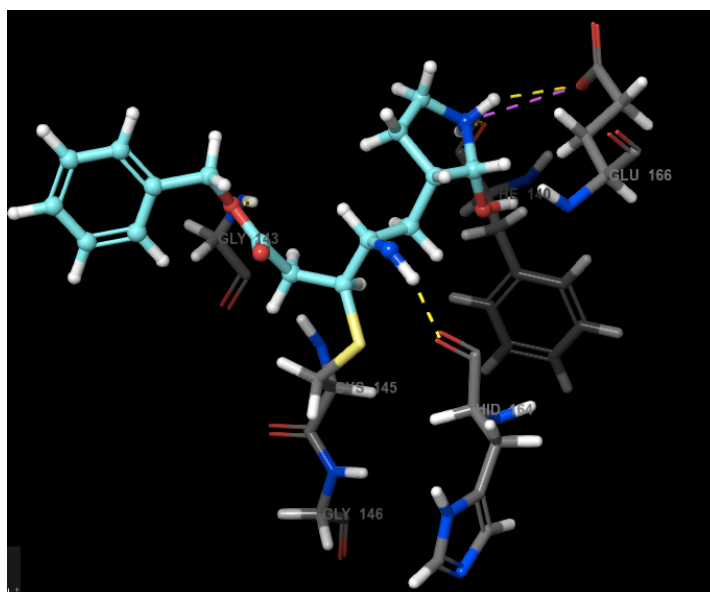


Figure 2.5: COVID-19 M<sup>pro</sup> in complex with N3 showing interactions with amino acid residues

One of the main causes of Covid-19 related death is acute lung injury. SARS-CoV-2 spike (S) proteins bind to the receptor angiotensin-converting enzyme 2 (ACE2) to enter human cells.<sup>89, 90</sup> ACE2 is a type I membrane protein expressed on cells in the kidney, heart, gastrointestinal tracts, blood vessels and type I and II alveolar cells in the lungs.<sup>89</sup> ACE2 enzyme catalyses the conversion of angiotensin II (AngII), a vasoconstrictor, to angiotensin (1-7). AngII also mediates cell proliferation by stimulating various cytokines. ACE2 regulates the vasoconstrictor and profibrotic effects of AngII. Ang (1-7) has vasodilatory and antifibrotic actions. SARS-CoV-2 infection leads to downregulation of ACE2 expression, followed by excessive production of AngII by angiotensin converting enzyme (ACE) that converts Ang (1-7) to AngII. Once the virus enters and infects the host cells, a host immune response and inflammation cascade begin via antigen presenting cells and macrophages. Uncontrolled release of pro-inflammation cytokines results in acute lung respiratory damage (ARDS). Favalli et al. reported that Covid-19 and rheumatoid arthritis have similar pathophysiology. They also suggested that anti-rheumatoid drugs can be used for Covid-19 treatment.<sup>91</sup> Chloroquine and hydroxychloroquine, that are also used to treat RA, were initially used to treat Covid-19 pneumonia.<sup>91</sup>

Several studies searching for HTAs point towards compounds inhibiting the host's pyrimidine synthetic pathway to impede virus infections, indicating that the replication of viruses is widely dependent on the aforementioned pathway.<sup>92</sup> Once again, DHODH represents a viable target and teriflunomide a potential treatment. In addition, DHODH inhibition provides anti-inflammatory effects.<sup>93</sup> As leflunomide and teriflunomide are capable of regulating lymphocytes and the release of cytokines and chemokines, they can be speculated to be effective against ARDS due to cytokine

storm. Several clinical trials to evaluate the potential of leflunomide as Covid-19 treatment are ongoing.<sup>94</sup>

Independent of our work, a small-scale clinical trial of Leflunomide as a treatment for Covid-19 revealed that patients treated with leflunomide recovered faster and cleared virus in fewer days than the blank-controlled patients. The study was however, conducted on a group of only ten people, where, five were administered leflunomide and the other half were not. The control group did not receive a placebo either. The study was based on findings, that, DHODH inhibitors are able to rescue mice from severe influenza-A-virus infection by antiviral and immune-repression of pathological inflammation. Moreover, treating SARS-CoV-2 infected cells with teriflunomide conferred a profound antiviral efficacy of  $EC_{50} = 6 \mu\text{mol/L}$ .<sup>94</sup>

Following these results, the safety of leflunomide on SARS-CoV-2 infected patients with post-symptomatic viral shedding, was evaluated and compared with interferon  $\alpha$ -2a treatment alone, by the same research group. Asymptomatic patients and patients with mild symptoms are known to shed virus for a long-term (22.5 days on average).<sup>95</sup> Even after resolved symptoms and observed improvement in initially abnormal CT imaging, some patients remain viral RNA-positive. A combination treatment group received leflunomide and interferon  $\alpha$ -2a while the control group only received interferon  $\alpha$ -2a. Interferon  $\alpha$ -2a is a wide biologically activity cytokine.<sup>96</sup> It regulates several genes involved in antiviral and antiproliferative activities.<sup>97</sup> As per their observation, patients given a combination of leflunomide and interferon  $\alpha$ -2a did not have a substantially shorter length of hospital stay than patients treated with interferon alone.<sup>98</sup> This result points to a conclusion that leflunomide is not a viable treatment for post-symptomatic SARS-CoV-2 viral shedding.

Another detailed study on the suppression of SARS-CoV-2 by DHODH inhibition was conducted by Xiong R. *et al*<sup>92</sup> in Wuhan. According to the study, the inhibition of the DHODH enzyme resulted in reduced proliferation of SARS-CoV-2 in cells and, furthermore, this crucial strategy can be used to treat Covid-19 disease due to the immune response suppression of DHODH inhibitors.<sup>99</sup> From 280,000 compounds, the group identified two candidates, **S312** and **S418**, with  $IC_{50}$ s of 29.2 nM and 7.5 nM respectively. These compounds are approximately two and seven times more potent than teriflunomide ( $IC_{50} = 307.1 \text{ nM}$ ).<sup>93</sup> Structures of the identified compounds are not yet released.

An initiative called the COVID Moonshot was launched to accelerate the development of a COVID antiviral. The initiative is an open source with no intellectual property constraints where<sup>100</sup> scientists can submit and view drug designs and experimental data to inspire new ideas.<sup>101</sup> We were approached by collaborators (Prof F. von Delft, Dr A. Aimon) at Diamond Lightsource to offer our expertise in this endeavour.

In this study we have continued our investigation on the effect of substituting a trifluoromethyl (CF<sub>3</sub>) with pentafluorosulfanyl (SF<sub>5</sub>) group and applied this to both leflunomide and teriflunomide on DHODH inhibition to determine its potential, both as a COVID treatment and an immunomodulator. Alliancing with the COVID Moonshot initiative and with the aim of advancing the search for COVID antivirals, we tested the effects of teriflunomide analogues, together with several other compounds, donated by eMolecules<sup>®</sup>, on M<sup>pro</sup>.

## 2.2 Results and Discussion

### 2.2.1 Comparing DHODH inhibiting potency of SF<sub>5</sub>-containing analogues against known DHODH inhibitors

Virtual screening is a useful tool to find ligand hits, and to assist lead optimisation in structure based drug discovery. With the help of a computational strategy, and the large number of protein-ligand complexes available in the Protein Data Bank (PDB), one could predict the binding affinity of the ligands in question towards a receptor site of interest. Using Schrödinger Maestro, a molecular modelling software, we docked our ligands in complex with crystal structures of proteins obtained from the PDB database. Schrödinger Glide is a scoring functionality that enables you to evaluate binding affinity of ligands.<sup>102</sup>

Glide finds all the possible binding locations of the ligands in the active site of the receptor and produces a set of initial ligand conformations. Different ligand poses can then be generated. Ligand pose refers to a complete specification of the ligand; position and orientation relative to the receptor, core conformation, and rotamer group conformations.<sup>103</sup> Using Glide score, different ligand poses can be ranked. Scoring is related to the strength of interaction between the ligand and the protein, which is expressed as binding free energy.<sup>104</sup> Therefore, more negative values represent tighter binders. The binding free energy is described as a sum of the intermolecular interactions between the ligand and the protein and the internal steric energy of the ligand.<sup>105,106</sup>

Liu *et al.*<sup>73</sup> in their paper, disclosed that the carbonyl group on the polar head of teriflunomide forms a hydrogen bond with water which in turn is bound to Arg136 while the enolic OH binds to Tyr356. In addition, the CF<sub>3</sub> containing aromatic ring made several hydrophobic interactions with amino acid residues in the tunnel. Leban *et al.*<sup>107</sup> and Davies *et al.*<sup>108</sup> reported that, apart from the direct hydrogen bond with Tyr356, there are two hydrogen bond interactions with Arg265 and Gln47 mediated by a water molecule.

We performed our own docking studies using the crystal structure of human DHODH in complex with teriflunomide obtained from the protein data bank (PDB ID: 1D3H) on Schrödinger Maestro<sup>102</sup> and compared it against literature findings.<sup>73</sup>

Our docking studies show slight variations in the interactions. We obtained 5 poses of teriflunomide in the human DHODH binding pocket and scrutinised the pose that gave the best Glide score. We observed the carbonyl forming an interaction with Thr360 via a water molecule rather than a direct hydrogen bond with Arg136 as mentioned in the literature. The hydroxyl group formed a hydrogen bond through the oxygen with Arg136 and with a water which in turn is bound to Thr360 and Gln47. The nitrile was found to make two interactions with Tyr356 (Figure 2.6). The trifluoromethyl containing aromatic group made several hydrophobic interactions with amino acid residues Pro364 and Met111.

A co-crystal structure solved by Liu *et al* showed that the phenyl group bearing the trifluoromethyl phenyl group only partially filled the binding cavity. This justifies the lack of inhibitor-protein interactions and low HDHODH potency exhibited by teriflunomide (Figure 2.7).<sup>109</sup>

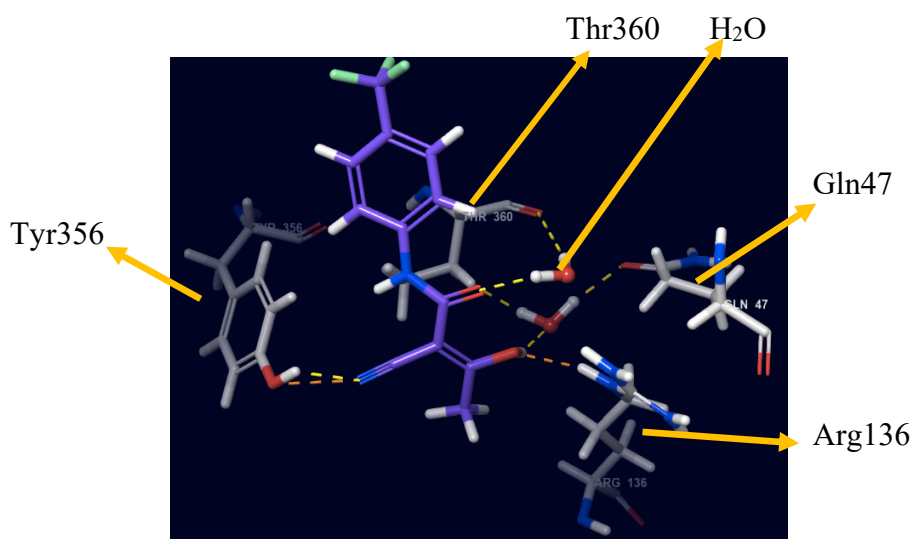


Figure 2.6: Teriflunomide (blue) in HDHODH binding pocket, docked using Schrödinger Maestro. Hydrogen bonding shown by yellow dashed lines. Amino acid residues are shown in grey (C), blue (N), red (O) & white (H)







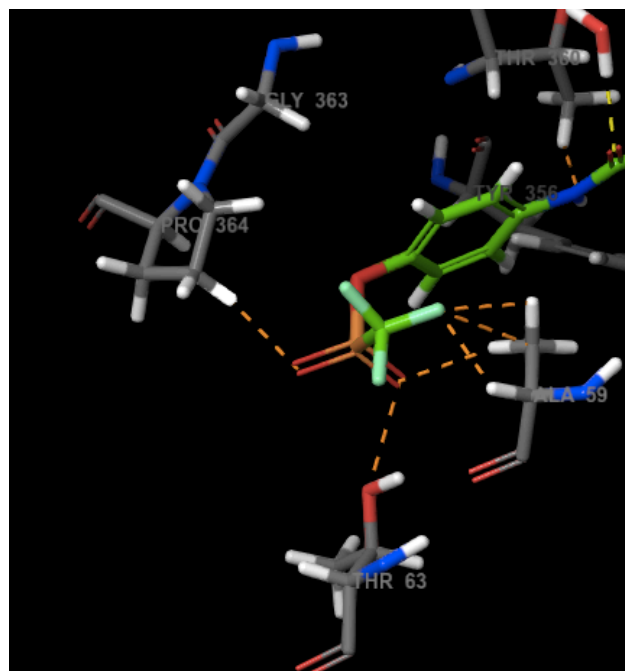


Figure 2.11:  $\text{OSO}_2\text{CF}_3$  group interaction with DHODH. Brown dashes indicate hydrophobic clashes

A comparison of teriflunomide and  $\text{OSO}_2\text{CF}_3$ -teriflunomide (**2.1**) reveals the pronounced bulky nature of the  $\text{OSO}_2\text{CF}_3$  functional group (Figures 2.12)

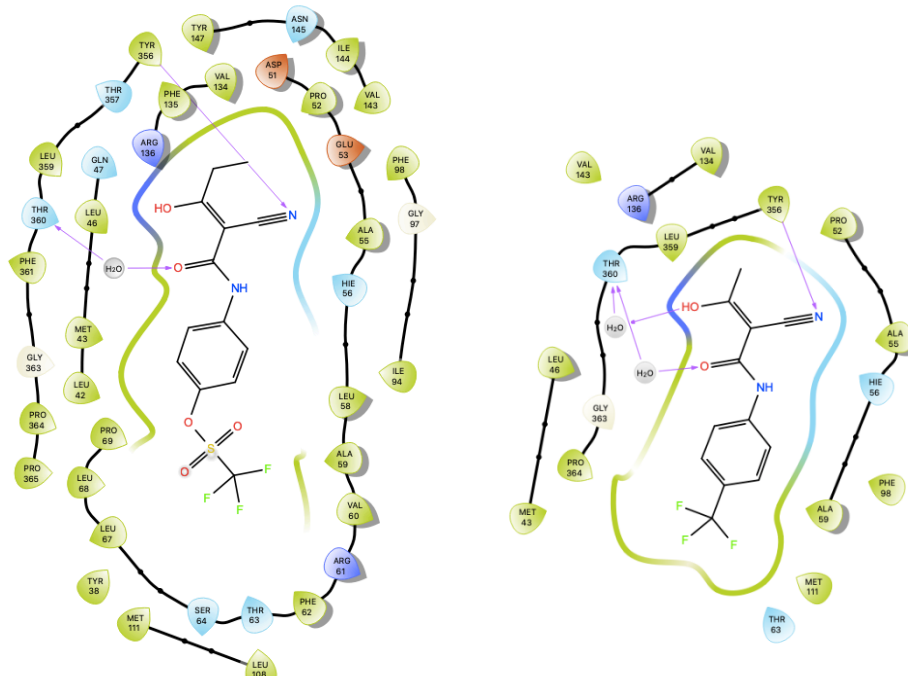


Figure 2.12: Ligand interaction diagram of teriflunomide and  $\text{OSO}_2\text{CF}_3$ -substituted teriflunomide (**2.1**)

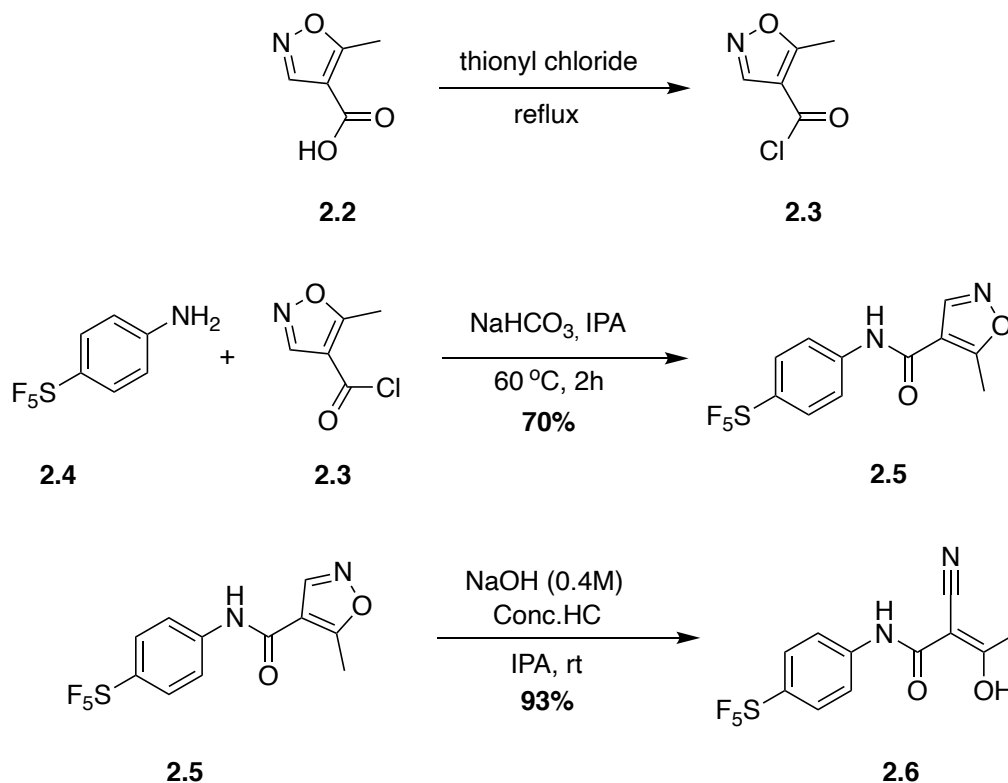
The sulfur pentafluoride group is an ideal substitute for the trifluoromethyl group as it is more lipophilic as proven by their Hansch hydrophobicity constants;  $\pi = 1.51$  for  $\text{SF}_5$  and  $\pi = 1.09$  for  $\text{CF}_3$ .<sup>19</sup> Moreover, the  $\text{SF}_5$  group has superior steric demand than  $\text{CF}_3$  with van der Waals volumes of  $49.2 \text{ cm}^3\text{mol}^{-1}$  and  $20.5 \text{ cm}^3\text{mol}^{-1}$  respectively.<sup>110,111</sup> Therefore, we proposed the synthesis of a

pentafluorosulfanyl-containing teriflunomide analogue to augment its binding affinity. To verify this hypothesis, we tested the compounds head to head through a commercial assay.

To synthesise SF<sub>5</sub>-teriflunomide (**2.6**), we first prepared SF<sub>5</sub>-leflunomide (**2.5**), which when treated with sodium hydroxide, provided its teriflunomide equivalent (Scheme 4.3).

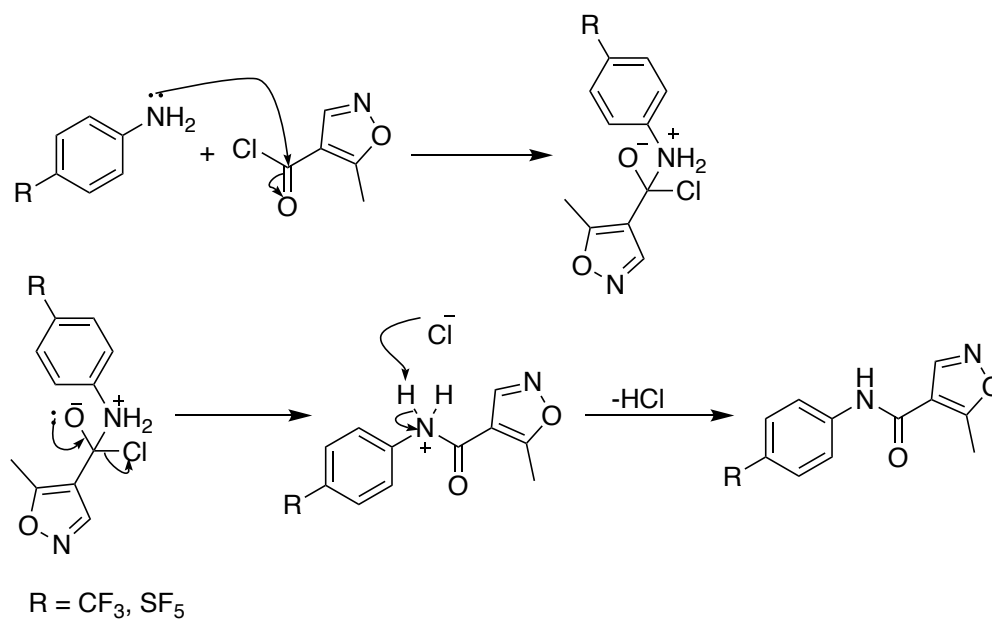
The compounds were synthesised using the same procedure used for preparing teriflunomide.<sup>112</sup> Reacting commercially available **2.4** and **2.3** in isopropyl alcohol (IPA) yielded **2.5**. In the absence of a base, 2 equivalence of amine (**2.4**) will be needed to scavenge the hydrochloric acid generated as a by-product (Scheme 2.4). However, the aniline is too expensive and too weak a base to be used in this manner in a commercial process.

Use of a base is required to drive the equilibrium towards the product. The reaction between an acid chloride and an amine is much faster compared to the hydrolysis of the acyl chloride, as nitrogen is a better nucleophile than oxygen. Therefore, an aqueous alkali can be used as base as part of a Schotten-Baumann procedure.<sup>113,114</sup> Most commonly, sodium hydroxide is the base of choice for this procedure. Other bases that are commonly used include piperidine and triethylamine. However, the isoxazole ring is base sensitive and in the presence of these strong bases, the isoxazole ring would open up to form teriflunomide derivative. To be able to isolate pure SF<sub>5</sub>-leflunomide, we used a weak base; sodium bicarbonate (NaHCO<sub>3</sub>), which was reported as the most preferred acid scavenger for the synthesis of leflunomide. The acid chloride, **2.3**, is an expensive reagent (1g = £165)<sup>115</sup>. However, its acid derivative, 5-methylisoxazole-4-carboxylic acid, is relatively low-priced (1g = £39.20)<sup>116</sup> and the acid can easily be activated using chlorinating agents such as thionyl chloride, oxalyl chloride, benzoyl chloride, POCl<sub>3</sub>, or PCl<sub>3</sub> in excess. Formation of the acid chloride can be monitored by TLC by taking a small amount of the sample and converting it to the methyl ester by addition of methanol. Once the reaction is completed or substantial amounts of acid chloride are formed, excess chlorinating agent and by products should be removed. Thionyl chloride and oxalyl chloride make ideal chlorinating agents, under fume hoods, as the by-products evolved are gases that can be easily removed by evaporation under vacuum at reasonable temperatures. The acyl chloride can then be deployed immediately in the amide coupling step. The mechanism of the amide coupling is shown in Scheme 2.5.

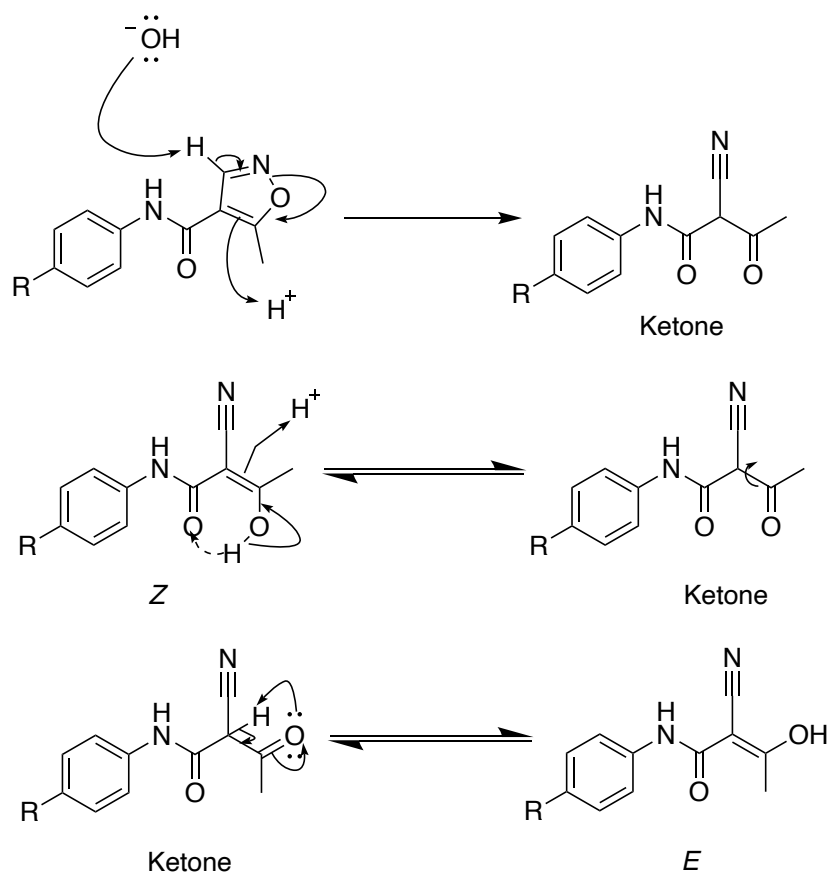


Scheme 2.3: Synthesis of SF<sub>5</sub>-Leflunomide **2.5** and SF<sub>5</sub>-Teriflunomide **2.6**

The acid chloride was added to a suspension of the aniline and NaHCO<sub>3</sub> in IPA and the reaction was stirred at 60 °C. Dissolution of NaHCO<sub>3</sub> is not necessary for the reaction as it can scavenge HCl as a suspended solid. It is preferable to carry out the reaction in a relatively highly concentrated solution for improved yields. The product precipitates out when cooled to ambient temperature. The isolated product **2.5** could be used without further purification for the synthesis of SF<sub>5</sub>-teriflunomide (**2.6**). 3- and 5- unsubstituted isoxazoles are known to be unstable towards alkali and strong bases.<sup>117</sup> Sodium hydroxide is assumed to abstract the C3 proton and the negatively charged species is acidified with HCl to obtain the open ring form. The latter can exist in two geometric forms (*Z* or *E*). The *Z*-isomer is energetically favoured as an internal hydrogen bond is formed between the hydroxyl and the keto group<sup>118</sup> (Scheme 2.6). The presence of this bond also helps the compound to penetrate through cell membranes. The intramolecular hydrogen bond stabilized conformation is potentially less polar while being more lipid soluble due to the hydrogen donor and acceptor not being available to form bonds with water, moreover masked H-bonds tend to be effluxed less.<sup>119</sup> Removal of one hydrogen-bond donor and acceptor atom makes the molecule less recognizable by the P-glycoprotein (P-gp), which is an efflux pump involved in multi-drug transport.<sup>120</sup> P-gp interacts with substrates by forming hydrogen bonds.<sup>121</sup> However, such intramolecular interactions could interfere with the interaction of the compound with its target enzyme-DHODH.<sup>118</sup>



Scheme 2.4: Amide coupling mechanism



Scheme 2.5: Base-mediated ring opening of isoxazoles

Studies by Kujawski *et al.* showed that the presence of the internal hydrogen bond in the *Z* configuration decreases the interaction between teriflunomide and tyrosine or arginine in DHODH. It was stated that even the *E* isomer of teriflunomide provide a stronger teriflunomide-amino acid (tyrosine or arginine) interaction.<sup>118</sup>

Figure 2.13 shows the X-ray structure of *Z*-SF<sub>5</sub>-teriflunomide (**2.6**) that we obtained from soaking it in dichloromethane (DCM) proving the configuration of the product as well as an intramolecular H-bond between the OH and adjacent amide carbonyl group.

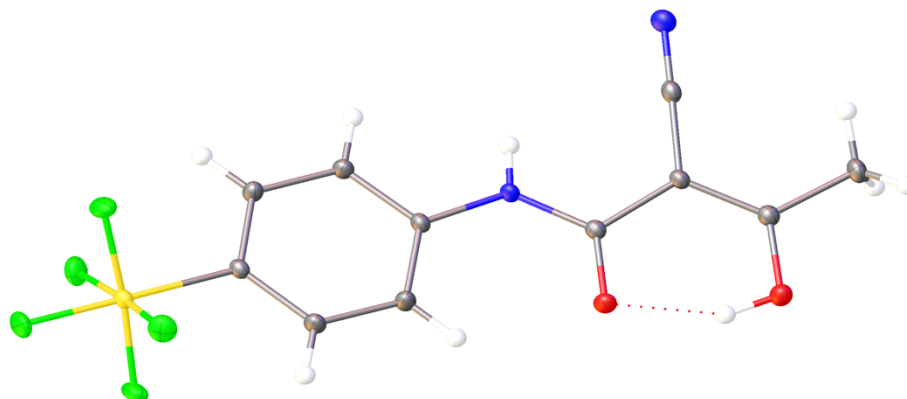


Figure 2.13: X-ray structure of (*Z*)-2.6

Figure 2.14 exhibits SF<sub>5</sub>-teriflunomide (**2.6**) in the DHODH binding pocket, docked using Schrodinger Maestro. Interactions between the ligand and the binding pocket are the same as our prior mentioned findings on teriflunomide in the same binding site. The hydroxyl group forms a direct bond with Arg136 as well as hydrogen bonds with Gln47 and Thr360 via a water molecule. Nitrile bonds with Tyr356. And finally the carbonyl forms a water mediated bond with Thr360. Several hydrophobic interaction are formed between the aromatic ring and amino acid residues lining the hydrophobic pocket.

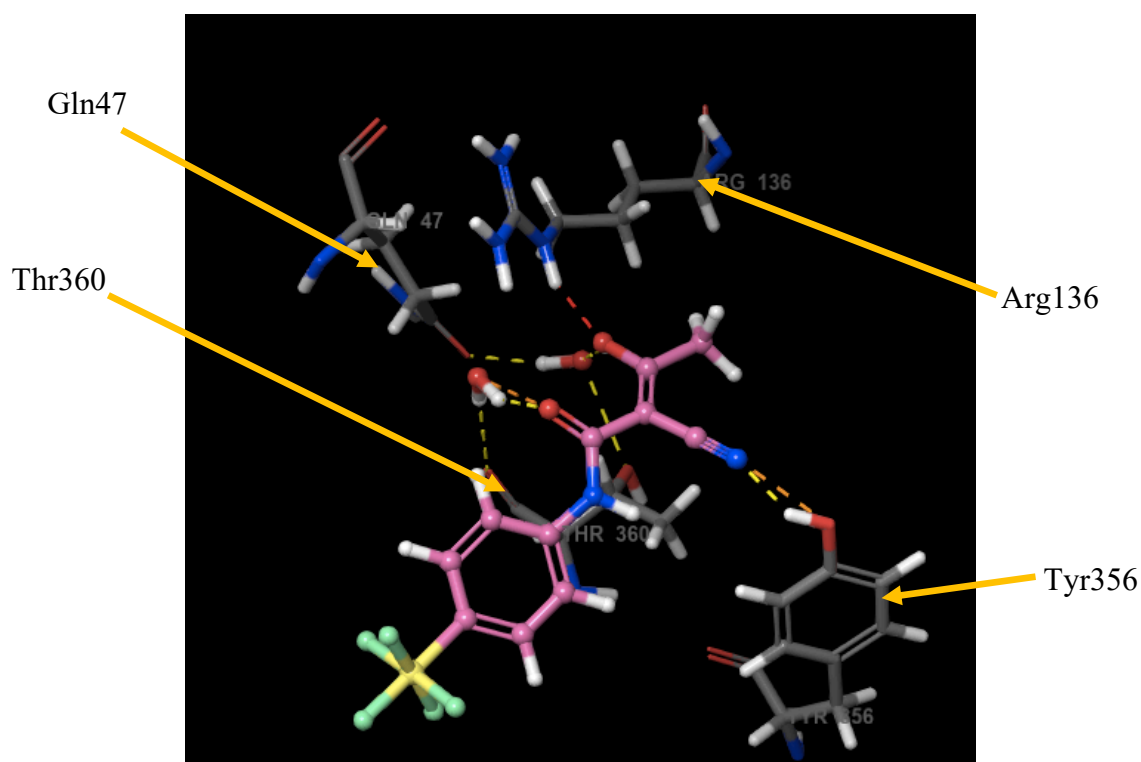


Figure 2.14: SF<sub>5</sub>-substituted teriflunomide (**2.6**) in DHODH binding pocket.

Figures 2.15 and 2.16 demonstrate the bulkiness of SF<sub>5</sub> and that it is able to fill more of the binding pocket in comparison to the less bulky CF<sub>3</sub>.

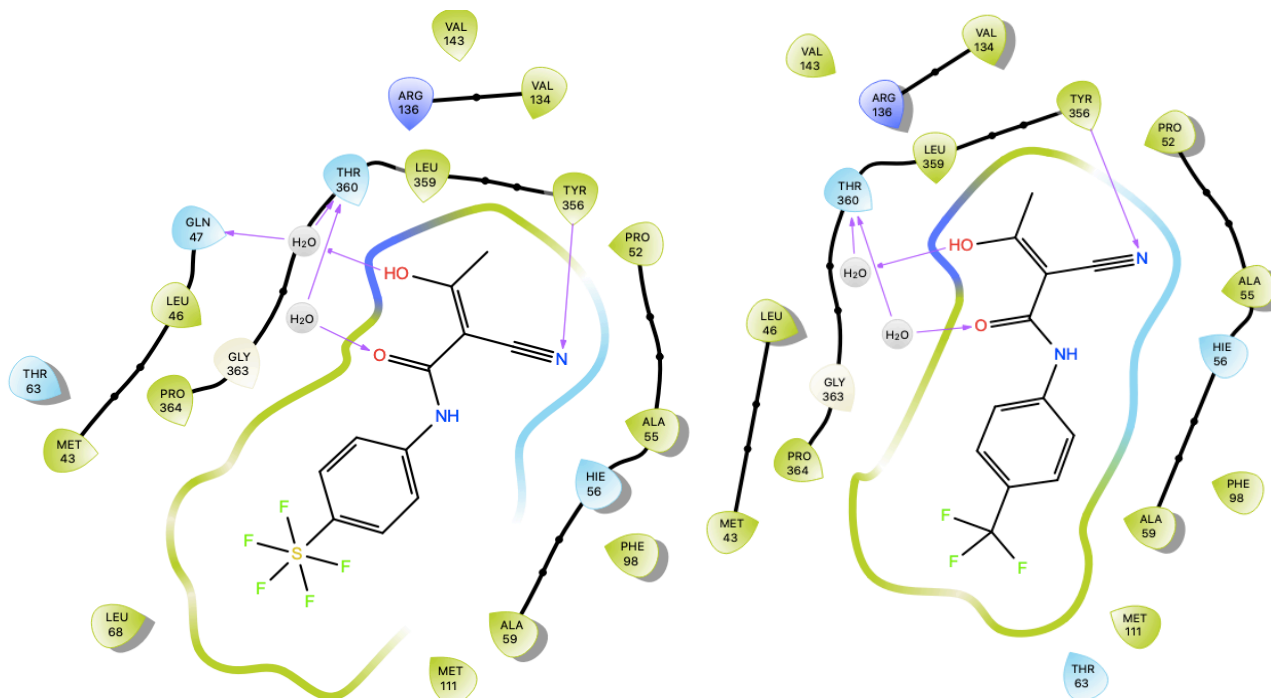


Figure 2.15: Comparing ligand interaction diagrams of SF<sub>5</sub>-teriflunomide (**2.6**) and teriflunomide

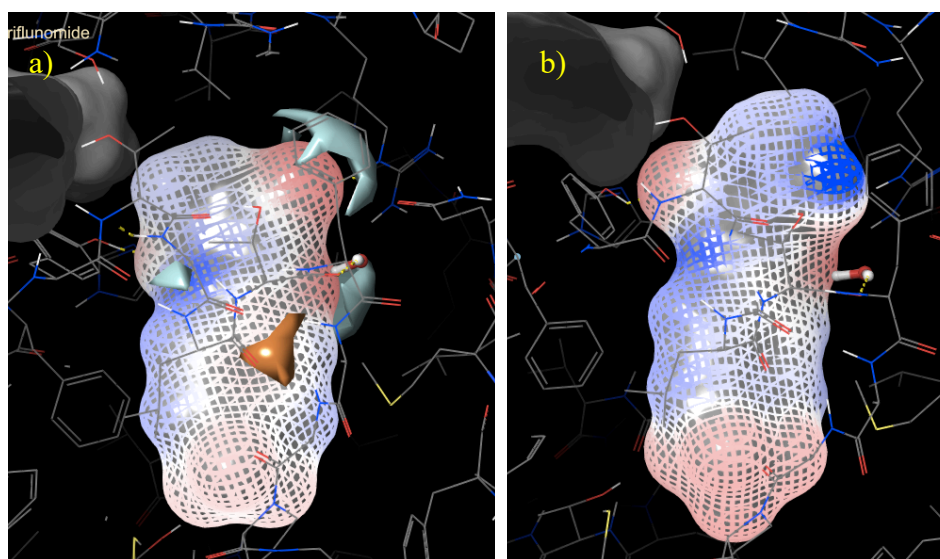


Figure 2.16: a) Electrostatic potential of teriflunomide; b) Electrostatic potential of **2.6**

Similar analysis was performed comparing SF<sub>5</sub>-teriflunomide (**2.6**) and OSO<sub>2</sub>CF<sub>3</sub>-teriflunomide (**2.1**, Figure 2.17). Visibly, the OSO<sub>2</sub>CF<sub>3</sub> moiety is bulkier than a SF<sub>5</sub> group and therefore, occupies more of the binding pocket as well as forming additional hydrogen bonds. While teriflunomide and SF<sub>5</sub>-teriflunomide (**2.6**) embody a polar head and hydrophobic tail; the OSO<sub>2</sub>CF<sub>3</sub> analogue possesses a

tail that is both polar and hydrophobic. However, any hydrophobic interactions made by the compounds are not visible in these molecular docking images.

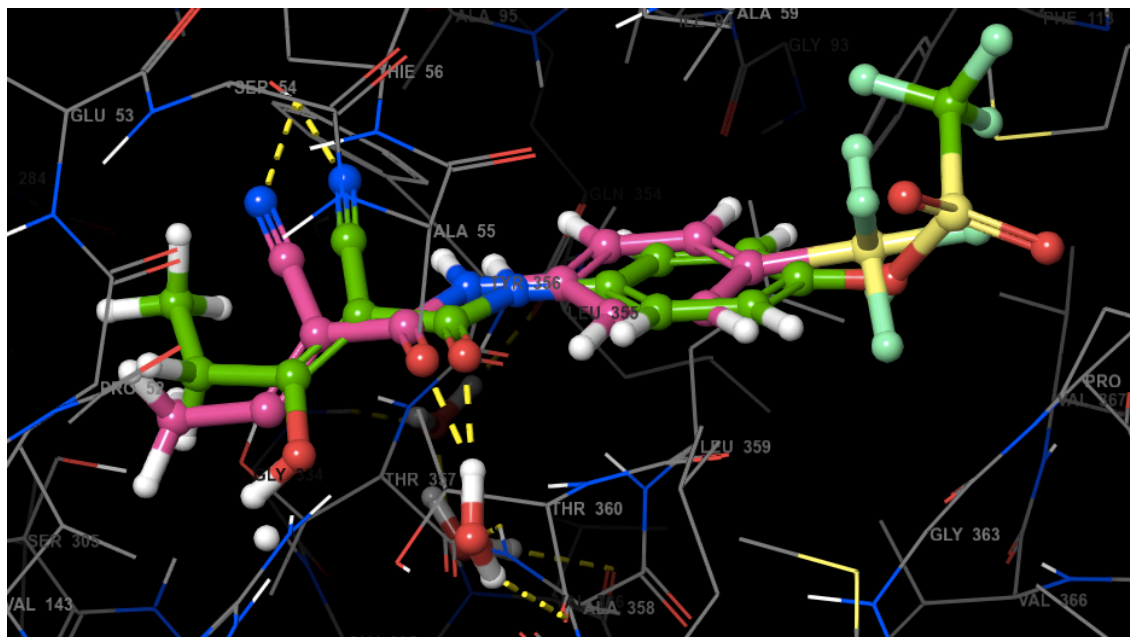
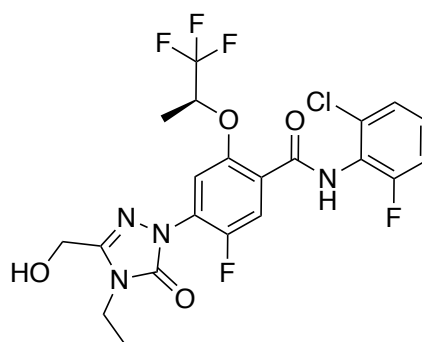


Figure 2.17: Overlapping of  $SF_5$ -teriflunomide (**2.6**) and  $OSO_2CF_3$ -teriflunomide (**2.1**). Green:  $OSO_2CF_3$ -teriflunomide, salmon pink:  $SF_5$ -teriflunomide

Following our docking studies, we tested  $SF_5$ -leflunomide (**2.5**) and  $SF_5$ -teriflunomide (**2.6**) against teriflunomide and BAY-2402234 as standard, internal controls. The biophysical tests were carried out by Reaction Biology Corp®.

Bayer developed a novel, potent, and selective DHODH inhibitor, BAY-2402234 (Figure 2.18), that inhibits HDHODH enzyme with an  $IC_{50}$  of 1.2 nM. It was developed as a potential treatment for acute myeloid leukaemia (AML).<sup>122</sup> BAY-2402234 also binds at the ubiquinone binding site. It is a notable DHODH inhibitor that is in phase I clinical trials. BAY-2402234 was included in our HDHODH inhibition table due to its high affinity and the presence of a trifluoromethyl group.



BAY-2402234

Figure 2.18: BAY-2402234

Table 2.1 shows a comparison of  $IC_{50}$  and  $pIC_{50}$  of  $SF_5$ -leflunomide (**2.5**),  $SF_5$ -teriflunomide (**2.6**), and leflunomide against teriflunomide and BAY-2402234. As anticipated,  $SF_5$ -leflunomide is more





BAY-2402234 gave the best potency with an  $IC_{50}$  of 1.8 nM in our outsourced assay, which is comparable to its literature value, 1.2 nM. As well as the hydrophilic interactions, BAY-2402234 makes hydrophobic interactions with a large set of non-polar residues such as Leu42, Met43, Leu46, etc. With its bigger size, and the combination of hydrophobic and hydrophilic groups, BAY-2402234, is able to fill the DHODH active site to a greater degree. Figures 2.19 and 2.20 display the several hydrogen bonds and interactions formed by BAY-2402234 in the HDHODH binding pocket.

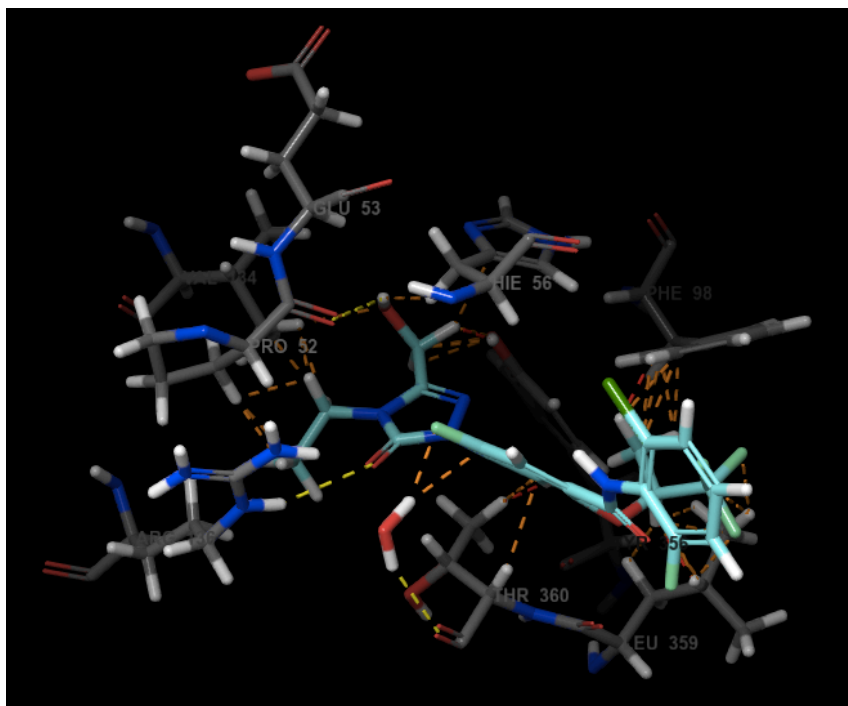


Figure 2.19: HDHODH in complex with BAY-2402234. Dashed lines indicate hydrogen bonds and aromatic hydrogen bonds.

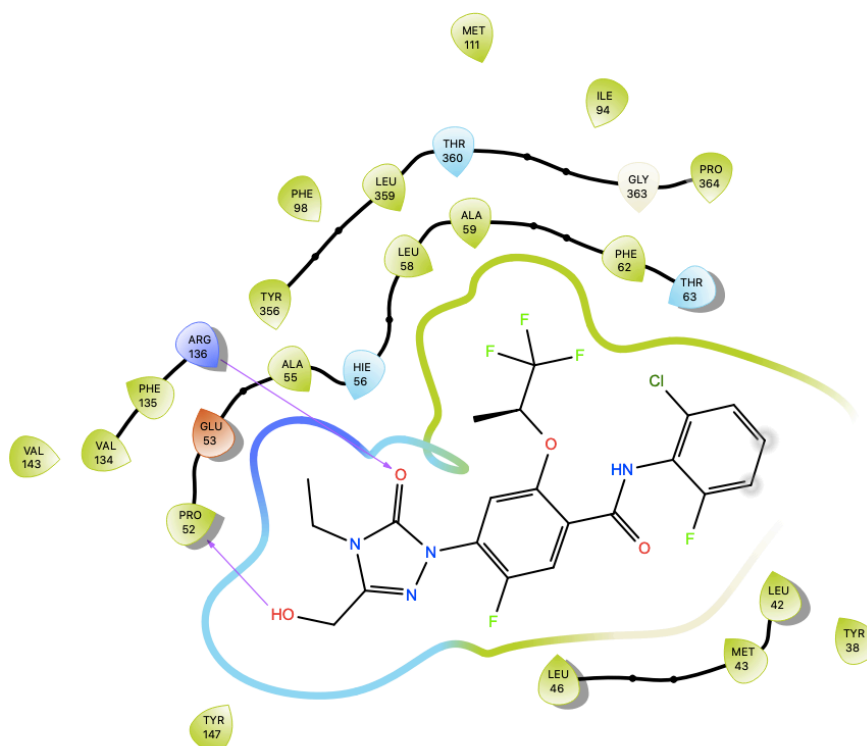


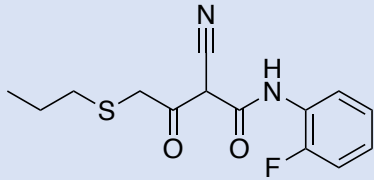
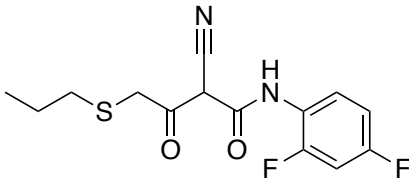
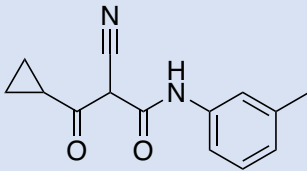
Figure 2.20: Ligand interaction diagram of BAY-2402234

The Bayer compound, BAY-2402234, proved to have the most affinity towards HDHODH. We anticipate an increase in affinity of the Bayer compound if the CF<sub>3</sub> group is substituted with the SF<sub>5</sub>.

### 2.2.2 Identifying a SARS-CoV-2 M<sup>pro</sup> inhibitor

The **N3** inhibitor that irreversibly inhibits CoVM<sup>pro</sup>s contains an  $\alpha$ ,  $\beta$  unsaturated ester which enables it to form a covalent bond with the Cys145 residue (Figure 2.4). It also makes multiple hydrogen bonds with amino acid residues in the substrate binding pocket. In addition the amino acid chains (Ala, Val and Leu) part of the ligand provide **N3** flexibility, which is a favourable aspect for protein-ligand interaction.

Through a combination of high throughput screening and structure-based virtual screening, over 10,000 compounds including drugs, drug candidates and other pharmacologically active compounds were assayed as inhibitors of M<sup>pro</sup>. Teriflunomide and its SF<sub>5</sub> analogue consist of a covalent warhead capable of performing a Michael addition with the S $\gamma$  atom of Cys145. In addition to these two compounds, 14 other potential candidates donated by eMolecules<sup>®</sup> were provided for assays. Out of the 16 tested, a singleton hit (compound **2.7**, Figure 2.21, Entry 16, Table 2.2) was identified which, gave a promising IC<sub>50</sub> of 0.23  $\mu$ M. The other compounds did not show a satisfactory inhibition of SARS CoV-2. Due to its singleton nature, we had limited confidence in its suitability as a M<sup>pro</sup> inhibitor.

Entry	Compound	IC <sub>50</sub> vs M <sup>pro</sup> ( $\mu$ M)
1		>99
2		>99
3		>99

4		>99
5		>99
6		>99
7		>99
8		>99
9		>99
10		>99
11		>99
12		>99
13		>99

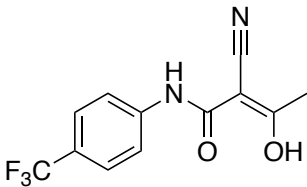
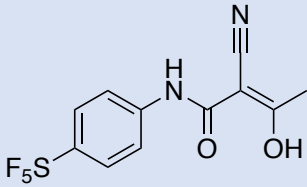
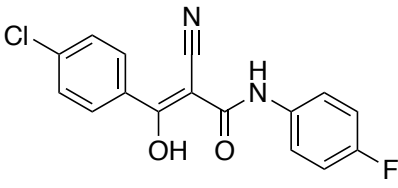
14	 <p style="text-align: center;"><b>Teriflunomide</b></p>	>99
15	 <p style="text-align: center;"><b>2.6</b></p>	>99
16	 <p style="text-align: center;"><b>2.7</b></p>	0.23

Table 2.2: Compounds donated to the Covid Moonshot initiative

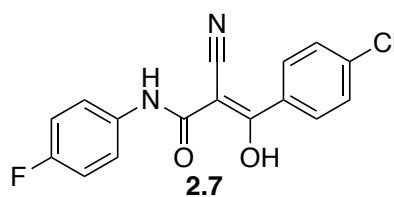


Figure 2.21: Compound 2.7 with  $IC_{50} = 0.23 \mu M$  against  $M^{pro}$  (fluorescence assay)

Figure 2.22 shows SARS-CoV-2  $M^{pro}$  in complex with our singleton hit.

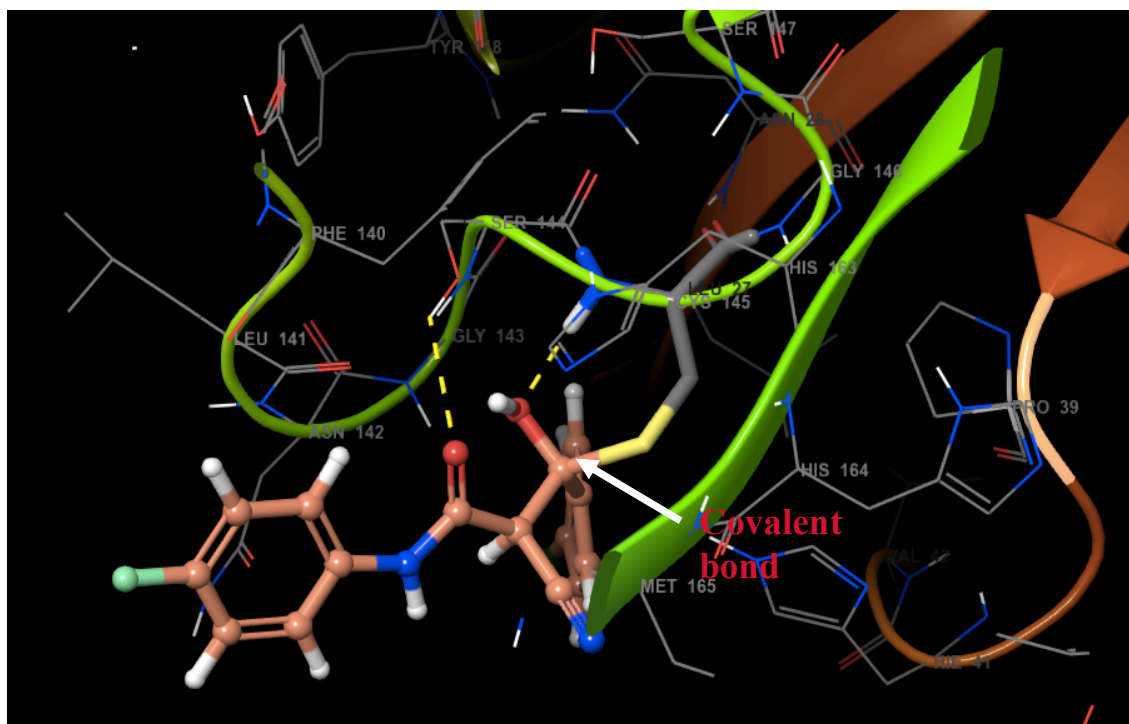


Figure 2.22: SARS-CoV-2 M<sup>pro</sup> in complex with 4.6

Docking image reveals ligand **2.7**, (shown in orange) could covalently bind to the S $\gamma$  atom of Cys145 residue (S $\gamma$  in yellow), following a Michael addition. Besides the covalent bond, two hydrogen bonds (yellow dashes) are formed between the O-H and Cys145, as well as the carbonyl and Ser144. In addition, hydrogen bonds to aromatic hydrogens (aromatic hydrogen bonds) and several hydrophobic interactions are observed.

Once compound **2.7** was identified to have little activity against SARS-CoV-2 M<sup>pro</sup>, it was tested for HDHODH affinity via a fluorescence assay run by Reaction Biology Corp®. Although it has structural similarities to teriflunomide, it was found to be inactive. Upon inspection using the docking software, we found that **2.7** occupies the binding pocket differently to teriflunomide. Figure 2.23 shows both teriflunomide and **2.7** in the HDHODH binding pocket. Evidently, the hydrogen bond donors and acceptors on **2.7** lie in the hydrophobic tunnel of HDHODH. Thus, **2.7** is unable to interact with the binding pocket, making it inactive against HDHODH.

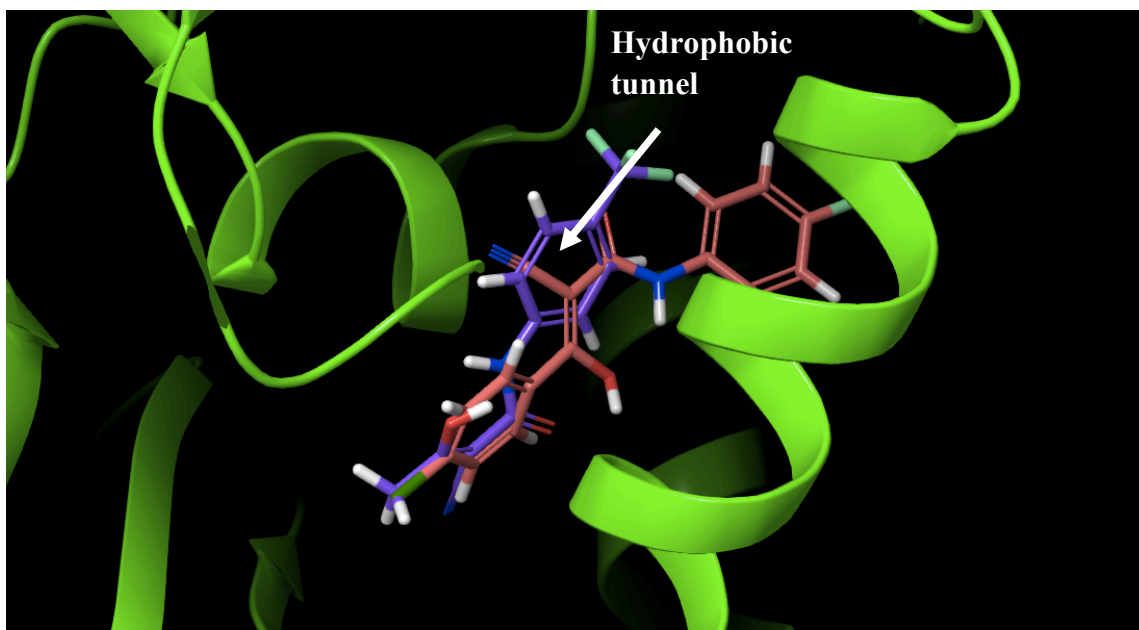


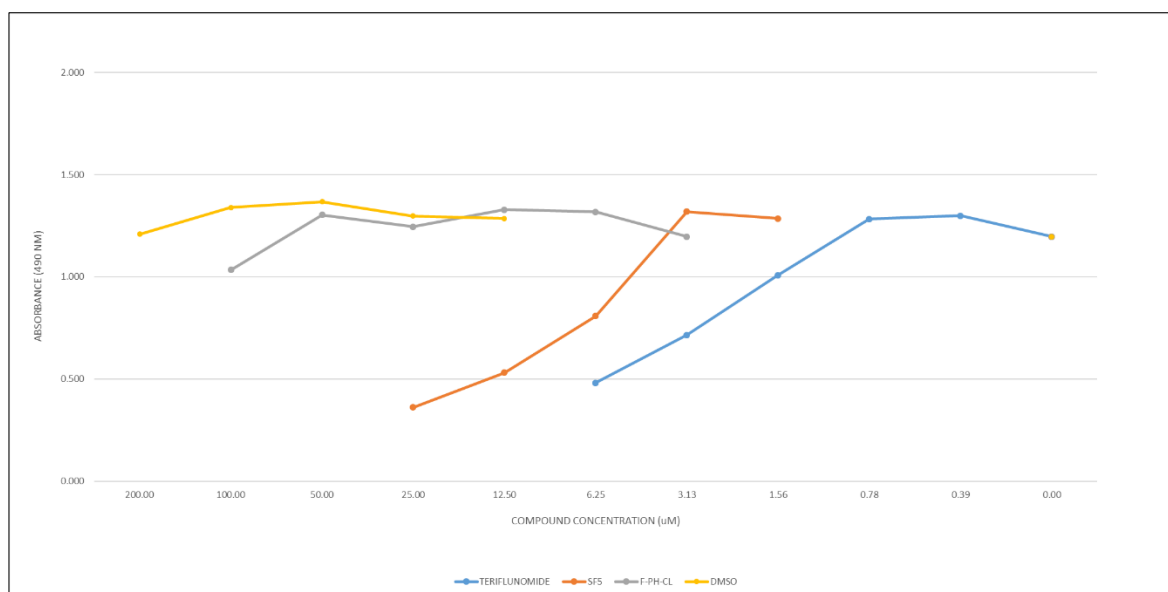
Figure 2.23: HDHODH in complex with teriflunomide (purple) and 4.6 (orange)

As HDHODH is a druggable target against SARS-CoV-2, we were interested in knowing the inhibitory effect of teriflunomide, SF<sub>5</sub>-teriflunomide (**2.6**) and **2.7** against SARS-CoV-2.

The outer surface of coronaviruses contain a spike (S) protein which facilitates its entry into host cells. The S1 subunit of S protein attaches to ACE2 receptor which is found on the surface of target cells. In addition to this, transmembrane protease, serine 2 (TMPRSS2) processes S protein into its constituent subunits, S1 and S2 thus allowing the virus to fuse into the plasma membrane of the host cell.

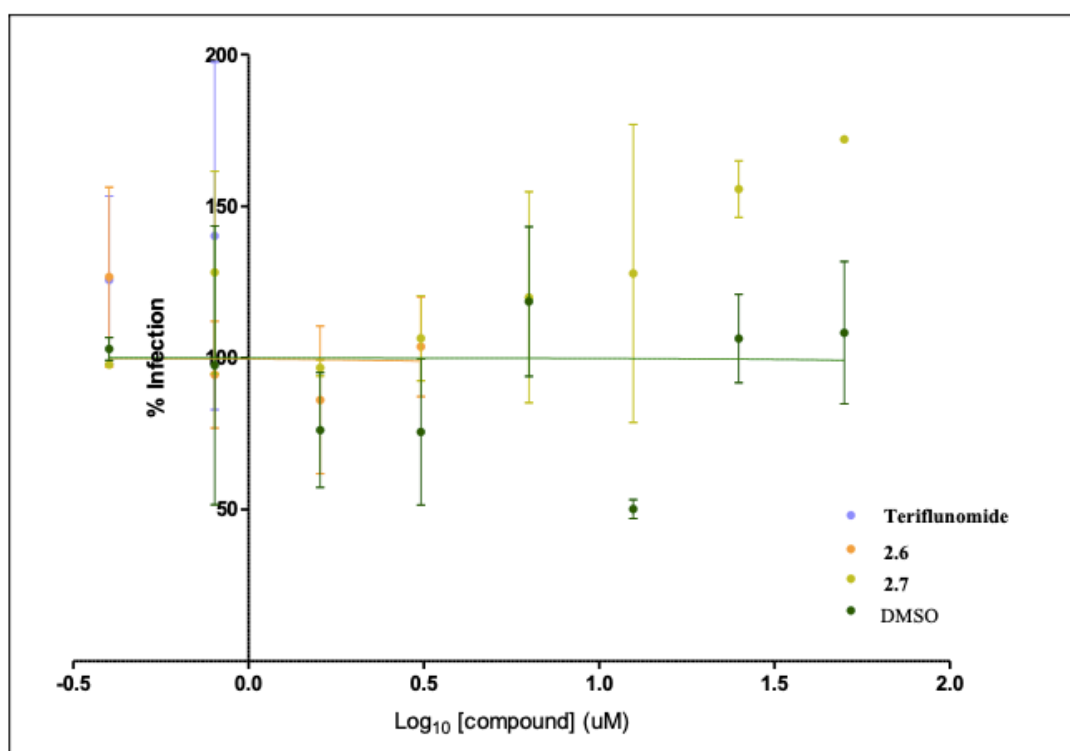
Cell-based assays were run by Dr M. Derveni from Dr Edward Wright's group at the University of Sussex.

Cytostatic drugs inhibit cell growth and multiplication. Teriflunomide was the most cytostatic with effects at concentrations above 0.78  $\mu$ M and **2.7** the least cytostatic. SF<sub>5</sub>-teriflunomide (**2.6**) had cytostatic effects at concentrations  $>3.1$   $\mu$ M and DMSO had no measurable effect. Graph 2.1 shows the cytostatic effect of teriflunomide and its analogues. Greater the cytostatic effect, lower the absorbance.



Graph 2.1: Effect of the teriflunomide compounds on HEK293T/17 viability using a colourimetric (MTS) assay. F-Ph-Cl denotes compound 2.7.

The infection inhibition assay showed that none of the three compounds had an inhibitory effect against SARS-CoV-2 infection in the infected cells. Graph 2.2 shows % infection against a range of concentrations ( $\log_{10}[\text{compound}]$ ) that was found to be non-toxic in the toxicity assay. The normalised data show that teriflunomide and SF<sub>5</sub>-teriflunomide (**2.6**) have no effect on the efficiency of infection while compound **2.7** appears to be acting as an agonist with increased concentration.



Graph 2.2: Effect of teriflunomide and its analogues on SARS-CoV-2 infection of HEK293T/17 cells. F-Ph-Cl denotes compound 2.7

Work by R. Xiong *et al.* however shows that teriflunomide has potential to be a covid antiviral following an in vivo test. Furthermore, they all showed low toxicity to SARS-CoV-2 susceptible Vero E6 cells.<sup>92</sup>

## 2.3 Conclusion

SF<sub>5</sub> substituted leflunomide (**2.5**) and teriflunomide (**2.6**) have been synthesised and tested for affinity towards the HDHODH binding pocket. Biophysical assays conveyed an approximately two-fold greater affinity for SF<sub>5</sub>-teriflunomide (**2.6**) towards HDHODH compared with teriflunomide. Molecular binding studies also revealed that the bulky SF<sub>5</sub> group fills the binding pocket better than the CF<sub>3</sub> group. In comparison, OSO<sub>2</sub>CF<sub>3</sub>-teriflunomide (**2.1**, lit IC<sub>50</sub> = 150 nM) fills the binding pocket better than both **2.6** and teriflunomide from our molecular docking studies.

A singleton hit (**2.7**) with structural similarities to teriflunomide was identified to have affinity towards SARS-CoV-2 M<sup>pro</sup> active site in the low micromolar range. Testing it against HDHODH, however, revealed no affinity.

Teriflunomide, **2.6** and **2.7** did not give satisfactory inhibition of SARS-CoV-2 infection, besides they were found to be cytostatic in HEK293T/17 cells.

## 2.4 Experimental

### 2.4.1 Chemistry

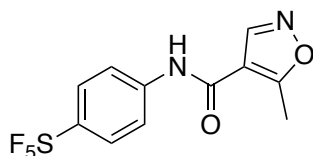
4-(Pentafluorosulfanyl)aniline was obtained from Fluorochem and 5-Methyl-4-isoxazolecarbonyl chloride was bought from Apollo Scientific.

Magnesium sulfate and sodium bicarbonate were obtained from Fisher Scientific. Preparative TLC was obtained from Analtech. Solvents and reagents were purchased from commercial suppliers and were used without purification. All reactions were performed in a fume hood.

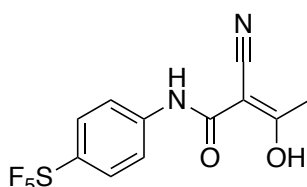
NMR spectra were recorded on Varian 500 MHz or 400 MHz spectrometers and chemical shifts are reported in ppm, usually referenced to TMS as an internal standard. LCMS were performed by Shimadzu LCMS-2020 equipped with a Gemini® 5µm C18 110Å column and percentage purities were ran over 30 minutes in water/acetonitrile with 0.1% formic acid (5 min at 5%, 5%-95% over 20 min, 5 min at 95%) with the UV detector at 254 nm. Mass spectrometry: ESI mass spectra were obtained using a Bruker Daltonics Apex III, using Apollo ESI as the ESI source. For EI mass spectra, a Fissions VG Autospec instrument was used at 70 eV. All analyses were run by Dr. Iain Goodall at the University of Greenwich. Analyses are for the molecular ion peak [M]<sup>+</sup> and are given in m/z, mass to charge ratio. Melting points were determined using a Stanford Research Systems Optimelt and are uncorrected.

The reactions for synthesis and purity of product were monitored by thin layer chromatography using TLC plates.



**5-Methyl-N-[4-(pentafluoro- $\lambda^6$ -sulfanyl)phenyl]-1,2-oxazole-4-carboxamide (2.5)**


4-(Pentafluorosulfanyl)aniline (500 mg, 2.28 mmol, 1.0 equiv.) was dissolved in isopropanol (IPA) (4 mL) followed by the addition of NaHCO<sub>3</sub> (201 mg, 2.39 mmol, 1.05 equiv.). The mixture was heated to 60 °C and 5-methyl-4-isoxazolecarbonyl chloride (0.2 mL, 2.28 mmol, 1.0 equiv.) was added dropwise. The reaction was followed by TLC and after 2 hours of stirring, the reaction was allowed to cool to ambient temperature. The white precipitate formed was filtered under vacuum and washed with water and toluene. The product was dried. A colourless powder was isolated as pure product (530 mg, 71%). <sup>1</sup>H NMR (600 MHz, CDCl<sub>3</sub>) δ 8.47 (s, 1H, NH), 7.77 – 7.72 (m, 2H, ArH), 7.67 (d, *J* = 8.8 Hz, 2H, ArH), 7.55 (s, 1H, ArH), 2.77 (s, 3H, CH<sub>3</sub>); <sup>13</sup>C NMR (151 MHz, CDCl<sub>3</sub>) δ 174.3 (C=O), 159.2 (C=N), 149.7 (C-SF<sub>5</sub>), 147.3 (ArC), 139.8 (ArC), 127.2 (2C, m, ArC), 119.5 (2C, ArC), 111.6 (ArC), 12.7 (CH<sub>3</sub>); <sup>19</sup>F NMR (400 MHz, CDCl<sub>3</sub>) δ 84.62 (p, *J* = 150 Hz), 63.34 (d, *J* = 150 Hz). LCMS Purity (UV) = 97%, *t*<sub>R</sub> 20.1 min; HRMS – ESI (*m/z*) found 329.0385, calc. for [C<sub>11</sub>H<sub>9</sub>F<sub>5</sub>N<sub>2</sub>O<sub>2</sub>S][H]<sup>+</sup>:329.0383; IR (neat)  $\nu_{\max}$ /cm<sup>-1</sup>: 3366 (N-H), 1663 (C=O), 824 (S-F); mp = 167 – 168 °C.

**(2Z)-2-Cyano-3-hydroxy-N-[4-(pentafluoro- $\lambda^6$ -sulfanyl)phenyl]but-2-enamide (2.6)**


Compound **2.5** (304 mg, 0.93 mmol, 1.0 equiv.) was suspended in a mixture of IPA (2 mL) and water (2 mL). To the stirred mixture was added dropwise an aqueous solution of NaOH (39% in water) until the solution reached a pH of circa 12. At this point, all of the starting material dissolved in the solvent. The solution was filtered and concentrated. Concentrated HCl was added to the filtrate until pH 3. Precipitate appeared that was filtered, washed with water and dried under vacuum to obtain pure product as colourless powder (283 mg, 93%). <sup>1</sup>H NMR (600 MHz, CDCl<sub>3</sub>) δ 7.79 – 7.74 (m, 2H, ArH), 7.62 (d, *J* = 8.8 Hz, 2H, ArH), 2.38 (s, 3H, CH<sub>3</sub>); N-H and O-H not found; <sup>13</sup>C NMR (151 MHz CDCl<sub>3</sub>) δ 189.2 (C=O), 167.5 (CN), 150.2 (C-SF<sub>5</sub>), 138.6 (ArC), 127.3 (2C, ArC, m), 120.2 (2C, ArC), 116.1(C), 80.6 (C), 22.1 (CH<sub>3</sub>); <sup>19</sup>F NMR (400 MHz, CDCl<sub>3</sub>) δ 84.82 (p, *J* = 150.4 Hz), 63.34 (d, *J* = 150.4 Hz). HPLC Purity (UV) = 99%, *t*<sub>R</sub> 17.9 min; HRMS – ESI (*m/z*) found 328.0247, calc. for [C<sub>11</sub>H<sub>9</sub>F<sub>5</sub>N<sub>2</sub>O<sub>2</sub>S][H]<sup>+</sup>:327.0227; IR (neat)  $\nu_{\max}$ /cm<sup>-1</sup>: 3312 (N-H), 2219 (CN), 1641 (C=O), 1589 (C=C), 825 (S-F); mp = 167 – 170 °C.

#### **2.4.2 Toxicity assay and SARS-CoV-2 infection inhibition assay**

HEK293T/17 cells were transiently transfected with human ACE2 and TMPRSS2. The three compounds were added to the HEK293T/17 cells in concentrations ranging from 200 to 0.4  $\mu\text{M}$  followed by addition of SARS-CoV-2. Control wells included virus and target cell without ligands/DMSO and target-cell only wells. Furthermore, a toxicity assay (MTS assay) was carried out to assess cell viability. HEK293T/17 at a concentration of  $4 \times 10^5$  cells/mL was added to each well containing teriflunomide and its analogues (200 to 0.4  $\mu\text{M}$  concentration range) as well as to a control well with only DMSO. A cell only control well was also set up. After incubating the wells for 48 hours in a 37 °C/5% CO<sub>2</sub> incubator they were examined microscopically. 20 mL of MTS reagent was then added to the wells and incubated for 4 hours.

Microscopic examination of the cells showed healthy cells at concentrations between 50 – 0.4  $\mu\text{M}$ . Cells in DMSO-only wells showed no visible difference to the cell-only control wells. Addition of MTS reagent revealed cytostatic effect of teriflunomide.

## Chapter 3.0 A Library of SF<sub>5</sub> Containing Small molecules

### 3.1 Introduction

Small organic molecules are indispensable as they can be used as powerful tool compounds (chemical probes) to explore biological systems and as therapeutics.<sup>124</sup> Owing to the relative dearth and high cost of commercially available pentafluorosulfanyl containing compounds, we synthesised several SF<sub>5</sub>-comprising small molecules via a simple amide bond construction. The majority of the amides in this library were synthesised to increase SF<sub>5</sub>-containing building block space, which can be useful scaffolds for others to expand upon according to their interests. During the process, a couple of compounds were synthesised to be analysed as potential Covid-19 antivirals as part of an international collaboration.

Jonathan Clayden states in his paper that amide is king in medicinal chemistry.<sup>125</sup> Their notable stability as well as exceptional polarity make them prevalent in medicinal chemistry. The high polarity allows amide-containing drugs to interact with biological receptors and enzymes.<sup>125</sup> Moreover, amide bonds link amino acids to form proteins, therefore, are pivotal for peptide synthesis.<sup>126</sup> An amide typically consists of a hydrogen bond donor (N-H) and an acceptor (C=O) site and possesses a unique ability to form relevant hydrogen bonding interactions.<sup>127</sup> This characteristic is of particular interest when developing drug-like compounds as it can contribute to improved binding affinity. Nevertheless, amide activity can be compromised *in vivo* by enzymatic cleavage resulting in toxic metabolites.<sup>128</sup> Amides are also present in industrial materials such as detergents, polymers and lubricants. These are adequate reasons as to why amide bond formation is one of the most common reactions carried out by medicinal and synthetic chemists.<sup>129</sup>

We coupled commercially available 3- and 4-pentafluorosulfanylbenzoyl chlorides with a range of amines to build our library.

Morpholine and piperazine are privileged backbones, due to their versatile binding properties. They are often used as substituents in drugs and medicinal chemistry. They have the potential to improve pharmacokinetic properties such as water solubility and metabolic stability of molecules although, they are not always crucial for direct receptor binding.<sup>130</sup> Several drug molecules contain piperazine and morpholine *viz.* moclobemide (antidepressant), gefitinib (anticancer agent), cyclizine (anti-sickness drug), and amoxapine (antidepressant) (Figure 3.1). Piperazine and morpholine are frequently used as handles to modulate lipophilicity while achieving desired pharmaceutical properties, especially solubility.

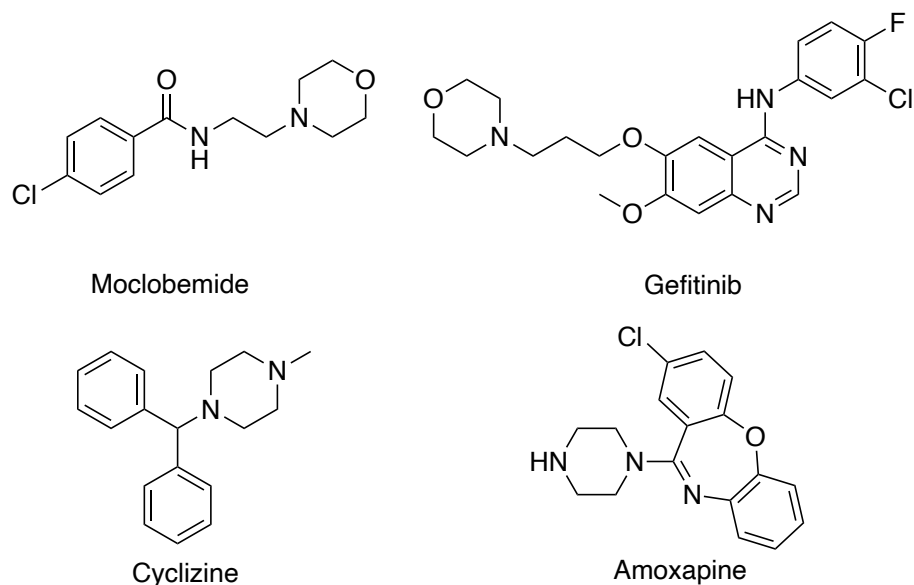


Figure 3.1: Piperazine and morpholine containing drugs

The highly functionalised piperidine core is found in several natural products. It possesses a range of biological activities like antibacterial, antimalarial, anti-inflammatory properties, giving it tremendous importance in medicinal chemistry. It is considered a privileged structure due to its affinity for multiple targets<sup>131</sup>. Moreover piperidine is one of the most used heterocycles in pharmaceutical agents, typically as a linker or to improve a drug's pharmacokinetic profile, in particular, transportation.<sup>132</sup> Industrially pyridine is used to synthesise piperidine. Like piperidine, pyridine possesses several properties that make it attractive to a medicinal chemist. Similar to piperazine and morpholine, piperidine possesses properties like basicity, water solubility, hydrogen bond forming ability and its small molecular size makes pyridine an interesting substituent in drug discovery.

A novel small molecule library generated by combining the aforementioned privileged scaffolds with the sought after SF<sub>5</sub> moiety via an amide link can serve useful as part of high-throughput screening. A couple of compounds from the amide linked library have been screened against SARS-CoV-2 main protease (M<sup>pro</sup>, also known as 3CL<sup>pro</sup>) as potential inhibitors as part of the COVID Moonshot project, which was mentioned in Chapter 2.0. The Moonshot project obtained several compounds through crowdsourcing, which were screened using high throughput crystallography and computational chemistry to identify covalent and non-covalent M<sup>pro</sup> inhibitors. As discussed in Chapter 2.0, M<sup>pro</sup> is an essential protease in the life cycle of SARS-CoV-2 that has been recognized as a druggable target. Chapter 2 discussed inhibitors designed based on a covalent warhead design

strategy. Such inhibitors were anticipated to irreversibly modify the cysteine catalytic residue, Cys145, resulting in the inhibition of M<sup>pro</sup> protease.

This chapter will discuss non-covalent inhibitors of M<sup>pro</sup>. Covalently bound inhibitors that may give longer half-life of action but may lead to off-target toxicity and side effects. Research into developing non-covalent inhibitors is therefore essential.

Based on the structure of M<sup>pro</sup>, machine learning approaches and insights from past literature on SARS and MERS, drug designers across the world have contributed over 10,000 individual molecule designs to the COVID Moonshot initiative. Remdesivir is an antiviral that was initially produced to combat hepatitis C and a cold like virus called respiratory syncytial virus albeit being ineffective for both the diseases. Remdesivir however, showed potency against viruses in the coronavirus family in a cell and animals-based study. In SARS-CoV and MERS-CoV it works by interrupting the production of the virus by interfering with one of the key enzymes, RNA-dependent RNA polymerase (RdRp), which the virus needs to replicate RNA.<sup>133,134</sup> Early studies showed that Remdesivir accelerated recovery of COVID-19 patients and it was the first drug to be authorised to treat hospitalised patients. Following its success, Nguyen *et al.* investigated Remdesivir's exact target of action.<sup>135</sup> *In vitro* analysis showed that the EC<sub>50</sub> value of remdesivir for SARS-CoV-2 is 0.77  $\mu$ M.<sup>135</sup> By combining a few techniques such as molecular docking, umbrella sampling, and steered molecular dynamics they tested Remdesivir's affinity towards RdRp and M<sup>pro</sup>. Their combined studies revealed that Remdesivir has affinity towards both the targets mentioned with slightly weaker affinity towards M<sup>pro</sup>. For example, the work spent on pulling remdesivir from the M<sup>pro</sup> binding site was calculated to be significantly lower than the amount of work spent on retrieving remdesivir from RdRp. The calculated values are  $106.2 \pm 11.6$  kcal/mol for M<sup>pro</sup> and  $144.6 \pm 19.2$  kcal/mol for RdRp.

While electrostatic interactions stabilize the RdRp-Remdesivir complex, van der Waals interactions dominate in the M<sup>pro</sup>-Remdesivir complex. Figure 3.2 shows a few non-covalent warheads identified in M<sup>pro</sup> as part of Covid Moonshot program. **TRY-UNI-714a760b-6** was initially identified and by fragment merge, the other two compounds (**ADA-UCB-6c2cb422-1** & **MAT-POS-b3e365b9-1**) were synthesised. In an antiviral assay, **ADA-UCB-6c2cb422-1** showed antiviral activity (IC<sub>50</sub> = 3.1  $\mu$ M) similar to Remdesivir (IC<sub>50</sub> = 1.7  $\mu$ M, Figure 3.3). To add to this series, we synthesised a small number of compounds by modifying **TRY-UNI-714a760b-6** which were analysed in the M<sup>pro</sup> binding site using Schrodinger Maestro. The synthesised compounds have also been contributed to COVID Moonshot for further analysis such as M<sup>pro</sup> inhibition assay.

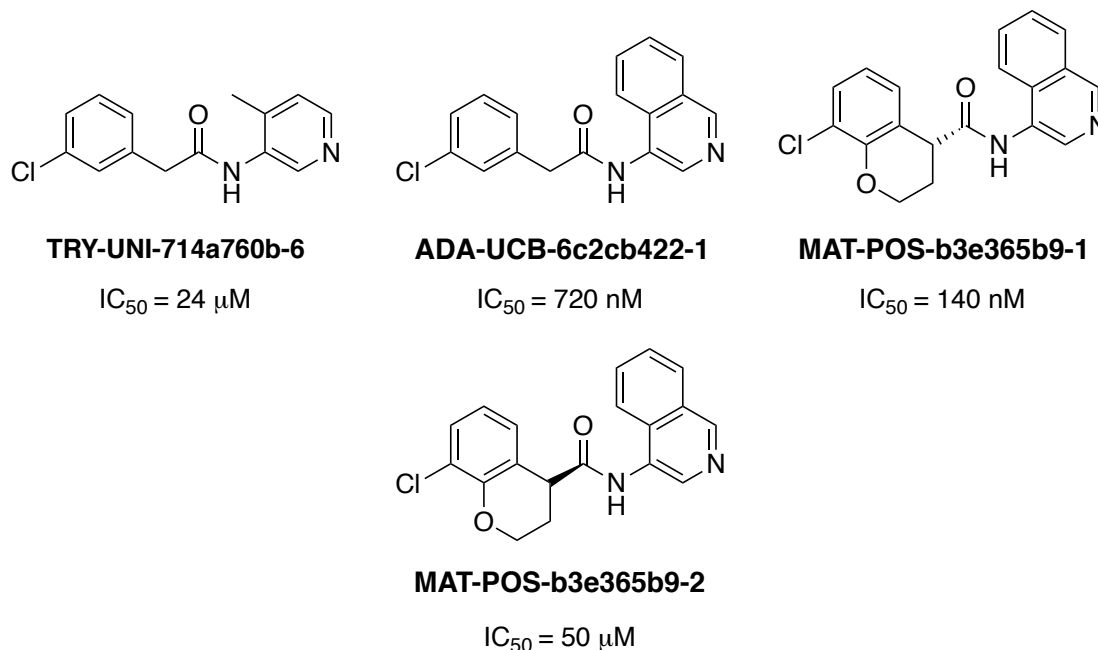


Figure 3.2: Non-covalent warheads showing promising IC<sub>50</sub> following fluorescence M<sup>pro</sup> inhibition assay

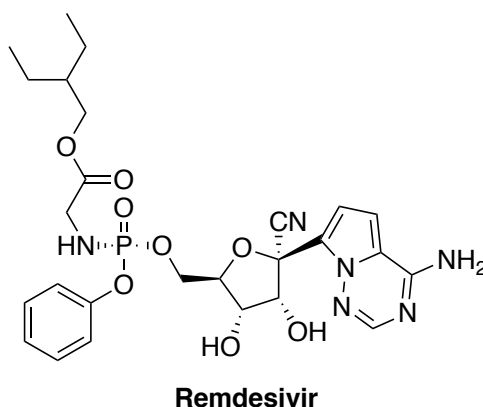


Figure 3.3: Remdesivir, an RNA antiviral

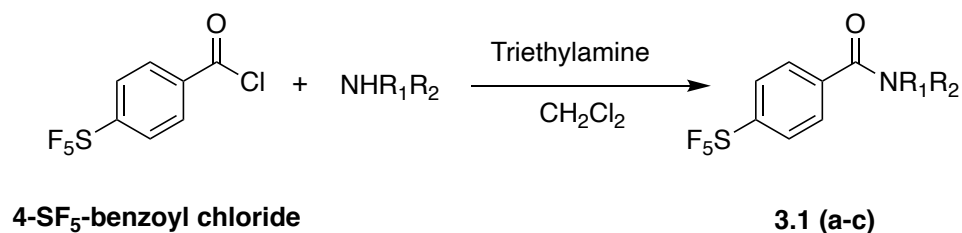
## 3.2 Results and Discussion

### 3.2.1 Synthesis

Amide couplings were initially attempted by combining amines with 4-pentafluorosulfanylbenzoyl chloride in the presence of triethylamine base as an HCl scavenger and dichloromethane (DCM) as the solvent (Table 3.1).

Attempted coupling of 4-pentafluorosulfanyl benzoyl chloride with 1-methyl-piperazine (**3.1c**) led to poor yields and the free benzoic acid was detected in the crude reaction mixture, suggesting acid chloride hydrolysis. Hence, the coupling agent HATU (hexafluorophosphate azabenzotriazole tetramethyl uronium), was added, to enable reaction of the acid, leading to improved yields (Figure

3.4). Much to our surprise, even in the absence of a coupling agent, reaction with morpholine and the acid chloride delivered excellent yield (93%).



Entry	Compound	NR <sub>1</sub> R <sub>2</sub>	Isolated Yield (%)
1	3.1a		76
2	3.1b		93
3	3.1c		10

Table 3.1: Amide coupling products of 4-SF<sub>5</sub>-benzoyl chloride and heterocycles

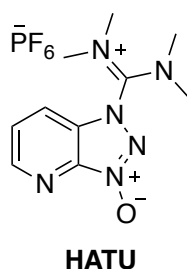
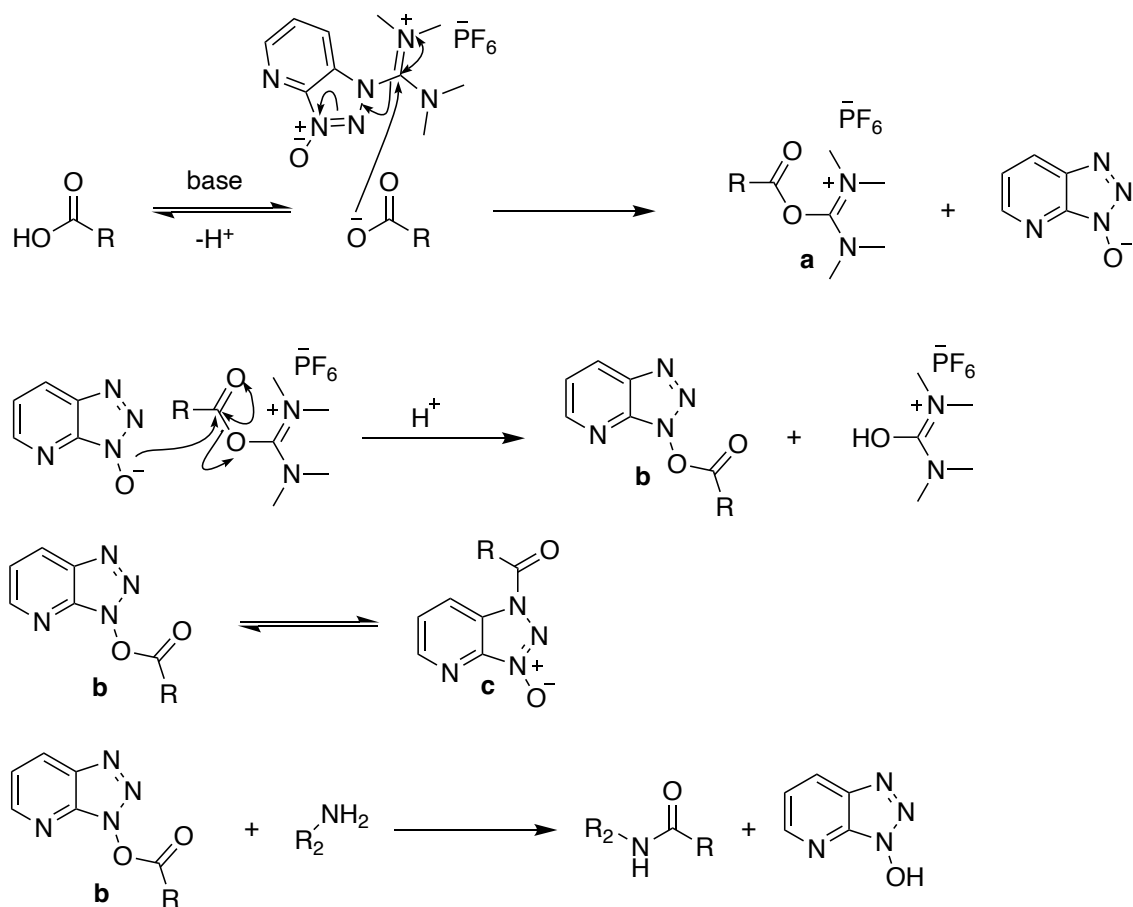


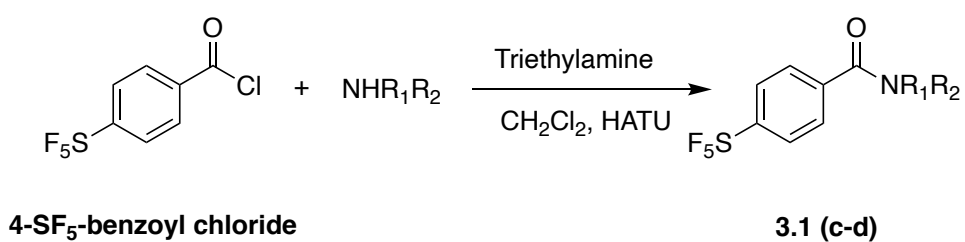
Figure 3.4: Amide coupling agent hexafluorophosphate azabenzotriazole tetramethyl uronium

HATU is a popular phosphonium based coupling reagent used for simple amide couplings as well as long chain peptide synthesis.<sup>136</sup> The precise mechanism of HATU mediated coupling is unknown. A mechanism proposed by Reszka *et al.* is shown in Scheme 3.1. An active species **a** is initially generated upon reaction between the carboxylic acid and the benzotriazole species. **a** is involved in the formation of an ester, **b**, which exists in equilibrium with its corresponding N-oxide, **c**.<sup>137</sup> The amine reacts with either **b** or **c** to deliver the amide coupled product.



Scheme 3.1: HATU mediated peptide bond formation mechanism<sup>136</sup>

Coupling 1-methyl-piperazine and 1-Boc-piperazine with 4-SF<sub>5</sub>-benzoyl chloride in the presence of HATU rendered excellent yields (80% and 91% respectively, Table 3.2)

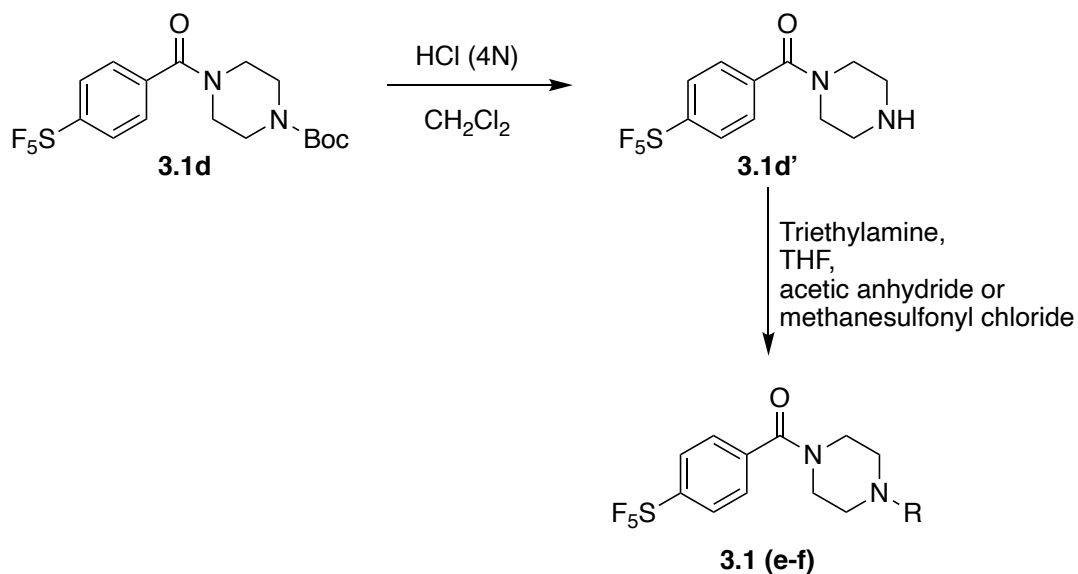


Entry	Compound	NR <sub>1</sub> R <sub>2</sub>	Isolated Yield (%)
1	3.1c		83
2	3.1d		91

Table 3.2: Yields of amide coupling products in the presence of HATU



**3.1d** was successfully deprotected and further functionalised as its amide (**3.1e**) and sulphonamide (**3.1f**) derivatives (Scheme 3.2 & Table 3.3).



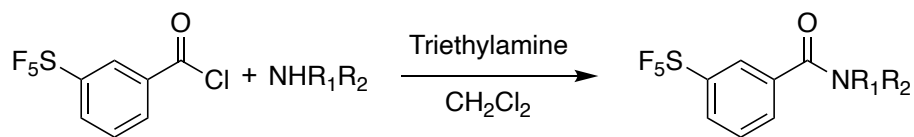
Scheme 3.2: Boc-deprotection of **3.1d** and further coupling of the free amine

Entry	Compound	NR <sub>1</sub> R <sub>2</sub>	Isolated (%)	Yield
1	<b>3.1e</b>		82	
2	<b>3.1f</b>		48	

Table 3.3: Yields of acetamide and sulphonamide analogues.

The same reactions were performed on **3-SF<sub>5</sub>-benzoyl chloride**. Only piperidine (**3.2a**) was coupled in the absence of HATU as it gave excellent yield (97%). Yields were generally low in comparison with **4-SF<sub>5</sub>-benzoyl chloride** couplings. The carbonyl carbon of **4-SF<sub>5</sub>-benzoyl chloride** is more electropositive than the carbonyl carbon of **3-SF<sub>5</sub>-benzoyl chloride**. This is a reasonable rationale

for the reduction in yields. Yield is significantly low in the case of 1-methyl-piperazine (17%, **3.2b**). The reduction in yield was mainly due to difficulty in purification (crude yield, 40%).



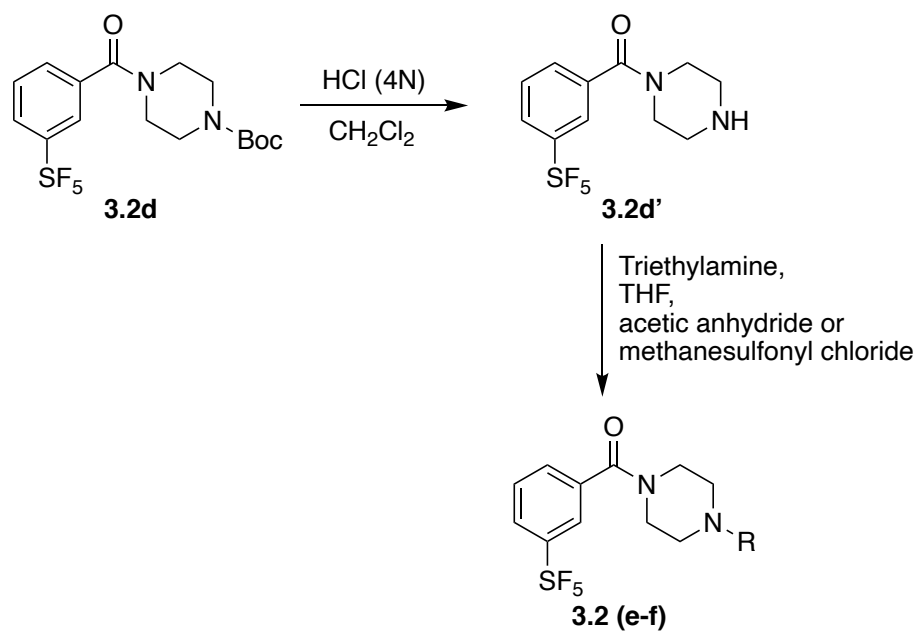
**3-SF<sub>5</sub>-benzoyl chloride**

**3.2 (a-d)**

Entry	Compound	NR <sub>1</sub> R <sub>2</sub>	Coupling agent	Isolated Yield (%)
1	<b>3.2a</b>		-	97
2	<b>3.2b</b>		HATU	17
3	<b>3.2c</b>		HATU	53
4	<b>3.2d</b>		HATU	73

Table 3.4: Amide coupling products of 3-SF<sub>5</sub>-benzoyl chloride and heterocycles

Similar to **3.1(e-f)**, **3.2(e-f)** were synthesised in excellent yields (Scheme 3.3 and Table 3.5).



Scheme 3.3: Boc-deprotection of **3.1d** and further coupling of the free amine

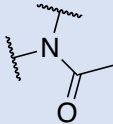
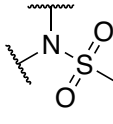
Entry	Compound	NR <sub>1</sub> R <sub>2</sub>	Yield %
1	3.2e		47
2	3.2f		80

Table 3.5: Yields of acetamide and sulfonamide analogues (3- SF<sub>5</sub>-benzoyl chloride

To assist rapid purification of solution phase reactions solid supported scavenger resins are often used, especially in peptide syntheses that involve multiple steps.<sup>138</sup> In several of our amide couplings, we utilised MP-Trisamine (macroporous polystyrene-bound nucleophilic scavenger), which is a powerful scavenger for acidic or electrophilic species such as acid chlorides.<sup>139,17,18</sup> Simply stirring the crude reaction mixture with 3 equivalents of MP-Trisamine for 1-2 hours eliminates the need for a base wash. Upon filtration, the reaction mixture is free of the acid chloride.

Compounds **3.3(a-b)** are analogues of **TRY-UNI-714a760b-6** representing a bioisosteric replacement of chlorine with CF<sub>3</sub> and SF<sub>5</sub> (Figure 3.5) and the 4-methyl chain has been replaced with a carboxamide group. The attempted strategy to synthesise **3.3(a-b)** did not yield the desired products, instead cyclised derivatives **3.3(c-d)** were obtained (Scheme 3.4). The hypothesis is that **3.3(a-b)** are formed initially in the presence of ammonia and are rapidly cyclised to **3.3(c-d)** under reflux conditions (Scheme 3.5). **3.3c** was crystallised by diffusion method using hexane and dichloromethane to obtain colourless crystals whereby an X-ray structure was obtained (Figure 3.6).

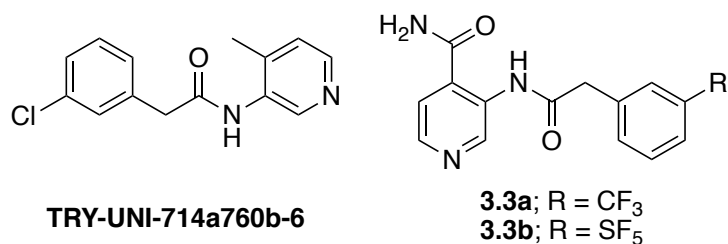
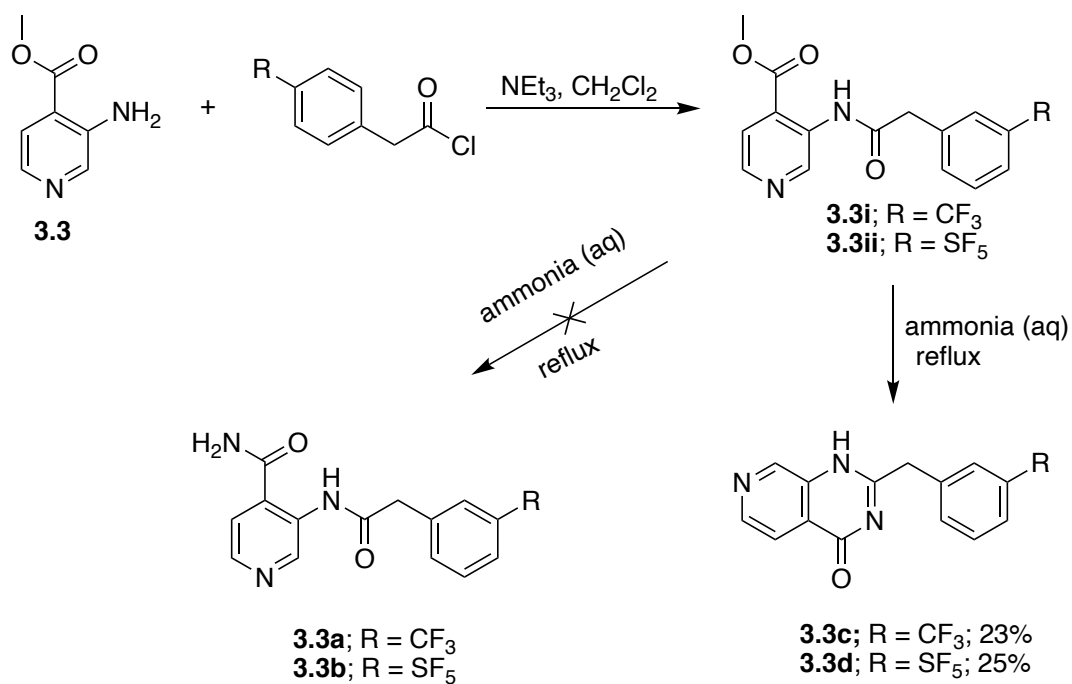
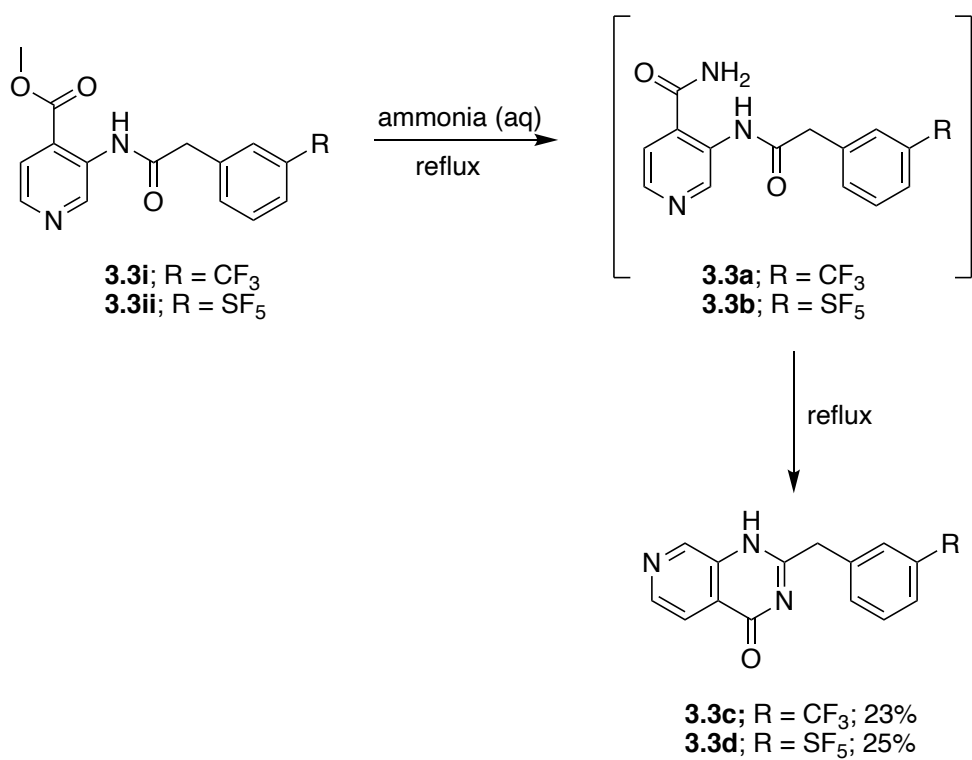


Figure 3.5: Analogues of **TRY-UNI-714a760b-6** (**3.3a-b**)



Scheme 3.4: Unexpected Synthesis of 3.3(c-d)



Scheme 3.5: An intermediate 3.3(a-b) maybe formed prior to cyclisation

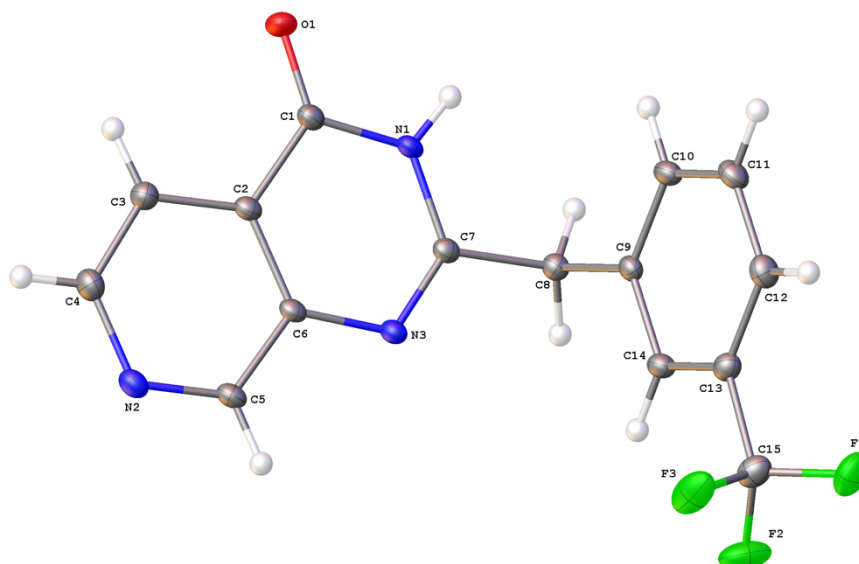
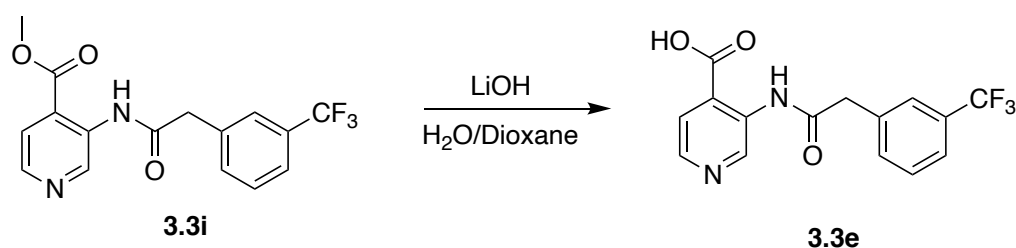


Figure 3.6: X-ray structure of **3.3c**

Attempts to synthesise compounds **3.3(a-b)** were futile. However, the synthesis of **3.3e** was achieved following the hydrolysis of **3.3i** by Dr Dan Guest, a Sussex collaborator on this project (Scheme 3.6).



Scheme 3.6: Ester hydrolysis of **3.3i** to afford **3.3e**

### 3.2.2 Modelling

Molecular docking was performed on **3.3 (c-d)** and compared with **TRY-UNI-714a760b-6**, **ADA-UCB-6c2cb422-1** and **3.3 (a-b)**. In figure 3.7, we present a ligand interaction diagram of **3.3 (a-b)** with M<sup>PRO</sup> of SARS-CoV-2. **3.3a** forms hydrogen bonding with His41 and Cys145 residues. A pi-pi aromatic interaction is formed by both ligands through respective pyridine rings. **3.3b** also forms several hydrogen bonds through the amino and carbonyl groups. The hydrophobic heads of the ligands must be forming several hydrophobic interactions with amino acid residues such as Leu167, Ala191, etc that are in close proximity. Figure 3.8 shows the pose of **TRY-UNI-714a760b-6** that has the best binding affinity in the M<sup>PRO</sup> binding pocket, as determined by the software. Orientation of the ligand is quite different to that of **3.3 (a-b)**. The piperidine ring carrying the polar functionalities is essentially in the same region as the other two ligands. However, the hydrophobic tail has flipped in orientation. The hydrophobic tail is now in proximity with amino acid residues Ser144 and Asn142 that are non-hydrophobic. Similar to **3.3b**, **TRY-UNI-714a760b-6** forms a pi-pi interaction with His41 and a hydrogen bond with Glu166.

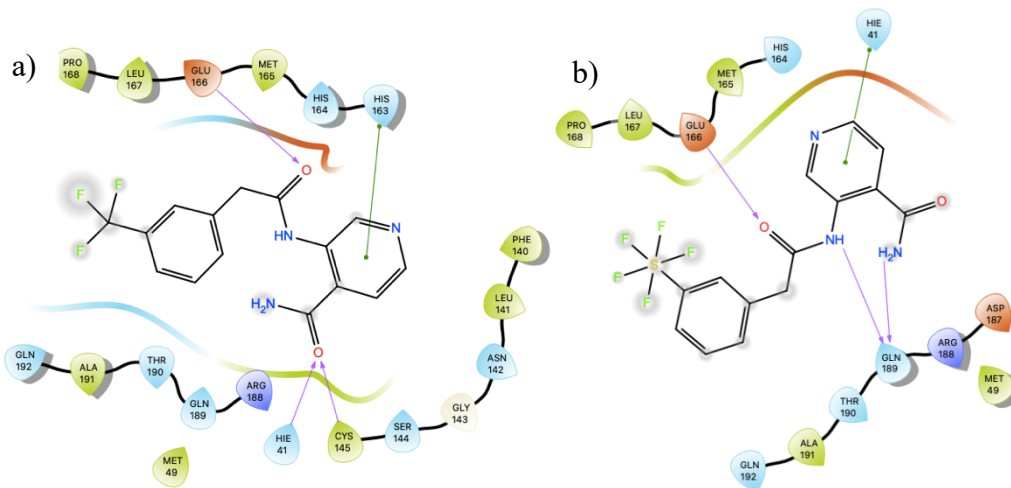


Figure 3.7: Ligand interaction diagram of **3.3(a-b)** in complex with  $M^{pro}$  of SARS-CoV-2

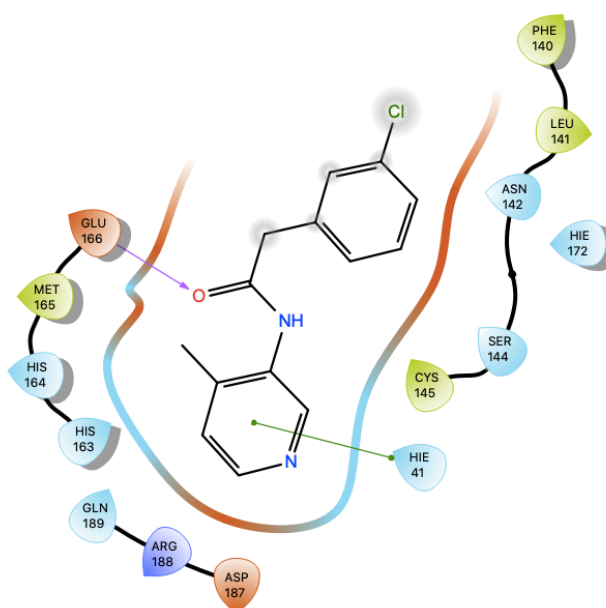


Figure 3.8: **TRY-UNI-714a760b-6**; HIE denotes histidine

**ADA-UCB-6c2cb422-1** docked in the  $M^{pro}$  binding site is shown in Figure 3.9. The ligand has lost the pi-pi interaction between the pyridine ring and His41 residue due to the increased distance between the species. However, the ligand is able to contribute hydrophobic interactions as well as a hydrogen bond with Cys145 and Glu166, to aid binding. **ADA-UCB-6c2cb422-1** has a different orientation compared to **3.3 (a-b)** as well as **TRY-UNI-714a760b-6**.

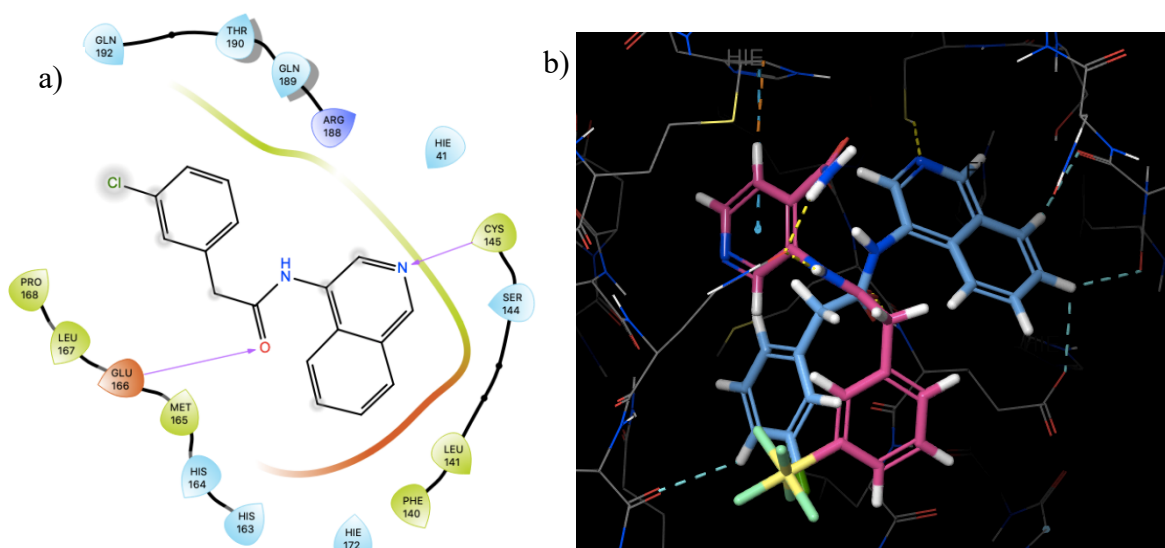


Figure 3.9: a); Ligand interaction diagram of ADA-UCB-6c2cb422-1, b); ADA-UCB-6c2cb422-1 (blue) and 3.3c (pink) in complex with  $M^{pro}$ ; blue dashed lines indicate aromatic hydrogen bonds.

ADA-UCB-6c2cb422-1 and 3.3d have similar poses as can be seen in Figure 3.10. The ligand 3.3d makes several hydrophobic interactions as well as aromatic hydrogen bonds while the pi-pi stacking and hydrogen bond with Cys145 are non-existent. Hydrogen bonds that arise between aromatic hydrogens and hydrogen bond acceptors are referred to as ‘aromatic hydrogen bonds’, by Schrodinger Maestro. Aromatic hydrogens can act as hydrogen bond donors due to partial charges on the ring carbon and hydrogen atoms.<sup>19</sup>

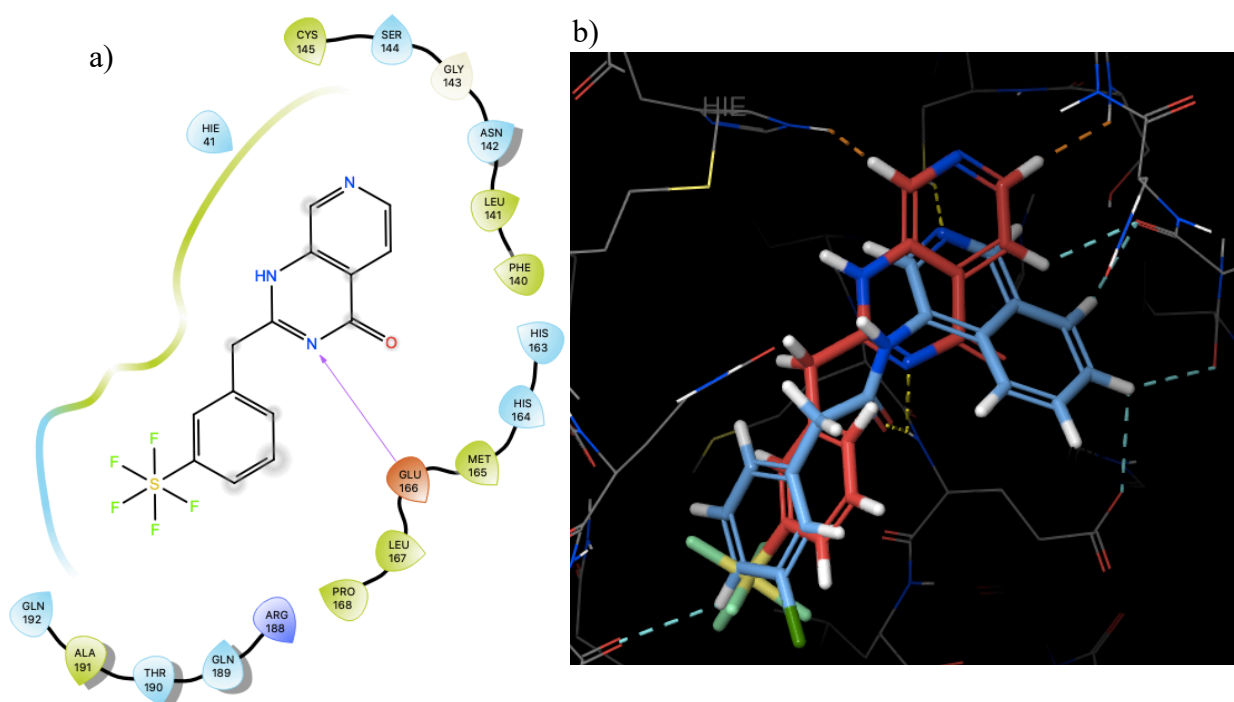


Figure 3.10: a) ligand interaction diagram of 3.3d, b) 3.3d (red) overlapped with ADA-UCB-6c2cb422-1 (blue), blue dashed lines indicate aromatic hydrogen bonds, hydrophobic clashes in brown and H-bonds yellow.

Ligand 3.3c has quite a different orientation when binding compared to the other ligands (Figure 3.11). It makes one hydrogen bond like 3.3c with Glu166. Unlike 3.3d, 3.3c does not form many aromatic hydrogen bonds. It has the potential to form a hydrophobic interaction with Met49.

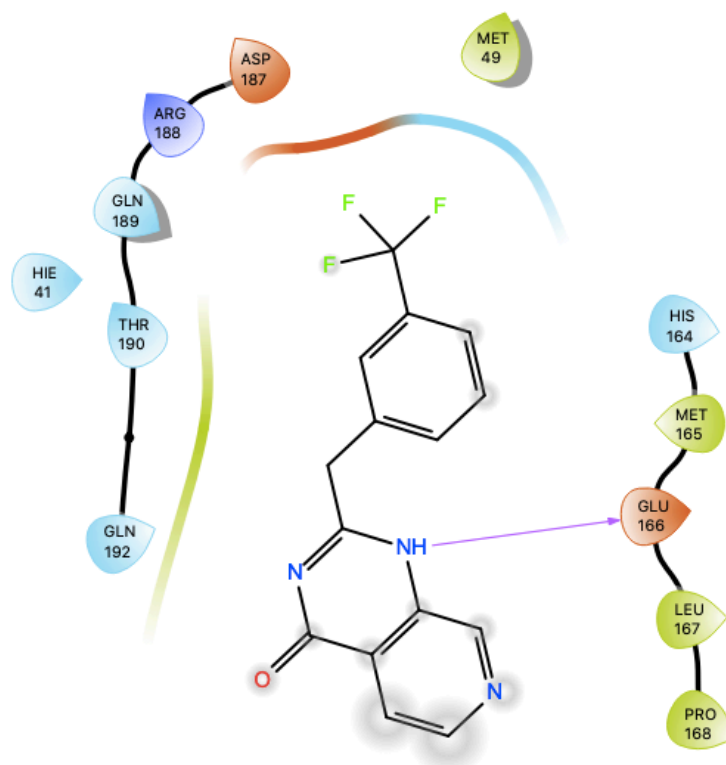


Figure 3.11: Ligand interaction diagram of 3.3c

**3.3e** interacts with the  $M^{\text{pro}}$  binding point through multiple hydrogen bonds including aromatic hydrogen bonds and hydrophobic clashes (Figure 3.12).

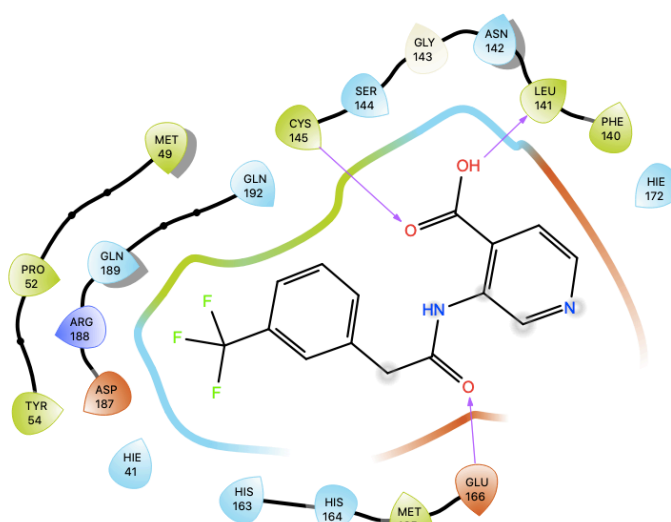


Figure 3.12: Ligand interaction diagram of 3.3e

Analysis of the ligand interaction diagrams reveals that ligands **3.3 (a-b)** are the better predicted binders at the  $M^{\text{pro}}$  binding site.

A fluorescence assay revealed that ligand **3.3 (e)** did not have significant inhibition below 20  $\mu\text{M}$  concentration. Ligands **3.3 (c-d)** did not show any inhibition even at higher concentrations (Figure 3.13).<sup>142</sup>



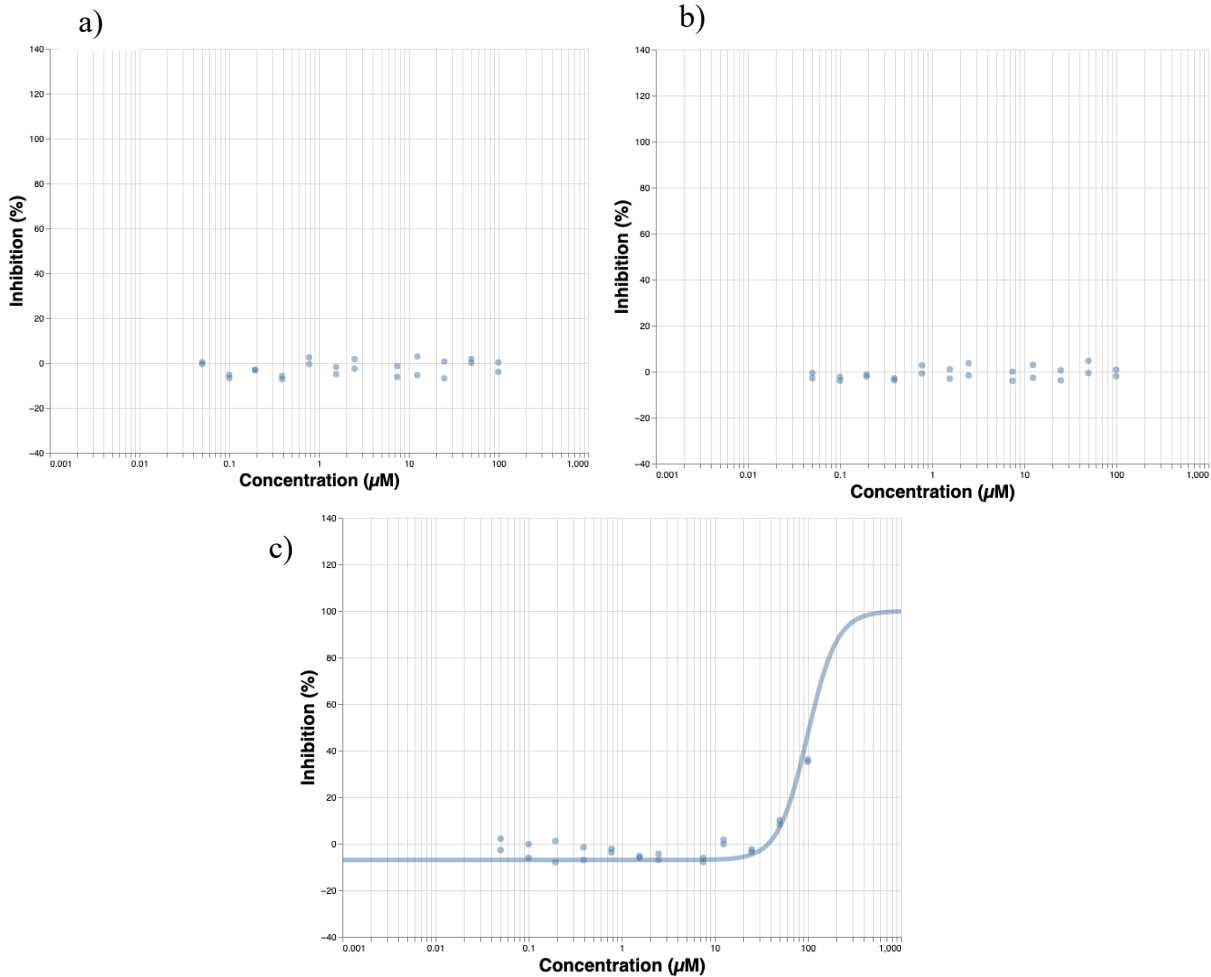


Figure 3.13: Dose response curve for ligands 3.3c (a), 3.3d (b) and 3.3e (c). [Graphs taken from www.covid.postera.ai](http://www.covid.postera.ai).

The figures below demonstrate the dose response curves of **TRY-UNI-714a760b-6** and **ADA-UCB-6c2cb422-1** (Figure 3.14).<sup>142</sup> Percentage inhibition of **ADA-UCB-6c2cb422-1** drops after 10  $\mu\text{M}$  concentration. Inhibition drops for **TRY-UNI-714a760b-6** at much higher concentrations (>100  $\mu\text{M}$ )

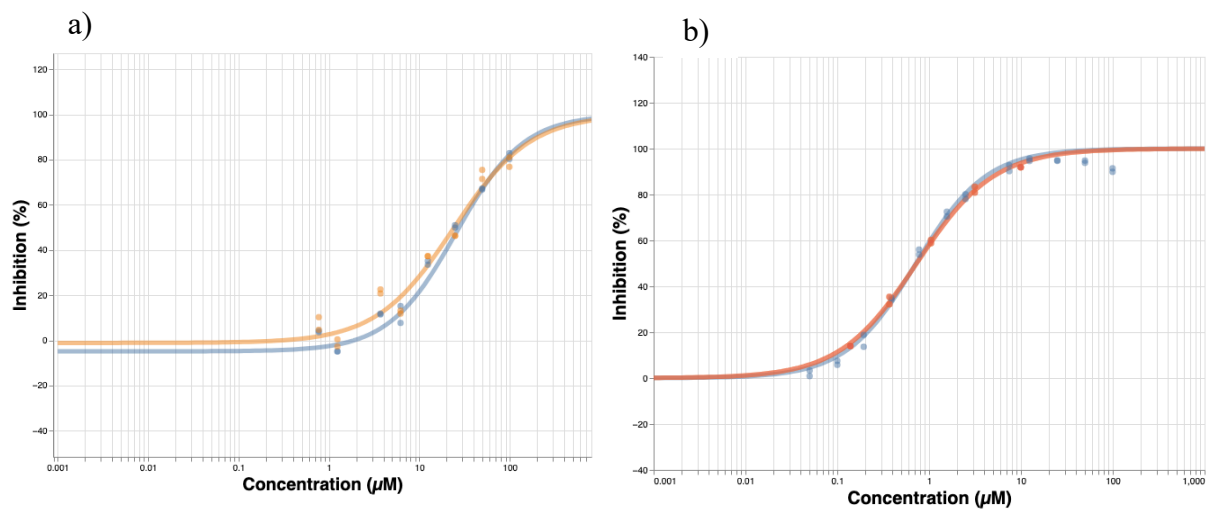


Figure 3.14: Dose response curves of a) **TRY-UNI-714a760b-6** and b) **ADA-UCB-6c2cb422-1**. [Graphs taken from www.covid.postera.ai](http://www.covid.postera.ai)

Even though, the binding modes of **ADA-UCB-6c2cb422-1** and ligand **3.3d** were similar from the docking studies, **3.3d** hardly inhibited the virus. None of the compounds synthesised had superior inhibitory effect compared to the original ligands, **TRY-UNI-714a760b-6** and **ADA-UCB-6c2cb422-1**. Although possible activity of ligands **3.3(a-b)** could not be determined, analysing an analogue (**TRY-UNI-714a760b-20**) of **TRY-UNI-714a760b-6** with a nitrile in the place of chlorine revealed a decrease in inhibition of viral activity (61  $\mu\text{M}$ ). On the other hand, adding an electron-donating group improved the inhibition (4  $\mu\text{M}$ ) (Figure 3.15).

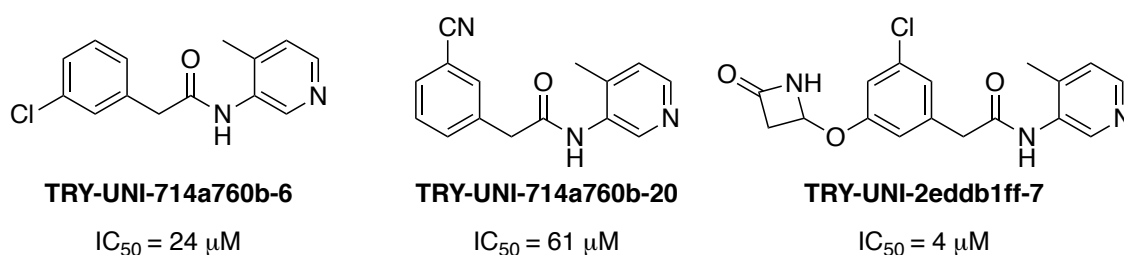
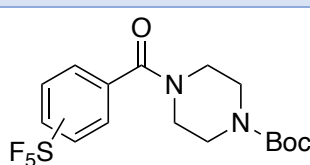
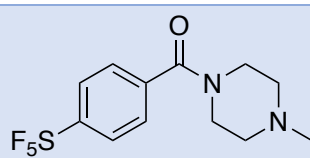
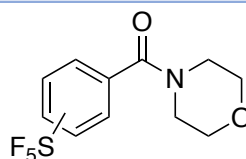
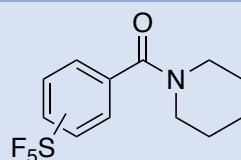


Figure 3.15: Comparison of TRY-UNI analogues with electron-donating and withdrawing substituents

### 3.3 Conclusion

To conclude, a library of compounds has been synthesised by coupling *N*-heterocycles with 3 and 4- $\text{SF}_5$ -benzoyl chlorides in order to expand  $\text{SF}_5$ -building block space (Table 3.6). Moreover, two compounds [**3.3(c-d)**] from the library were analysed *in vitro* (Table 3.7) and *in silico* for their biological activity as inhibitors of SARS-Cov-2  $\text{M}^{\text{pro}}$  and were found to be inactive.

Entry	Compounds
1	
2	
3	
4	



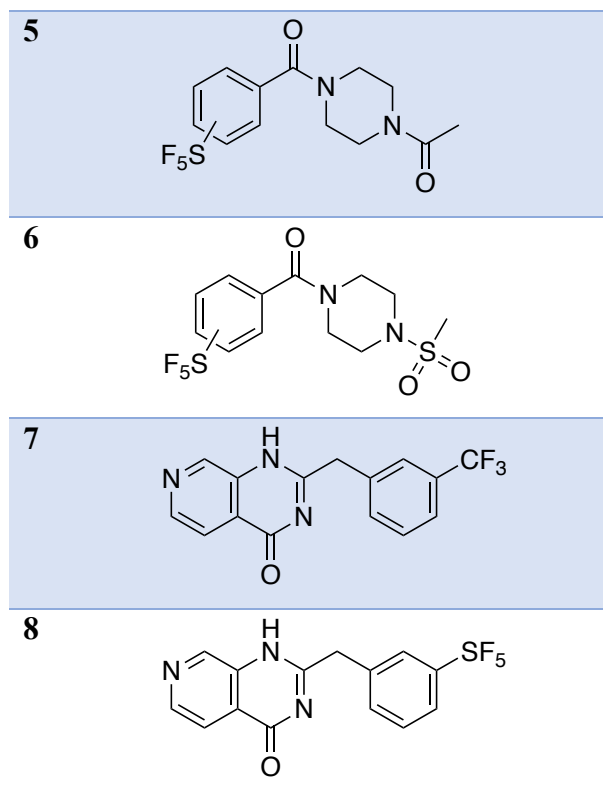


Table 3.6: Library of amides synthesised

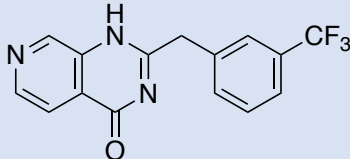
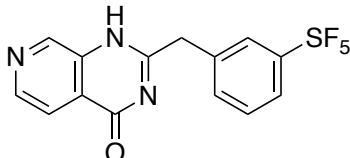
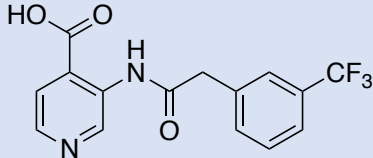
Entry	Compounds	IC <sub>50</sub> (μM)
1		>99
2		>99
3		>99

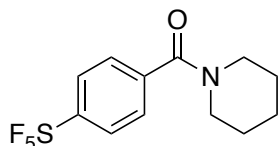
Table 3.7: Compounds tested for antiviral activity

### 3.4 Experimental

All reagents were purchased from Merck, Fisher Scientific UK Ltd, SpiroChem AG, Fluorochem Ltd, and used without further purification. <sup>1</sup>H NMR spectra were recorded on Varian VNMRS 600 MHz spectrometers, at room temperature, using deuterated solvent for calibration ((CD<sub>3</sub>Cl at 7.26 ppm, (CD<sub>3</sub>)<sub>2</sub>SO at 2.50 ppm or CD<sub>3</sub>OD at 3.31 ppm). <sup>13</sup>C NMR analyses were recorded on Varian VNMRS 600 MHz spectrometers, at room temperature, using deuterated solvent for calibration (CDCl<sub>3</sub> at 77.16 ppm, (CD<sub>3</sub>)<sub>2</sub>SO at 39.52 ppm or CD<sub>3</sub>OD at 49.00 ppm). <sup>19</sup>F NMR were recorded on Varian VNMRS 376 MHz spectrometers, at room temperature, using deuterated solvent for calibration. Chemical shifts are reported in ppm, usually referenced to TMS as an internal

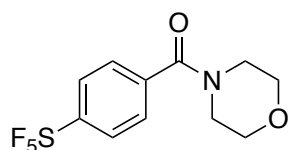
standard, and data reported as s = singlet, d = doublet, t = triplet, q = quadruplet, p = pentet, ddd = doublet of doublets of doublets, m = multiplet; integration. Mass spectrometry analyses were conducted by Dr Abdul-Sada. ESI mass spectra were obtained using a Bruker Daltonics Apex III, using Apollo ESI as the ESI source; EI mass spectra were obtained using a Fissions VG Autospec instrument used at 70 eV. Elemental analyses were conducted by Mr Stephen Boyer from the London Metropolitan University. Melting points were determined using a Stanford Research Systems Optimelt and are uncorrected. LCMS were performed by Shimadzu LCMS-2020 equipped with a Gemini® 5µm C18 110Å column and percentage purities were ran over 30 minutes in water/acetonitrile with 0.1% formic acid (5 min at 5%, 5%-95% over 20 min, 5 min at 95%) with the UV detector at 254 nm.

#### [4-(Pentafluoro-λ<sup>6</sup>-sulfanyl)phenyl](piperidin-1-yl)methanone (3.1a)



Triethylamine (247.4 mg, 2.44 mmol, 1.3 equiv.) was added to piperidine (176.0 mg, 2.07 mmol, 1.1 equiv.) dissolved in dichloromethane (2 mL) followed by dropwise addition of 4-(pentafluorosulfanyl) benzoyl chloride (500.0 mg, 1.88 mmol, 1.0 equiv.). The reaction mixture was stirred at room temperature overnight. It was then diluted with dichloromethane (5 mL) and washed with 2M HCl (10 mL x 3). The aqueous layers were extracted with dichloromethane (15 mL x 3), dried over MgSO<sub>4</sub>, filtered and concentrated in *vacuo*. The crude was purified over a column of silica (dichloromethane:methanol, 9:1) to obtain a colourless solid as the title compound (451.0 mg, 76%). <sup>1</sup>H NMR (600 MHz, CDCl<sub>3</sub>) δ 7.74 (d, *J* = 8.4 Hz, 2H, ArH), 7.43 (d, *J* = 8.4 Hz, 2H, ArH), 3.66 (m, 2H, CH<sub>2</sub>), 3.24 (m, 2H, CH<sub>2</sub>), 1.63 (m, 4H, (CH<sub>2</sub>)<sub>2</sub>), 1.47 (m, 2H, CH<sub>2</sub>). <sup>13</sup>C NMR (151 MHz, CDCl<sub>3</sub>) δ 168.0 (C=O), 154.1 (p, *J* = 17.8 Hz, ArC-SF<sub>5</sub>), 139.9 (ArC), 127.1 (2ArC), 126.2 (m, 2ArC-CSF<sub>5</sub>), 48.6 (C), 43.1 (C), 26.4 (C), 25.4 (C), 24.3 (C); <sup>19</sup>F NMR (400 MHz, CDCl<sub>3</sub>) δ 83.75 (m, F), 62.53 (d, *J* = 150.0 Hz, 4F); LCMS Purity (UV) = 95%, *t*<sub>R</sub> 19.5 min; HRMS – ESI (*m/z*) found 316.0789, calc. for [C<sub>12</sub>H<sub>14</sub>F<sub>5</sub>NOS][H]<sup>+</sup>:316.0789; IR (neat) *v*<sub>max</sub>/cm<sup>-1</sup>: 2945, 1627, 817; mp 84.5 - 86.7 °C.

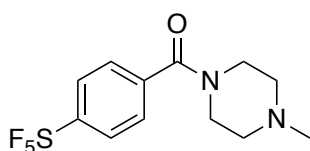
#### [4-(Pentafluoro-λ<sup>6</sup>-sulfanyl)phenyl](morpholino)methanone (3.1b)



To morpholine (180.3 mg, 2.07 mmol, 1.1 equiv.), dissolved in dichloromethane (2 mL) was added triethylamine (247.0 mg, 2.44 mmol, 1.3 equiv.), followed by dropwise addition of 4-(pentafluorosulfanyl) benzoyl chloride (500.0 mg, 1.88 mmol, 1.0 equiv.). The reaction mixture was stirred at room temperature overnight. The reaction mixture was diluted with dichloromethane (5

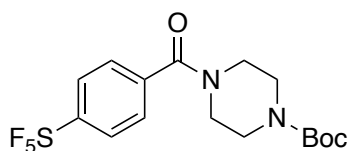
mL) and the organic layer was washed with 2M HCl (10 mL x 3). The combined aqueous layers were extracted with dichloromethane (15 mL x 3). The organic layers were dried over MgSO<sub>4</sub>, filtered and concentrated in *vacuo*. The crude material was purified over a column of silica (dichloromethane:methanol, 9:1) to afford a colourless solid as the title compound (556.0 mg, 93%). <sup>1</sup>H NMR (600 MHz, CDCl<sub>3</sub>) δ 7.58 (d, *J* = 8.1 Hz, 2H, ArH), 7.30 (d, *J* = 8.1 Hz, 2H, ArH), 3.33 (m, 8H, ((CH<sub>2</sub>)<sub>4</sub>); <sup>13</sup>C NMR (151 MHz, CDCl<sub>3</sub>) δ 168.1 (C=O), 154.2 (p, *J* = 17.7 Hz, ArC-SF<sub>5</sub>), 138.7 (ArC), 127.4 (2ArC), 126.3 (m, 2ArC), 66.5 (2C, N-(CH<sub>2</sub>)<sub>2</sub>), 47.9 (CH<sub>2</sub>), 42.4 (CH<sub>2</sub>); <sup>19</sup>F NMR (400 MHz, CDCl<sub>3</sub>) δ 83.40 (p, *J* = 150.3, F), 62.39 (d, *J* = 150.3 Hz, 4F); LCMS Purity (UV) = 95%, *t*<sub>R</sub> 18.3 min; HRMS – ESI (*m/z*) found 340.0394, calc. for [C<sub>11</sub>H<sub>12</sub>F<sub>5</sub>NO<sub>2</sub>S] [Na]<sup>+</sup>: 340.0401. IR (neat) *v*<sub>max</sub>/cm<sup>-1</sup>: 3734 (CH), 1626 (s, C=O), 818 (SF<sub>5</sub>); mp 72 – 73 °C.

**(4-Pentafluoro-λ<sup>6</sup>-sulfanylphenyl)(4-methylpiperazin-1-yl)methanone (3.1c)**



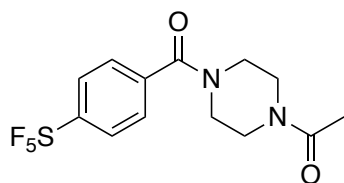
To 1-methyl piperazine (188.0 mg, 1.88 mmol, 1.0 equiv.), dissolved in dichloromethane (2 mL) was added triethylamine (190.3 mg, 1.88 mmol, 1.0 equiv.), followed by dropwise addition of 4-(pentafluorosulfonyl) benzoyl chloride (250.0 mg, 0.94 mmol, 0.5 equiv.) and HATU (391.2 mg, 0.94 mmol, 0.5 equiv.). The reaction mixture was stirred at room temperature overnight and then diluted with dichloromethane (10 mL). The reaction mixture was filtered and the organic filtrate was washed with water (10 mL x 3) and the aqueous layer extracted with dichloromethane (10 mL x 3). The organic layer was then dried over MgSO<sub>4</sub>, filtered and concentrated in *vacuo*. The crude product was purified over a column of silica (dichloromethane:methanol, 9:1) to afford a yellow solid as the title compound (257 mg, 83%). <sup>1</sup>H NMR (600 MHz, CDCl<sub>3</sub>) δ 7.78 (m, 2H, ArH), 7.52 (m, 2H, ArH), 3.78 (m, 2H, CH<sub>2</sub>), 3.39 (m, 2H, CH<sub>2</sub>), 2.50 (m, 4H, (CH<sub>2</sub>)<sub>2</sub>), 2.30 (s, 3H, CH<sub>3</sub>). <sup>13</sup>C NMR (151 MHz, CDCl<sub>3</sub>) δ 168.0 (C=O), 153.9 (m, ArC-SF<sub>5</sub>), 136.6 (ArC), 130.1 (ArC), 129.1 (ArC), 127.1 (m, ArC-CSF<sub>5</sub>), 124.9 (m, ArC-CSF<sub>5</sub>), 54.8 (2C), 47.6 (C), 45.9 (CH<sub>3</sub>), 42.2 (C); <sup>19</sup>F NMR (400 MHz, CDCl<sub>3</sub>) δ 83.50 (m, F), 62.67 (d, *J* = 150.3 Hz, 4F); LCMS Purity (UV) = 98%, *t*<sub>R</sub> 11.6 min. HRMS – ESI (*m/z*) found 331.0901, calc. for [C<sub>12</sub>H<sub>15</sub>F<sub>5</sub>N<sub>2</sub>OS][H]<sup>+</sup>: 331.0898. IR (neat) *v*<sub>max</sub>/cm<sup>-1</sup> 2811.3, 1613.5, 822.4; mp 159.7 – 160.2 °C.

***tert*-Butyl 4-(4-pentafluoro-λ<sup>6</sup>-sulfanyl) benzoyl piperazine-1-carboxylate (3.1d)**



To *N*-Boc piperazine (385.5 mg, 2.07 mmol, 1.1 equiv.), dissolved in dichloromethane (3 mL) was added triethylamine (247.0 mg, 2.44 mmol, 1.3 equiv.) and the mixture was stirred for a few minutes. HATU (787.1 mg, 2.07 mmol, 1.1 equiv) was added to this solution followed by dropwise addition of 4-(pentafluorosulfanyl) benzoyl chloride (500.0 mg, 1.88 mmol, 1.0 equiv.). The reaction mixture was stirred at room temperature overnight. The reaction mixture was diluted with dichloromethane (5 mL) and the precipitate formed was discarded after gravity filtration. MP-Trisamine scavenger resin (520.0 mg, 3.0 mmol, 1.6 equiv.) was added to the filtrate and after 3 hours, the scavenger was removed by gravity filtration. The crude material was purified over a column of silica (dichloromethane:methanol, 9:1) to obtain a white solid as the title compound (352.0 mg, 76%). <sup>1</sup>H NMR (600 MHz, CDCl<sub>3</sub>) δ 7.67 (m, 2H, ArH), 7.37(m, 2H, ArH), 3.78 –3.49 (m, 4H), 3.40 –3.32 (m, 4H), 1.32 (s, 9H, (CH<sub>3</sub>)<sub>3</sub>); <sup>13</sup>C NMR (151 MHz, CDCl<sub>3</sub>) δ 168.4 (C=O), 154.6 –153.9 (m, 2C, C=O, ArC-SF<sub>5</sub>), 138.8 (ArC), 127.4 (2ArC), 126.5 (2ArC), 80.5 (C), 47.4 (2C), 42.1 (2C), 28.3 (3C); <sup>19</sup>F NMR (400 MHz, CDCl<sub>3</sub>) δ 83.32 (p, *J* = 150.2 Hz, F), 62.47 (d, *J* = 150.2 Hz, 4F); LCMS Purity (UV) = 97%, *t*<sub>R</sub> 21.5 min; HRMS - ESI (*m/z*) found: 439.1078, calc. for [C<sub>16</sub>H<sub>21</sub>F<sub>5</sub>N<sub>2</sub>O<sub>3</sub>S][Na]<sup>+</sup>: 439.1085. IR (neat) *v*<sub>max</sub>/cm<sup>-1</sup> 2920, 1637, 1279, 816; mp: 151 – 153 °C.

### 1-{4-[4-(Pentafluoro-λ<sup>6</sup>-sulfanyl)benzoyl]piperazin-1-yl}ethan-1-one (3.1e)

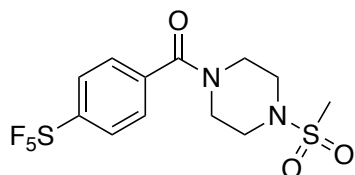


Compound **3.1d** was dissolved in dichloromethane (2 mL) and treated with HCl in dioxane (4M, 6.0 equiv.) overnight to remove the Boc group. The reaction was monitored by TLC. Following the completion of the reaction, it was concentrated in *vacuo* to obtain the HCl salt (4-[4-(pentafluoro-λ<sup>6</sup>-sulfanyl)benzoyl]piperazinyl hydrochloride, **3.1d'**), as a colourless solid. Compound **3.1d'** was used without purification in the following step.

To **3.1d'** (80.0 mg, 0.2 mmol, 1.0 equiv.), dissolved in THF (1.0 mL), was added triethylamine (20.0 mg, 0.2 mmol, 1.0 equiv.). The reaction mixture was stirred for 30 minutes, followed by which, acetic anhydride (20 mg, 0.2 mmol, 1.0 equiv.) was added to the mixture and this was stirred at room temperature overnight. The crude was dissolved in dichloromethane (5 mL) and passed through a hydrophobic frit, to collect the organic layer. Afterwards, the crude material was purified over a column of silica (dichloromethane:methanol; 7:3) to obtain the pure product as a colourless solid (59 mg, 82%). <sup>1</sup>H NMR (600 MHz, CDCl<sub>3</sub>) δ 7.81 (d, *J* = 8.4 Hz, 2ArH), 7.49 (d, *J* = 8.4 Hz, 2ArH), 3.89 –3.64 (m, 4H, piperazine), 3.56 (s, 3H, CH<sub>3</sub>), 3.47 –3.30 (m, 4H, piperazine); <sup>13</sup>C NMR (151 MHz, CDCl<sub>3</sub>) δ 169.2 (Ar-C=O), 168.5 (C=O), 154.6 (m, ArC-SF<sub>5</sub>), 138.4 (ArC), 127.5 (2ArC),

126.6 (2ArC), 47.3 (bs, C), 46.1 (bs, C), 42.1 (bs, C), 41.3 (bs, C), 21.4 (CH<sub>3</sub>) <sup>19</sup>F NMR (400 MHz, CDCl<sub>3</sub>) δ 83.32 (p, *J* = 150.4 Hz, 1F), 62.96 (d, *J* = 150.4 Hz, 4F); HPLC Purity (UV) = 95%, *t*<sub>R</sub> 13.3 min; HRMS – ESI (*m/z*) found 381.0665, calc. for [C<sub>13</sub>H<sub>15</sub>F<sub>5</sub>N<sub>2</sub>O<sub>2</sub>S][Na]<sup>+</sup>:381.0667; IR (neat) *v*<sub>max</sub>/cm<sup>-1</sup> 2917(C-H), 1633 (C=O), 1625(C=O), 820 (S-F); mp 158 – 160 °C.

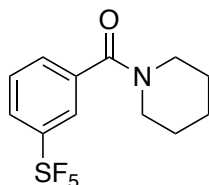
**(4-Pentafluoro-λ<sup>6</sup>sulfanyl phenyl)(4-(methylsulfonyl)piperazin-1-yl)methanone (3.1f)**



To crude **3.1d'** (82.0 mg, 0.23 mmol, 1.0 equiv.) dissolved in THF (3.0 mL) was added triethylamine (23.0 mg, 0.23 mmol, 1.0 equiv.) and the mixture was stirred for 30 minutes. Methanesulfonyl chloride (32.0 mg, 0.28 mmol, 1.2 equiv.) was added to the reaction mixture, which was stirred overnight at room temperature. The reaction mixture was quenched with dichloromethane (5 mL) and water (5 mL) then passed through a hydrophobic frit.

The crude was purified over column of silica (dichloromethane:methanol; 3:2) to get the pure product as a colourless solid (43 mg, 48%). <sup>1</sup>H NMR (600 MHz, CDCl<sub>3</sub>) δ 7.83 (d, *J* = 8.2 Hz, ArH, 2H), 7.50 (d, *J* = 8.2 Hz, ArH, 2H), 3.90 (m, CH<sub>2</sub>, 2H), 3.52 (m, CH<sub>2</sub>, 2H), 3.34 (m, CH<sub>2</sub>, 2H), 3.18 (m, CH<sub>2</sub>, 2H), 2.81 (s, CH<sub>3</sub>, 3H); <sup>13</sup>C NMR (151 MHz, CDCl<sub>3</sub>) δ 168.4 (C=O), 154.8 (m, C-SF<sub>5</sub>), 138.1 (ArC), 127.5 (ArC, 2C), 126.7 (ArC, 2C), 47.2 (CH<sub>2</sub>), 46.0 (CH<sub>2</sub>), 45.5 (CH<sub>2</sub>), 41.8 (CH<sub>2</sub>), 35.1 (CH<sub>3</sub>); <sup>19</sup>F NMR (376 MHz, CDCl<sub>3</sub>) δ 82.99 (p, *J* = 150.3 Hz, 1F), 62.51 (d, *J* = 150.3 Hz, 4F); HRMS - ESI (*m/z*) found 417.0342, calc. for [C<sub>12</sub>H<sub>15</sub>F<sub>5</sub>N<sub>2</sub>O<sub>3</sub>S<sub>2</sub>][Na]<sup>+</sup>:417.0349; Anal. calc (%) for C<sub>12</sub>H<sub>15</sub>F<sub>5</sub>N<sub>2</sub>O<sub>3</sub>S<sub>2</sub>: C, 36.55; H, 3.83; N, 7.10; found (%): C, 36.65; H, 3.69; N, 6.98. IR (neat) *v*<sub>max</sub>/cm<sup>-1</sup> 2187 (C-H), 1637 (C=O), 1322 (S=O), 821 (S-F); mp 163 – 164 °C.

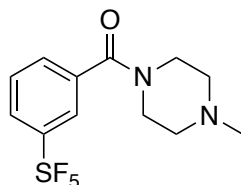
**[3-(Pentafluoro-λ<sup>6</sup>-sulfanyl)phenyl](piperidin-1-yl)methanone (3.2a)**



This was made as for its **3.1a**-analogue, from piperidine (175.8 mg, 2.07 mmol, 1.1 equiv.), triethylamine (247.0 mg, 2.44 mmol, 1.3 equiv.), and 3-(pentafluorosulfanyl)benzoyl chloride (500.0 mg, 1.88 mmol, 1.0 equiv.). It was obtained as a colourless solid (572.0 mg, 97%). <sup>1</sup>H NMR (600 MHz, CDCl<sub>3</sub>) δ 7.72 (m, 2H, ArH), 7.47 (m, 2H, ArH), 3.46 (m, 4H, 2CH<sub>2</sub>), 1.63 (m, 4H, 2CH<sub>2</sub>), 1.47 (m, 2H, CH<sub>2</sub>). <sup>13</sup>C NMR (151 MHz, CDCl<sub>3</sub>) δ 167.9 (C=O), 153.7 (C-SF<sub>5</sub>, p, <sup>2</sup>*J*<sub>F,C</sub> = 17.5 Hz), 137.3 (ArC), 129.8 (ArC), 128.9 (ArC), 126.6 (ArC-CSF<sub>5</sub>, m), 124.6 (ArC-CSF<sub>5</sub>, m), 48.6 (N-CH<sub>2</sub>), 43.2(N-CH<sub>2</sub>), 26.3 (2CH<sub>2</sub>), 25.4 (CH<sub>2</sub>); <sup>19</sup>F NMR (376 MHz, CDCl<sub>3</sub>) δ 83.60 (p, *J* = 150.0 Hz), 62.44

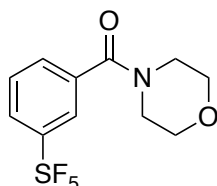
(d,  $J = 150.0$  Hz); LCMS Purity (UV) = 96%,  $t_R$  21.0 min; HRMS – ESI ( $m/z$ ) found 316.0785, calc. for  $[C_{12}H_{14}F_5NOS][H]^+$ : 316.0789; IR (neat)  $\nu_{max}/cm^{-1}$ : 3680, 1633, 820; mp 88 – 90 °C.

### (3-(Pentafluoro- $\lambda^6$ -sulfanyl)phenyl)(4-methylpiperazin-1-yl)methanone (3.2b)



To *N*-methylpiperazine (207.0 mg, 2.07 mmol, 1.1 equiv.), dissolved in dichloromethane (2 mL) was added triethylamine (247.4 mg, 2.44 mmol, 1.3 equiv.) together with HATU (787.0 mg, 2.07 mmol, 1.1 equiv.) and, finally, 3-(pentafluorosulfanyl)benzoyl chloride (500.0 mg, 1.88 mmol, 1.0 equiv.) was added dropwise. The reaction mixture was stirred at room temperature overnight, then filtered and the filtrate was stirred with MP Trisamine (3 equiv.) for 3 hours to remove the unreacted acid chloride. The crude product was purified over a column of silica (dichloromethane:methanol; 9:1) to give a colourless gum as the title compound (107 mg, 17%).  $^1H$  NMR (600 MHz,  $CDCl_3$ )  $\delta$  7.79 (ArH, m, 2H), 7.53 (ArH, m, 2H), 3.80 ( $CH_2$ , bs, 2H), 3.41 ( $CH_2$ , bs, 2H), 2.50 ( $CH_2$ , bs, 2H), 2.36 ( $CH_2$ , bs, 2H), 2.32 ( $CH_3$ , s, 3H);  $^{13}C$  NMR (151 MHz,  $CDCl_3$ )  $\delta$  168.1 (C=O), 153.9 (ArC-SF<sub>5</sub>, p,  $^2J_{FC} = 17.8$  Hz), 136.6 (ArC), 130.1 (ArC), 129.1 (ArC), 127.1 (ArC, p,  $^2J_{FC} = 4.4$  Hz), 124.9 (ArC, p,  $^2J_{FC} = 4.4$  Hz), 55.0 (C), 54.5 (C), 47.6 (C), 45.8 (C), 42.2 (C);  $^{19}F$  NMR (376 MHz,  $CDCl_3$ )  $\delta$  83.45 (1F, p,  $J = 150.1$  Hz), 62.83 (4F, d,  $J = 150.1$  Hz); LCMS Purity (UV) = 97%,  $t_R$  7.1 min; HRMS - ESI ( $m/z$ ) found:331.0896, calc. for  $[C_{12}H_{15}F_5N_2OS][H]^+$ :331.0898; IR (neat)  $\nu_{max}/cm^{-1}$ : 3499 (C-H), 1614 (C=O), 823 (S-F).

### [3-(Pentafluoro- $\lambda^6$ -sulfanyl)phenyl](morpholino)methanone (3.2c)

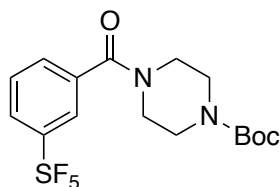


To morpholine (180.30 mg, 2.07 mmol, 1.1 equiv.), dissolved in dichloromethane (2 mL), was added triethylamine (246.90 mg, 2.44 mmol, 1.3 equiv.) and the mixture was stirred for a few minutes. HATU (787.10 mg, 2.07 mmol, 1.1 equiv.) was added to this solution followed by dropwise addition of 3-(pentafluorosulfanyl)benzoyl chloride (500.0 mg, 1.88 mmol, 1.0 equiv.). The reaction mixture was stirred at room temperature overnight then diluted with dichloromethane (5 mL) and the precipitate formed was discarded after gravity filtration. MP-Trisamine (520.0 mg, 3.00 mmol, 1.6 equiv.) was added to the filtrate and stirred for 3 hours after which the scavenger was removed by gravity filtration. The crude was purified over a column of silica (dichloromethane:methanol, 9:1) to



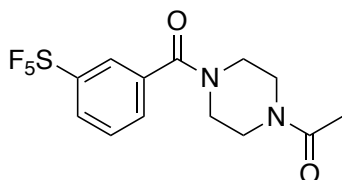
obtain a colourless solid as the title compound (317.0 mg, 53%).  $^1\text{H}$  NMR (600 MHz,  $\text{CDCl}_3$ )  $\delta$  7.75 – 7.71 (m, 2H, ArH), 7.50 – 7.43 (m, 2H, ArH), 3.75 – 3.63 (m, 4H,  $(\text{CH}_2)_2$ ), 3.57 – 3.26 (m, 4H,  $(\text{CH}_2)_2$ );  $^{13}\text{C}$  NMR (151 MHz,  $\text{CDCl}_3$ )  $\delta$  168.0 (C=O), 153.8 (p,  $J = 17.7$  Hz, ArCSF<sub>5</sub>), 136.2 (ArC), 130.1 (ArC), 129.1 (ArC), 127.2 (p,  $J = 4.5$  Hz, (ArC-CSF<sub>5</sub>)), 124.9 (p,  $J = 4.5$  Hz, ArC-CSF<sub>5</sub>), 66.6 (4C);  $^{19}\text{F}$  NMR (376 MHz,  $\text{CDCl}_3$ )  $\delta$  84.29 – 82.21 (m), 62.66 (d,  $J = 150.4$  Hz); LCMS Purity (UV) = 97%,  $t_{\text{R}}$  18.3 min; HRMS – ESI ( $m/z$ ) found 340.0384, calc. for  $[\text{C}_{11}\text{H}_{12}\text{F}_5\text{NO}_2\text{S}][\text{Na}]^+$ : 340.0401; IR (neat)  $\nu_{\text{max}}/\text{cm}^{-1}$  2858, 1644, 821; mp 63 – 64 °C.

### ***tert*-Butyl 4-(3-pentafluoro- $\lambda^6$ -sulfanyl benzoyl)piperazine-1-carboxylate (3.2d)**



To *N*-Boc piperazine (385.5 mg, 2.07 mmol, 1.1 equiv.), dissolved in dichloromethane (3 mL) was added triethylamine (247.0 mg, 2.44 mmol, 1.3 equiv.) and the mixture was stirred for a few minutes. HATU (787.2 mg, 2.07 mmol, 1.1 equiv.) was added to this solution followed by dropwise addition of 3-(pentafluorosulfanyl)benzoyl chloride (500.0 mg, 1.88 mmol, 1.0 equiv.) and the reaction mixture was stirred at room temperature overnight. After completion of the reaction, it was diluted with dichloromethane (10 mL) and the precipitate formed was removed by filtration. MP Trisamine (520 mg, 3 mmol, 1.6 equiv.) was added to the filtrate then removed by gravity filtration after 3 hours of stirring. The crude material was purified over a column of silica (dichloromethane:methanol, 9:1) to obtain a colourless solid as the title compound (573.0 mg, 73%).  $^1\text{H}$  NMR (600 MHz,  $\text{CDCl}_3$ )  $\delta$  7.81(m, 2H, ArH), 7.53 (m, 2H, ArH), 3.51 (m, 4H,  $(\text{CH}_2)_2$ ), 3.39 (m, 4H,  $(\text{CH}_2)_2$ ), 1.45 (s, 9H,  $(\text{CH}_3)_3$ );  $^{13}\text{C}$  NMR (151 MHz,  $\text{CDCl}_3$ )  $\delta$  168.4 (C=O), 154.5 (C=O), 154.0 (ArC-SF<sub>5</sub>), 136.3 (ArC), 130.1 (ArC), 129.2 (ArC), 127.4 (ArC-CSF<sub>5</sub>), 125.0 (ArC-CSF<sub>5</sub>), 80.5 (C), 47.5 (2C, m), 42.9 (2C, m), 28.3 (3C);  $^{19}\text{F}$  NMR (376 MHz,  $\text{CDCl}_3$ )  $\delta$  83.20 (m, F), 62.67 (d,  $J = 150.1$  Hz, 4F); LCMS Purity (UV) = 99%,  $t_{\text{R}}$  20.4 min. HRMS – ESI ( $m/z$ ) found 439.1078, calc. for  $[\text{C}_{16}\text{H}_{21}\text{F}_5\text{N}_2\text{O}_3\text{S}][\text{Na}]^+$ : 439.1085; IR (neat)  $\nu_{\text{max}}/\text{cm}^{-1}$  2977, 1685, 1626, 1243, 828; mp 153 – 155 °C.

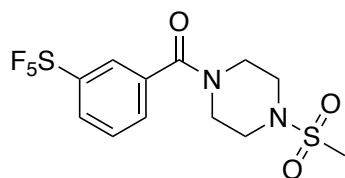
### **1-[4-[3-(Pentafluoro- $\lambda^6$ -sulfanyl)benzoyl]piperazin-1-yl]ethanone (3.2e)**



Compound **3.2d** (573 mg, 1.38 mmol, 1.0 equiv.) in dichloromethane (2 mL) was treated with HCl in dioxane (4M, 5.0 equiv.) overnight. The reaction mixture was concentrated in *vacuo* to afford the HCl salt, **3.2d'** (4-[3-(pentafluoro- $\lambda^6$ -sulfanyl)benzoyl]piperazin hydrochloride) as a colourless solid (376 mg, 92%).

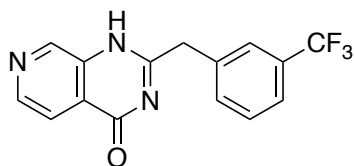
To **3.2d'** (0.100 g, 0.28 mmol, 1.0 equiv.), dissolved in THF (3 mL) was added triethylamine (0.028 g, 0.28 mmol, 1.0 equiv.) and stirred for 30 minutes. Acetic anhydride (0.028 g, 0.28 mmol, 1.0 equiv.) was added to the mixture and stirred overnight at room temperature. The reaction mixture was concentrated in *vacuo* and purified by flash chromatography (dichloromethane:methanol; 9:1) to obtain the pure product as a colourless oil (47.0 mg, 47%).  $^1\text{H}$  NMR (600 MHz,  $\text{CDCl}_3$ )  $\delta$  7.84 – 7.81 (m, 1H, ArH), 7.80 – 7.79 (m, 1H, ArH), 7.57 – 7.51 (m, 2H, ArH), 3.88 – 3.28 (m, 8H, ArH), 2.11 (s, 3H,  $\text{CH}_3$ );  $^{13}\text{C}$  NMR (151 MHz,  $\text{CDCl}_3$ )  $\delta$  169.3 (C=O, MeCO), 168.4 (C=O), 154.0 (t,  $^2J_{\text{FC}} = 18.0$  Hz, ArC), 136.0 (ArC), 130.2 (ArC), 129.3 (ArC), 127.7 – 127.4 (m, ArC), 125.0 (ArC), 47.4 (bs,  $\text{CH}_2$ ), 45.9 (bs,  $\text{CH}_2$ ), 42.4 (bs,  $\text{CH}_2$ ), 41.4 (bs,  $\text{CH}_2$ ), 21.3 ( $\text{CH}_3$ );  $^{19}\text{F}$  NMR (376 MHz,  $\text{CDCl}_3$ )  $\delta$  83.19 (p,  $J = 150.3$  Hz, F), 62.78 (d,  $J = 150.3$  Hz, 4F); LCMS Purity (UV) = 96%,  $t_{\text{R}}$  13.5 min; HRMS - ESI ( $m/z$ ) found 381.0662, calc. for  $[\text{C}_{13}\text{H}_{15}\text{F}_5\text{N}_2\text{O}_2\text{S}][\text{Na}]^+$ : 381.0667; IR (neat)  $\nu_{\text{max}}/\text{cm}^{-1}$  2917 (C-H), 1633 (C=O), 1322 (S=O), 821 (S-F).

### (3-Pentafluoro- $\lambda^6$ -sulfanyl phenyl)(4-(methylsulfonyl)piperazin-1-yl)methanone (**3.2f**)



To crude **3.2d'** (75 mg, 0.21 mmol, 1.0 equiv.), dissolved in THF (3 mL) was added triethylamine (21 mg, 0.21 mmol, 1.0 equiv.) and stirred for 30 min. Methylsulfonyl chloride (24 mg, 0.21 mmol, 1.0 equiv.) was added to the reaction mixture and stirred overnight at room temperature. The reaction was followed by TLC. After completion of the reaction, it was separated over dichloromethane (5 mL) and water (5 mL). The biphasic layers were passed through a hydrophobic frit to obtain the organic phase which was concentrated in *vacuo*. The crude was then purified over a column of silica, (dichloromethane:methanol; 3:2) to obtain the title compound as a colourless solid (66mg, 80%).  $^1\text{H}$  NMR (600 MHz,  $\text{CDCl}_3$ )  $\delta$  7.86 – 7.82 (m, 1H, ArH), 7.82 – 7.80 (m, 1H, ArH), 7.57 – 7.54 (m, 2H, ArH), 4.03 – 3.47 (m, 4H,  $\text{CH}_2$ ), 3.38 – 3.14 (m, 4H,  $(\text{CH}_2)_2$ ), 2.81 (s, 3H,  $\text{CH}_3$ );  $^{13}\text{C}$  NMR (151 MHz,  $\text{CDCl}_3$ )  $\delta$  168.4 (C=O), 154.2 – 153.8 (m, C-SF<sub>5</sub>), 135.7 (ArC), 130.2 (ArC), 129.4 (ArC), 127.8 – 127.6 (m, ArC), 125.2 – 125.0 (m, ArC), 47.4 ( $\text{CH}_2$ ), 45.5 (2C,  $(\text{CH}_2)_2$ ), 42.0 ( $\text{CH}_2$ ), 35.0 ( $\text{CH}_3$ );  $^{19}\text{F}$  NMR (376 MHz,  $\text{CDCl}_3$ )  $\delta$  83.32 (p,  $J = 150.4$  Hz, 1F), 62.96 (d,  $J = 150.4$  Hz, 4F); LCMS Purity (UV) = 98%,  $t_{\text{R}}$  15.6 min; HRMS - ESI ( $m/z$ ) found 417.0349, calc. for  $[\text{C}_{12}\text{H}_{15}\text{F}_5\text{N}_2\text{O}_2\text{S}][\text{Na}]^+$ : 417.0342; IR (neat)  $\nu_{\text{max}}/\text{cm}^{-1}$  2007 (C-H), 1616 (C=O), 1342 (S=O), 826 (S-F); mp 159 – 160 °C.

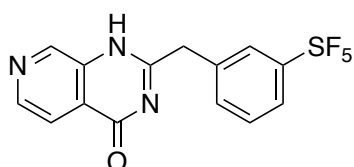
**2-{{3-(Trifluoromethyl)phenyl}methyl}-3H,4H-pyrido[3,4-d]pyrimidin-4-one (3.3c)**



To methyl 3-aminopyridine-4-carboxylate (100.0 mg, 0.66 mmol, 1.0 equiv.) in dichloromethane (5 mL) was added triethylamine (134.0 mg, 1.32 mmol, 2.0 equiv.) followed by dropwise addition of 3-(trifluoromethyl)phenyl acetyl chloride (220.0 mg, 0.99 mmol, 1.5 equiv.). The reaction mixture was stirred at room temperature for 48 h and monitored by TLC. After 48 h, it was diluted by dichloromethane (10 mL), washed with 2M HCl (10 mL x 3) and the aqueous layer was extracted with dichloromethane (25 mL). Combined organic layers were washed with sodium bicarbonate (25 mL), brine (15 mL x 3), dried over MgSO<sub>4</sub>, filtered and concentrated in *vacuo*. The crude material was purified over a column of silica (dichloromethane:methanol; 19:1) to obtain a colourless solid, **3.3i**, (144 mg, 65%). The product was then refluxed with 7M ammonia in methanol (10 mL) for 48 hours. The crude was diluted with dichloromethane (15 mL) and washed with 2M HCl (10 mL x 2). The combined organic layers were dried over MgSO<sub>4</sub>, filtered, and concentrated in *vacuo*. The crude was purified over a column of silica (dichloromethane:methanol; 97:3) to obtain the title compound as a colourless solid (30 mg, 23%). The pure product was crystallised using diffusion method (hexane:dichloromethane). Crystallization of **3.3c** was achieved by soaking it in minimum amount of dichloromethane.

<sup>1</sup>H NMR (600 MHz, (CD<sub>3</sub>)<sub>2</sub>SO) δ 12.79 (s, 1H, NH), 8.94 (s, 1H, ArH), 8.59 (d, *J* = 5.1 Hz, 1H, ArH), 7.89 (d, *J* = 5.1 Hz, 1H, ArH), 7.77 (s, 1H, ArH), 7.67 (d, *J* = 7.8 Hz, 1H, ArH), 7.62 (d, *J* = 7.8 Hz, 1H, ArH), 7.58 – 7.52 (m, 1H, ArH), 4.08 (s, 2H, CH<sub>2</sub>); <sup>13</sup>C NMR (151 MHz, CD<sub>3</sub>OD) δ 161.5 (C=O), 158.1 (ArC), 149.8 (ArC), 145.1 (ArC), 143.9 (ArC), 136.7 (ArC), 132.5 (ArC), 130.6 (q, <sup>2</sup>*J*<sub>FC</sub> = 32.0 Hz, ArC-CF<sub>3</sub>), 129.2 (ArC), 126.4 (ArC), 125.5 (q, <sup>3</sup>*J*<sub>FC</sub> = 4.0 Hz, ArC), 124.2 (q, <sup>1</sup>*J*<sub>FC</sub> = 271.4 Hz, ArC), 123.7 (q, <sup>3</sup>*J*<sub>FC</sub> = 4.0 Hz, ArC), 118.4 (ArC), 40.5 (CH<sub>2</sub>); <sup>19</sup>F NMR (376 MHz, CDCl<sub>3</sub>) δ -62.71 (s, 3F); HRMS – ESI (*m/z*) found 306.0845, calc. for [C<sub>15</sub>H<sub>10</sub>F<sub>3</sub>N<sub>2</sub>O][H]<sup>+</sup>:306.0869; LCMS Purity (UV) = 90%, *t*<sub>R</sub> 14.9 min; IR (neat) *v*<sub>max</sub>/cm<sup>-1</sup>: 2769 (NH), 1704 (C=O), 1329 (CF<sub>3</sub>).

**2-{{3-(Pentafluoro-λ<sup>6</sup>-sulfanyl)phenyl}methyl}-3H,4H-pyrido[3,4-]pyrimidin-4-one (3.3d)**



To 2-[3-(pentafluoro- $\lambda^6$ -sulfanyl)phenyl]acetic acid (120.0 mg, 0.46 mmol, 1.0 equiv.) was added thionyl chloride (201.0  $\mu$ L, 2.76 mmol, 6 equiv.) and 2 drops of DMF. The reaction was refluxed under argon overnight. The reaction was followed by LCMS and following completion of the reaction, it was concentrated in *vacuo* to obtain **3.3d'** (2-[3-(pentafluoro- $\lambda^6$ -sulfanyl)phenyl]acetyl chloride). The crude was taken through to the following steps without purifications (115 mg, 0.4 mmol).

To methyl 3-aminopyridine-4-carboxylate (41.0 mg, 0.27 mmol, 1.0 equiv.) in dichloromethane (5 mL) was added triethylamine (55.0 mg, 0.54 mmol, 2.0 equiv.) followed by dropwise addition of **3.3d'** (115.0 mg, 0.40 mmol, 1.5 equiv.). The reaction mixture was stirred at room temperature for 48 h and monitored by TLC. After 48 h, it was diluted with dichloromethane (10 mL), washed with 2M HCl (10 mL x 3) and aqueous layer extracted with dichloromethane (25 mL). Combined organic layers were washed with sodium bicarbonate (25 mL), brine (15 mL x 3), dried over MgSO<sub>4</sub>, filtered and concentrated in *vacuo*. The crude was purified over a column of silica (dichloromethane:methanol; 19:1) to obtain a colourless solid, **3.3ii**, (144 mg, 65%). **3.3ii** was then refluxed with 7M ammonia in methanol (10 mL) for 48 hours. The crude was diluted with dichloromethane (15 mL) and washed with 2M HCl (10 mL x 2). The combined organic layers were dried over MgSO<sub>4</sub>, filtered, and concentrated in *vacuo*. The crude was purified over a column of silica (dichloromethane:methanol; 97:3) to obtain the title compound as a colourless solid (9 mg, 25%). <sup>1</sup>H NMR (600 MHz, CDCl<sub>3</sub>)  $\delta$  11.85 (s, 1H, NH), 9.20 (s, 1H, ArH), 8.76 (d,  $J$  = 5.1 Hz, 1H, ArH), 8.05 (d,  $J$  = 5.1, 1H, ArH), 7.97 (dd,  $J$  = 8.0 Hz, 1.9 Hz, 1H, ArH), 7.71 – 7.67 (m, 1H, ArH), 7.64 (d,  $J$  = 7.7 Hz, 1H, ArH), 7.49 – 7.44 (m, 1H, ArH), 4.19 (s, 2H, CH<sub>2</sub>); <sup>13</sup>C NMR (151 MHz, CDCl<sub>3</sub>)  $\delta$  161.7 (C=O), 156.0 (ArC), 154.3 – 153.7 (m, ArC-SF<sub>5</sub>), 151.1 (ArC), 146.3 (ArC), 143.5 (ArC), 136.2 (ArC), 132.3 (ArC), 129.2 (ArC), 126.8 (m, ArC), 126.0 (ArC), 125.1 (m, ArC), 118.1 (ArC), 41.5 (C).

<sup>19</sup>F NMR (376 MHz, CDCl<sub>3</sub>)  $\delta$  87.64 – 85.94 (p,  $J$  = 148.4 Hz, 1F), 65.21 (d,  $J$  = 148.4 Hz, 4F); HRMS-ESI ( $m/z$ ) found 364.0543, calc. for [C<sub>14</sub>H<sub>10</sub>F<sub>5</sub>N<sub>3</sub>OS][H]<sup>+</sup>:364.0527; LCMS Purity (UV) = 92%,  $t_R$  16.18 min; IR (neat)  $\nu_{max}/cm^{-1}$ : 2854 (NH), 1672 (C=O), 834 (SF<sub>5</sub>).

## Chapter 4.0 SF<sub>5</sub>-Substituted Oxindole Scaffolds as Kinase Inhibitors

### 4.1 Introduction

The oxindole scaffold is ubiquitously found in the tissues and body fluids of mammals, as well as in many natural products and biologically active compounds.<sup>143</sup> One of its many applications comprises antitumor activity by inhibiting tyrosine receptors such as PDGFR (platelet-derived growth factor receptor), VEGFR (vascular endothelial growth factor receptor), etc.<sup>144</sup>

Protein kinases are enzymes that catalyse the transfer of a  $\gamma$ -phosphate of adenosine triphosphate (ATP, Figure 4.1) often to a hydroxyl residue of a protein leading to a structural change in the protein and an intracellular signal.<sup>145</sup> They are part of a huge superfamily and many kinases and isoforms exist. The human kinome contains 518 protein kinases that are classified according to the amino acid residue they phosphorylate.<sup>146</sup> Most kinases recognise serine/threonine residue known as serine/threonine kinases (STK). Another major class of kinases are tyrosine kinases (TK) and as the name implies, they phosphorylate tyrosine specifically. However, tyrosine phosphorylation is relatively rare (1.8 %) compared to serine (86.4%) and threonine (11.8%) phosphorylation.<sup>147</sup> A few kinases, known as dual-specificity tyrosine phosphorylation-regulated kinases (DYRK), phosphorylate on both tyrosine and serine/threonine amino acid side residues.<sup>148</sup>

Oxindole scaffolds are widely used as protein kinase inhibitors as the NH-C=O groups form hydrogen bonds with the backbone of the hinge segment of the kinase ATP binding domain.<sup>149</sup> Of these oxindoles, 3-pyrrolylmethylidene oxindoles are of particular interest as they inhibit receptor tyrosine kinases (Figure 4.1).<sup>150,151</sup>

Tyrosine kinases are cell surface receptors with receptor tyrosine kinase (RTK) part of the larger family of protein tyrosine kinases.<sup>152</sup> These consist of epidermal growth factor receptor (EGFR), nerve growth factor receptor (NGFR), platelet-derived growth factor receptor (PDGFR), vascular endothelial growth factor receptor (VEGFR), fibroblast growth factor receptor (FGFR), insulin receptor, and insulin like growth factor receptor (IGFR).<sup>146</sup>

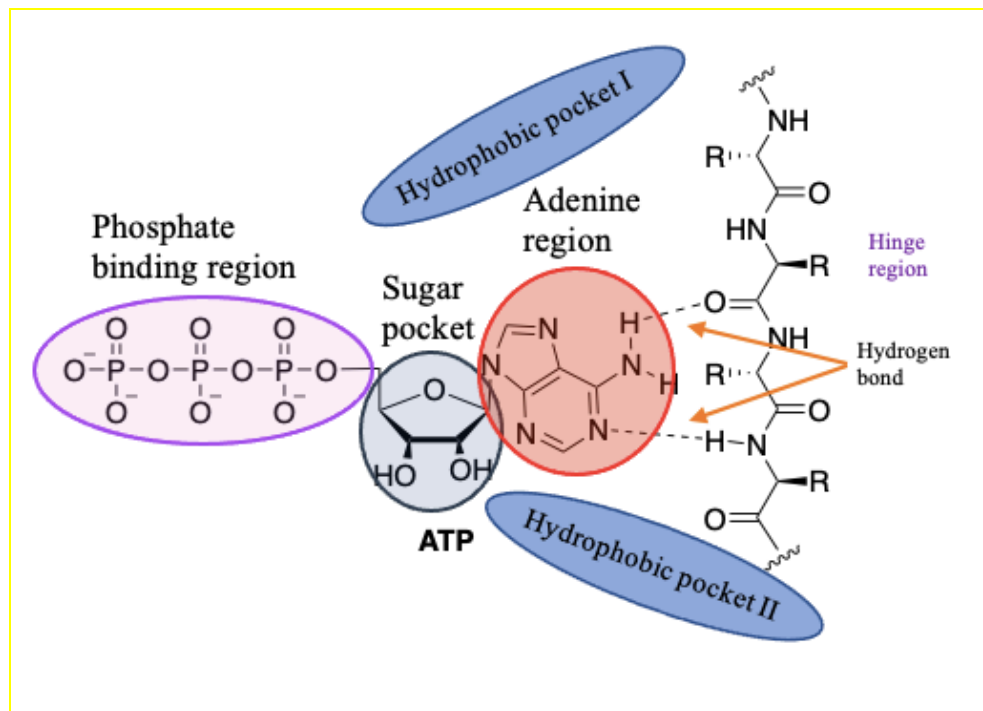


Figure 4.1: ATP binding mode

All RTKs consist of an extracellular domain encompassed with a ligand-binding site, a hydrophobic transmembrane  $\alpha$ -helix, and a cytosolic domain containing a protein-tyrosine kinase activity region (Figure 4.2).<sup>153</sup> Most RTKs dimerise in response to growth factor ligand binding. A protein kinase of each receptor monomer phosphorylates a distinct set of tyrosine dimer pairs. This process is termed autophosphorylation. Protein domains, Src homology-2 (SH2) and phosphotyrosine-binding (PTB) domains recognise phosphotyrosine and bind to them. Binding of these protein domains to an activated RTK allows simultaneous activation of multiple intracellular signalling pathways.<sup>154</sup> Ultimately, this causes a cellular response.<sup>155</sup>

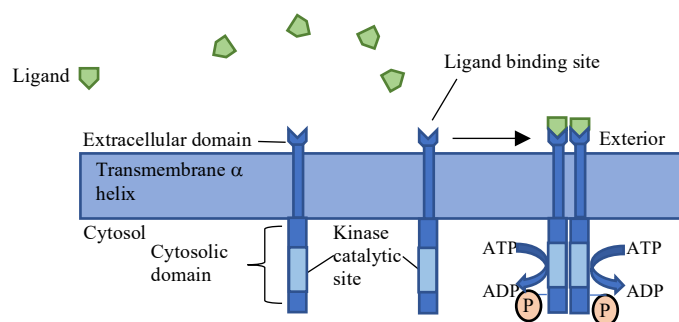


Figure 4.2: RTK autophosphorylation

RTK activation regulates various biological processes like cell growth and cell survival. Dysregulation of RTKs caused by mutation is related to development and progression of many human cancers. Therefore, RTKs are an attractive therapeutic target. Small molecule RTK inhibitors can modify the dysregulated functions of the receptors by directly inhibiting the tyrosine kinase activity. They achieve inhibition by mimicking the binding mode of the ATP molecule. Growth factors are signalling proteins that regulate cell growth and survival from conception to death. Some growth factors are considered hormones and those that regulate cell growth are classified

as growth factors. They act in three ways: mitogens induce cell proliferation, trophic factors promote growth and survival factors inhibit apoptosis. Growth factors can have multiple effects in the same cell or different roles in different cells. Abnormalities in growth factor signalling is the basis of many types of cancers. Major growth factor families that will be mentioned in this chapter and their biological activity are summarised in Table 4.1

<b>Signalling molecule</b>	<b>Major biological activity</b>
<b>Neurotrophins</b>	
Nerve growth factor (NGF)	Neuronal differentiation and survival
<b>Epidermal growth factor (EGF)</b>	Cell proliferation
<b>Fibroblast growth factor (FGF)</b>	Repair and regeneration of tissues
<b>Transforming growth factor (TGF)-<math>\beta</math> family</b>	
Bone morphogenetic proteins (BMP) (>30)	Osteogenesis
<b>Platelet-derived growth factor (PDGF) family</b>	
PDGF	Tissue repair
Vascular endothelial growth factor (VEGF)	Regulation of vascular development
<b>Hematopoietic growth factors</b>	
Stem cell factor (KIT) FMS like tyrosine kinase 3 ligand (FLT3)	Cell survival and proliferation
<b>Insulin like growth factor</b>	Fetal growth, mitogenic, glucose homeostasis

*Table 4.1: Growth factor families and their biological activity*

Prominent oxindole based small molecule kinase inhibitors include nintedanib, which acts as triple kinase inhibitor with activity against vascular endothelial growth factor receptor (VEGFR), fibroblast growth factor receptor (FGFR) and platelet-derived growth factor receptor (PDGFR) kinases resulting in angiogenesis inhibition, suppressed vascularization and proliferation of tumour tissues causing starvation and death of tumour cells. Other triple kinase inhibitors of VEGFR, FGFR and PDGFR kinases are orantinib (SU 6668) and SU4984. The latter specifically inhibits FGFR1 with an  $IC_{50}$  of 10-20  $\mu$ M.<sup>156</sup> Sunitinib is a multitargeted tyrosine kinase inhibitor that inhibits VEGFR-1, VEGFR-2, c-KIT (stem-cell factor receptor), FLT3 (FMS like tyrosine kinase 3), PDGFR $\alpha$  and PDGFR $\beta$  in both biochemical and cellular assays. It is an FDA approved treatment for advanced renal cell cancer and imatinib-resistant gastrointestinal stromal tumours. Semaxanib was the first pyrrole indoline-2-one to be tested clinically as a potent inhibitor of VEGFRs and PDGFRs for anti-angiogenesis properties. It selectively inhibits VEGFR. It had proceeded to clinical studies but was halted due to toxicity issues (Figure 4.3).

Angiogenesis is the development of new blood vessels from the existing vascular system<sup>157</sup> whereas vasculogenesis is the *de novo* formation of primitive vascular network.<sup>158</sup>

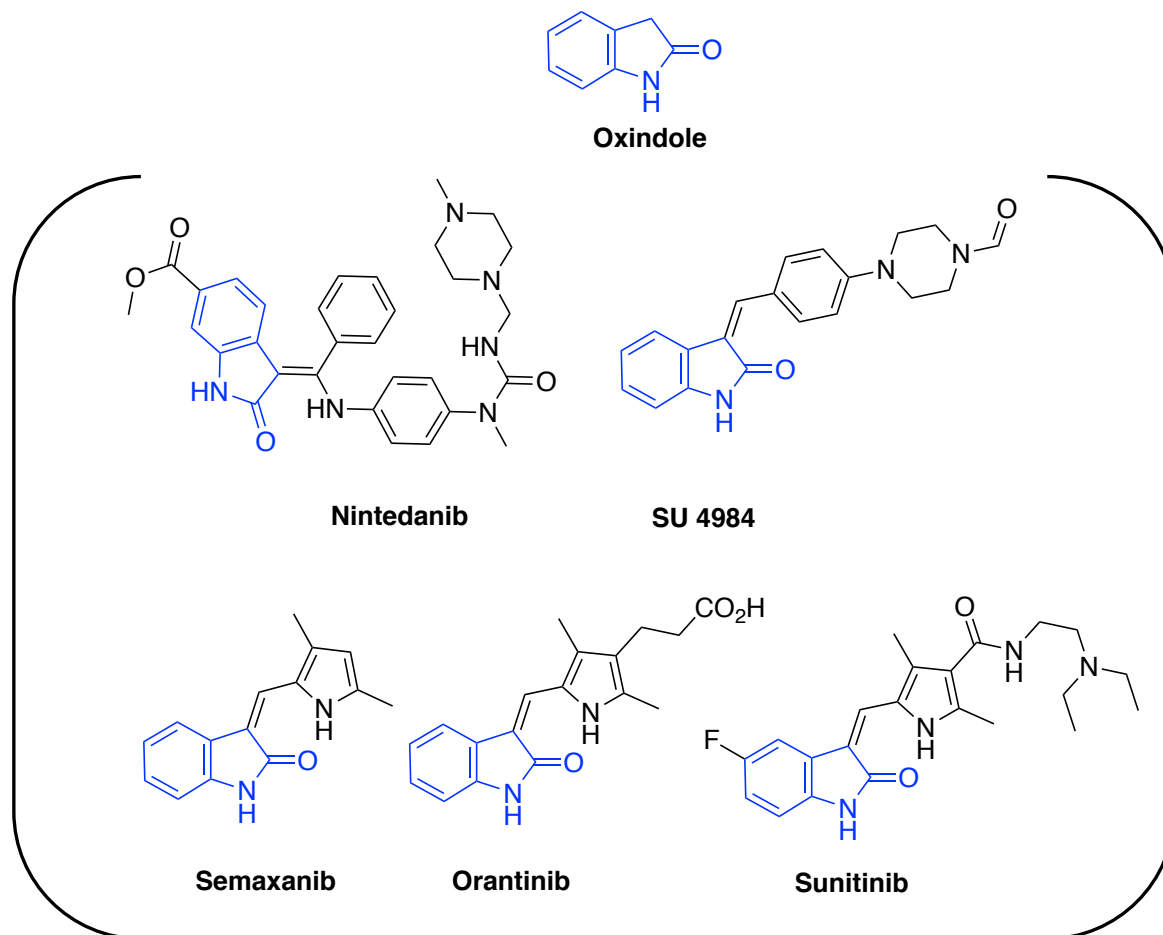


Figure 4.3: Oxindole-based RTKIs

The C5 and C6 carbons of the oxindole moiety on the pyrrole indoline-2-one derivatives occupy a hydrophobic pocket, hydrophobic pocket II, in the ATP binding site. Therefore, modification of highly active pyrrole indoline-2-one derivatives at these positions is common.

In 2017, Sansook. et al<sup>159</sup>, from the Spencer group, published their work on oxindole-based kinase inhibitors containing a pentafluorosulfonyl moiety at positions C5 and C6. Their compounds were tested against a panel of protein kinases following which a few compounds showing low nM potency against bone morphogenic protein-2 inducible gene (BMP2K), PDGFR2, PDGFR $\alpha$ , and VEGFR3 were identified. The structures and respective IC<sub>50</sub> are shown in Figure 4.4. BMP-2 comes under the transforming growth factor- $\beta$  (TGF- $\beta$ ) superfamily and binds to serine-threonine kinase receptor type II unlike PDGFR and VEGFR.



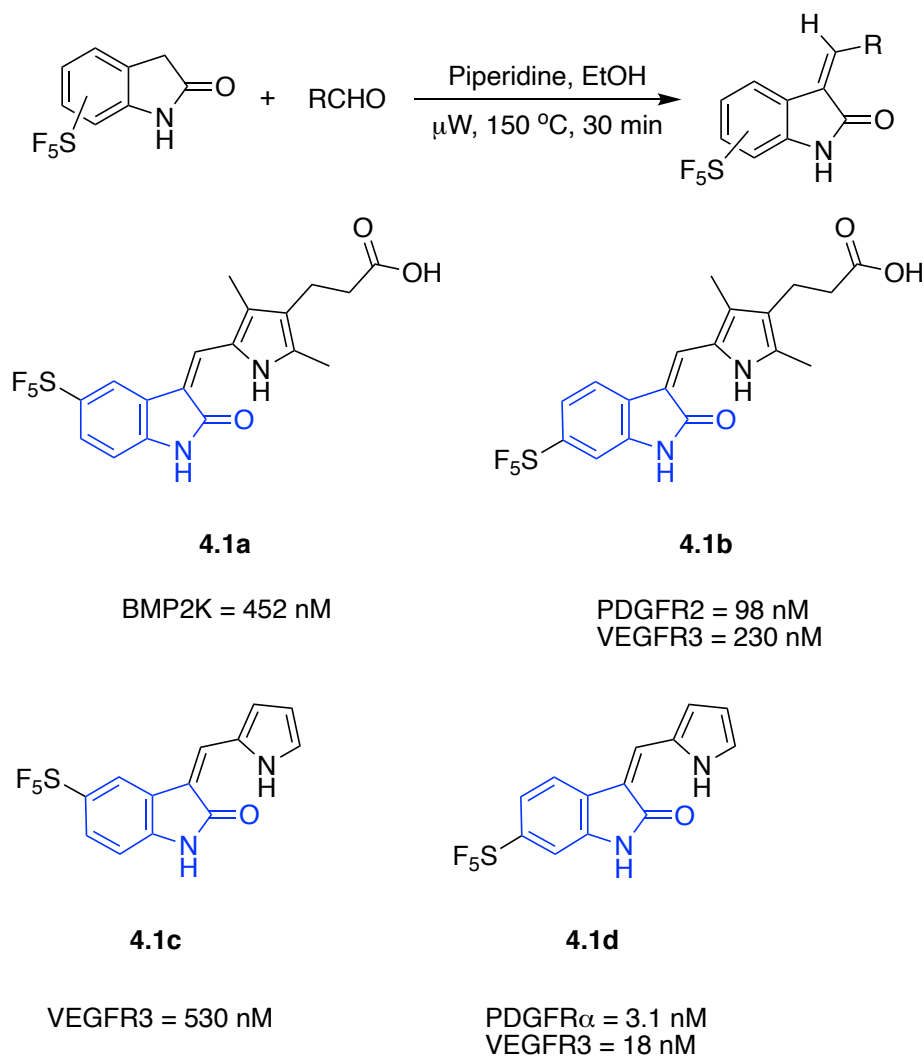


Figure 4.4: Oxindole-based kinase inhibitors with  $IC_{50}$  values

In addition to being potent RTK inhibitors, oxindoles and spirooxindoles are credited to have a wide range of applications in medicinal chemistry.<sup>160,161</sup> Spirocyclic compounds are both conformationally rigid and flexible. Their rigidity make them an ideal substituent when absorption and permeability of a molecule is restricted.<sup>162</sup> On the other hand they are more flexible compared to flat aromatic heterocycles and can adapt to many a variety of proteins.<sup>162</sup> Spirooxindoles are found as core structures of many naturally occurring alkaloids such as mitraphylline, horsfiline, etc with encouraging pharmacological activity (Figure 4.5).

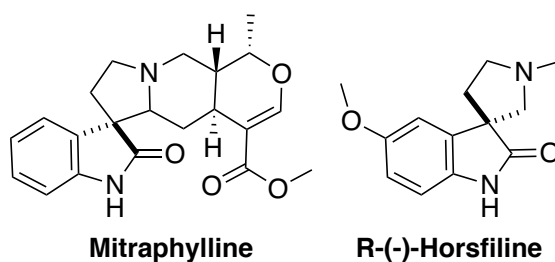


Figure 4.5: Spirocyclic oxindoles in nature

Besides antiproliferative activity, they possess antiviral, antifungal, antibacterial and antihypertensive activities.<sup>143</sup> In this study we synthesised five more SF<sub>5</sub> containing oxindoles and a nitro-substituted analogue, to widen the range of SF<sub>5</sub> containing biologically active scaffolds. In addition biological activity of Semaxanib was compared with two novel SF<sub>5</sub>-analogues of Semaxanib.

## 4.2 Results and discussion

### 4.2.1 Synthesis

Figure 4.6 demonstrates the oxindoles synthesised by a microwave assisted Knoevenagel reaction. Yields and conditions are shown in Table 4.2.

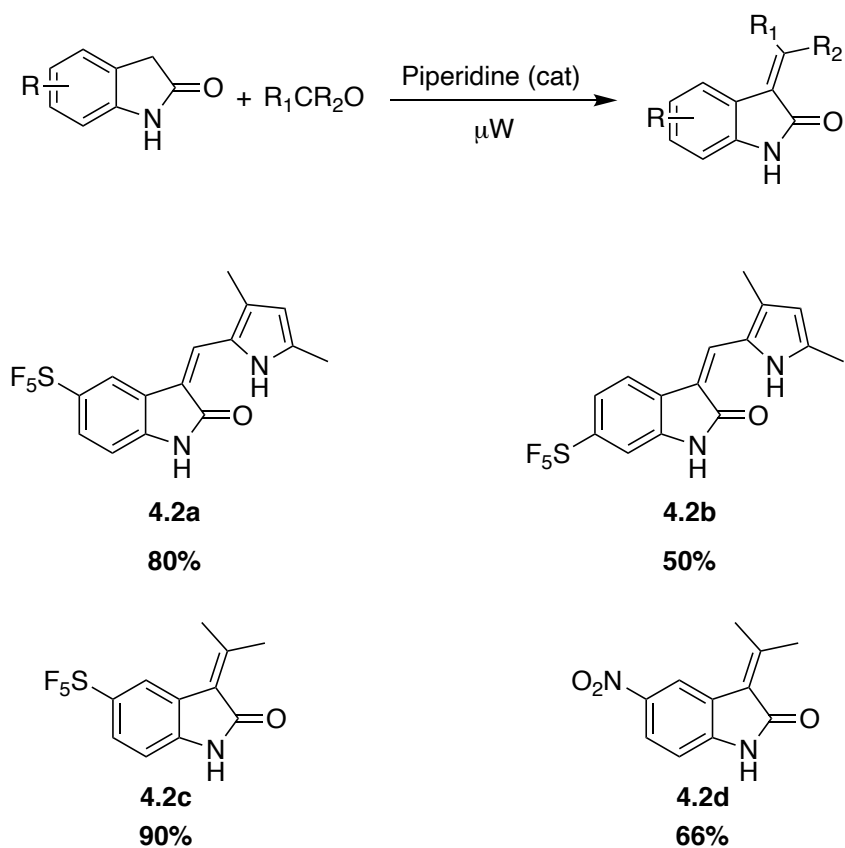


Figure 4.6:  $\mu W$ -mediated Knoevenagel synthesis

Entry	Temperature °C	Solvent	Time (min)	Product yield (%)
1	150	Ethanol	30	4.2a (80)
2	150	Ethanol	30	4.2b (50)
3	100	Acetone	20	4.2c (90)
4	100	acetonitrile	20	4.2d (66)

Table 4.2: Various conditions for MW-mediated Knoevenagel

Sansook. *et. al.*'s microwave-mediated Knoevenagel condensation conditions (Figure 4.4) were followed to synthesise compounds **4.2a** and **4.2b**. For entries 3 and 4, the conditions were slightly modified. Compound **4.2c** was synthesised with an excess of acetone to dissolve the reaction components. In this case acetone acted both as a solvent and a reagent. Soon after combining the oxindole, acetone and piperidine, product was observed, which precipitated out of the solution as an orange solid. Nevertheless, the reaction mixture was microwave irradiated until completion of the reaction, i.e. 20 min, as monitored by TLC. Following a simple work-up, the pure product was obtained at 90% yield and was crystallised in acetone, affording single crystals suitable for X-ray structure determination (Figure 4.7).

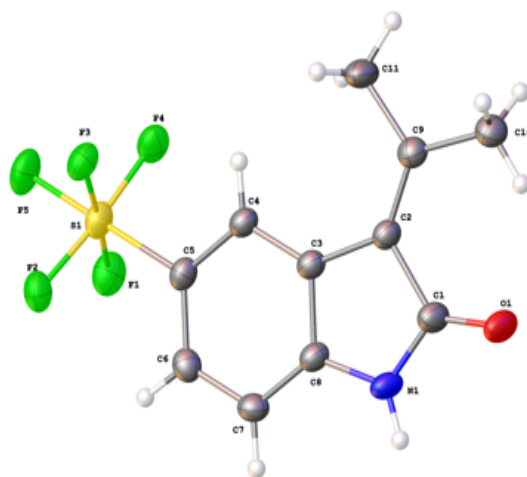


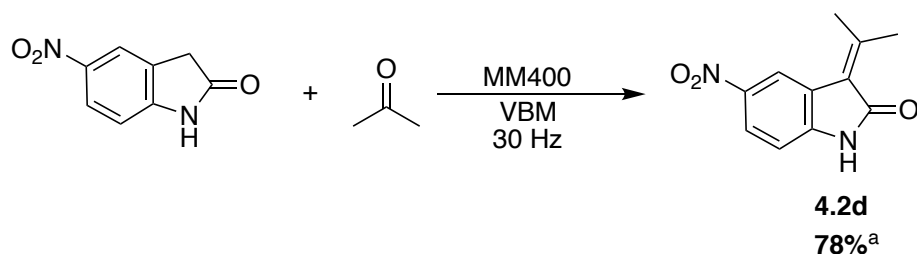
Figure 4.7: X-ray structure of **4.2c**

Upon realising that simple Knoevenagel products could be recrystallised using acetonitrile, **4.2d** was synthesised in acetonitrile and the crude was recrystallised in the same solvent, yielding pure product in 68% yield. A quick search in the literature revealed the same reaction carried out in acetone by stirring for 14 hours at room temperature to obtain 86% yield.<sup>163</sup> The purity of the compound was not reported. We then attempted the synthesis of **4.1c** in acetonitrile at 100 °C for 20 minutes in the microwave as opposed to the initial synthesis in ethanol at 150 °C by Sansook *et al.* Purification of **4.1c** was not as simple as the prior mentioned compounds. When synthesised in acetonitrile, we observed both *Z* and *E* isomers in the <sup>1</sup>H NMR spectrum of the crude mixture in an approximate 9:1 ratio. However, the *E*-isomer could not be isolated from the mixture. The crude product was subjected to reverse phased column chromatography followed by normal phased column to obtain pure *Z* isomer in 77% yield. The <sup>1</sup>H NMR spectrum of the product was compared with the reported literature spectrum to confirm its configuration. Equilibrium between *Z* and *E* isomers has been reported in polar solvents or in the presence of light.<sup>164</sup> *E* isomers of pyrrole indoline-2-one derivatives are known to convert back into their respective *Z* isomers in the dark, perhaps due to the intramolecular hydrogen bonding between the carbonyl oxygen and NH group of the pyrrole ring.<sup>165</sup> Pyrrole indoline-2-one derivatives predominantly exists as *Z* isomers due to this intramolecular hydrogen bonding. A NOESY experiment would confirm the configuration by showing interaction between

the proton at C4 position and the vinyl proton.<sup>166</sup> A study which investigated isomerisation of 3-substituted indolin-2-ones revealed that pyrrole indoline-2-ones with no *N*-substitution on the pyrrole are isolated as *Z*-isomers and are converted to *E*-isomers after exposure to fluorescent light.<sup>165</sup> As occurrence of isomerisation is also reported while in solution, we came to a conclusion that part of **4.1c** isomerised into its *E*-isomer while in solution in the NMR tube (exposed to light) rather than the method of synthesis producing a mixture of isomers. Another drawback of using acetonitrile as the solvent is that it could potentially react with the ketone or aldehyde to give an additional Knoevenagel condensation product.<sup>167</sup>

The synthesis of 3-pyrrolylmethylidene oxindoles in acetonitrile using the aforementioned conditions were not considered favourable as two column purifications were needed to obtain the pure product. Sansook *et al*'s conditions provided pure **4.1c** in 74% yield following a normal phase column. Therefore compounds **4.2a** and **4.2b** were synthesised following the said method.

Mechanochemical synthesis is another attractive method that is an environmentally friendly alternative for traditional routes. It provides mild/short reaction conditions, simplicity and often solvent-free conditions.<sup>168</sup> Mechanochemical Knoevenagel condensation is a known method of synthesis.<sup>169,170</sup> We attempted the synthesis of **4.2d** in a vibratory ball mill (VBM, Scheme 4.1). Table 4.4 shows various conditions utilized for the synthesis. Reactions were attempted in steel jars (SST) and zirconium oxide jars (ZrO<sub>2</sub>); with and without catalyst, and for various reaction times. Under mechanochemical conditions, reactions performed in the absence of catalyst did not yield any product. Zirconia jars were best suited for mechanochemical Knoevenagel condensation as opposed to steel jars. Zirconia is extremely hard<sup>171</sup> and chemically inert.<sup>172</sup> These jars provide high impact and iron free milling. Steel jars are also able to provide high impact milling. However, grinding in steel jars can result in iron contaminated product. The <sup>1</sup>H NMR spectra of crude reaction mixtures from steel jars tend to be highly noisy due to the presence of paramagnetic iron particles.<sup>173</sup>



Scheme 4.1: Mechanochemical Knoevenagel condensation, a: Following conditions in Entry 5 from Table 4.4

Entry	Jar	No of balls	Time (min)	Catalyst	% conversion by $^1\text{H}$ NMR (product:starting material)
1	SST (10 mL)	1	180	-	-
2	SST (10 mL)	1	60	Piperidine	16:84
3	SST (10 mL)	1	90	Piperidine	44:56
4	ZrO <sub>2</sub> (25 mL)	1	90	-	-
5	ZrO <sub>2</sub> (25 mL)	1	90	Piperidine	100:0

Table 4.3: Various conditions used for mechanochemical Knoevenagel synthesis

**4.2d** synthesised via ball milling under conditions in entry 5, yielded 78% of pure product (by  $^1\text{H}$  NMR) as a brown solid without further purifications. Figure 4.8 shows the proton NMR of **4.2d** in DMSO following mechanochemical synthesis. As expected the NMR shows three aromatic protons between 6.98 ppm and 8.27 ppm, two aliphatic peaks between 2.41 and 2.54 ppm with each peak integrating to three protons and an NH peak at 11.14 ppm.

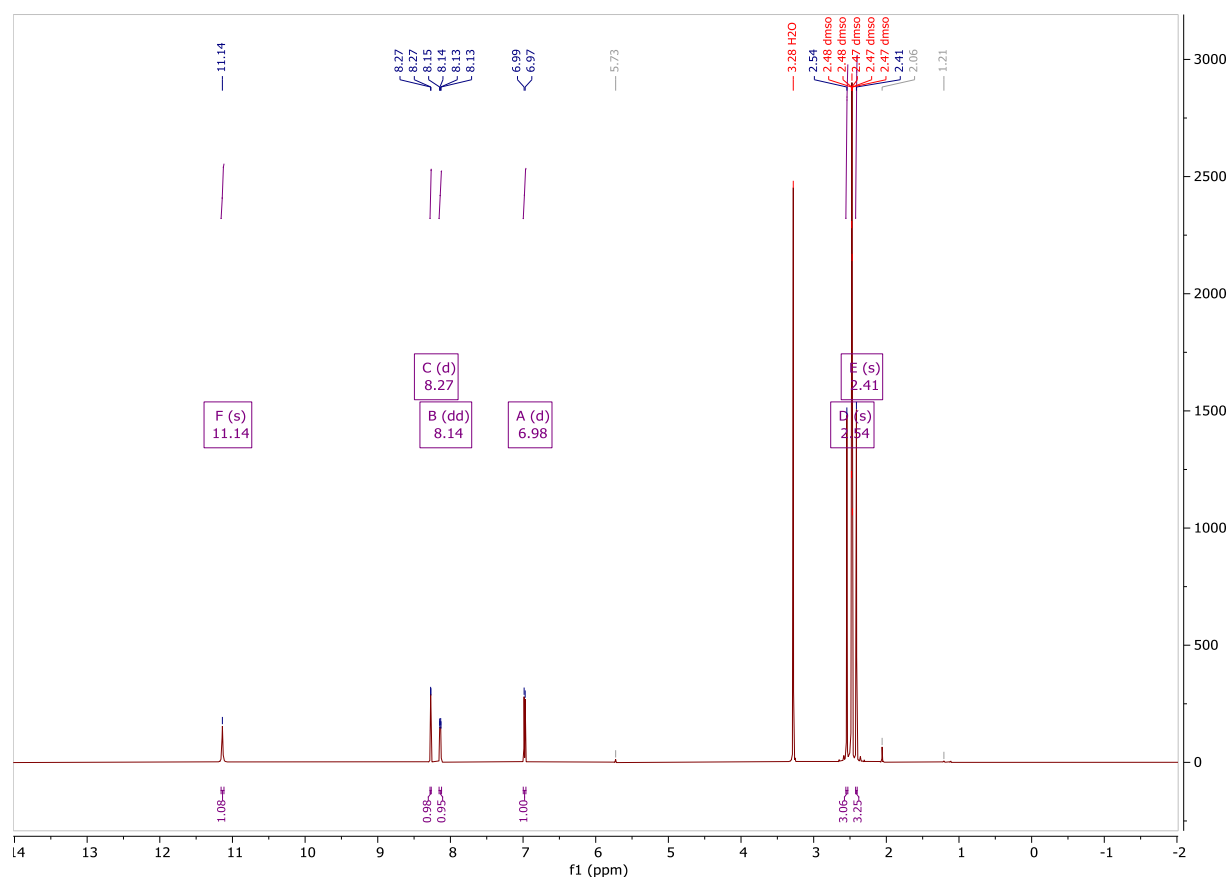
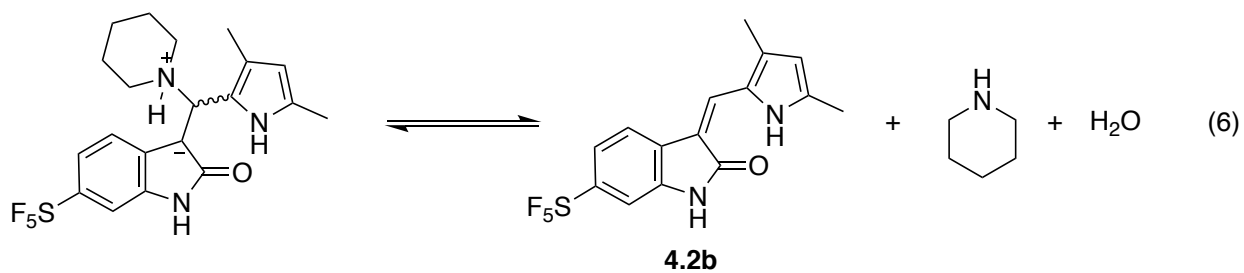
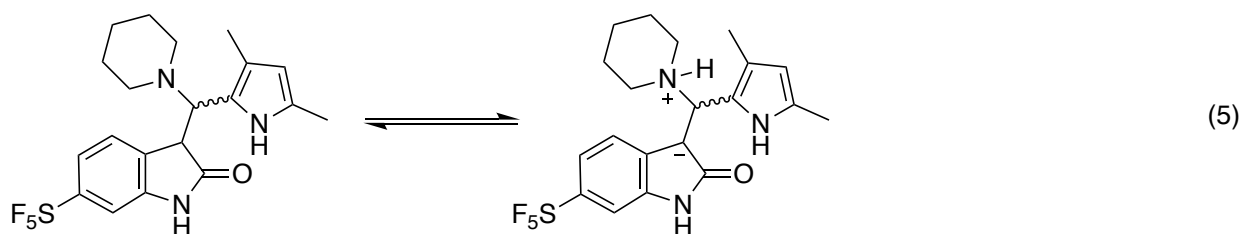
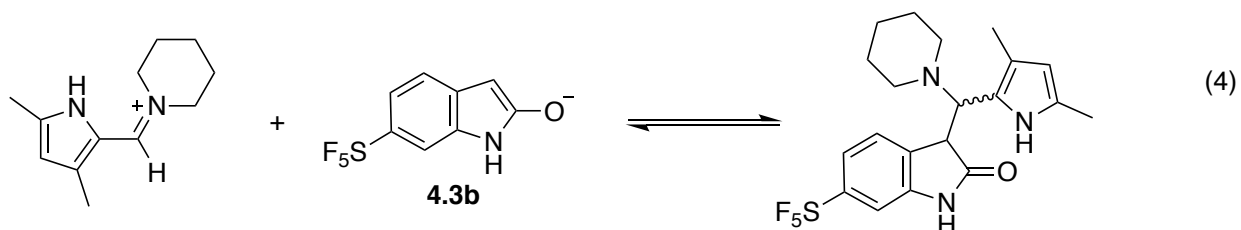
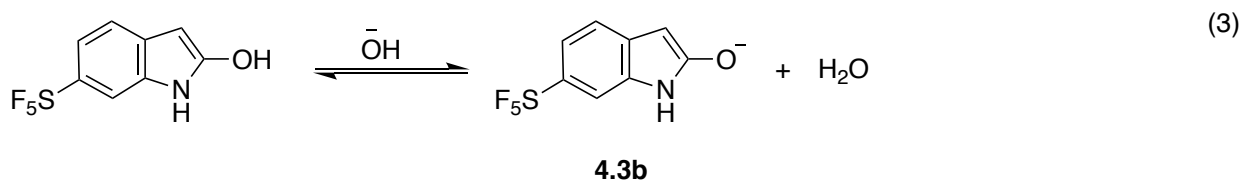
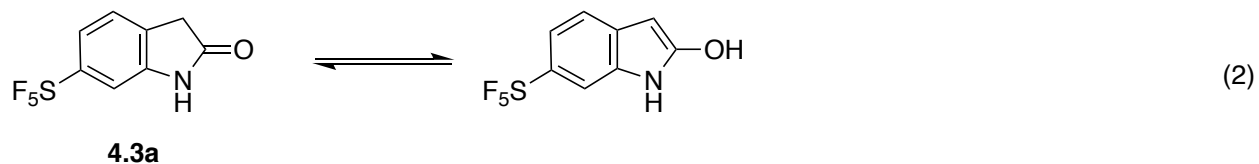
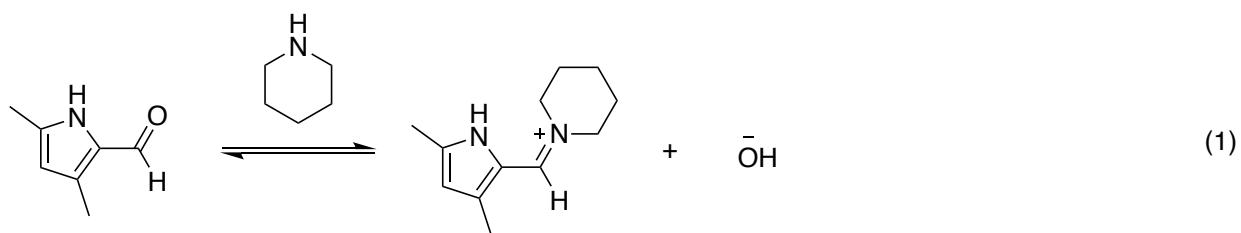


Figure 4.8: Proton NMR of **4.2d** from ballmill experiment (entry 5)

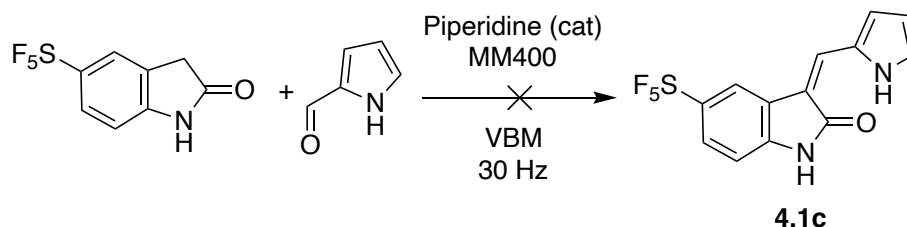
Scheme 4.2 shows the reaction steps of mechanism of the piperidine catalysed Knoevenagel condensation. Ellen V. Dalessandro et. al. proposed a mechanism for the piperidine catalysed Knoevenagel condensation reaction which proceeds via deprotonation of acetyl acetone (pKa 8.93) by piperidine (pKaH 11.28) to generate the nucleophile which attacks the respective iminium.<sup>174</sup> In

the following mechanism, we have proposed the formation of an enolate which would serve as the nucleophile. The keto-enol tautomerisation occurs readily in solvent and when combined with simple ketones like acetone, the reaction proceeds spontaneously under room temperature.



Scheme 4.2: Reaction steps of the mechanism of the piperidine catalysed Knoevenagel condensation

Subsequently, the synthesis of **4.1c** was also attempted under mechanochemical conditions in a zirconia jar. However the reaction did not yield any product (Scheme 4.3). Unlike the aforementioned reaction, both reactants were in the solid state.



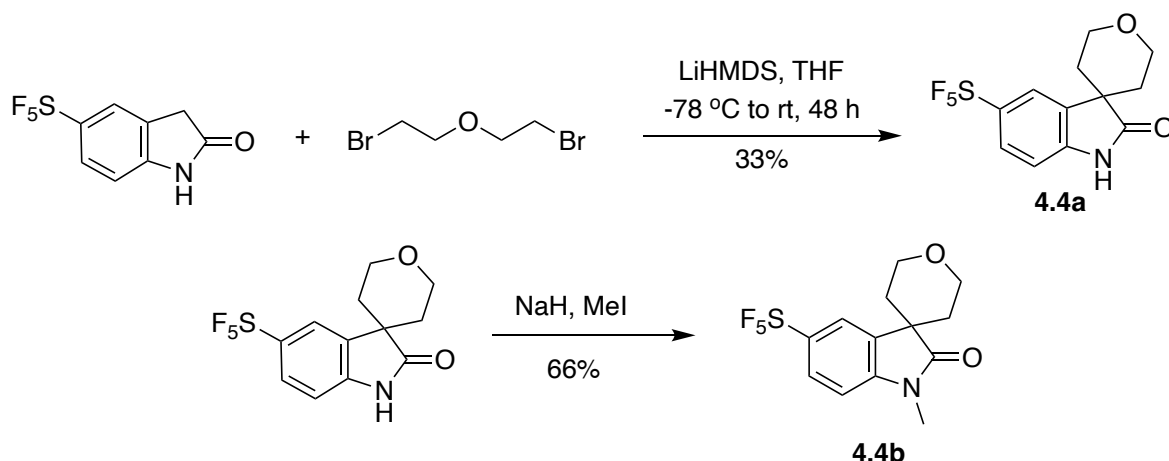
*Scheme 4.3: Mechanochemical synthesis of 4.1c*

Often, solids clump together preventing proper mixing of the reagents. Introducing a liquid additive in  $\mu\text{L}$  amounts; known as liquid assisted grinding (LAG) can circumvent this issue.<sup>56,175</sup> The solvent acts as a lubricant and enhances overall mixing and reaction kinetics.<sup>56</sup> We reasoned that Liquid assisted grinding (LAG) could be a better option for Knoevenagel condensations when the starting materials are in the solid state. Temperature might have been another factor that impeded the formation of **4.1c**. Temperature cannot be controlled while using a vibratory ball miller. It is solely dependent on the energy released during the milling process. For reagents with high melting points such as 5-pentafluorosulfanyl-2-oxindole (mp: 179–181 °C)<sup>176</sup>, higher temperatures might be required to activate mixing.

Further investigation on the mechanochemical Knoevenagel synthesis was not carried out due to time limits. Regardless, the synthesis of 3-substituted oxindoles via a mechanochemical route has proven to be a viable and environmentally friendly option.



Synthesis of the spirocyclic oxindoles **4.4a** and **4.4b** proceeded via different routes to the above mentioned oxindoles (Scheme 4.4).



*Scheme 4.4: Synthesis and N-methylation of spirocyclic oxindole*

Compound **4.4a** was synthesised adopting a method published for the synthesis of non-substituted spirooxindole.<sup>177</sup> Condensation of 5-SF<sub>5</sub>-2-oxindole and 2-bromoethyl ether was performed in the presence of an organic base, LiHMDS, in THF to obtain **4.4a** in 33% yield. Figure 4.9 shows the crystal structure of **4.4a**. The latter was subsequently methylated by MeI in the presence of NaH to obtain **4.4b** in moderate yields (66%).

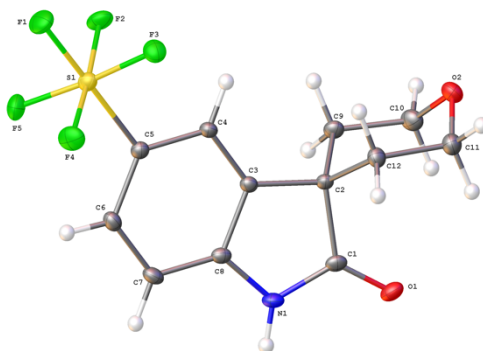


*Figure 4.9: Crystal structure of 4.4a*

#### 4.2.2 Modelling (performed using Schrodinger Maestro Version 12.6.144)

Protein kinases share a common three dimensional folding that consists of two lobes; N-terminal and C-terminal lobe. Between these two lobes is the ATP-binding site, which is a flexible hinge region, that connects the two lobes (Figure 4.10). The active site consists of several structural elements required for enzymatic activity. The activation loop which is typically 20 to 30 residues begins with a conserved DFG motif (Asp-Phe-Gly, Figure 4.11) which extends to an APE motif (usually Ala-Pro-Glu). In an active kinase, this loop forms a cleft that binds substrate. The Asp residue of the DFG motif in an active conformation binds to a magnesium ion that interacts directly with an oxygen atom of the  $\beta$  phosphate of ATP. The DFG phenylaniline creates a hydrophobic regulatory spine

(hydrophobic pocket II) by fitting into a hydrophobic pocket between one residue from the N-lobe and one from the C-lobe. The Asp residue orientates and conceives a position which allows interaction with  $Mg^{2+}$ . Once the above mentioned interaction takes place a conserved Glu residue of the C-helix forms a salt bridge with a Lys residue. After the formation of the salt bridge, the lysine side chain forms hydrogen bonds with oxygen atoms of the  $\alpha$  and  $\beta$  phosphates of ATP.

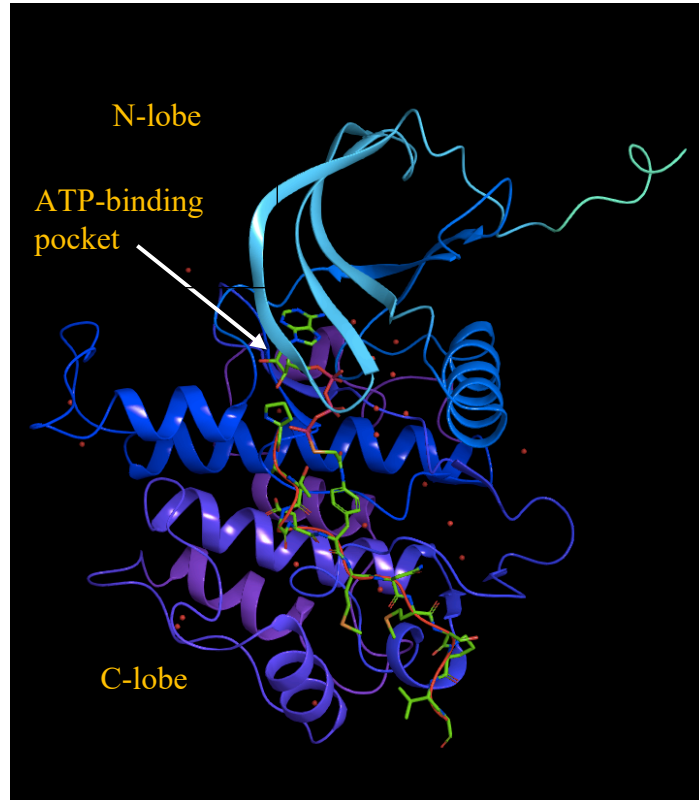


Figure 4.10: A typical protein kinase domain displaying ATP binding pocket occupied by an inhibitor (PDB: 1GAG)

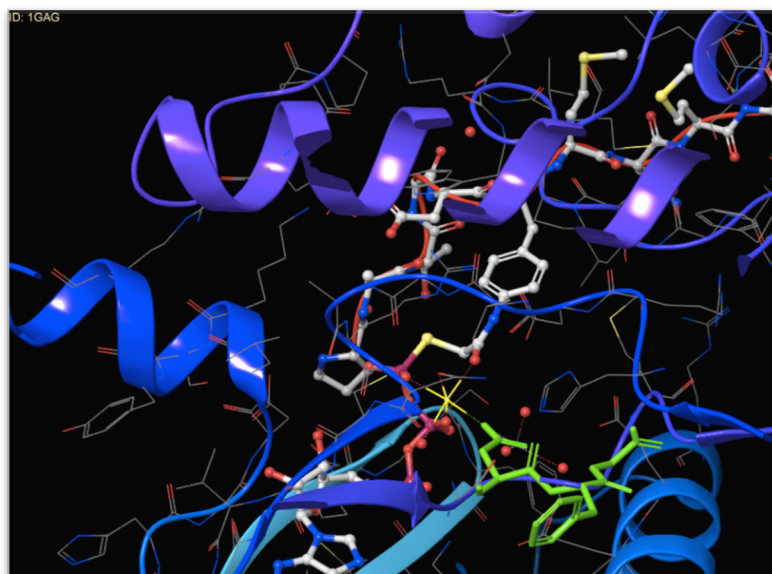


Figure 4.11: Zoomed in image of the ATP binding site. DFG motif in green interacting (dashed green line) with  $Mg^{2+}$  (yellow)

Most small molecule kinase inhibitors bind in the region of the ATP binding site. In this study, we integrated SF<sub>5</sub> on to carbons C5 and C6 of Semaxanib, which is an experimental stage drug that specifically inhibits VEGFR2. SF<sub>5</sub> moiety is hypothesised to form hydrophobic interactions in the hydrophobic pocket II.

Indoline-2-one of Semaxanib binds in a similar fashion to the ATP's purine ring. The pyrrole forms van der Waals interaction with the hydrophobic pocket I located outside the ATP binding pocket (Figure 4.12). The indoline-2-one moiety forms two hydrogen bond interactions with Glu917 and Cys919 residues in the adenine pocket and an aromatic pi-pi interaction with the phenylalanine of the DFG motif.

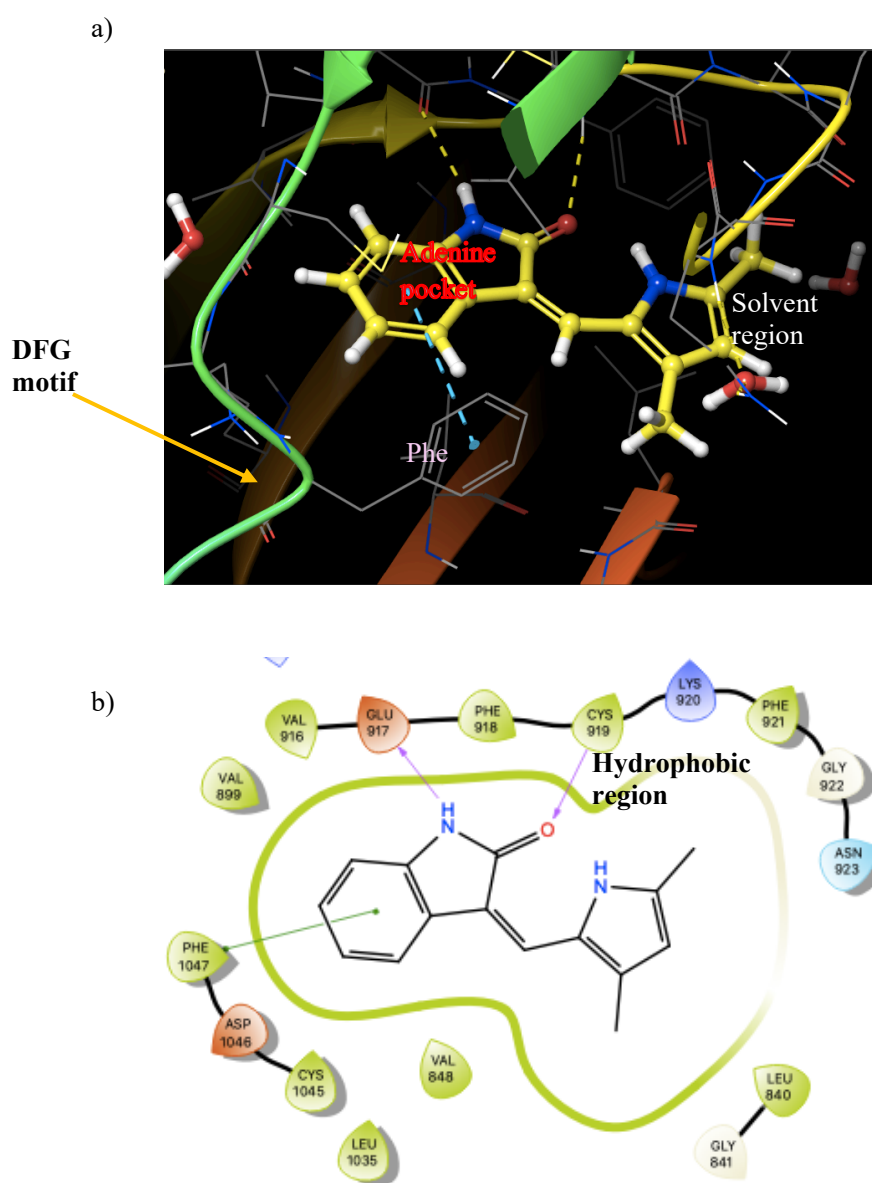


Figure 4.12: Semaxanib (yellow) in complex with VEGFR2. a) Highlights adenine pocket and solvent region. Blue dashed line indicates aromatic pi-pi interaction. Hydrogen bonds shown as yellow dashes. b) Hydrophobic interaction between pyrrole and hydrophobic amino acid residues. PDB: 4AGD

When docking **4.2b** in VEGFR-2 we observed that the indoline-2-one is no longer able to occupy the adenine pocket (Figure 4.13). The bulkiness of the SF<sub>5</sub> pushes the oxindole ring into the hydrophobic pocket and the pyrrole into the solvent region. The aromatic pi-pi bond between Phe (DFG motif) and the oxindole endures. However, hydrogen bond interactions with Glu917 and Cys919 disappear. The oxygen of the oxindole forms a (solvent region) hydrogen bond interaction with a water molecule. SF<sub>5</sub> moiety must be forming van der Waals interactions with Lys868 and Ala866 in the hydrophobic binding pocket.

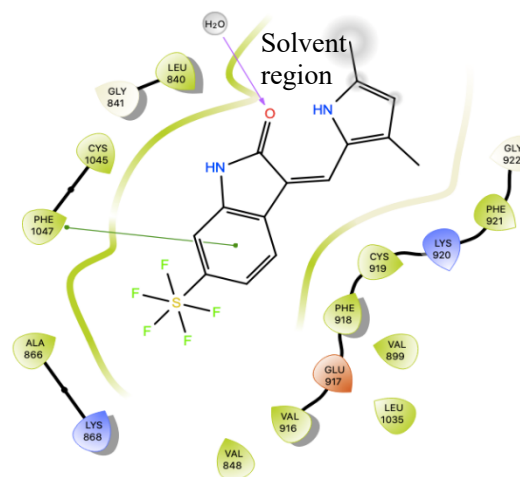
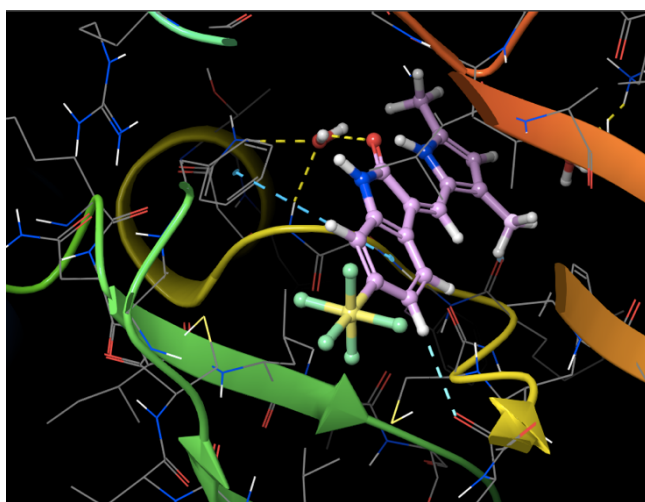


Figure 4.13: **4.2b** (pink) in complex with VEGFR-2. Dashed lines indicate hydrogen bonds (yellow), aromatic interactions (light blue) and pi-pi interactions (dark blue)

The same analysis was performed on **4.2a**. Incorporating SF<sub>5</sub> at position 5, forces the compound further away from the DFG motif and the adenine pocket resulting in no interaction between the oxindole and the adenine pocket except for an aromatic hydrogen bonding with the Cys919 residue (light blue dashed line). Nevertheless, the pyrrole NH forms a hydrogen bond with Leu840 (Figure 4.14).

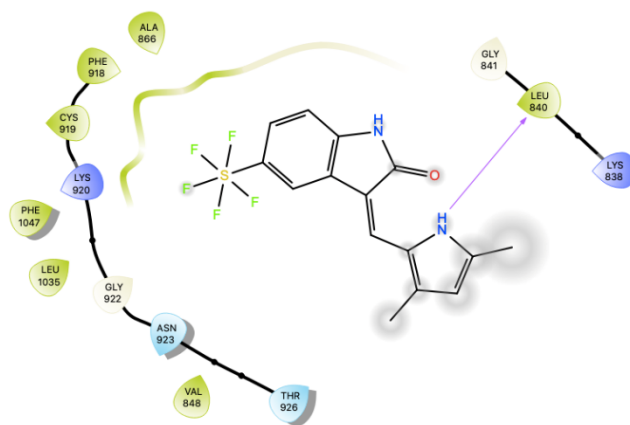
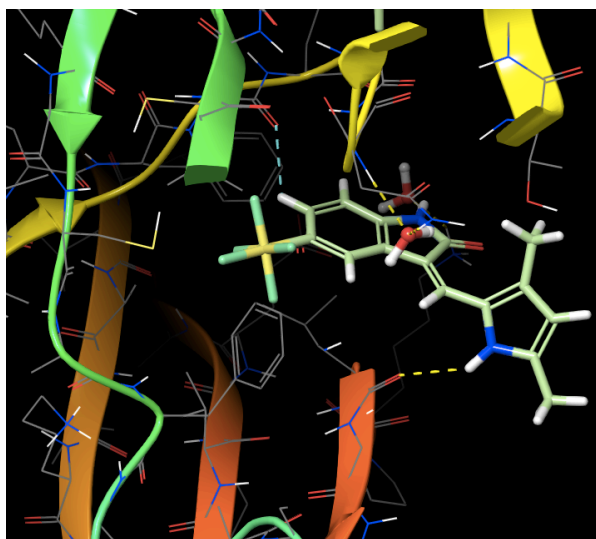


Figure 4.14: **4.2a** (light green) in complex with VEGFR-2. Dashed lines indicate hydrogen bonds (yellow) and aromatic interactions (light blue)

We compared our modelling analysis with a crystal structure of Sunitinib bound to VEGFR-2. Sunitinib contains a fluorine at position C5. Therefore, it seemed logical to compare SF<sub>5</sub>-substituted Semaxanib and Sunitinib to understand the role of a halogen at the site.

The oxindole and pyrrole moieties of Sunitinib and Semaxanib overlap perfectly in the binding pocket (Figure 4.15). Consequently, Sunitinib forms interactions similar to those in Semaxanib, in the adenine pocket and the hydrophobic pocket. In addition, Sunitinib forms multiple water mediated hydrogen bonds in the solvent region. Fluorine is in close proximity to the  $\beta$ -carbon of phenylalanine, favouring van der Waals interactions. The fluorine atom is also a bio-isostere of proton which slows down metabolism of the drug. As fluorine and proton are similar in size, it does not affect the orientation and positioning of the drug in the binding pocket. These findings also apply to PDGFR- $\beta$  binding pocket as they share a similar protein structure.

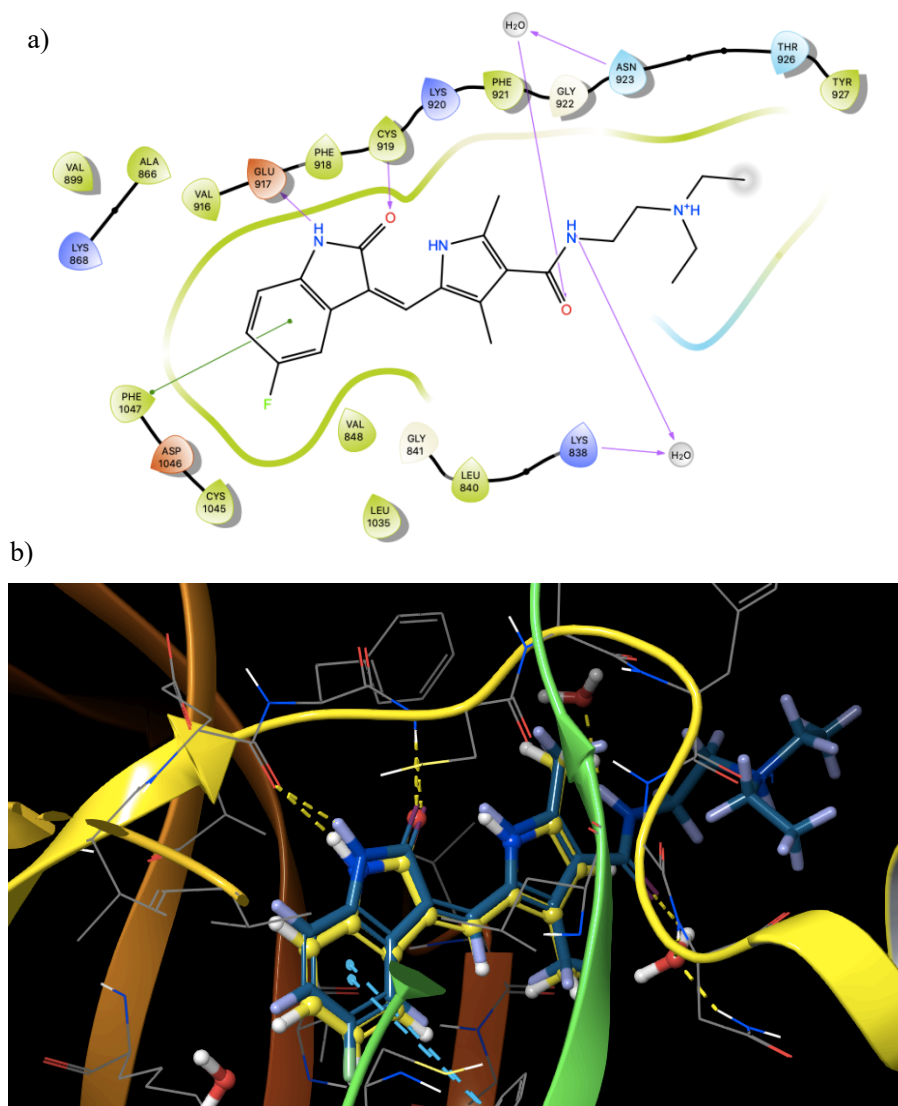


Figure 4.15 a) Sunitinib in complex with VEGFR-2. b) An overlap of Sunitinib and Semaxanib

From our docking studies, it is apparent that a bulky ligand in the adenine pocket is not favourable for binding. SAR studies have shown that substitution of electron withdrawing groups at such as NO<sub>2</sub>

or CF<sub>3</sub> at positions C5 and C6 are undesirable. Alternatively substitution of electron donating and polar groups enhance binding affinity. A para substitution of an electron withdrawing group weakens the oxindole N-H bond. Subsequently the hydrogen bond interaction between the NH and amino acid residues becomes weaker.

Out of interest we modelled compounds **4.4a** and **4.4b** to get similar results to that of **4.2a** and **4.2b**. The spiro cycle was expected to form interactions in the solvent region through the oxygen but none could be observed.

### 4.2.3 *In Vitro* Analysis

A biochemical assay showed Semaxanib to inhibit VEGFR2 giving an IC<sub>50</sub> of 1.5 μM (lit. 1.04 ± 0.53 μM).<sup>178</sup> Compounds **4.2a** and **4.2b** did not show any satisfactory inhibition to generate IC<sub>50</sub> values. At 10 μM, **4.2a** exhibits 27% inhibition of VEGFR2 while **4.2b** only gives 23% inhibition at the same concentration.

Entry	Compound <sup>a</sup>	IC <sub>50</sub> (μM)
1	Semaxanib	1.5
2	<b>4.2a</b>	- <sup>b</sup>
3	<b>4.2b</b>	- <sup>b</sup>

Table 4.4: Biochemical kinase assay of Semaxanib and its SF<sub>5</sub> counterparts. <sup>a</sup>n = 1; 10-dose IC<sub>50</sub> mode with 2-fold serial dilutions, starting at 10 μM. <sup>b</sup> % inhibition at 10 μM; **4.2a** (27%); **4.2b** (23%)

## 4.3 Conclusion

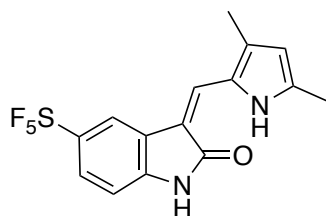
To conclude, SF<sub>5</sub> and NO<sub>2</sub>-substituted oxindoles were modified by substituting at position-3 via Knoevenagel condensation, in the microwave. Knoevenagel condensation was also explored by means of mechanochemistry. Modification of oxindole includes synthesis of a spirocyclic compound and *N*-methylating it. An *in silico* study of SF<sub>5</sub>-counterparts of Semaxanib, **4.2a** and **4.2b**, in the VEGFR-2 active site and comparing them with Semaxanib, revealed that SF<sub>5</sub> is too bulky a substituent that impedes the ligands' interaction with the adenine pocket. A radioactive assay carried out showed **4.2a** and **4.2b** to have no inhibition activity validating our *in silico* observation.

## 4.4 Experimental

All reagents were purchased from Merck, Fisher Scientific UK Ltd, SpiroChem AG, Fluorochem Ltd, and used without further purification. The milling treatments were carried out in a Retsch MM400 vibratory ball mill (VBM) operated at 30 Hz. <sup>1</sup>H NMR spectra were recorded on Varian

VNMRS 600 MHz spectrometers, at room temperature, using deuterated solvent for calibration ( $(\text{CD}_3)_2\text{CO}$ ) at 2.05 ppm,  $(\text{CD}_3)_2\text{SO}$  at 2.50 ppm, or  $\text{CD}_3\text{OD}$  at 3.31 ppm).  $^{13}\text{C}$  NMR analyses were conducted by Rémi Legay from the University of Caen, and spectra recorded on Bruker Avance III 600 MHz spectrometers, at room temperature, using deuterated solvent for calibration ( $(\text{CD}_3)_2\text{CO}$ ) at 29.84, 206.26 ppm,  $(\text{CD}_3)_2\text{SO}$  at 39.52 ppm, or  $\text{CD}_3\text{OD}$  at 49.00 ppm).  $^{19}\text{F}$  NMR were recorded on Varian VNMRS 376 MHz spectrometers, at room temperature, using deuterated solvent for calibration. Chemical shifts are reported in ppm, usually referenced to TMS as an internal standard, and data reported as s = singlet, d = doublet, t = triplet, q = quadruplet, p = pentet, ddd = doublet of doublets of doublets, m = multiplet; integration. Mass spectrometry analyses were conducted by Dr Abdul-Sada. ESI mass spectra were obtained using a Bruker Daltonics Apex III, using Apollo ESI as the ESI source; EI mass spectra were obtained using a Fissions VG Autospec instrument used at 70 eV. Elemental analyses were conducted by Mr Stephen Boyer from the London Metropolitan University. Melting points were determined using a Stanford Research Systems Optimelt and are uncorrected. LCMS were performed by Shimadzu LCMS-2020 equipped with a Gemini® 5 $\mu\text{m}$  C18 110Å column and percentage purities were ran over 30 minutes in water/acetonitrile with 0.1% formic acid (5 min at 5%, 5%-95% over 20 min, 5 min at 95%) with the UV detector at 254 nm.

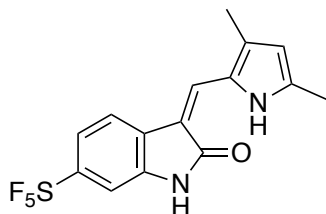
**(3Z)-3-[(3,5-Dimethyl-1H-pyrrol-2-yl)methylidene]-5-(pentafluoro- $\lambda^6$ -sulfanyl)-2,3-dihydro-1H-indol-2-one (4.2a)**



In a 10 mL microwave vial equipped with a stirrer bar was added 5-(pentafluorosulfanyl)-1,3-dihydro-indol-2-one (0.096 g, 0.37 mmol, 1.0 equiv.), 3,5-dimethyl-1H-pyrrole-2-carbaldehyde (0.062 g, 0.5 mmol, 1.3 equiv.), ethanol (2.5 mL) and 3 drops of piperidine. The vessel was then sealed using a rubber microwave septum and placed into the microwave cavity. The reaction mixture was subjected to microwave irradiation by ramping to 150 °C with 200 W of power. It was held at that temperature for 30 min. The vessel was then cooled to ambient temperature and solvent removed in *vacuo*. The crude was purified over a column of C18 silica (100% acetonitrile) to obtain the pure product as a red solid (0.137 g, 80%).  $^1\text{H}$  NMR (600 MHz,  $(\text{CD}_3)_2\text{CO}$ )  $\delta$  13.46 (s, NH), 10.15 (s, NH), 8.21 (s, ArH), 7.91 (s, ArH), 7.60 (d,  $J = 8.6$  Hz, ArH), 7.10 (d,  $J = 8.6$  Hz, ArH), 6.06 (s, C=H), 2.38 (3H, s,  $\text{CH}_3$ ), 2.35 (3H, s,  $\text{CH}_3$ );  $^{13}\text{C}$  NMR (151 MHz,  $(\text{CD}_3)_2\text{CO}$ )  $\delta$  169.8 (C=O), 147.7 (m, ArC-SF<sub>5</sub>), 140.0 (ArC=C), 138.0 (ArC), 134.4 (ArC), 127.4 (ArC), 126.6 (ArC), 125.4 (m, ArC-CSF<sub>5</sub>), 123.0 (ArC), 115.5 (ArC), 113.3 (m, ArC-CSF<sub>5</sub>), 110.5 (C=C), 108.5 (ArC), 12.9 ( $\text{CH}_3$ ), 10.7( $\text{CH}_3$ );  $^{19}\text{F}$  NMR (376 MHz,  $(\text{CD}_3)_2\text{CO}$ )  $\delta$  87.2 (1F, m, equatorial), 63.74 (1F, d,  $J = 148.1$  Hz,

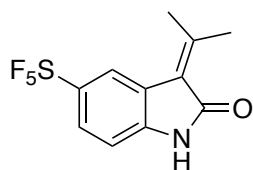
axial); LCMS Purity (UV) = 100%,  $t_R$  23.6 min; HRMS – ESI ( $m/z$ ) found 365.0737, calc. for  $[C_{15}H_{13}F_5N_2OS][H]^+$ :365.0742; IR (neat)  $\nu_{max}/cm^{-1}$  3060 (N-H), 1659 (C=O), 820 (S-F); mp 203 – 205 °C.

**(3Z)-3-[(3,5-Dimethyl-1H-pyrrol-2-yl)methylidene]-6-(pentafluoro- $\lambda^6$ -sulfanyl)-2,3-dihydro-1H-indol-2-one (4.2b)**



In a 10 mL microwave vial equipped with a stirrer bar was added 6-(pentafluorosulfanyl)-1,3-dihydro-indol-2-one (0.100 g, 0.4 mmol, 1.0 equiv.), 3,5-dimethyl-1H-pyrrole-2-carbaldehyde (0.062 g, 0.5 mmol, 1.3 equiv.), ethanol (2.5 mL) and 3 drops of piperidine. The vessel was then sealed using a rubber microwave septum and placed into the microwave cavity. The reaction mixture was irradiated with 200 W of power. When at 150 °C it was held by moderation of power for 30 min. The vessel was then cooled to room temperature and solvent removed in *vacuo*. The aqueous layer was extracted using ethyl acetate (3 x 20 mL), washed with brine (3 x 20 mL), dried over  $MgSO_4$ , filtered under gravity and concentrated in *vacuo*. The crude was purified over a column of C18 silica (100% acetonitrile) (70 mg, 50%) to get an orange solid.  $^1H$  NMR (600 MHz,  $(CD_3)_2CO$ )  $\delta$  13.52 (1H, s, NH), 10.02 (1H, s, NH), 7.82 (1H, d,  $J = 8.5$  Hz, ArH), 7.79 (1H, s, ArH), 7.48 (1H, d,  $J = 8.5$  Hz, ArH), 7.41 (1H, s, ArH), 6.08 (1H, s, C=H), 2.36 (3H, s,  $CH_3$ ), 2.38 (3H, s,  $CH_3$ ).  $^{13}C$  NMR (151 MHz,  $(CD_3)_2CO$ )  $\delta$  169.6 (C=O), 138.7 (ArC-SF<sub>5</sub>), 137.3 (ArC=C), 135.0 (ArC), 130.2 (ArC), 127.7 (ArC), 126.0 (ArC-CSF<sub>5</sub>), 118.6 (ArC), 117.0 (ArC), 113.6 (ArC-CSF<sub>5</sub>), 110.0 (ArC), 106.8. (ArC), 54.1 (C=C), 12.9 ( $CH_3$ ), 10.7 ( $CH_3$ ).  $^{19}F$  NMR (376 MHz,  $(CD_3)_2CO$ )  $\delta$  86.32 (1F, m), 63.74 (4F, d,  $J = 148.1$  Hz); LCMS Purity (UV) = 100%,  $t_R$  23.7 min; HRMS – ESI ( $m/z$ ) found 389.2959, calc. for  $[C_{15}H_{13}F_5N_2O_3S][Na]^+$ :387.0561. IR (neat)  $\nu_{max}/cm^{-1}$  3559, 1650, 814; mp 199 – 201 °C.

**5-(Pentafluoro- $\lambda^6$ -sulfanyl)-3-(propan-2-ylidene)-2,3-dihydro-1H-indol-2-one (4.2c)**

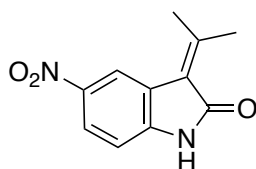


In a 10 mL microwave vial equipped with a stirrer bar was added 5-(pentafluorosulfanyl)-1,3-dihydro-indol-2-one (0.096 g, 0.37 mmol, 1.0 equiv.) in acetone (2 mL) followed by 3 drops of piperidine. The vessel was then sealed using a rubber microwave septum and placed into the microwave cavity. The reaction mixture was irradiated with 200 W of power. When at 100 °C, it was held by moderation of power for 20 min. The vessel was then cooled to room temperature. The



reaction mixture was extracted with ethyl acetate (3 x 20 mL), washed with water (20 mL), dried over MgSO<sub>4</sub>, filtered under gravity and concentrated in *vacuo*. Orange solid was obtained as pure compound without further purification (0.100 g, 90%). Crystallization by mixed solvents, dichloromethane and hexane, provided orange crystals. <sup>1</sup>H NMR, (600 MHz, (CD<sub>3</sub>OD) δ 2.39 (3H, s, CH<sub>3</sub>), 2.59 (3H, s, CH<sub>3</sub>), 6.94 (1H, d, *J* = 8.5 Hz, ArH), 7.65 (1H, d, *J* = 8.5 Hz, ArH), 7.87 (1H, s, ArH); N-H not observed. <sup>13</sup>C NMR (600 MHz, CD<sub>3</sub>OD) δ 21.9 (CH<sub>3</sub>), 24.0 (CH<sub>3</sub>), 108.2 (C=C), 120.7 (C, ArC-CSF<sub>5</sub>, m), 121.8 (ArC), 123.6 (ArC), 125.6 (ArC-CSF<sub>5</sub>, m), 142.5 (ArC), 147.6 (ArC-SF<sub>5</sub>, m), 159.0 (C=C), 169.6 (C=O); <sup>19</sup>F NMR, (376 MHz, CD<sub>3</sub>OD) δ 62.9 (4F, d, *J* = 147.8 Hz, equatorial), 85.3 (1F, p, *J* = 147.8, axial); LCMS Purity (UV) = 99%, *t*<sub>R</sub> 18.5 min; HRMS – ESI (*m/z*) found 322.0285, calc. for [C<sub>11</sub>H<sub>10</sub>F<sub>5</sub>NOS][Na]<sup>+</sup>:322.0295; IR (neat) *v*<sub>max</sub>/cm<sup>-1</sup> 3062 (N-H), 2925 (C-H), 1694 (C=O), 1618 (C=C), 813 (S-F); mp 191 – 194 °C.

### 5-Nitro-3-(propan-2-ylidene)-2,3-dihydro-1H-indol-2-one (4.2d)



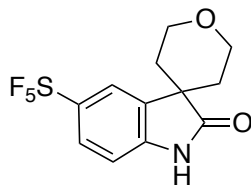
#### Microwave reaction:

In a 10 mL microwave vial equipped with a stirrer bar was added 5-nitro-2-oxindole (0.50 g, 2.9 mmol, 1.0 equiv.), acetone (0.25 mL, 3.4 mmol, 1.2 equiv.), acetonitrile (5 mL) and 3 drops of piperidine. The vessel was then sealed using a rubber microwave septum and placed into the microwave cavity. The reaction mixture was irradiated with 200 W of power and heated to 100 °C in a CEM Explorer. When at 100 °C it was held by moderation of power for 20 min. The vessel was then cooled to ambient temperature and the reaction mixture was concentrated in *vacuo*. The crude was recrystallized in acetonitrile to obtain a brown solid as pure product (0.411 g, 66%).

#### Solventless reaction:

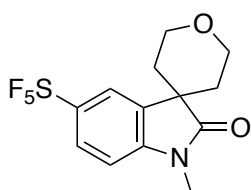
5-nitro-2-oxindole (242.0 mg, 1.36 mmol, 1.0 equiv.), acetone (200.0 μL, 2.71 mmol, 2.0 equiv.) and piperidine (40.2 μL) were mechanically activated in a Retsch MM400 vibratory ball-mill for 90 minutes at 30 Hz in 25 mL zirconia jar with one, 1.2 cm dia. ball. The product was suspended in acetone (10 mL) and filtered to obtain the pure product as a brown solid (229.0 mg, 78%).

<sup>1</sup>H NMR (600 MHz, (CD<sub>3</sub>)<sub>2</sub>SO) δ 10.96 (1H, s, NH), 8.21 (1H, s, ArH), 8.11 (1H, dd, *J* = 8.6, 2.0 Hz, ArH), 6.94 (1H, d, *J* = 8.6 Hz, ArH), 2.52 (3H, s, CH<sub>3</sub>), 2.38 (3H, s, ArH). <sup>13</sup>C NMR (151 MHz, (CD<sub>3</sub>)<sub>2</sub>SO) δ 169.0 (C=O), 160.0 (ArC), 146.6 (ArC), 141.9 (ArC), 125.0 (ArC-H), 124.1 (ArC-NH), 121.5 (C=ArC), 118.9 (ArC-H), 109.4 (ArC-H), 25.5 (CH<sub>3</sub>), 23.2 (CH<sub>3</sub>); HRMS – ESI (*m/z*) found 241.0584, calc. for [C<sub>11</sub>H<sub>10</sub>N<sub>2</sub>O<sub>3</sub>][Na]<sup>+</sup>:241.0584; IR (neat) *v*<sub>max</sub>/cm<sup>-1</sup> 1694 (C=O), 1509 (N-O stretch); LCMS Purity (UV) = 100%, *t*<sub>R</sub> = 14.6 min; mp 228 – 230 °C.

**5-(Pentafluoro- $\lambda^6$ -sulfanyl)-1,2-dihydrospiro[indole-3,4'-oxan]-2-one (4.4a)**

5-(Pentafluorosulfanyl)-1,3-dihydro-indol-2-one (0.500 g, 1.93 mmol, 1.0 equiv.) dissolved in tetrahydrofuran (10 mL) was added to LiHMDS (1M) in tetrahydrofuran (5.80 mL, 5.80 mmol, 3.0 equiv.) at -78 °C. After an hour of stirring, 1-bromo-2-(2-bromoethoxy)ethane (0.448 g, 1.93 mmol, 1.0 equiv) was added to the mixture and warmed to ambient temperature. The reaction was stirred for 46 hours and quenched with water. The reaction mixture was extracted with ethyl acetate (3 x 20 mL), washed with brine (3 x 20 mL), dried over MgSO<sub>4</sub>, filtered under gravity and concentrated in *vacuo*. The crude material was purified over a column of silica (hexane:ethyl acetate; 4:1) to get a pink solid as the title compound (210 mg, 33%).

<sup>1</sup>H NMR (600 MHz, CD<sub>3</sub>OD)  $\delta$  7.82 (1H, s, ArH), 7.71 (1H, d,  $J$  = 8.6 Hz, ArH), 7.01 (1H, d,  $J$  = 8.6 Hz, ArH), 4.22 (2H, m, OCH<sub>2</sub>), 3.88 (2H, m, OCH<sub>2</sub>), 1.95 (2H, m, CH<sub>2</sub>), 1.82 (2H, m, CH<sub>2</sub>); <sup>13</sup>C NMR (151 MHz, (CD<sub>3</sub>)<sub>2</sub>CO)  $\delta$  180.7 (C=O), 147.8 (m, ArC-SF<sub>5</sub>), 144.3 (ArC), 135.2 (ArC), 126.7 (m, ArC-CSF<sub>5</sub>), 121.2 (m, ArC-CSF<sub>5</sub>), 109.0 (ArC), 62.0 (2C), 44.6 (C), 32.5 (2C); <sup>19</sup>F NMR (376 MHz, (CD<sub>3</sub>)<sub>2</sub>CO)  $\delta$  86.41 (4F, m), 64.09 (F, d,  $J$  = 148.1 Hz); LCMS Purity (UV) = 98%,  $t_R$  = 20.2 min; HRMS – ESI ( $m/z$ ) found 329.0535, calc. for [C<sub>12</sub>H<sub>12</sub>F<sub>5</sub>NO<sub>2</sub>S]: 329.0509; IR (neat)  $\nu_{max}/cm^{-1}$  3303, 1690, 1101, 818; mp 247 – 249 °C.

**1-methyl-5-(pentafluoro- $\lambda^6$ -sulfanyl)-1,2-dihydrospiro[indole-3,4'-oxan]-2-one (4.4b)**

Sodium hydride (11 mg, 0.45 mmol, 1.5 equiv ) was added to a round bottomed flask and purged with argon. Dry dimethyl formamide (15 mL) was then added to the flask followed by compound **4.4a** (0.1g, 0.30 mmol, 1.0 equiv) and stirred for 1 hour. To this mixture was added methyl iodide (0.213 g, 1.50 mmol, 5.0 equiv) and stirred overnight at room temperature. The reaction mixture was quenched with water (10 mL), extracted with ethyl acetate (10 mL x 3), washed with brine (20 mL), dried over MgSO<sub>4</sub>, filtered and concentrated in *vacuo*. The crude material was purified over a column of silica (hexane:ethyl acetate; 4:1) to get a yellow solid as the title compound(68 mg, 66%).

<sup>1</sup>H NMR (600 MHz, CDCl<sub>3</sub>)  $\delta$  7.71 (ArH, dd,  $J$  = 8.6, 1.9 Hz, 1H), 7.68 (ArH, d,  $J$  = 1.9 Hz, 1H), 6.86 (ArH, d,  $J$  = 8.6 Hz, 1H), 4.25 (CH<sub>2</sub>, ddd,  $J$  = 12.0, 9.5, 3.0 Hz, 2H), 3.89 (CH, dt,  $J$  = 12.0, 4.3 Hz, 2H), 3.22 (s, 3H), 1.91 (ddd,  $J$  = 13.4, 9.5, 4.3 Hz, 2H), 1.82 (dt,  $J$  = 13.4, 3.0 Hz, 2H). <sup>13</sup>C NMR (151 MHz, CDCl<sub>3</sub>)  $\delta$  179.5 (C=O), 148.8 (ArC, p, <sup>2</sup> $J_{FC}$  = 17.7, 17.2 Hz), 145.1 (ArC), 134.0 (ArC),

126.7 (ArC-H, p,  $^3J_{FC} = 4.7$  Hz), 120.9 (ArC-H, p,  $^3J_{FC} = 4.7$  Hz), 107.3 (ArC-H), 62.6 (2C), ((CH<sub>2</sub>)<sub>2</sub>), 44.4 (C), 32.7 (2C, (CH<sub>2</sub>)<sub>2</sub>), 26.3 (CH<sub>3</sub>). <sup>19</sup>F NMR (376 MHz, CDCl<sub>3</sub>) δ 86.61 – 84.84 (p,  $J = 150.1$  Hz), 64.42 (d,  $J = 150.1$  Hz); HRMS – ESI ( $m/z$ ) found 344.0743, calc. for [C<sub>13</sub>H<sub>14</sub>F<sub>5</sub>NO<sub>2</sub>S][H]<sup>+</sup>: 344.0744; IR (neat)  $\nu_{\max}/\text{cm}^{-1}$  2947 (C-H, st), 1727 (C=O), 1258 (N-C, methyl), 828 (S-F); LCMS Purity (UV) = 95%,  $t_R$  18.7 min; mp: 158 – 158 °C.

## Chapter 5.0 Synthesis and Biological Evaluation of SF<sub>5</sub>-Containing Diazepines

### 5.1 Introduction

Since their discovery in the late 1950s,<sup>179</sup> benzodiazepines (BZDs or 1,4-diazepam) have been widely employed to treat a broad spectrum of neurological disorders such as anxiety, insomnia, seizure disorders and certain kinds of spasticity.<sup>180,181,182,183</sup> The first 1,4 diazepam to be discovered, chlordiazepoxide (Librium<sup>®</sup>, Figure 5.1)<sup>184</sup>, was fundamentally purposed to treat anxiety disorders. In 1963, diazepam (Valium<sup>®</sup>)<sup>185</sup> was revealed as an even more potent BZD. Its therapeutic benefits were not limited to anxiety; several other CNS disorders including epilepsy and alcohol withdrawal were treated with diazepam.<sup>186,187,180</sup> Since then several drugs with the 1,4-BZD nucleus have been developed and used.

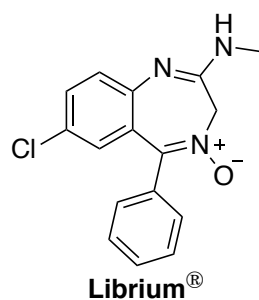
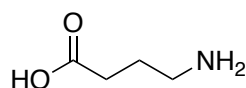


Figure 5.1: Chlordiazepoxide

For around 15 years after their discovery, BZDs were widely prescribed without significant knowledge of their mode of action. Although, each BZD differs in its structure activity relationship (SAR), in general all BZDs produce a clinical effect by enhancing the actions of  $\gamma$ -aminobutyric acid (GABA, Figure 5.2). GABA is a major neurotransmitter of the nervous system,<sup>188</sup> found in high concentrations in the cortex and limbic system.<sup>189</sup>



**GABA**

Figure 5.2:  $\gamma$ -Aminobutyric acid

During a synaptic neuronal process, GABA binds to GABA receptors found in the plasma membrane. This allows ion channels to open and negatively charged chloride ions to enter the neuron.<sup>190</sup> The overall negative change in the transmembrane potential limits other neurotransmitters from binding, thus reducing the excitability of neurons. There are three known GABA receptors: GABA<sub>A</sub>, GABA<sub>B</sub> and GABA<sub>C</sub>. The GABA<sub>A</sub> receptor has modulatory binding

sites for BZDs, barbiturates, general anaesthetics and picrotoxin (Figure 5.3) other than GABA. GABA<sub>B</sub> and GABA<sub>C</sub> receptors are resistant to drugs that modulate GABA<sub>A</sub>.<sup>191,192,193</sup>

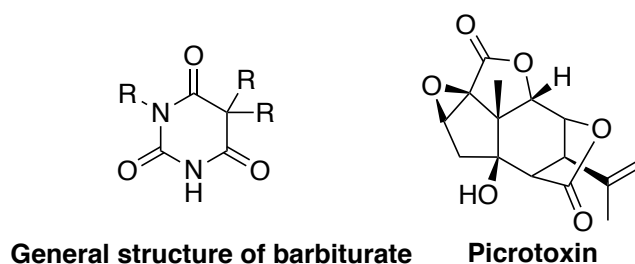


Figure 5.3: Barbiturate & Picrotoxin

GABA<sub>A</sub> receptor is a chloride ion channel typically formed by 5 subunits, each with multiple isoforms. There are 19 known GABA<sub>A</sub> subunit families:  $\alpha$ 1–6,  $\beta$ 1–3,  $\gamma$ 1–3,  $\delta$ ,  $\epsilon$ ,  $\theta$ ,  $\pi$ , and  $\rho$ 1–3.<sup>194</sup> Most commonly they are constructed of 2 copies of an  $\alpha$ <sub>1</sub> subunit, 2 copies of  $\beta$ <sub>2</sub> and a single  $\gamma$ <sub>2</sub> subunit. This composition can vary depending on age, brain region as well as subcellular distribution. The benzodiazepine binding sites form in a specific pocket at the intersection of  $\alpha$  and  $\gamma$  subunits (Figure 5.4). BZDs only have affinity towards the  $\alpha$  subunit and in particular towards isoforms 1, 2, 3, and 5, as they possess a histidine residue: H101, H101, H126, and H105, respectively.<sup>195,196</sup> The histidine residue is small enough to accommodate BZDs in the binding pocket. Isoforms 4 and 6 possess arginine residue. These larger side chains would sterically clash with classical BZDs, so do not have affinity for them.<sup>193</sup>

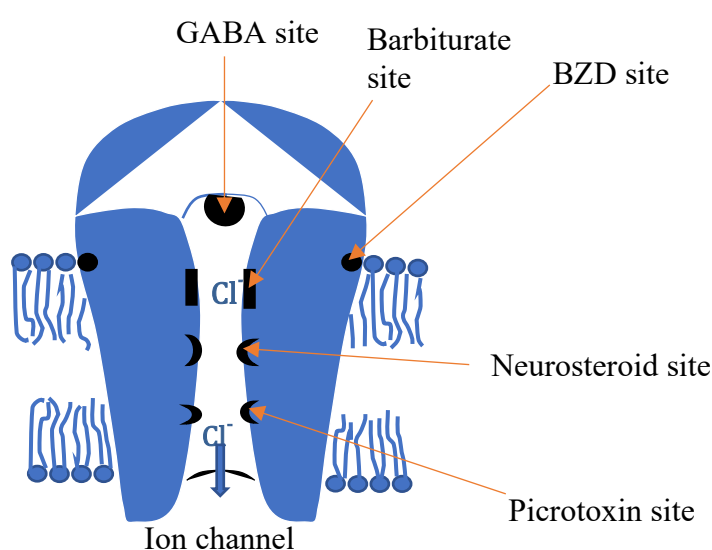


Figure 5.4: GABA<sub>A</sub> receptor with target sites

There are two types of drugs on the market, classified based on their inhibition: orthosteric and allosteric.<sup>197</sup> Orthosteric drugs bind at the active site and allosteric ones bind elsewhere on the protein surface.<sup>198</sup>

BZDs, barbiturates and general anaesthetics are positive allosteric modulators (PAM) of GABA receptor, while picrotoxin is a negative allosteric modulator. A PAM works by binding to an allosteric site while modifying the conformation of the orthosteric site to cause boosting of a signal or increased activity. When BZDs and other PAM bind to their binding sites, they allosterically change the conformation of the GABA<sub>A</sub> receptor site, altering the ion channels and allowing increased chloride ion flow into the cell by increasing the permeability of the central pore to chloride ions.<sup>199</sup>

BZDs enhance the effectiveness of GABA in a unique way by lowering the concentration required for opening the channel. Unlike barbiturates and other GABA<sub>A</sub> modulators, BZDs do not act directly to open chloride ion channels. This notable difference makes BZDs a safer set of drugs in comparison.<sup>200</sup> An overdose of non-BZD drugs is lethal due to their direct action on the chloride ion channels.<sup>201</sup>

As mentioned, 1,4-BZDs are successful drugs in treating several CNS disorders. Figure 5.5 illustrates a list of prominent 1,4-BZDs in the market.<sup>202</sup>

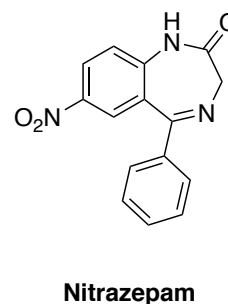
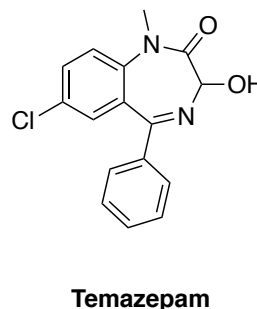
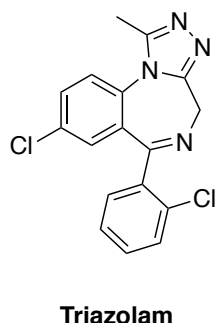
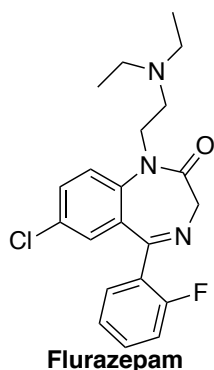
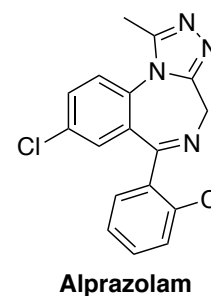
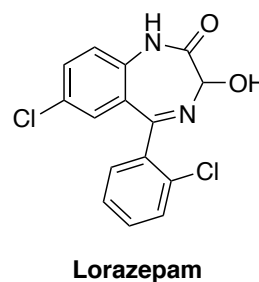
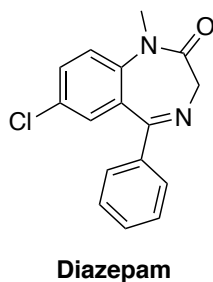
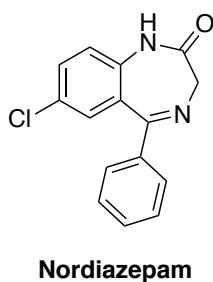
**Hypnotics:****Tranquilizers:**

Figure 5.5: Pharmacologically active 1,4-benzodiazepines

Figure 5.6 shows the basic structure of a 1,4-BZD. Early SAR studies identified the 7-membered imino ring B, as an essential structure for binding affinity towards the BZD binding site on the GABA<sub>A</sub> receptor. Additional SAR and quantitative SAR (QSAR) studies revealed that the lipophilicity of several BZDs has contributed in improving binding affinity.<sup>203</sup>

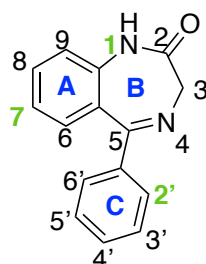


Figure 5.6: 1,4 benzodiazepine skeleton

Moreover, the carbonyl group at position 2 and the C=N double bond are crucial for high binding affinity. Removal of the carbonyl group results in a decrease of binding affinity by two orders of magnitude and saturation of the 4,5 double bond results in a complete loss of in vitro affinity.<sup>202</sup> SAR studies by Sternbach *et al.* revealed that positions 7, 2' and 1 are key regions in the molecule, and functionalising them can potentially improve binding affinity.<sup>204</sup> The most important being position 7 followed by 2'. Increasing lipophilicity and electronegativity at position 7, seemingly

improved receptor affinity whereas having electron donors at the same position had the opposite effect. Having an electrophilic and bulky substituents (mainly halogens; F and Cl) at position 2', enhanced the binding affinity of the BZD analogues, e.g. flunitrazepam, and clonazepam. A methyl group on position 1 improved the activity. Substituting the 1- and 2-positions with an imidazo- or triazolo-ring could heighten the binding affinity for 1,4-BZDs with low affinity. However, modifying 1,4-BZDs that have high binding affinity in this manner, does not appear to boost ligand binding affinity.<sup>205</sup> Another spot of interest is position 3. Position 3 is often substituted with a hydroxy group which accelerates elimination of the drug.

Benzodiazepines are titled 'privileged scaffolds' owing to their affinity for multiple receptor sites.<sup>206</sup> Other than GABA receptor, BZDs bind to CCK receptors (cholecystokinin receptor), AMPA ( $\alpha$ -amino-3-hydroxy-5-methyl-4-isoxazolepropionic acid receptor), gastrin receptors etc. Apart from CNS activity, BZDs are researched for their antitumour, anti-HIV, anti-inflammatory, anti-viral, anti-malarial and anti-bacterial properties.<sup>202,207,208,209,210</sup>

The modification of benzodiazepines at position 7 by the incorporation of an SF<sub>5</sub> seemed, at first sight, to be an ideal research endeavour. It is intriguing to discover how SF<sub>5</sub>'s enhanced lipophilicity and electronegativity<sup>211</sup> would alter the fate of the resulting compound in the BZD binding site of the GABA<sub>A</sub> receptor.

The prevailing lack of SF<sub>5</sub> containing biologically active compounds in the literature<sup>111</sup> is another matter that is addressed as part of this synthesis. Besides, there were no known SF<sub>5</sub> containing benzodiazepines, to the best of our knowledge, at the onset of this study.

Convinced by the vast pharmacological profile of BZDs and with the aim of studying the effect of a SF<sub>5</sub> vs e.g. Cl group on the GABA<sub>A</sub> receptor, we synthesized some 1,4-BZDs functionalized with an SF<sub>5</sub> group.

As position 7 is the most important position in terms of ligand binding affinity, we incorporated SF<sub>5</sub> here, which is comparable to nordiazepam. The nordiazepam analogue was further modified at position 1 by *N*-methylation to obtain a diazepam analogue, and finally we modified a BZD derivative at position 2' via C-H activation (Figure 5.7).

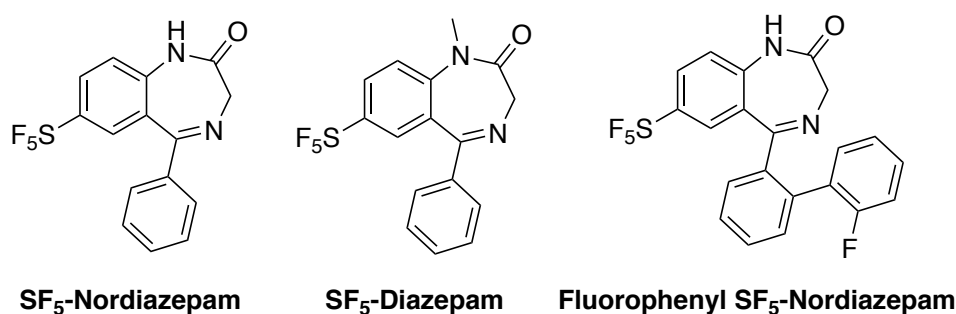


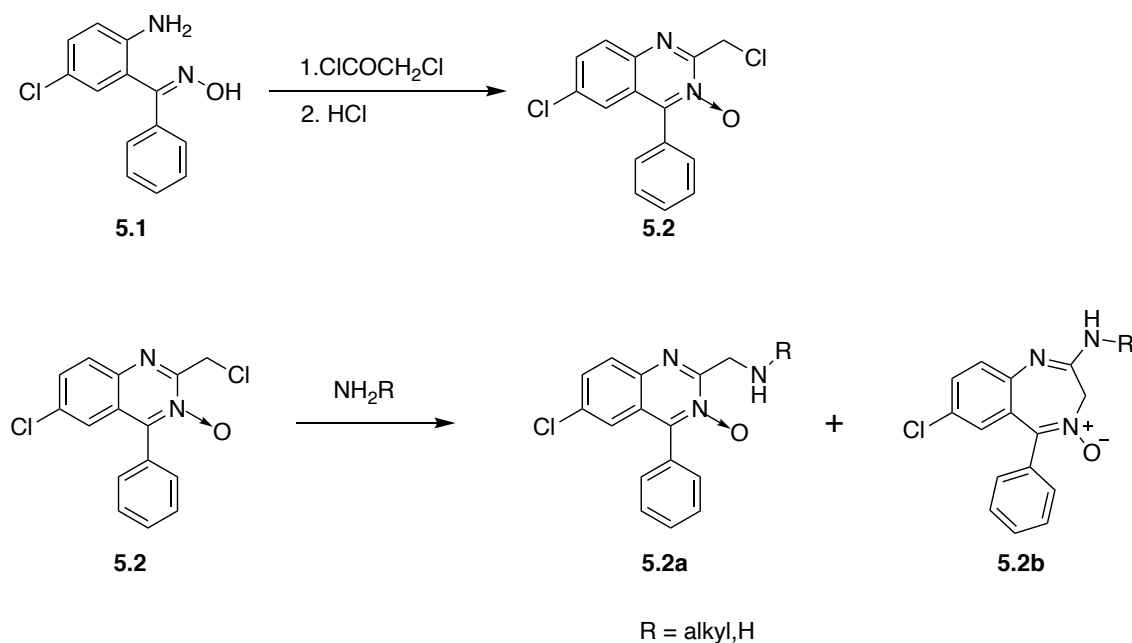
Figure 5.7: Modification of BZD at positions 7, 1 and 2'



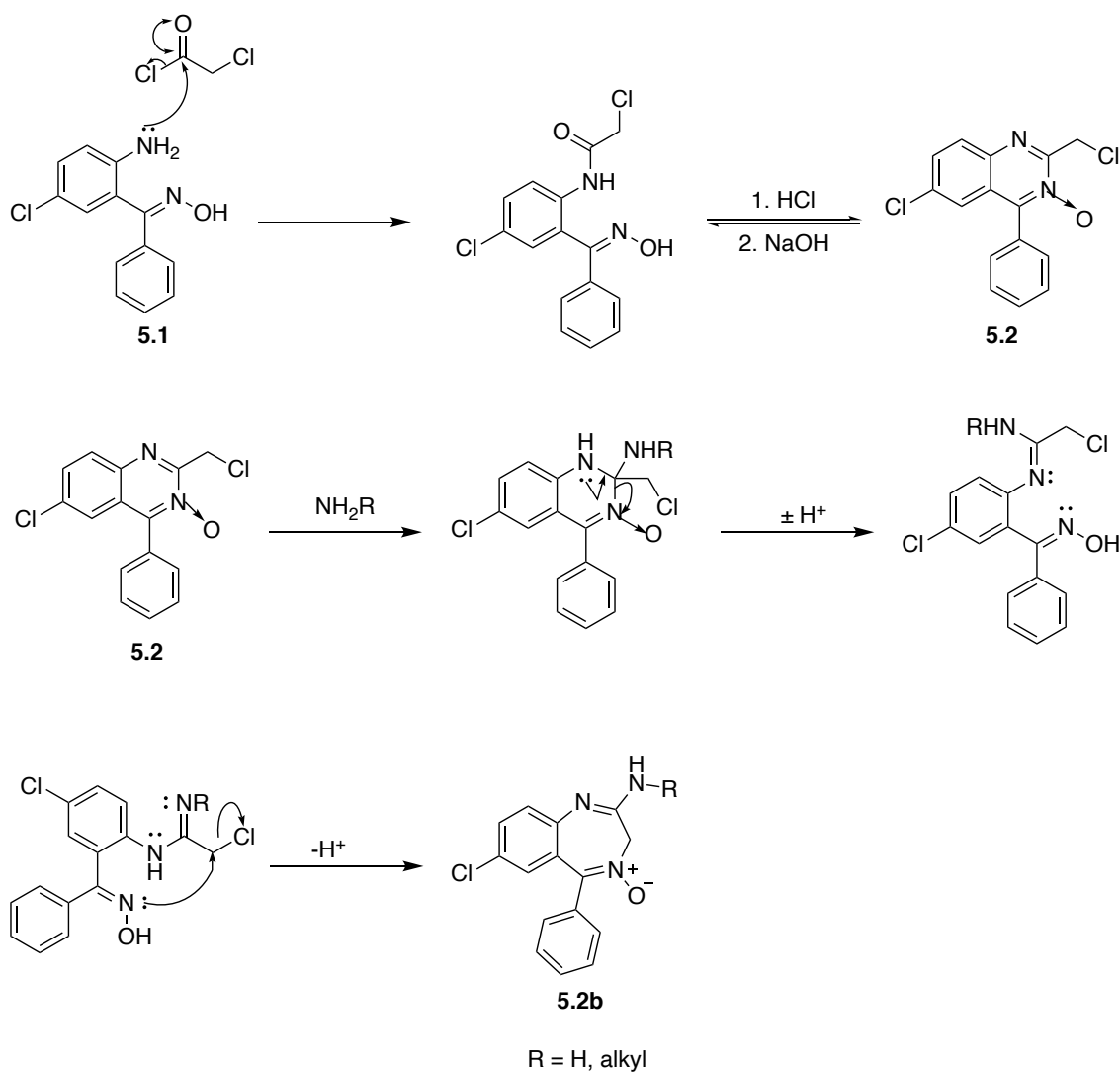
## 5.2 Results and Discussion

### 5.2.1 Synthesis

The original synthesis of 1,4-BZDs was described when L.H. Sternbach and E. Reeder<sup>212</sup> attempted to prepare secondary amino derivatives of quinazoline 3-oxides as part of a project to develop new tranquilizers. 6-Chloro-2-chloromethyl-4-phenylquinazoline 3-oxide (**5.2**, Scheme 5.1) was treated with primary amines to obtain the expected products in a few cases (**5.2a**). In addition to this, they observed a different compound in all the reactions. The infrared and ultraviolet absorption spectra indicated a structural change in these compounds; to be specific, a ring enlargement (Scheme 5.2). In fact these compounds were 2-amino derivatives of 7-chloro-5-phenyl-3H-1,4-benzodiazepine 4-oxide (**5.2b**).<sup>212</sup>

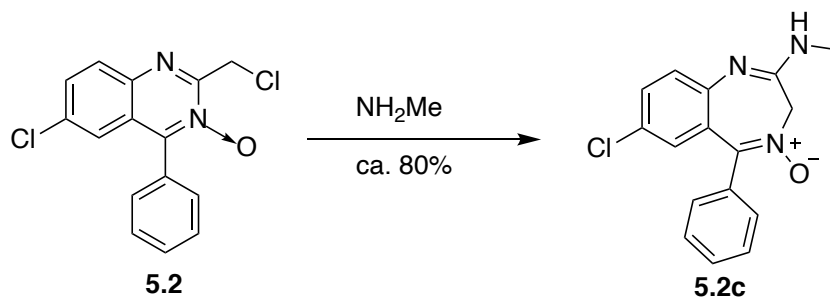


Scheme 5.1: Synthesis of chlordiazepoxide analogues



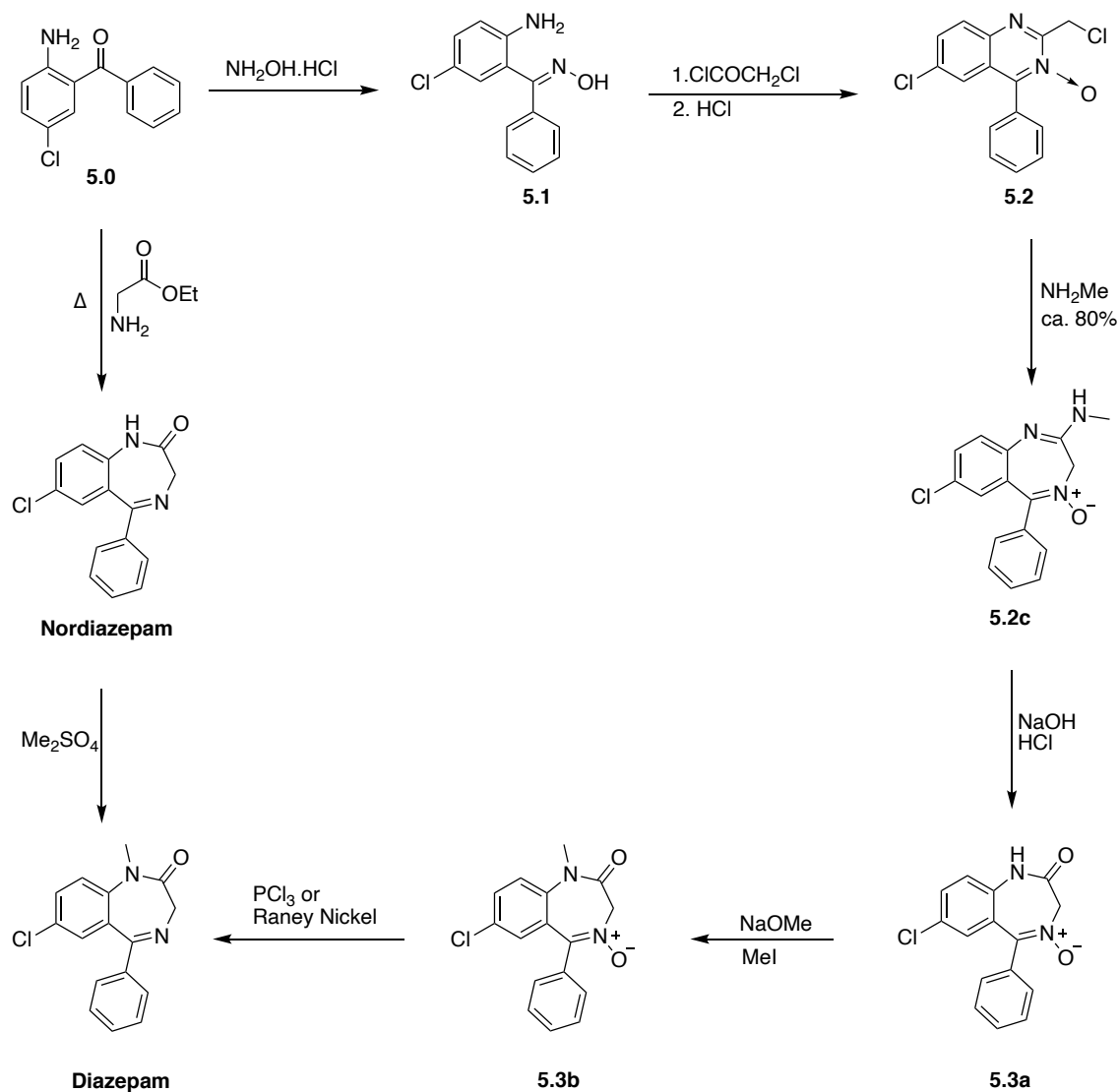
Scheme 5.2: Mechanism showing formation of chlordiazepoxide<sup>213</sup>

To investigate the unfamiliar side products formed, Sternbach and Reeder reacted 6-chloro-2-chloromethyl-4-phenylquinazoline 3-oxide with methylamine. The reaction only generated the rearranged 7-membered ring also in high yields (Scheme 5.3).



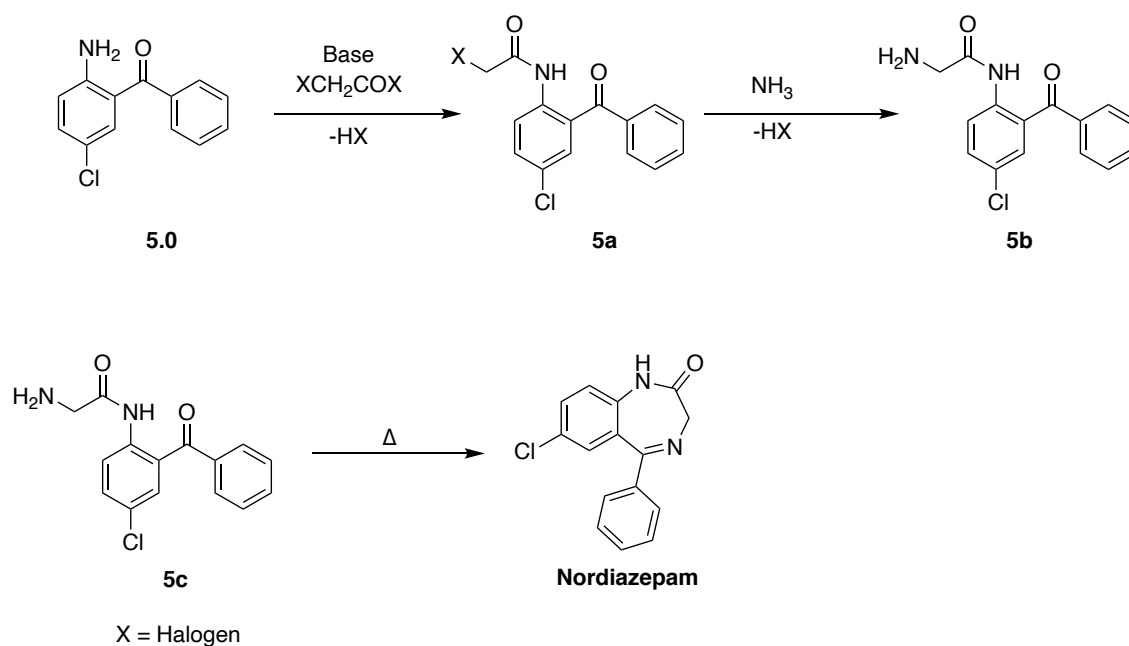
Scheme 5.3: Chlordiazepoxide synthesis

Later they realised that 1,4-BZDs possessed much more pronounced pharmacological activity than benzodiazepine 4-oxides of the type **5.2c**.<sup>204</sup> Hence, a large number of 1,4-BZDs were synthesised. Scheme 5.4 shows the earliest methods to synthesise diazepam, developed by Leo. H. Sternbach and colleagues. 2-Aminobenzophenones were treated with glycine ethyl ester hydrochloride in pyridine to yield 1,4-BZDs in a single step, generally in yields of about 50%.<sup>214</sup>



Scheme 5.4: Routes to diazepam developed by Hoffmann-La Roche Inc.

In 1971 Sternbach *et.al.* devised an improved multi-step route to synthesise 1,4-BZDs, which furnished the desired products in overall yields frequently exceeding 70%. An example of this method is illustrated in Scheme 5.5.<sup>204</sup>



*Scheme 5.5: A multi-step route to synthesis 1,4-BZDs<sup>215</sup>*

Other approaches utilised *N*-protected, such as benzoxycarbonyl, phthaloyl, or azido, glycine derivatives, to first synthesise the intermediate (**5a**) followed by deprotection and cyclisation (Figure 5.8).<sup>204</sup>

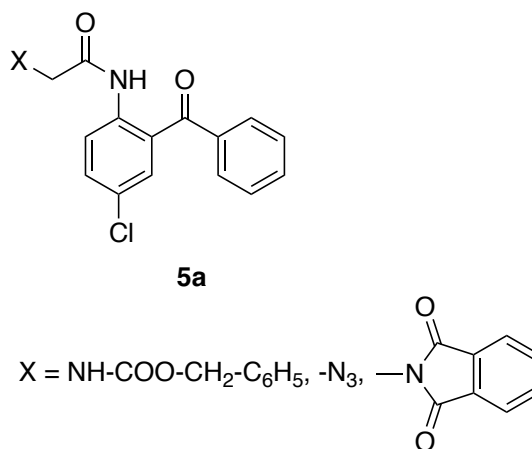
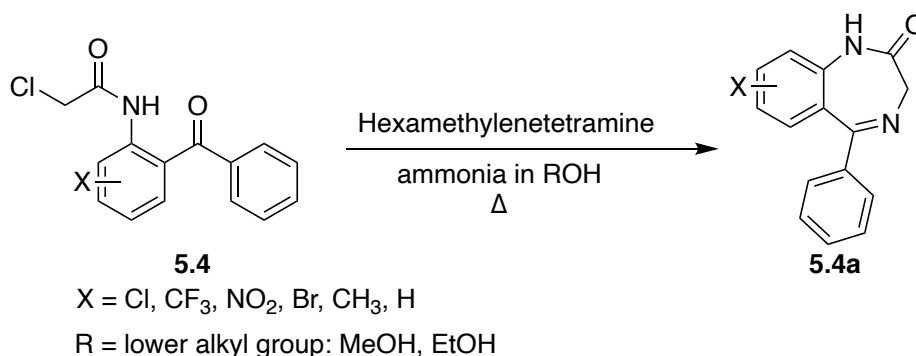


*Figure 5.8: N-protected glycine derivatives.*

Subsequently in 1976, Hoffmann-La Roche Inc., published an approach that utilises hexamethylenetetramine to synthesise 5-phenyl-1,4-benzodiazepines (Scheme 5.6).<sup>216</sup> It was stated that this approach gives good yields when the nitrogen on **5a** is substituted, especially methylated. However, when the nitrogen contains a hydrogen, “consistently good yields are not obtained.”<sup>216</sup>



*Scheme 5.6: Preparing 1,4-BZD with hexamethylenetetramine*

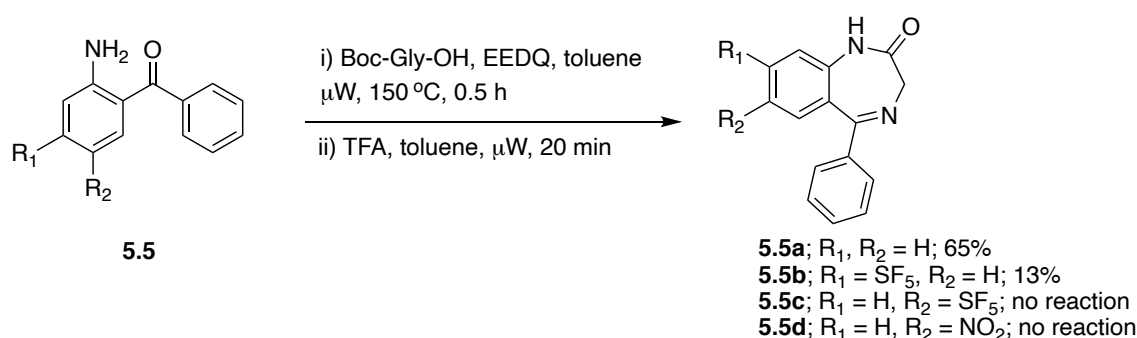
In 2011, a one pot, microwave mediated synthesis of 1,4-BZDs of the type **5.4a** was reported by Mwande-Maguene *et al.*<sup>217</sup> The reactions were reported to give good yields (80-86%), in less than an hour.

Microwave mediated reactions are preferred over conventional heating methods because, they generally produce clean and high yielding reactions in minimum time.<sup>218</sup> For this reason, we opted for a one pot microwave route to synthesise SF<sub>5</sub>-substituted BZD analogues.

Commercially available 2-amino-5-pentafluorosulfanyl-benzophenone was coupled under microwave irradiation with Boc-Gly-OH, and DCC as the coupling agent, in toluene at 150 °C for 30 min, followed by Boc-deprotection with TFA.<sup>42,219</sup> However, the attempt was unsuccessful and one speculation for the failure was the poor nucleophilicity of the aniline. To validate this hypothesis, we attempted the same reaction with 2-amino-5-nitrobenzophenone as the nitro group has an electronic effect fairly close to that of the SF<sub>5</sub> group ( $\sigma_p = 0.68$ <sup>211</sup> for SF<sub>5</sub> and  $\sigma_p = 0.78$ <sup>220</sup> for NO<sub>2</sub>). The result was, as postulated, unsuccessful.

Although position-8 on the BZD ring was not a region of interest in terms of biological activity, we were curious about the electronic effect a pentafluorosulfanyl group would lead to at this position. Again, we used the microwave approach for the attempted synthesis of **5.5b** (Scheme 5.7).

The reaction was moderately successful with **5.5b** formed in 13% yield with a purity of only 88% by LCMS. The unsubstituted benzodiazepine **5.5a** was synthesised in 65% yield.



*Scheme 5.7: Microwave assisted, one pot synthesis of 1,4 BZDs*

Unperturbed in this approach, we next attempted the microwave mediated route, utilizing **5.5** and Boc-Gly-OH but with EEDQ as the coupling agent (Table 5.1). Moreover, the coupling reaction mixture was worked up and the anticipated intermediate was isolated and purified before continuing to the next step, *viz.* Boc-group deprotection. This would enable us to establish whether this initial coupling step was responsible, or the cyclisation step, for the poor overall yield. We found that the coupling step was very low yielding for the reaction of **5.6b** and the reaction was also, disappointingly, again, unsuccessful for **5.6c**.

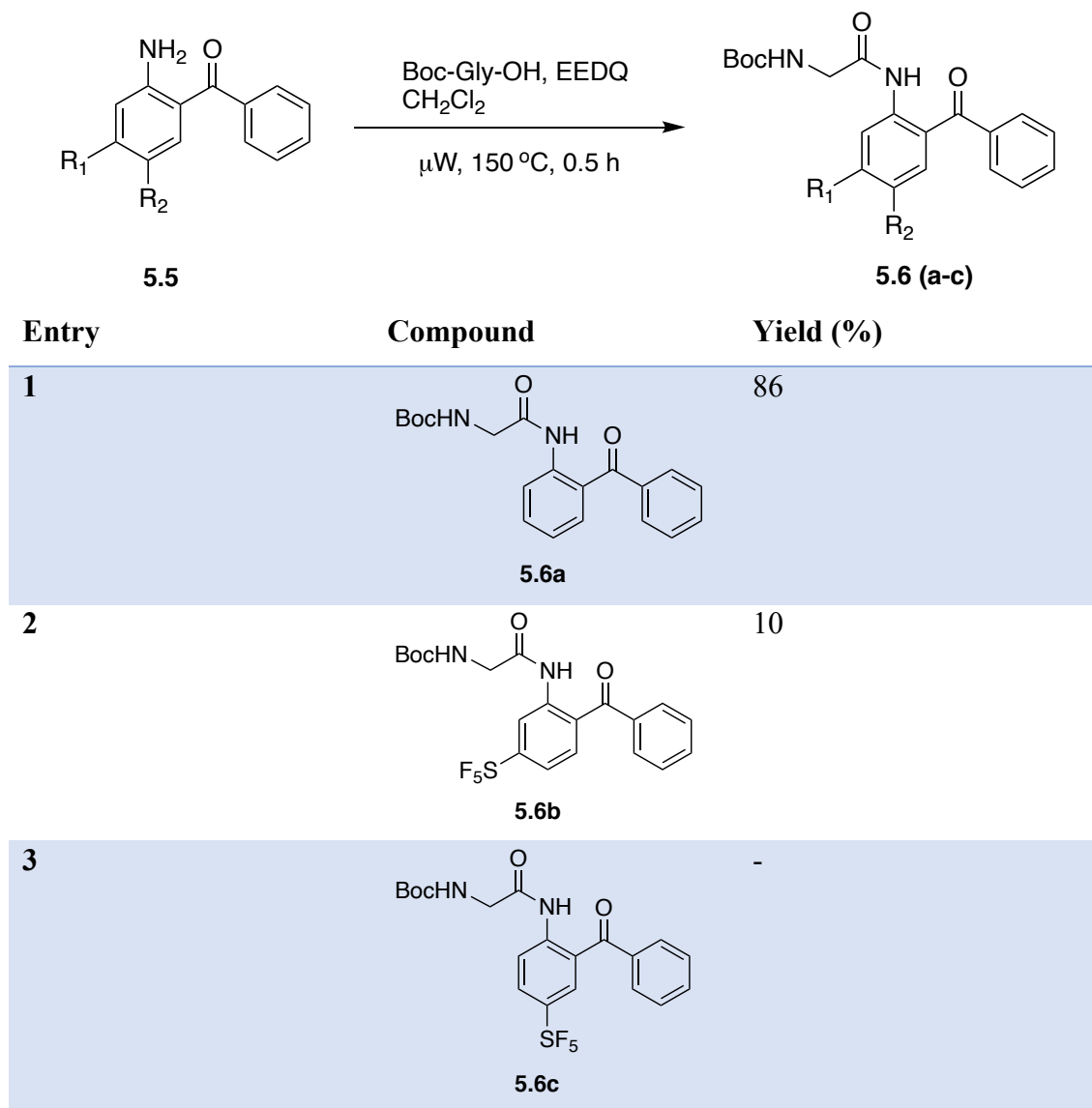
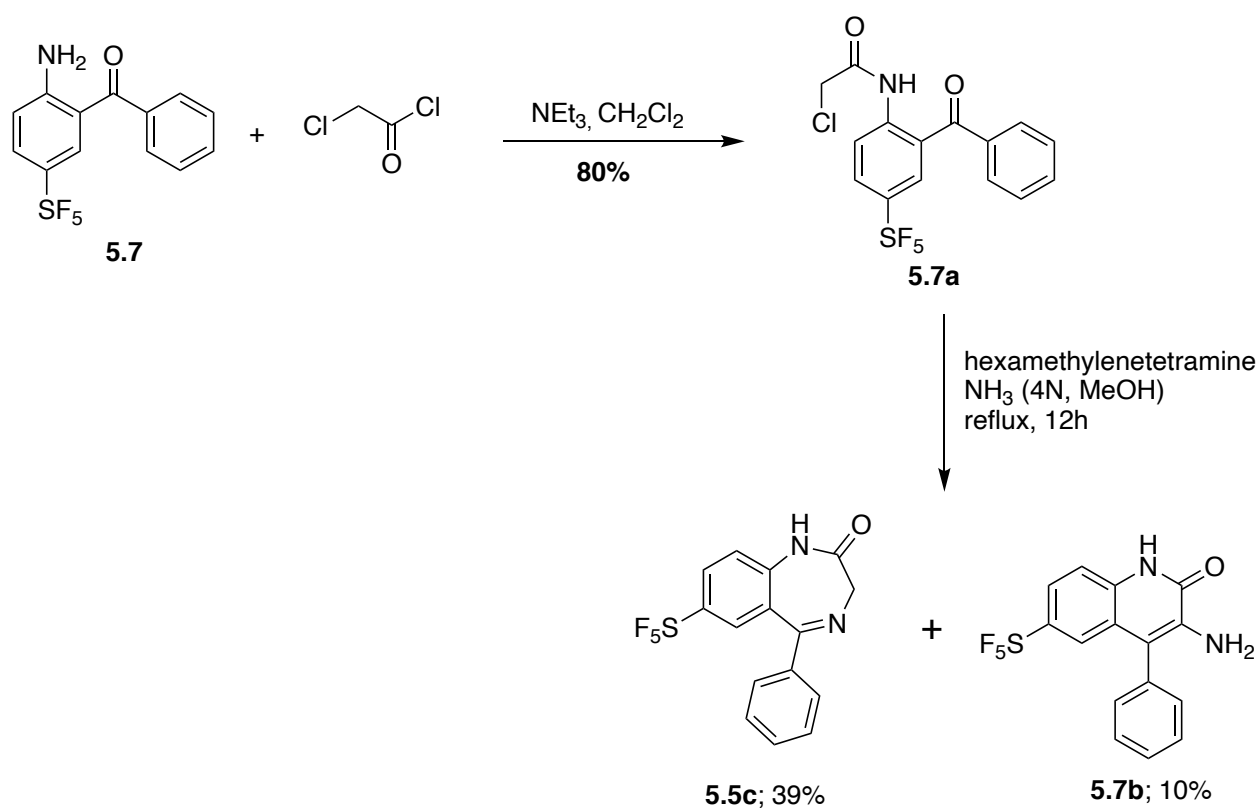


Table 5.1: Boc-Gly-OH coupling reactions

As the microwave approaches on the SF<sub>5</sub> derivatives were unsuccessful, yet worked on a standard 1,4-BZD core (entry 1), it was decided to synthesise the desired products using other approaches.

As above, a method published by Hoffmann-La Roche, using hexamethylenetetramine with ammonia as a reagent, was reported to be successful even for starting materials with electron-withdrawing substituents. This method was also reported to give good yields although none were stated. Accordingly, this was our next method of choice.

Scheme 5.8 shows the multi-step route to synthesise a SF<sub>5</sub>-substituted nordiazepam analogue (**5.5c**). **5.7** was acylated using chloroacetyl chloride then aminated with hexamethylenetetramine in the presence of ammonia (Scheme 5.8). Analysis of the crude mixture, gratifyingly, showed the presence of the expected product as well as a similar by-product, which we tentatively assigned the structure (**5.7b**), notably by the similarity of its <sup>1</sup>H NMR spectrum to that of its 4-chloro-derivative (**5.8**, Figure 5.13). The two products could be separated after a normal phase and a reverse phase column chromatographic purification. Formation of side products<sup>221</sup> of the type **5.7b** has been reported in Sternbach's paper but as a rare occurrence.<sup>214</sup> **5.7b** was observed each time this reaction was carried out. A similar side reaction was observed when 2-amino-4-pentafluorosulfanyl-benzophenone was reacted.



Scheme 5.8: Multi-step synthesis of SF<sub>5</sub> substituted nordiazepam

The <sup>1</sup>H NMR and <sup>13</sup>C NMR spectra of **5.5c** and **5.7b** are very similar. The obvious difference between these structural isomers would be the absence of a CH<sub>2</sub> in the case of **5.7b**. However, the NH<sub>2</sub> peak appears around the same region as the CH<sub>2</sub> on **5.5c**. Another notable difference is the distinct chemical shifts of the two NH peaks; NH on **5.7b** appears around δ = 12.2 ppm, whereas the NH peak of **5.5c** appears around δ = 10.5 ppm. The presence of NH<sub>2</sub> at δ = 3.19 as well as the second aromatic ring that is closer, further deshields the NH proton, and so, the chemical shift is shifted more downfield (δ = 12.2 ppm). Figure 5.9 shows the proton NMR spectrum of the mixture of the two compounds in deuterated methanol and Figure 5.10 highlights the NH<sub>2</sub> and CH<sub>2</sub> peaks of compounds **5.7b** and **5.5c**.

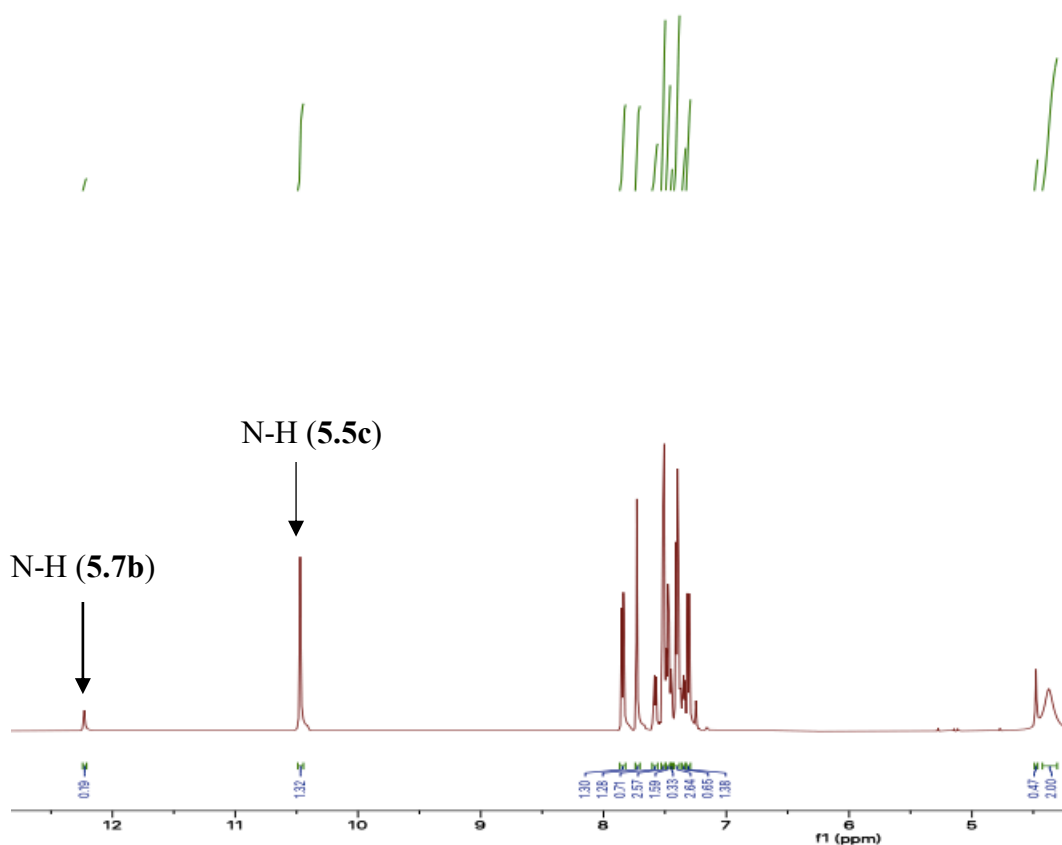


Figure 5.9:  $^1\text{H}$  NMR spectra of **5.5c** and **5.7b** mixture in  $\text{CD}_3\text{OD}$

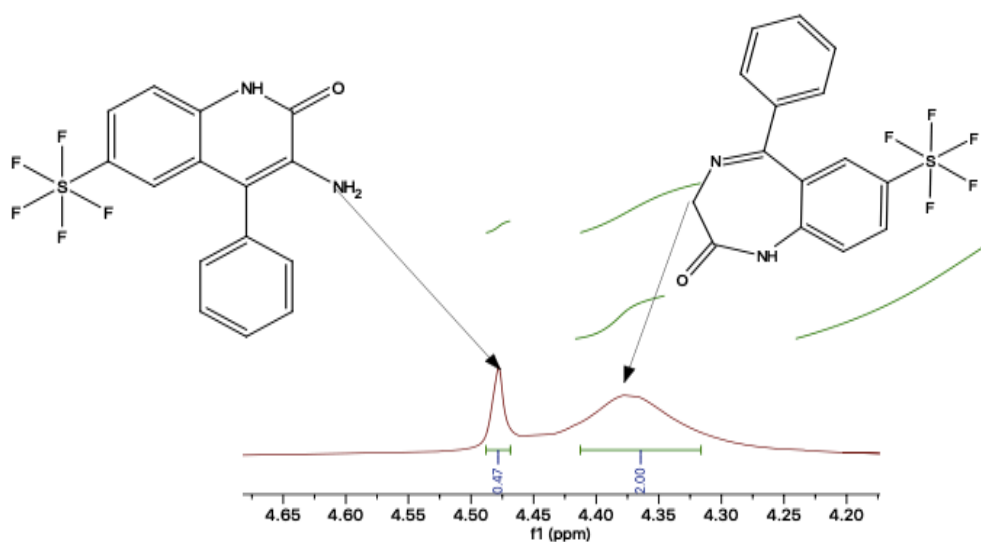


Figure 5.10: Comparing  $\text{NH}_2$  and  $\text{CH}_2$  peaks of **5.5c** and **5.7b** from  $^1\text{H}$  NMR mixture

Compound **5.5c** was crystallised by diffusion method using hexane and DCM to obtain colourless crystals and this confirmed both the regiochemistry of the  $\text{SF}_5$ -substituent and the formation of the BZD core (Figure 5.11).



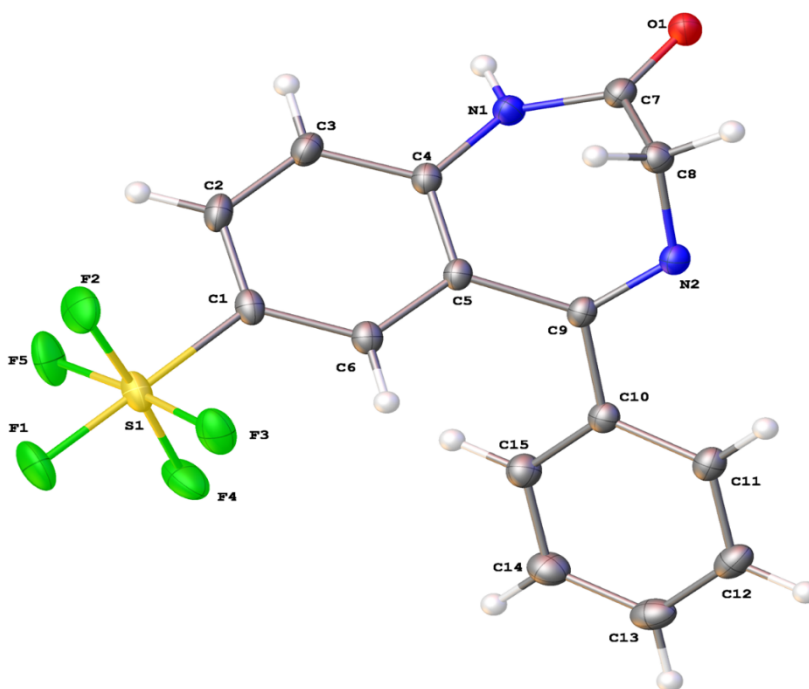


Figure 5.11: Crystal structure showing 5.5c

We were not successful in growing a crystal of compound **5.7b**. A  $^1\text{H}$  NMR sample of the latter, in  $\text{CD}_3\text{CN}$ , was subjected to a  $\text{D}_2\text{O}$  shake (Figure 5.12) and, as expected, the  $\text{NH}_2$  peak significantly diminished, after hydrogen exchange for deuterium, with its integration reducing from around 2H to 0.18H. At the same time the NH peak at  $\delta = 10.28$  ppm disappeared.

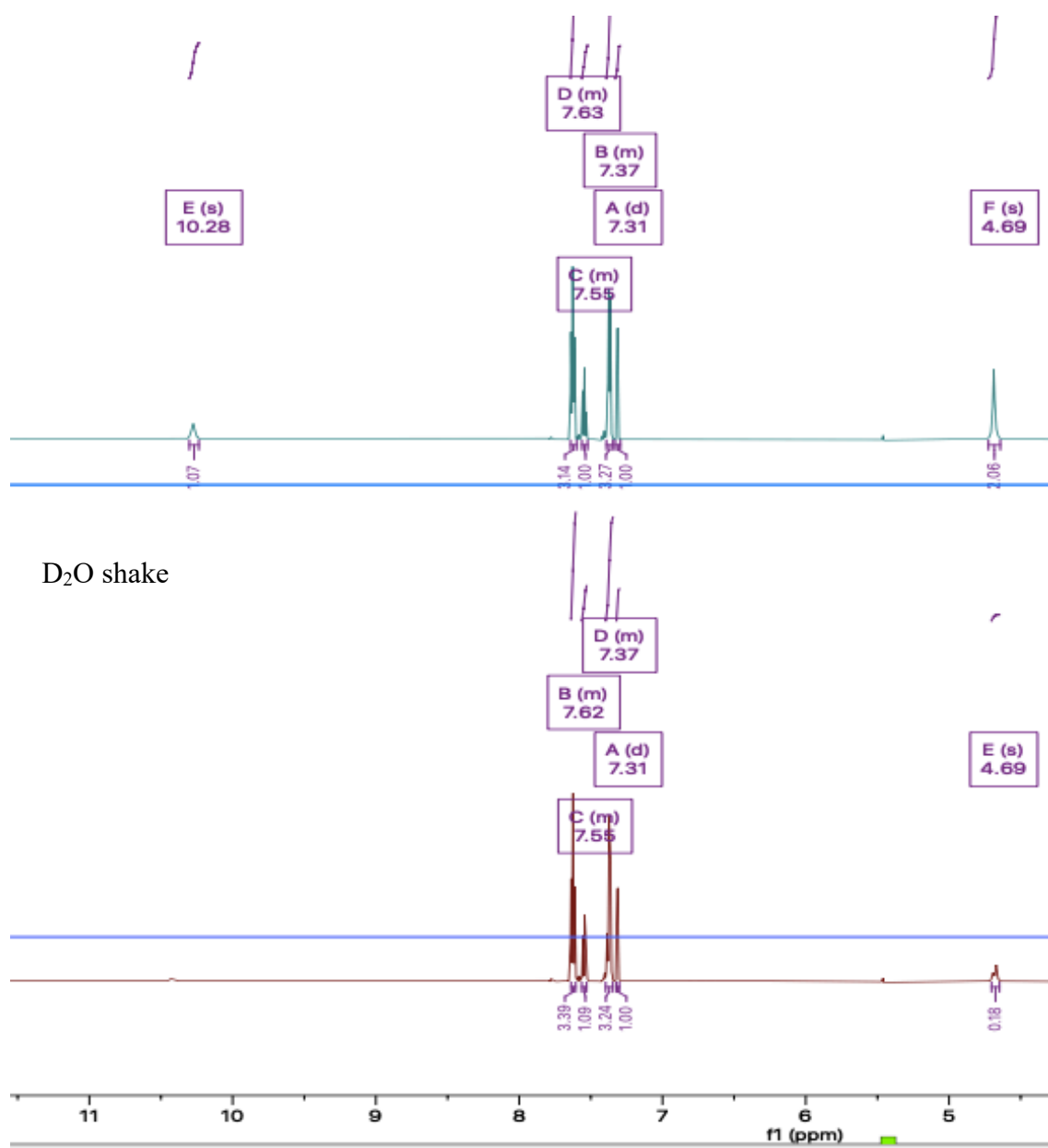


Figure 5.12: Comparing  $^1\text{H}$  NMR of **5.7b** before and after  $\text{D}_2\text{O}$  shake in  $\text{CD}_3\text{CN}$

The  $^1\text{H}$  NMR spectrum of **5.7b** was comparable with that of a similar Cl-substituted compound, from the literature (**5.8**, Figure 5.13).

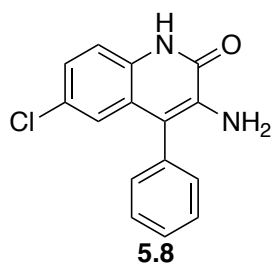


Figure 5.13: 4-chloro-derivative of **5.7b**

Tables 5.2 and 5.3 show proton NMR assignment of compounds **5.8** in  $\text{CDCl}_3$ <sup>222</sup> and **5.7b** in  $\text{CD}_3\text{CN}$  respectively. It can be seen that  $^1\text{H}$  NMR of **5.7b** agrees with that of **5.8**.

Chemical shift (ppm)	Multiplicity	Integration	Coupling constant (Hz)	Assignment
12.11	s	1		NH
7.61-7.20	m	7		ArH
7.03	d	1	2.1	ArH
4.44	s	2		NH <sub>2</sub>

Table 5.2:  $^1\text{H}$  NMR assignment of **5.8**

Chemical shift (ppm)	Multiplicity	Integration	Coupling constant (Hz)	Assignment
10.28	s	1		NH
7.64-7.60	m	3		ArH
7.56-7.52	m	1		ArH
7.39-7.35	m	3		ArH
7.31	d	1	2.5	ArH
4.69	s	2		NH <sub>2</sub>

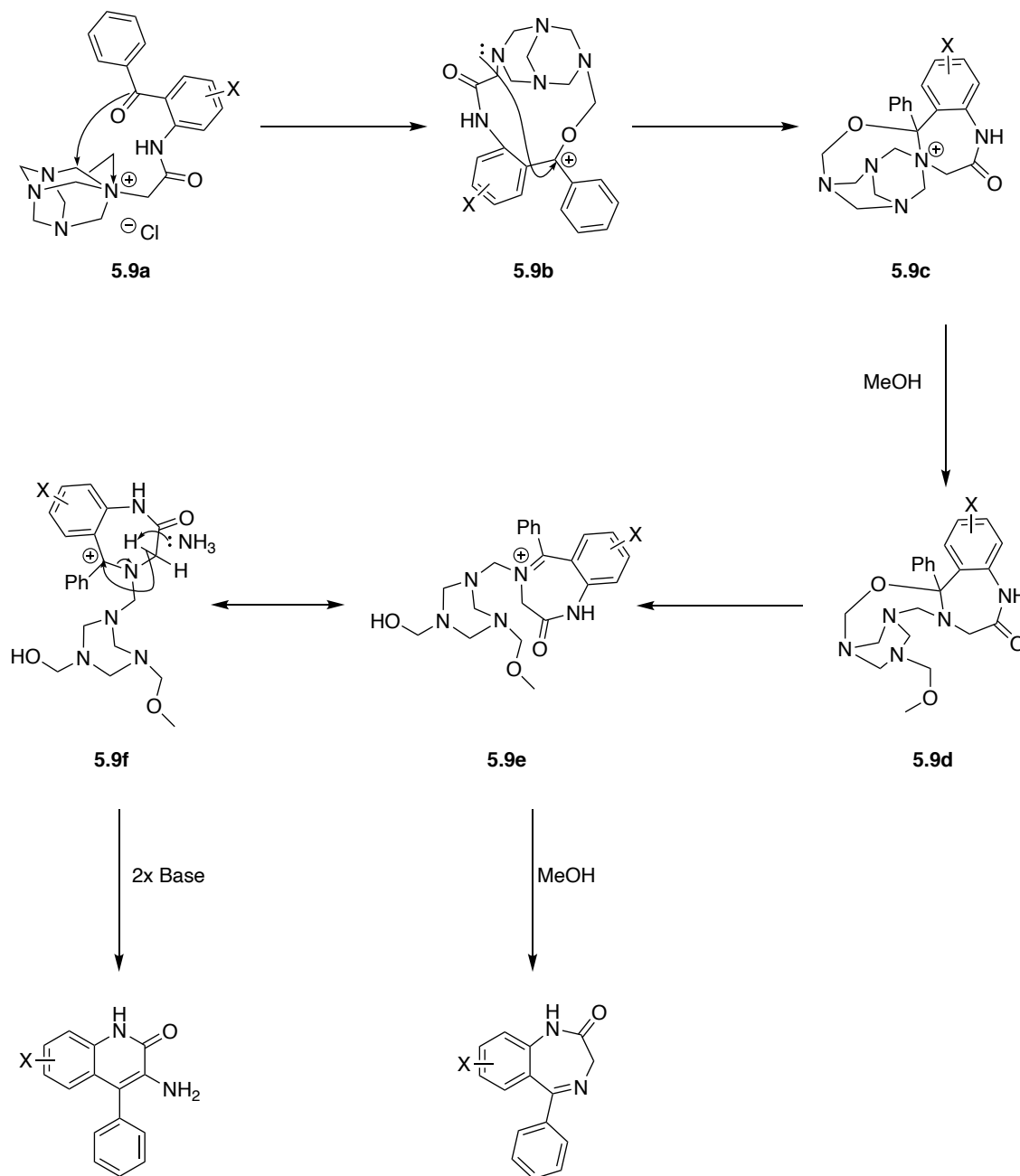
Table 5.3:  $^1\text{H}$  NMR assignment of **5.7b**

A mechanism proposed by Nikola Blazevic *et al.* in 1979<sup>223</sup> for the formation of 1,4-BZD in the presence of hexamethylenetetramine is shown in Scheme 5.9. It also shows the formation of the side product when two equivalence of a base is present.

The initial step of the mechanism shows a nucleophilic substitution which proceeds via  $\text{S}_{\text{N}}2$ . However, the carbonyl used is too poor a nucleophile and is unlikely to react in an  $\text{S}_{\text{N}}2$  fashion therefore, we believe the reaction would rather proceed via an  $\text{S}_{\text{N}}1$  (Scheme 5.10). In addition the carbocation generated can be stabilized by the  $\alpha$  nitrogen, and the reaction is in polar protic condition which favours  $\text{S}_{\text{N}}1$ .

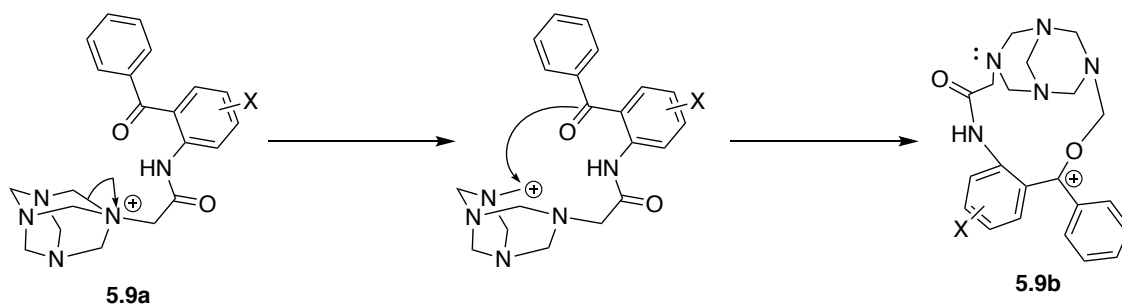
According to the proposed method (Scheme 5.9), after the formation of **5.21**, it undergoes alcoholysis to give the desired 1,4-BZD. Nikola Blazevic *et al.* reported that the formation of side product is due to the presence of base in the reaction. They refluxed the hexaminium salt in ethanol without any ammonia present and reported 1,4-BZD as the only product formed and in good yields, unless the equivalence of alcohol used for the solvolysis was insufficient. We propose a different

route towards the formation of the side product in Scheme 5.11. In the presence of ammonia, an enolate is generated which undergoes an aldol condensation followed by alcoholysis of hexaminium salt to generate the side product.

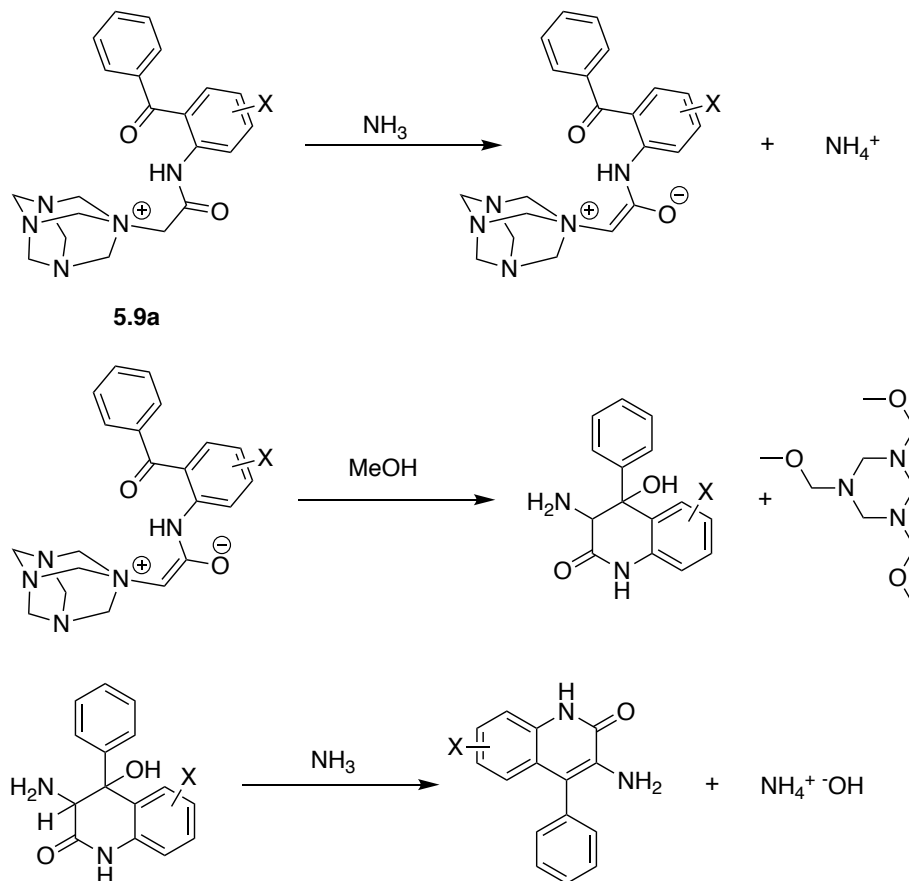


X = Cl, NO<sub>2</sub>, SF<sub>5</sub>, CF<sub>3</sub>, F

Scheme 5.9: Cyclisation to form 1,4-BZD as proposed by Nikola Blazevic et al.<sup>223</sup>



*Scheme 5.10:  $S_N1$  substitution to generate the intermediate*



*Scheme 5.11: Proposed mechanism for the formation of the side product*

Hexamethylenetetramine can hydrolyse to ammonia and formaldehyde. Formaldehyde is capable of reacting with 2-chloroacetamidobenzophenone to form imidazolidinones.<sup>224</sup> In 1976, a patent published by Hoffmann-La Roche<sup>216</sup> states that reacting compound of type **5.7a** (Scheme 5.8) with hexamethylenetetramine in the presence of ammonia gives improved yields compared to their prior art which utilizes hexamethylenetetramine alone to synthesise benzodiazepines. Ammonia assisted reactions were said to be good especially when position 1 of BZD is substituted. When position 1 is non-substituted, the hydrogen and oxygen forms a hydrogen bond and the electron withdrawing capability of group X determines the strength of this bond. Highly electron withdrawing groups weaken the N-H bond, thus making the hydrogen bond stronger. This favours reaction with formaldehyde to form imidazolidinones (Figure 5.14). Ammonia would scavenge any

formaldehyde formed, preventing imidazolidinone formation. Other side products such as quinazolines were reported by G.M. Clarke *et al.* although these were not observed in our experiments.<sup>224</sup>

In the above mentioned patent, the characteristic of solvent was stated as inert organic. The only requirement of the solvent is to dissolve the starting materials. Some of the solvents that could be used as reported were any lower alcohols such as methanol, ethanol, propanol, etc.<sup>216</sup>

According to G.M. Clarke *et al.*, formation of the side product proceeds via an epoxide intermediate (Figure 5.15). They also conveyed a dubiety towards the mechanism proposed by Nikola Blazevic *et al* as the intermediates from the proposed mechanism were not observed in their hands.

From a crude <sup>1</sup>H NMR spectrum of our reaction mixture, we only observed formation of 1,4 benzodiazepine and phenylquinolone together with 2-aminoacetamidobenzophenone. No epoxide was observed in our reactions.

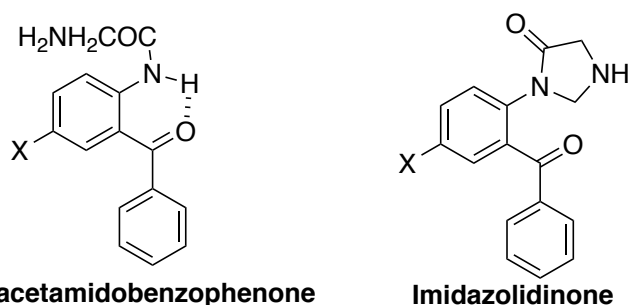


Figure 5.14: Intermolecular hydrogen bonding between N-H-O that favours the formation of imidazolidinone

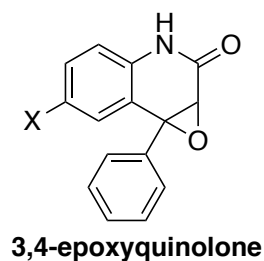
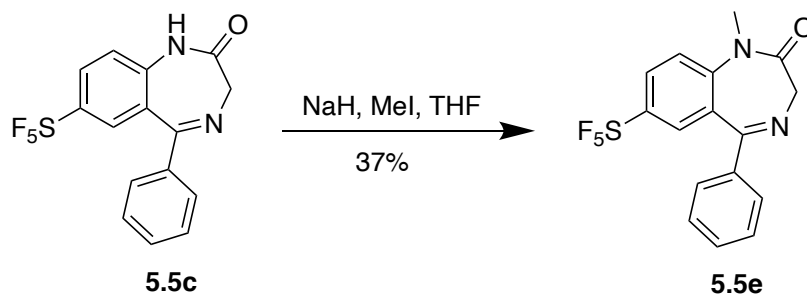


Figure 5.15: 3,4-epoxyquinolone Intermediate

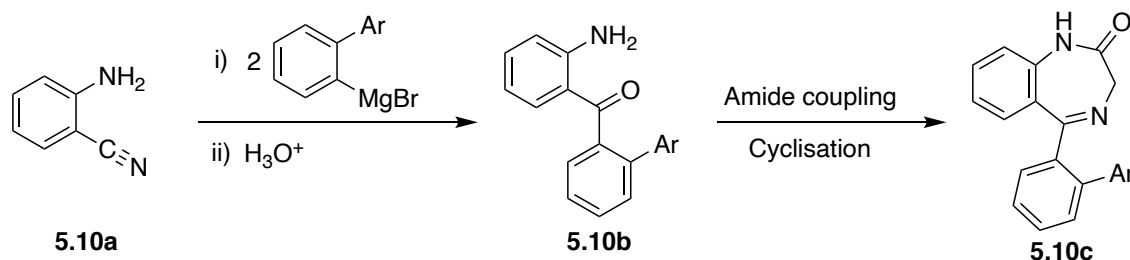
After the success with synthesising a SF<sub>5</sub> containing nordiazepam analogue, we moved on to addressing the methylation of it to form the diazepam counterpart. A standard *N*-methylation route using sodium hydride and methyl iodide was employed to synthesise SF<sub>5</sub>-diazepam (Scheme 5.12).



*Scheme 5.12: N-methylation to form SF<sub>5</sub>-diazepam*

The reaction was low yielding, again attributed to the electron poor ring. The yield calculated on recovered starting material is, however, 92%.

Functionalisation at position 2' with bulky and electrophilic substituents is desirable, as previously mentioned. Functionalised aromatic rings could make a good choice of substituent at this position. The aromatic ring can be made bulky and/or electrophilic. Introducing an aryl group at the 2'-position can be achieved by various routes. A typical method to do so is illustrated in Scheme 5.13.<sup>225</sup>

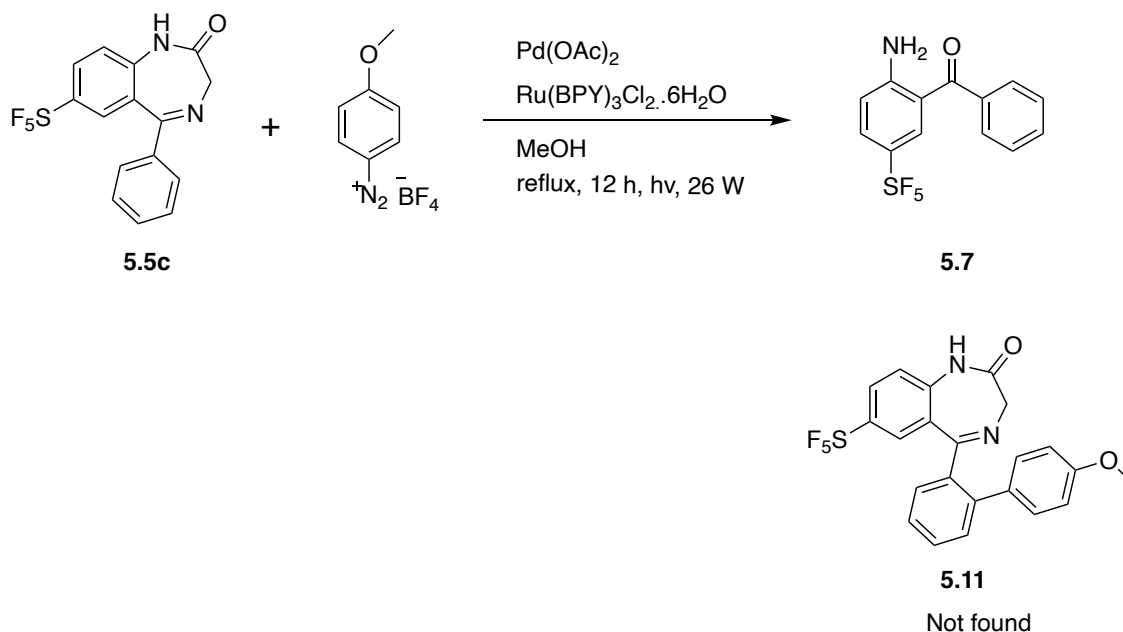


*Scheme 5.13: Multi-step route to arylate at position 2'*

The above route requires cryogenics, dry conditions and an acidic work up to yield the desired benzophenone. Having a bulky and electrophilic group on the benzophenone might also negatively affect the yield of the repetitive coupling, cyclisation steps to follow. When a range of ortho-substituted BZDs need to be generated, the above approach seems inefficient as these groups need to be coupled early on in the reaction. In addition, commercially available SF<sub>5</sub> containing aromatic building blocks are limited and expensive.

A better route to synthesise compounds of type **5.10c** would be to arylate in the last step. This would add atom and step economy. Late stage C-H activation to functionalise BZDs is an explored and established method within the Spencer group.<sup>225,226,227</sup> We were also interested in knowing if our methods work on SF<sub>5</sub> substituted BZDs.

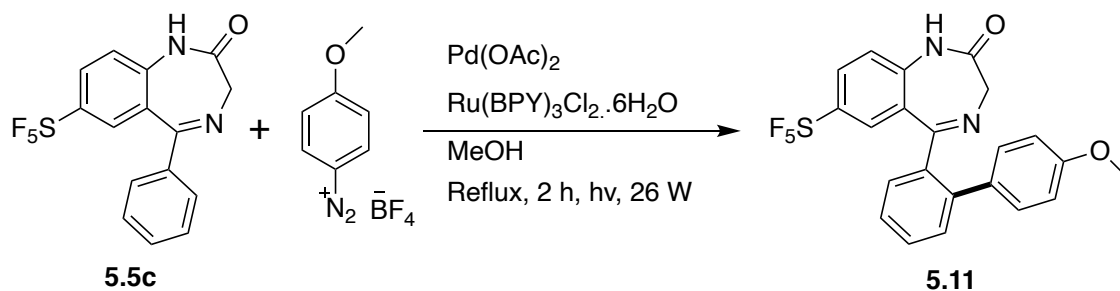
Our initial approach was to use visible-light catalysed procedure mediated by a Ru photocatalyst and Pd catalysis, as well as involving an available diazonium salt; 4-methoxy-benzenediazonium tetrafluoroborate.<sup>226</sup> The reaction was refluxed for 12 hours in methanol and the light source used was a 26W bulb (Scheme 5.14). However, the desired product was not obtained. To our surprise, instead of the arylated product we isolated **5.7**. The product was characterised by <sup>1</sup>H NMR spectroscopy and LCMS.



Scheme 5.14: Photocatalyzed Pd-mediated route for C-H activation

Sternbach *et al.* has reported mild acidic hydrolysis of 2-aminonitrobenzodiazepinones into 2-aminonitrobenzophenones. Heating **5.5c** for prolonged time (12 h) in the above conditions yielded **5.7**.

We were curious to learn if the desired product could be synthesised with a short period of heating under the same conditions. Therefore, **5.5c** was refluxed in MeOH for only 2 hours as shown in Scheme 5.15.



Scheme 5.15: Photocatalyzed synthesis of arylated BZD

Formation of product **5.11** was observed by LCMS (Figure 5.8). A peak with a retention time (*t<sub>R</sub>*) of 20.8 min showed a molecular mass for **5.11** at *m/z* = 468. The peak at *t<sub>R</sub>* 18.6 min indicated the mass of **5.5c**. The product could not be isolated, however, these data indicated that late stage



photocatalyzed C-H activation works on SF<sub>5</sub> substituted 1,4-BZDs. Due to the expensive nature of the SF<sub>5</sub> substituted amino benzophenone and the low yielding cyclisation step, we were reluctant to further explore photocatalyzed C-H activation.

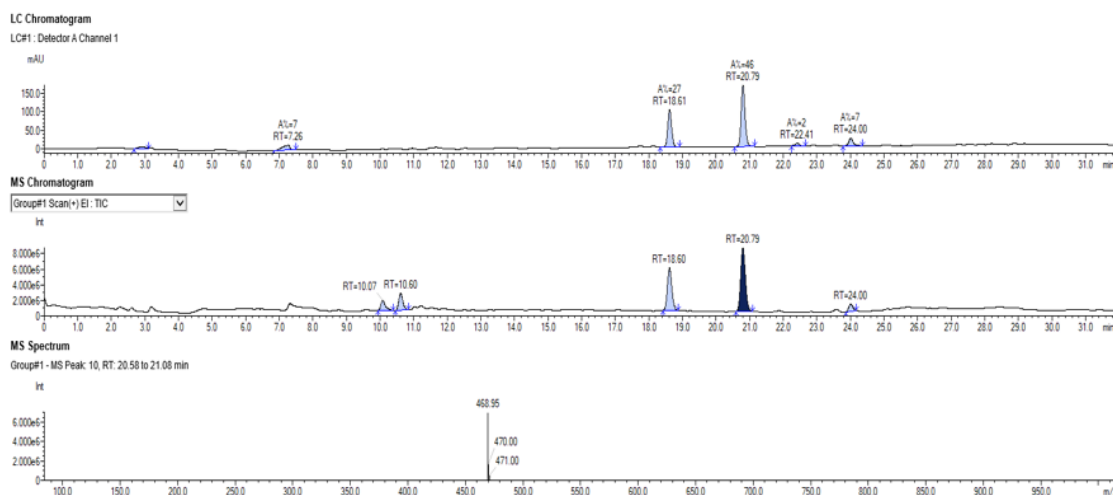
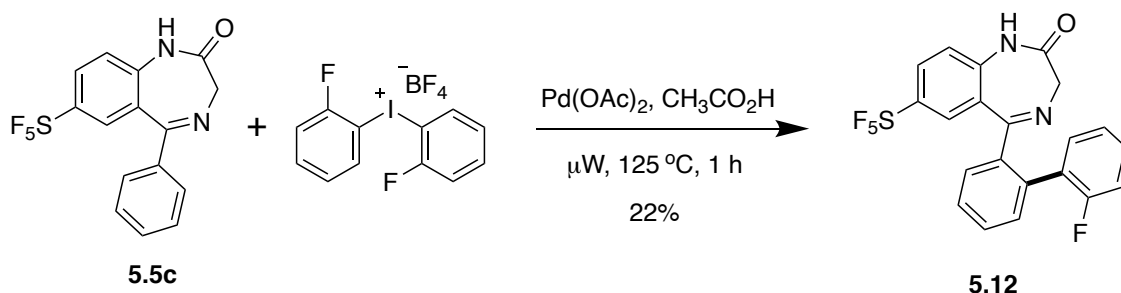


Figure 5.16: LCMS data showing the *m/z* of the desired product.

The Spencer group have previously published another Pd mediated C-H activation involving microwave chemistry and iodonium salts.<sup>225</sup> This method was appealing to us as it only used one metal catalyst and the work up was much simpler than the photocatalyzed method. An unoptimized attempt at Pd-catalysed C–H activation with iodonium salts, using our previously described conditions, involving microwave chemistry afforded the expected ortho-arylated product **5.12** (Scheme 5.16). This illustrates that catalytic C–H activation chemistry is now amenable to the synthesis of polyfluorinated BZDs and **5.12** was now available for biological assay.



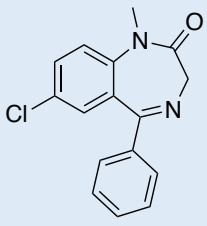
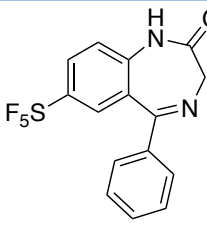
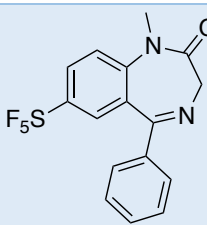
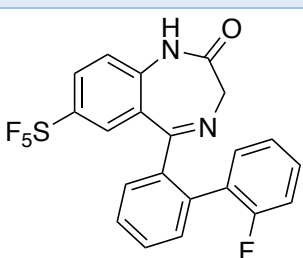
Scheme 5.16: MW mediated ortho-arylation

### 5.2.2 Modelling

The compounds were docked into the cryo-EM structure (PDB ID: 6HUP)<sup>193</sup> of the  $\alpha 1\beta 3\gamma 2L$  GABAA receptor at the interfacial benzodiazepine binding site between the principal (+)  $\alpha$  and complementary (–)  $\gamma$  subunit using Schrödinger Glide<sup>102,228</sup>. We evaluated their apparent binding affinity using the Glide score, which predicts possible binding of the ligands in the benzodiazepine

binding site of the receptor and produces a set of initial ligand conformations. However, the task of accurately estimating protein ligand binding affinities is beyond the capabilities of docking scoring functions and, hence Glide scores are not always congruent with experimental data.

A Glide score was determined for compounds **5.5c**, **5.5e** and **5.12** and was compared against diazepam and the metabolite, nordiazepam (Table 5.4). Diazepam showed similar binding in comparison with the SF<sub>5</sub>-substituted diazepam (**5.5e**) analogue. The SF<sub>5</sub>-substituted nordazepam analogue (**5.5c**), however gave a better Glide score suggesting it binds stronger than diazepam in the binding site. The Glide score of the ortho C-H activated analogue (**5.12**) was (-3.98 kcal/mol) very poor in comparison.

Entry	1,4-BZD	Glide score (kcal/mol)
1	 <p><b>Diazepam</b></p>	-4.74
2	 <p><b>5.5c</b></p>	-4.97
3	 <p><b>5.5e</b></p>	-4.74
4	 <p><b>5.12</b></p>	-3.98

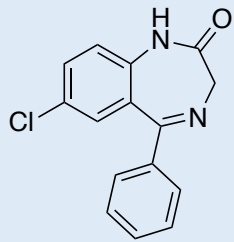
5	 <p data-bbox="746 443 917 474"><b>Nordiazepam</b></p>	-5.36
---	---	-------

Table 5.4: Glide score of diazepam versus SF<sub>5</sub>-substituted BZDs

Figure 5.17 shows diazepam interacting with the amino acid residues in the  $\alpha 1\beta 3\gamma 2L$  receptor. The dashed lines indicate hydrogen bonds and  $\pi$ - $\pi$  interactions. The chlorine atom interacts with the  $\alpha$ His102 side chain. The distance between the chlorine atom and the nitrogen on the  $\alpha$ His102 was measured as 2.89 Å. According to the literature, the polarized *N*-methyl group forms hydrogen bonds with Thr206, Tyr209 and the backbone of Tyr159 in a C-H----O fashion.<sup>229</sup> However, no such hydrogen bond interactions were observed in our modelling study.

Poses of **5.5c**, **5.5e** as well as their superpositions with diazepam and nordiazepam with the best Glide score docked in the  $\alpha 1\beta 3\gamma 2L$  receptor are shown in Figure 5.18.

The images show that there is no interaction between SF<sub>5</sub> and the amino acid side chains.

A direct comparison of **5.5e** and diazepam can be made. We calculated the distance between SF<sub>5</sub> and  $\alpha$ His102 to be 5.34 Å. This was calculated between the closest fluorine to  $\alpha$ His102, and  $\alpha$ His102. This distance is almost double the distance between chlorine and  $\alpha$ His102 on diazepam (2.89 Å). This could explain the lack of interaction between SF<sub>5</sub> and the  $\alpha$ His102. This applies to **5.5c** and **5.12**, as well (Figure 5.18 and 5.19).

The interaction of the chlorine in diazepam with the ring nitrogen on the histidine side chain can be defined as a halogen bond. The IUPAC definition of a halogen bond is: “a halogen bond occurs when there is evidence of a net attractive interaction between an electrophilic region associated with a halogen atom in a molecular entity and a nucleophilic region in another, or the same molecular entity.”<sup>230</sup> In a halogen bond the distance between the halogen and the nucleophile is less than the sum of the van der Waals radii of the atoms. The sum of van der Waals radii between chlorine and nitrogen = 3.34 Å and the distance calculated between them = 2.89 Å.

In contrast sum of the van der Waals radii between a F atom and nitrogen = 2.89 Å which is less than the distance between F on SF<sub>5</sub> and nitrogen (5.34 Å).

A halogen bond can also be described as a direct, non-covalent interaction between a nucleophilic region of a Lewis base with a halogen atom as a Lewis acid where the halogen atom is involved in a covalent bonding in an R-X manner (Figure 5.20, X = halogen). Anisotropic distribution of electronic charge around halogen atoms allows them to act as both a Lewis acid and base. Many covalently bonded halogens have positive electrostatic potential on their outer surface known as a  $\sigma$  hole. The positive sigma hole allows the halogen to bond with the negative Lewis base. In

addition, they possess negative charge on their equatorial sides due to the lone pairs. As per  $\sigma$  hole concept, fluorine lacks a positive  $\sigma$  hole on the outer surface as its charge distribution is spherical and so is incapable of interacting with the nucleophilic nitrogen on His102.

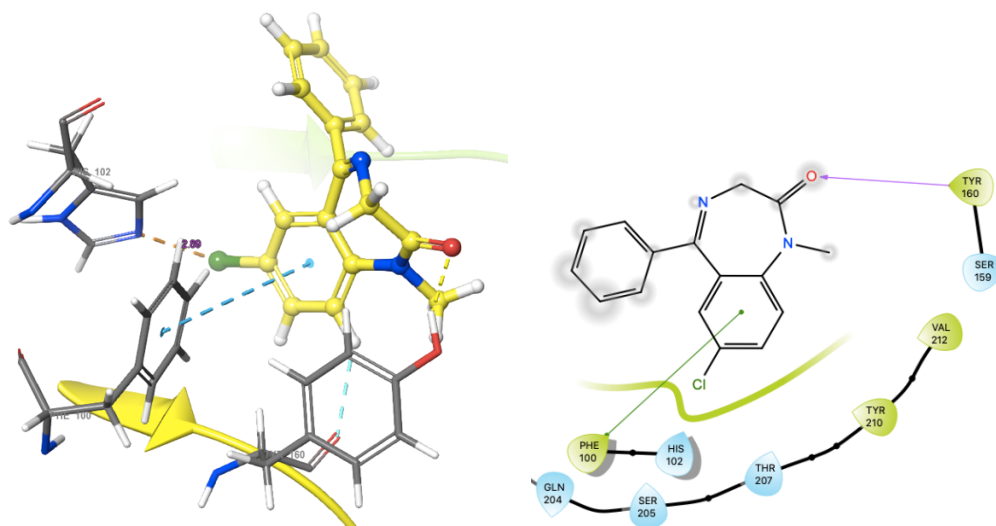


Figure 5.17:  $\alpha 1\beta 3\gamma 2L$  receptor in complex with diazepam (yellow)

Careful inspection of Figure 5.18d which shows an overlap of nordiazepam and **5.5c** in the GABA<sub>A</sub> receptor site, reveals that due to the bulky size of SF<sub>5</sub>, the positioning of SF<sub>5</sub>-nordiazepam is slightly different to that of nordiazepam and the SF<sub>5</sub> group is not oriented toward the nitrogen on His102 to form a bond.

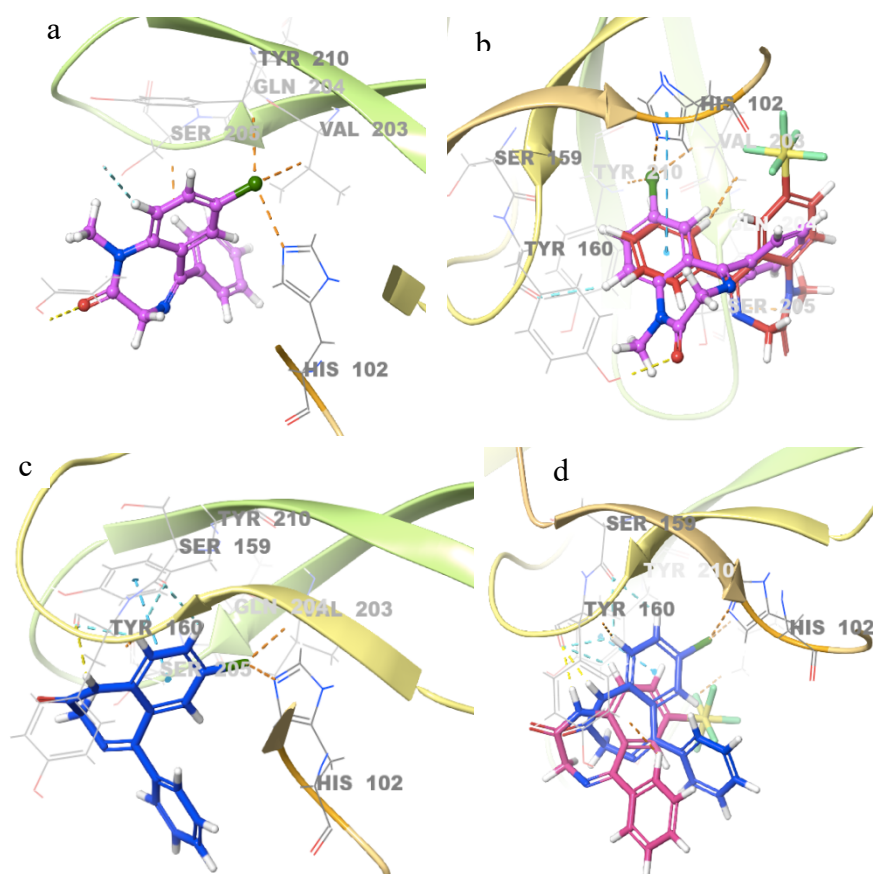


Figure 5.18: Benzodiazepines in complex with  $\alpha 1\beta 3\gamma 2L$  receptor a) Brown dashed lines show hydrophobic clashes between diazepam's (purple) chlorine and amino acid residues, His102, Val203, and Tyr210. b) diazepam (purple) overlapped with SF<sub>5</sub>-diazepam (5.5e, red). c) Interactions between nordiazepam (blue) and the benzodiazepine binding pocket and d) superposition of nordiazepam and SF<sub>5</sub>-nordiazepam (5.5c, pink). Yellow dashed lines indicate hydrogen bonds. Pi-pi interactions are indicated by blue dashed lines. SF<sub>5</sub>-diazepam and SF<sub>5</sub>-nordiazepam do not interact with the His102 which is a key interaction between diazepam and the binding pocket.

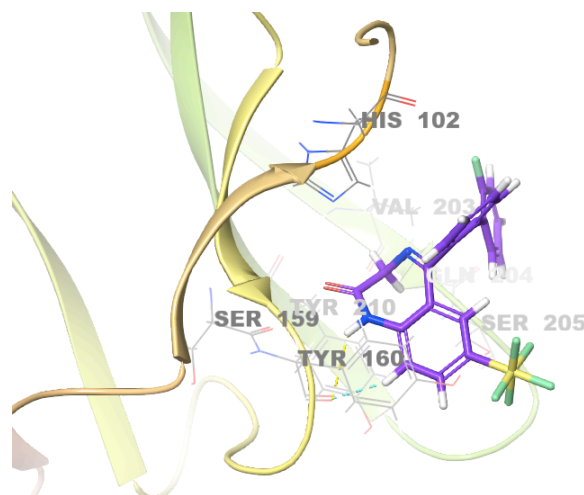


Figure 5.19: 5.12 (Violet) in complex with  $\alpha 1\beta 3\gamma 2L$  receptor shows no interaction with His102. Aromatic hydrogen bonds are indicated by blue dashed lines.

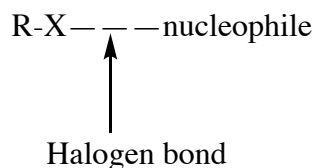
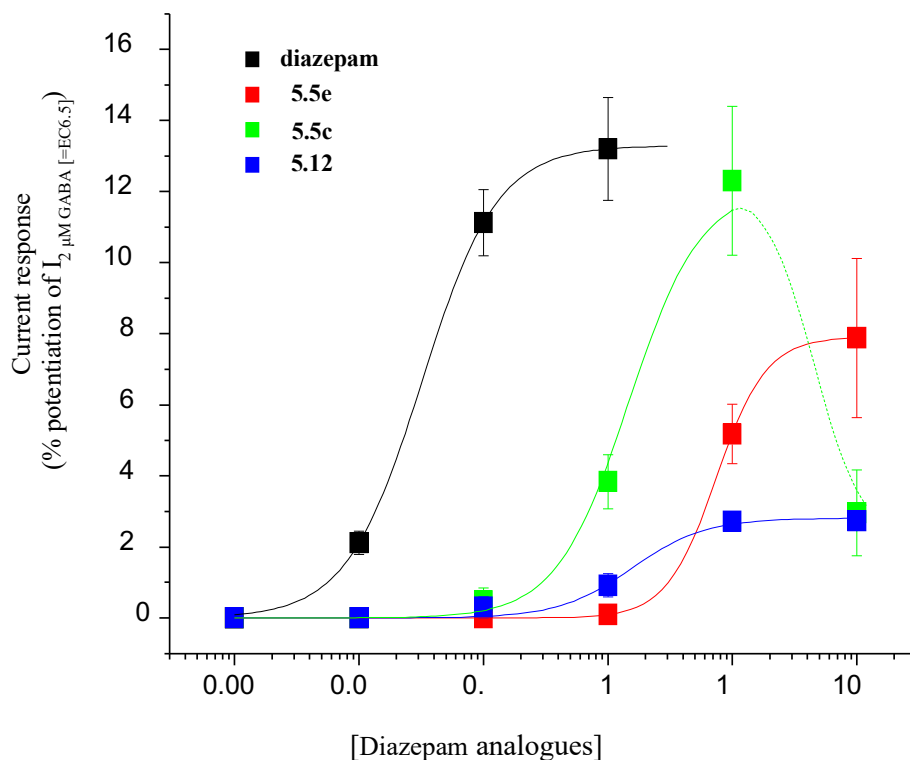


Figure 5.20: Demonstration of halogen bonding

With the benzodiazepines to hand and predictive docking studies, our next obvious step was to test out compounds in an assay. Biological studies were performed by Dr Trevor Smart at UCL. To access functionality of the BDZ ligands, whole-cell patch-clamp recording from human embryonic kidney cells expressing recombinant  $\alpha 1\beta 2\gamma 2L$  GABA<sub>A</sub>Rs were used. The analogues, 5.5c, 5.5e and 5.12 were compared to diazepam for their ability to potentiate 2 $\mu$ M GABA-induced currents ( $\sim$ EC<sub>6.5</sub>). The three SF<sub>5</sub>-diazepam analogues showed much lower potencies than diazepam (60- (5.5c), 70- (5.12), and 190-fold lower (5.5e)). The relative extent of potentiation was very low for 5.12,  $\sim$ half that of diazepam for 5.5e, or near equivalent with diazepam for 5.5c (Graph 5.1; Table 5.5). For 5.12, the efficacy level of the potentiation was reduced at the highest concentration of 100  $\mu$ M (Graph. 5.1). Such inhibition has been reported before for benzodiazepines like diazepam and flurazepam and could reflect increased desensitization of GABA<sub>A</sub>Rs. From these data, it is clear that substituting Cl on the benzo ring for SF<sub>5</sub> has a deleterious effect primarily on BDZ potency and to a large extent, also on their relative efficacy at GABA<sub>A</sub> receptors. This is likely to be due to disruption of the Cl –  $\alpha$ H102 interaction, which is known to be critical for BDZ modulation at GABA<sub>A</sub> receptors.

Concentration-response curves of the potentiation effects by **diazepam**, **5.5e**, **5.5c** and **5.12**



Graph 5.1: Whole-cell voltage-clamp tests of diazepam and the sulphur-pentafluoride diazepam analogues, **5.5c**, **5.5e** and **5.12** on  $\alpha 1\beta 2\gamma 2L$   $GABA_A$  receptors expressed in HEK cells

	<b>Diazepam</b>	<b>5.5e</b>	<b>5.5c</b>	<b>5.12</b>
Maximum Potentiation	133 ± 15 %	77 ± 20 %	138 ± 19 %	28 ± 2.5 %
Potency	7.518 ± 0.067	5.247 ± 0.121	5.780 ± 0.043	5.697 ± 0.076
pEC <sub>50</sub> ± SEM (EC <sub>50</sub> )	(30 nM)	(5.7 μM)	(1.7 μM)	(2.0 μM)
Number of cells	5	5	5	5

Table 5.5: In-Vitro studies of SF<sub>5</sub>-substituted BZDs in comparison with diazepam

### 5.3 Conclusion

Three SF<sub>5</sub>-substituted 1,4-BZDs were synthesised and were evaluated *in silico* and *in vitro*. Multiple approaches were tried before successfully synthesising the desired product; **5.5c**. While synthesising the mentioned compound, we isolated compound **5.7b** as a by-product. Synthesis of an

SF<sub>5</sub> *meta*-substituted BZD (**5.5b**) was attempted but failed due to separation issues from the by-product. *N*-methylated benzophenones when treated with hexamethylenetetramine gave 1,4 BZDs in good yields as reported by Blazevic and Sternbach. This may be a desirable approach for the synthesis of both the *meta* and *para*-SF<sub>5</sub>-substituted BZDs in the future.

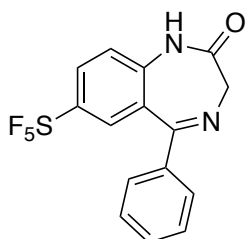
*In silico* calculations of the BZDs predicted that the SF<sub>5</sub>-substituted diazepam and nordazepam analogues are better or equivalent in activity in comparison with diazepam. However, *in vitro* binding studies showed the three SF<sub>5</sub>-diazepam analogues to have much lower potencies than diazepam. It can be appreciated that although Glide scoring is an ideal function for generating a library of compounds with potential biological activity by estimating binding affinity, it is not an absolute tool to predict accurate activity of ligands.

## 5.4 Experimental

### 5.4.1 Organic Chemistry

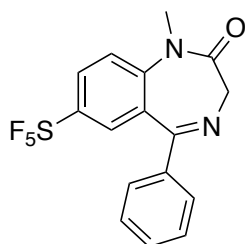
All commercially purchased materials and solvents were used without further purification unless specified otherwise. NMR spectra were recorded on a Varian VNMRS 600 (<sup>1</sup>H 600 MHz, <sup>13</sup>C 126 MHz) and VNMRS 400 (<sup>19</sup>F 376 MHz, <sup>2</sup>H 61 MHz and <sup>31</sup>P 162 MHz) spectrometer and prepared in deuterated solvents such as CDCl<sub>3</sub> and DMSO-d<sub>6</sub>. <sup>1</sup>H and <sup>13</sup>C chemical shifts were recorded in parts per million (ppm). Multiplicity of <sup>1</sup>H-NMR peaks are indicated by s – singlet, d – doublet, dd – doublets of doublets, t – triplet, pt – pseudo triplet, q – quartet, m – multiplet and coupling constants are given in Hertz (Hz). Electrospray ionisation – high resolution mass spectra (ESI-HRMS) were obtained using a Bruker Daltonics Apex III where Apollo ESI was used as the ESI source. All analyses were conducted by Dr A. K. Abdul-Sada. The molecular ion peaks [M]<sup>+</sup> were recorded in mass to charge (m/z) ratio. LC-MS spectra were acquired using Shimadzu LC-MS 2020, on a Gemini 5 m C18 110 Å. column. All X-ray analyses were performed at the UK National Crystallography Services, Southampton. Purifications were performed by flash chromatography on silica gel columns or C18 columns using a Combi flash RF 75 PSI, ISCO unit.

#### 7-(Pentafluoro-λ<sup>6</sup>-sulfanyl)-5-phenyl-2,3-dihydro-1H-1,4-benzodiazepin-2-one (**5.5c**)



Triethylamine (188 mg, 1.86 mmol, 2.0 equiv.) was added to a solution of 2-benzoyl-4-(pentafluoro- $\lambda^6$ -sulfanyl)aniline (0.300 g, 0.93 mmol, 1.0 equiv.) in dichloromethane (1 mL) and the mixture was stirred at room temperature. After an hour the mixture was cooled in an ice bath, and chloroacetyl chloride (0.210 g, 1.86 mmol, 2.0 equiv.) dissolved in dichloromethane (1 mL) and cooled in an ice bath was added dropwise to the reaction mixture. The reaction was stirred overnight at room temperature. The reaction was monitored by TLC and the crude was concentrated in *vacuo* and purified by flash chromatography (petroleum ether: ethyl acetate; 7:3) to obtain pure *N*-[2-benzoyl-4-(pentafluoro- $\lambda^6$ -sulfanyl)phenyl]-2-chloroacetamide as a clear solid (0.301 g, 0.75 mmol, 81%). Ammonium carbonate (0.360 g, 3.75 mmol, 5.0 equiv.) was suspended in a solution of ammonia (2M) in ethanol (5 mL) and stirred. Hexamethylenetetramine (0.531 g, 3.75 mmol, 5.0 equiv.) was added and refluxed. After 5 minutes of refluxing, a solution of *N*-(2-benzoyl-4-sulfur penta-fluoro phenyl)-2-chloroacetamide (0.301 g, 0.75 mmol, 1.0 equiv.) in dichloromethane (3 mL) was added and the reaction mixture was refluxed overnight. After cooling, the latter was concentrated in *vacuo* and dissolved in toluene (5 mL). *p*-Toluene sulfonic acid (6 mg, 0.03 mmol, 0.04 equiv.), was added to the solution and the mixture was refluxed for 1 hour. The crude was concentrated in *vacuo* and purified over a column of silica (hexane:ethyl acetate; 3:7), followed by a reverse phased column (C18, acetonitrile:water, 1:3) to obtain the pure product as a colourless solid (83 mg, 31%, 72 mg, 26% of *N*-(2-benzoyl-4-sulfur penta-fluoro phenyl)-2-chloroacetamide recovered).  $^1\text{H}$  NMR (600 MHz, Chloroform-*d*)  $\delta$  9.40 (s, 1H, NH), 7.87 (dd,  $J$  = 8.9, 2.6 Hz, 1H, ArH), 7.74 (d,  $J$  = 2.6 Hz, 1H, ArH), 7.53 – 7.50 (m, 2H, 2ArH), 7.50 – 7.47 (m, 1H, ArH), 7.41 (m, 2H, 2ArH), 7.25 (d,  $J$  = 8.9 Hz, 1H, ArH), 4.37 (s, 2H, CH<sub>2</sub>);  $^{13}\text{C}$  NMR (600 MHz, Chloroform-*d*)  $\delta$  172.1 (C=O), 169.8 (C=N), 148.1 (t,  $^1J_{F,C}$  = 18.9 Hz, ArC-SF<sub>5</sub>), 141.0 (ArC), 138.2 (ArC), 131.1 (ArC), 129.6 (2ArC), 129.5 (m, ArC), 129.1 – 129.01 (m, ArC), 128.5 (2ArC), 126.8 (ArC), 121.5 (ArC), 56.7 (CH<sub>2</sub>);  $^{19}\text{F}$  NMR (376 MHz, Chloroform-*d*)  $\delta$  83.51 (q,  $J$  = 150.5 Hz), 63.32 (d,  $J$  = 150.5 Hz); LCMS Purity (UV) = 96%,  $t_{\text{R}}$  18.1 min; HRMS - ESI ( $m/z$ ) found 385.0404, calc. for [C<sub>15</sub>H<sub>11</sub>F<sub>5</sub>N<sub>2</sub>OS] [Na]<sup>+</sup>: 385.0404; IR (neat)  $\nu_{\text{max}}$ /cm<sup>-1</sup>: 3089 (N-H), 1687 (C=O), 1610 (C=N), 824 (S-F); mp = 158 – 159 °C.

### 1-methyl-7-(pentafluoro- $\lambda^6$ -sulfanyl)-5-phenyl-2,3-dihydro-1H-1,4-benzodiazepin-2-one (5.5e)

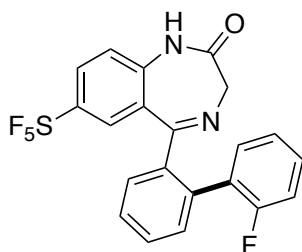


Sodium hydride (0.023 g, 0.94 mmol, 2.0 equiv.) was added to a solution of **5.5c** (0.170 g, 0.47 mmol, 1.0 equiv.) in dry THF (1 mL) and the mixture was stirred for 1 hour. Methyl iodide (0.133 g, 0.94 mmol, 2.0 equiv.) was added to the reaction mixture, which was stirred at room temperature



overnight. Crude product was washed with water (3 x15 mL), extracted with ethyl acetate (3 x15 mL), dried over MgSO<sub>4</sub>, filtered and concentrated in *vacuo*. The crude was purified over a column of silica (hexane:EtOAc; 7:3) to obtain a colourless solid as the title compound (0.066 g, 37%). <sup>1</sup>H NMR (600 MHz, Chloroform-d) δ 7.93 (dd, *J* = 9.1 Hz, 2.6 Hz, 1H, ArH), 7.73 (d, *J* = 2.6 Hz, 1H, ArH), 7.61 (m, 2H, ArH), 7.52 (m, 1H, ArH), 7.45(m, 3H, ArH), 4.90 (d, *J* = 11.0 Hz, 1H, CH), 3.79 (d, *J* = 11.0 Hz, 1H, CH), 3.44 (s, 3H, CH<sub>3</sub>); <sup>13</sup>C NMR (600 MHz, Chloroform-d) δ 169.8 (C=O), 168.8 (C=N), 148.4 (C-SF<sub>5</sub>), 146.1(ArC), 137.7 (ArC), 131.1 (ArC), 129.4 (2ArC), 128.7 (4ArC), 128.6(ArC), 121.2 (ArC), 56.9 (CH<sub>2</sub>), 34.9 (CH<sub>3</sub>); <sup>19</sup>F NMR (400 MHz, Chloroform-d) δ 83.10 (p, *J* = 150.4 Hz), 63.23 (d, *J* = 150.4 Hz); LCMS Purity (UV) = 96%, *t*<sub>R</sub> 19.5 min; HRMS - ESI(*m/z*) found 377.0749, calc. for [C<sub>16</sub>H<sub>13</sub>F<sub>5</sub>N<sub>2</sub>OS][H]<sup>+</sup>:377.0742; IR (neat) *v*<sub>max</sub>/cm<sup>-1</sup>: 1682 (C=O), 1611 (C=N), 835 (S-F); mp = 240 – 242 °C.

**5-{{[1,1'-Biphenyl]-2-yl}-7-(pentafluoro-λ<sup>6</sup>-sulfanyl)-2,3-dihydro-1H-1,4-benzodiazepin-2-one (5.12)**



**5.5c** (86 mg, 0.24 mmol, 1.0 equiv.), bis(2-fluorophenyl)iodonium tetrafluoroborate (145 mg, 0.36 mmol, 1.5 equiv.) and glacial acetic acid were combined in a 10 mL microwave vial. The vial was degassed and purged with argon before adding palladium (II) acetate (7 mg, 0.0089 mmol, and 0.01 equiv) and stirring at 125 °C in the microwave for 1 hour. Thereafter, the cooled reaction mixture was filtered through celite, washed with dichloromethane (50 mL) and concentrated in *vacuo*. The residue was dissolved in dichloromethane (15 mL), washed with sodium bicarbonate (20 mL) and the aqueous layer extracted with dichloromethane (20 mL x 3), dried over MgSO<sub>4</sub>, filtered and concentrated in *vacuo*. The bright red oil was purified over a column of silica (hexane:EtOAc; 1:4) to obtain a colourless solid as pure product (0.024 g, 22%). <sup>1</sup>H NMR (600 MHz, Chloroform-d) δ 9.49 (s,1H, NH), 7.82 –7.74 (m, 1H, ArH), 7.58 –7.53 (m, 2H, 2ArH), 7.50 (dd, *J* = 8.9, *J* = 2.5 Hz, 1H, ArH), 7.34 –7.30 (m, 2H, 2ArH), 7.07 –7.01 (m, 1H, ArH), 6.92 –6.84 (m, 2H, ArH), 6.78 (d, *J* = 8.9 Hz, 1H, ArH), 6.75 (pt, *J* = 9.0 Hz, 1H), 4.32 (s, 2H, CH<sub>2</sub>); <sup>13</sup>C NMR (600 MHz, Chloroform-d) δ 171.1 (C=O), 170.9 (C=N), 158.7 (ArC-F, d, <sup>1</sup>*J*<sub>F,C</sub> = 247.6 Hz), 148.6 –148.0(ArC-SF<sub>5</sub>), 139.5 (ArC), 138.9 (ArC), 135.7 (ArC), 131.3 (ArC), 131.0 (ArC), 130.4 (ArC), 130.2 (ArC), 129.5 (ArC, d, <sup>3</sup>*J*<sub>F,C</sub> = 7.9 Hz), 128.5 (2ArC), 128.2 (ArC), 127.8 (ArC, d, <sup>2</sup>*J*<sub>F,C</sub> = 15.6 Hz), 127.6 (ArC), 123.7 (ArC), 120.5 (ArC), 115.0 (ArC, d, <sup>2</sup>*J*<sub>F,C</sub> = 22.0 Hz), 56.5 (CH<sub>2</sub>); <sup>19</sup>F NMR (376 MHz, Chloroform-d) δ 83.40 (p, *J* = 150.7 Hz, axial F), 63.07 (d, *J* = 150.7 Hz, equatorial F); LCMS Purity (UV) = 98%, *t*<sub>R</sub>: 19.9 min; HRMS -ESI(*m/z*) found 457.0813, calc. for [C<sub>21</sub>H<sub>15</sub>F<sub>6</sub>N<sub>2</sub>OS][H]<sup>+</sup>:457.0809; IR

(neat)  $\nu_{\max}/\text{cm}^{-1}$ : 3064 (N-H), 1704 (C=O), 1616 (C=N), 1336 (C-F), 836 (S-F); mp = 190 – 191 °C.

#### 5.4.2 Computational ligand docking

Docking was performed using the solved cryo-EM structure of the  $\alpha 1\beta 3\gamma 2\text{L}$  receptor in complex with GABA and diazepam obtained from PDB (ID: 6HUP). The software used was Schrodinger Glide.

#### 5.4.3 Cell culture and recombinant GABA<sub>A</sub>R expression

HEK cells were maintained at 37°C, 95% CO<sub>2</sub>/ 5% O<sub>2</sub> in Dulbecco's Modified Eagle's Medium (DMEM) supplemented with 10% v/v fetal bovine serum and 100 U/ml penicillin/100 µg/ml streptomycin. Cells were transfected with cDNAs encoding enhanced green fluorescent protein (EGFP) and murine  $\alpha 1$ ,  $\beta 2$ ,  $\gamma 2\text{L}$  GABA<sub>A</sub>R<sub>1</sub> subunits in a 1:1:1:1 ratio using a standard calcium-phosphate precipitation method.

#### 5.4.4 Electrophysiology experiments

Whole-cell patch clamp recording from HEK cells was used to study GABA<sub>A</sub> receptor currents as described previously<sup>231</sup> using an Axopatch 200B Axon Instruments amplifier. Patch pipettes (resistance 3-5MΩ) were filled with a solution containing (mM): 120 KCl, 1 MgCl<sub>2</sub>, 11 EGTA, 30 KOH, 10 HEPES, 1 CaCl<sub>2</sub>, and 2 adenosine triphosphate; pH 7.11. The cells were continuously perfused with Krebs recording solution containing (mM): 140 NaCl, 4.7 KCl, 1.2 MgCl<sub>2</sub>, 2.52 CaCl<sub>2</sub>, 11 Glucose and 5 HEPES; pH 7.4. diazepam and SF<sub>5</sub>-analogues were first dissolved in DMSO (stock), and for functional electrophysiology experiments subsequently diluted at least 1000-fold in Krebs solution. Drug solutions were applied to recording cells via a Y-tube application system<sup>[30]</sup>.

The potentiating effects of diazepam, and analogues **2c**, **5c** and **6c** were evaluated in the presence of 2 µM GABA which was equivalent to a current approximately 6.5% of the GABA maximum response (EC<sub>6.5</sub>). The efficacy and potency for the potentiation by each ligand was established by fitting curves to the GABA current response-concentration relationship data points from each of the five individual experiments using the Hill equation,  $I / I_{\max \text{ pot}} = (1 / (1 + (\text{EC}_{50} / [\text{L}])^n))$ . The ligand potency, EC<sub>50</sub>, represents the concentration of the ligand ([L]) inducing 50% of the maximal potentiation current (in the presence of 2 µM GABA), and n is the Hill slope.

Since concentration response EC<sub>50</sub> data are distributed on a logarithmic scale, we converted these to pEC<sub>50</sub> values (pEC<sub>50</sub> = -log(EC<sub>50</sub>)) which are distributed on a linear scale. From pEC<sub>50</sub> values we calculated mean values ± sem, and to facilitate data-interpretation we re-transformed these mean

pEC<sub>50</sub> values into mean EC<sub>50</sub> values (Table 2). The relative efficacy for GABA current potentiation was calculated as a mean percentage  $\pm$  sem of the current induced by 2  $\mu$ M GABA alone.

## Chapter 6.0 Conclusion, Future Directions and Thesis Outcome

The importance of halogen containing fragments, and in particular, fluorine's role in medicinal chemistry was described in Chapter 1.<sup>4,232–234</sup> Recent years have seen a rise in molecules substituted with pentafluorosulfanyl (SF<sub>5</sub>) groups,<sup>22,235</sup> as direct access to aryl- and alkyl-SF<sub>5</sub> building blocks has been achieved.<sup>31,236</sup> Despite their popularity, SF<sub>5</sub> containing arenes remain an underdeveloped class of compounds in medicinal chemistry, mainly due to difficulty accessing the respective building blocks. Therefore, this thesis aimed to expand the repertoire of SF<sub>5</sub> in medicinal chemistry while exploring SF<sub>5</sub> as a bioisostere. In accord with the project's aim, a series of SF<sub>5</sub>-substituted aromatic compounds have been synthesised, some of which are SF<sub>5</sub> analogues of known drugs (teriflunomide, leflunomide, semaxanib, diazepam, and nordiazepam), while utilizing microwave and mechanochemistry when possible.

Chapter 2 discussed the scope of SF<sub>5</sub> as a bioisosteric replacement in leflunomide and its active form, teriflunomide (Figure 6.1). Compounds **2.5** and **2.6** (mentioned in Chapter 2) were synthesised and a biophysical assay conveyed an approximate two-fold greater affinity for **2.6** towards HDHODH compared with teriflunomide. Molecular binding studies also revealed that the bulky SF<sub>5</sub> group fills the binding pocket better than the CF<sub>3</sub> group.

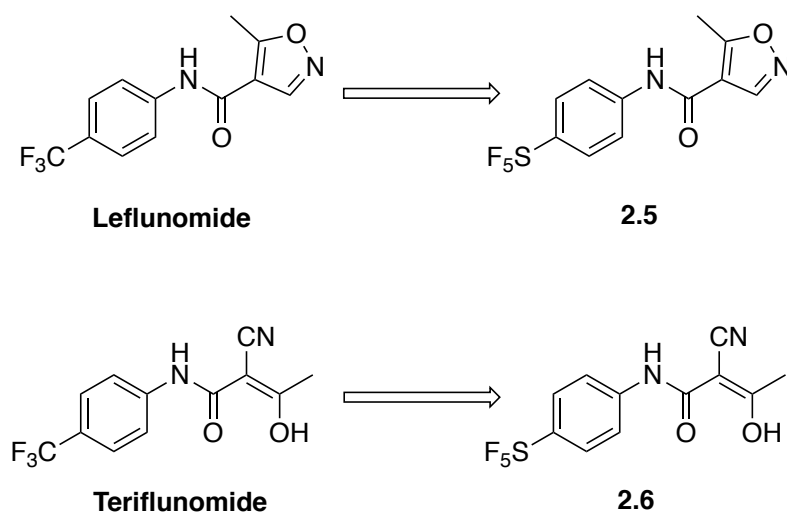
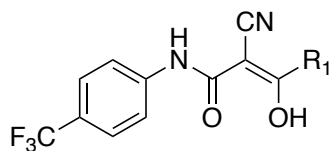


Figure 6.1: Leflunomide, teriflunomide and their SF<sub>5</sub> analogues

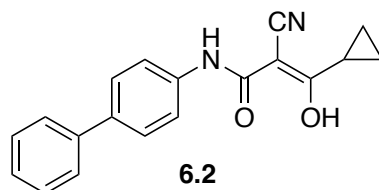
Johnson *et al.*<sup>108</sup> screened a series of compounds similar to teriflunomide, against *P. falciparum* DHODH (*Pf*DHODH) as well as the human DHODH (HDHODH). The series revealed that having a cyclopropane (compound **6.1**) in the place of the methyl group enhances binding affinity (Figure 6.2). Furthermore, replacement of CF<sub>3</sub> on teriflunomide with a phenyl significantly improved binding affinities. Figure 6.3 displays augmented binding affinity of compound **6.2** towards HDHODH.



**Teriflunomide**,  $R_1$ ; = Me,  $IC_{50}$ ; *PfDHODH* = 190.1  $\mu$ M, *HDHODH* = 0.261  $\mu$ M

**6.1**,  $R_1$ ; = ,  $IC_{50}$ ; *PfDHODH* = 92.5  $\mu$ M, *HDHODH* = 0.117  $\mu$ M

Figure 6.2: Teriflunomide vs cyclopropane analogue (6.1)



$IC_{50}$ ; *PfDHODH* = 223.6  $\mu$ M, *HDHODH* = 0.053  $\mu$ M

Figure 6.3: Binding affinity of 6.2 towards *PfDHODH* & *HDHODH*

Future studies on this work could involve synthesis and analysis of compound **6.3** and **6.4** for their *HDHODH* binding affinity (Figure 6.4).

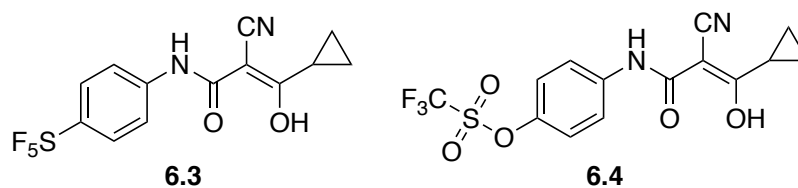


Figure 6.4: Compounds 6.3 and 6.4

Chapter 3 discussed the synthesis of a library of SF<sub>5</sub>-comprising small molecules via a simple amide bond construction. The synthesis involved coupling of amines such as morpholine, piperazine, piperidine, and pyridine with 3 and 4-SF<sub>5</sub>-benzoyl chlorides. To aid coupling of hydrolysed acid chlorides, HATU (hexafluorophosphate azabenzotriazole tetramethyl uronium), was used. In order to ease purification, solid supported scavenger resin, MP-Trisamine (microporous polystyrene-bound nucleophilic scavenger), was used to remove unreacted acid chloride from the reactions.<sup>237</sup>

A collaboration with the Covid Moonshot Consortium which is an open source initiative, lead to the synthesis of a couple of compounds related to **TRY-UNI-714a760b-6**. **TRY-UNI-714a760b-6** is a non-covalent M<sup>pro</sup> inhibitor. Compounds **3.3c** and **3.3d** were synthesised and analysed for their affinity towards M<sup>pro</sup> binding site (Figure 6.5). A fluorescence assay revealed that compounds **3.3c** and **3.3d** does not satisfactorily inhibit M<sup>pro</sup>. Analysis of similar compounds, **TRY-UNI-714a760b-20** (Figure 6.6), indicated that replacing chlorine on **TRY-UNI-714a760b-6** with electron withdrawing substituents can lead to a decrease in inhibition of viral activity.<sup>101</sup>

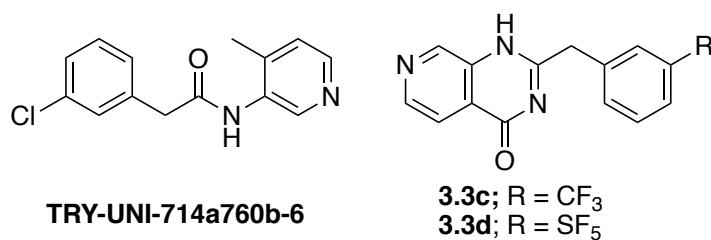


Figure 6.5: TRY-UNI-714a760b-6 and related compounds 3.3(c-d)

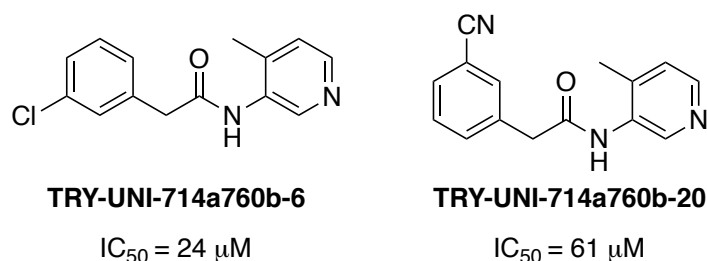


Figure 6.6: Comparing  $IC_{50}$ s of TRY-UNI-714a760b-6 & TRY-UNI-714a760b-20

Chapter 4 described the synthesis of a series of SF<sub>5</sub> substituted oxindoles to expand the repertoire of pentafluorosulfanyl chemistry in medicinal chemistry. Included in the series were two SF<sub>5</sub> cognates of Semaxanib.<sup>165</sup> Using molecular modelling and a radioactive kinase assay we compared activities of Semaxanib and its SF<sub>5</sub> counterparts in the VEGFR2 binding pocket to learn that SF<sub>5</sub> is too bulky a substituent to occupy the ATP-binding site, and in particular, it impedes the ligand's ability to interact with the adenine pocket. In addition, a NO<sub>2</sub>-substituted oxindole, and SF<sub>5</sub>-substituted spirooxindoles were synthesised via Knoevenagel condensation. The reaction was performed using microwave chemistry as well as mechanochemistry. Synthesis via mechanochemistry was successful when one of the reagents used was a liquid. Liquid assisted grinding could be employed to facilitate Knoevenagel condensation where, all the reagents are of solid state.

Analysis of SF<sub>5</sub> as a bioisostere was accomplished by replacing chlorine and nitro groups in Chapter 5 through developing SF<sub>5</sub>-substituted analogues of nordiazepam and diazepam (**5.5c** and **5.5e**). Benzodiazepine was functionalised at positions 1, 7 and 2' (Figure 6.7). Late stage C-H activation was performed on SF<sub>5</sub>-substituted nordiazepam (**5.5c**) via a microwave route as well as a visible-light catalysed procedure, while refluxing in methanol, to modify at position 2'. Both routes would yield the desired product however, heating **5.5c** for a prolonged time under the condition described in Chapter 5 (Scheme 5.14) yielded 2-benzoyl-4-(pentafluoro- $\lambda^6$ -sulfanyl)aniline.

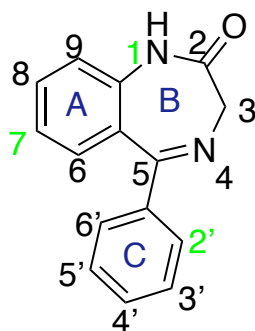


Figure 6.7: Benzodiazepine

*In vitro* binding studies showed the three SF<sub>5</sub>-diazepam analogues (**5.5c**, **5.5e**, & **5.12**) to have much lower potencies than diazepam. Substituting Cl on the benzodiazepine ring for SF<sub>5</sub> has a damaging effect on BZD potency as well as on their relative efficacy at GABA<sub>A</sub> receptors. The Cl -  $\alpha$ H102 interaction is known to be critical for BZD modulation at GABA<sub>A</sub> receptors. This interaction has been disrupted when substituted with SF<sub>5</sub> due to its bulkiness. The distance between F and  $\alpha$ H102 is too big for forming interactions.

As substitution of a bulky and electrophilic group at position 2' is known to improve the activity of the ligand, we propose synthesis of compound **6.5** (Figure 6.8).

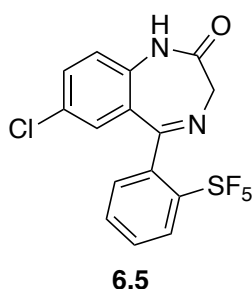


Figure 6.8: SF<sub>5</sub>-substituted at position 2'

The distance calculated between chlorine of compound **6.5** and His102 is 2.71 Å which is smaller than the distance between chlorine and His102 in diazepam (2.89 Å) and the Glide score obtained for this docking is -5.21 kcal/mol which is more negative than the one obtained for diazepam. This suggests that this compound might serve to be an adequate binder in the GABA<sub>A</sub> receptor, however, it is not conclusive and synthesis of the compound in question is required. Unfortunately, the SF<sub>5</sub>-containing starting material required to synthesis this compound is not commercially available, moreover, an expensive Home Office Scheduled Drugs License would probably be required to acquire and use a nordazepam precursor to **6.5**.

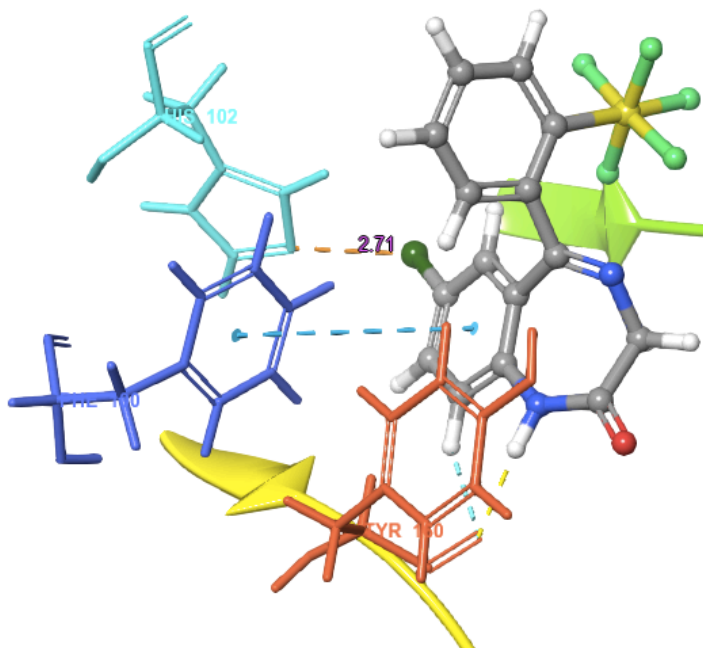


Figure 6.9: Compound 6.5 in complex with GABA<sub>A</sub> receptor

## 6.1 Thesis outcomes

### Publications:

1. A. Jose, R. K. Tareque, M. Mortensen, R. Legay, S. J. Coles, G. J. Tizzard, B. W. Greenland, T. G. Smart, M. C. Bagley and J. Spencer, *Tetrahedron*, 2021, 132020. This paper describes contents from Chapter 5.
2. Contents from Chapters 2, 3 & 4 are soon to be published.

### Poster presentations:

- A. Jose, J. Spencer and M. Bagley “Reagentless synthesis of sulfurpentafluoride containing aromatic compounds” RSC Fluorine conference 2019 on 11<sup>th</sup> April 2019, University of Southampton, Southampton.
- A. Jose, J. Spencer and M. Bagley “Incorporating SF<sub>5</sub> into privileged structures” Flow chemistry and reagentless synthesis on 30<sup>th</sup> September 2019, University of Southampton, Southampton.
- A. Jose, S. Ortoll, J. Spencer and M. Bagley “Scaffold synthesis using flow and microwave chemistry” Labfact management and collaboration meeting on 16<sup>th</sup> and 17<sup>th</sup> January, 2019, Caen, France.

### Oral presentations:

- A. Jose, J. Spencer and M. Bagley “Investigating the scope of SF<sub>5</sub> in medicinal chemistry” PhD symposium 2020, University of Sussex.



- A. Jose, J. Spencer and M. Bagley “Incorporating SF<sub>5</sub> into privileged structures” Labfact launch event, 2018, Southampton.

### Awards and Honours:

- 2019 Bader Prize for best returning Sussex Graduate

## 6.2 References

- 1 Turning Laboratories into Factories (LabFact) | Chemistry | University of Southampton, <https://www.southampton.ac.uk/chemistry/research/projects/lab-fact.page>, (accessed 1 May 2021).
- 2 Turning Laboratories into Factories, <https://www.labfact.eu/>, (accessed 22 April 2021).
- 3 P. Shah and A. D. Westwell, *J. Enzyme Inhib. Med. Chem.*, 2007, **22**, 527–540.
- 4 S. Purser, P. R. Moore, S. Swallow and V. Gouverneur, *Chem. Soc. Rev.*, 2008, **37**, 320–330.
- 5 N. V. Goncharov, R. O. Jenkins and A. S. Radilov, *J. Appl. Toxicol.*, 2006, **26**, 148–161.
- 6 J. Fried and E. F. Sabo, *J. Am. Chem. Soc.*, 1954, **76**, 1455–1456.
- 7 C. Heidelberger, N. K. Chaudhuri, P. Danneberg, D. Mooren, L. Griesbach, R. Duschinsky, R. J. Schnitzer, E. Plevin and J. Scheiner, *Nature*, 1957, **179**, 663–666.
- 8 M. B. van Niel, I. Collins, M. S. Beer, H. B. Broughton, S. K. F. Cheng, S. C. Goodacre, A. Heald, K. L. Locker, A. M. MacLeod, D. Morrison, C. R. Moyes, D. O’Connor, A. Pike, M. Rowley, M. G. N. Russell, B. Sohal, J. A. Stanton, S. Thomas, H. Verrier, A. Alan P. Watt and J. L. Castro, *J. Med. Chem.*, 1999, **42**, 2087–2104.
- 9 T. Besset, P. Jubault, X. Pannecoucke and T. Poisson, *Org. Chem. Front.*, 2016, **3**, 1004–1010.
- 10 S. Rossi, A. Puglisi, L. Raimondi and M. Benaglia, *ChemCatChem*, 2018, **10**, 2717–2733.
- 11 J. Wang, M. Sánchez-Roselló, J. L. Aceña, C. del Pozo, A. E. Sorochinsky, S. Fustero, V. A. Soloshonok and H. Liu, *Chem. Rev.*, 2014, **114**, 2432–2506.
- 12 W. A. Sheppard, *J. Am. Chem. Soc.*, 1962, **84**, 3072–3076.
- 13 W. A. Sheppard, *J. Am. Chem. Soc.*, 1962, **84**, 3064–3072.
- 14 R. W. Winter and G. L. Gard, *J. Fluor. Chem.*, 2004, **125**, 549–552.
- 15 D. A. Jackson and S. A. Mabury, *Environ. Toxicol. Chem.*, 2009, **28**, 1866.
- 16 G. Iakobson, J. Du, A. M. Z. Slawin and P. Beier, *Beilstein J. Org. Chem.* 11162, 2015, **11**, 1494–1502.
- 17 P. Adhikari, D. Bhattacharyya, S. Nandi, P. K. Kancharla and A. Das, *Org. Lett.*, 2021, **23**, 2437–2442.
- 18 W. R. Dolbier, *Guide to Fluorine NMR for Organic Chemists*, John Wiley & Sons, Inc., Hoboken, NJ, USA, 2016.

- 19 C. Hansch, R. M. Muir, T. Fujita, P. P. Maloney, F. Geiger and M. Streich, *J. Am. Chem. Soc.*, 1963, **85**, 2817–2824.
- 20 K. H. Ling, G. A. Leeson, S. D. Burmaster, R. H. Hook, M. K. Reith and L. K. Cheng, *Drug Metab. Dispos.*, 1995, **23**, 631–636.
- 21 M. V. Westphal, B. T. Wolfstädter, J.-M. Plancher, J. Gatfield and E. M. Carreira, *ChemMedChem*, 2015, **10**, 461–469.
- 22 P. R. Savoie and J. T. Welch, *Chem. Rev.*, 2015, **115**, 1131.
- 23 J. Ajenjo, B. Klepetářová, M. Greenhall, D. Bím, M. Culka, L. Rulišek and P. Beier, *Chem. - A Eur. J.*, 2019, **25**, 11375–11382.
- 24 R. D. Bowden, P. J. Comina, M. P. Greenhall, B. M. Kariuki, A. Loveday and D. Philp, *Tetrahedron*, 2000, **56**, 3399–3408.
- 25 O. S. Kanishchev and W. R. Dolbier, *Angew. Chemie Int. Ed.*, 2015, **54**, 280–284.
- 26 P. Kirsch and A. Hahn, *European J. Org. Chem.*, 2005, **2005**, 3095–3100.
- 27 X. Ou and A. F. Janzen, *J. Fluor. Chem.*, 2000, **101**, 279–283.
- 28 F. W. Hoover and D. D. Coffman, *J. Org. Chem.*, 1964, **29**, 3567.
- 29 T. Umemoto, L. M. Garrick and N. Saito, *Beilstein J. Org. Chem.*, 2012, **8**, 461–471.
- 30 I. Saidalimu, Y. Liang, K. Niina, K. Tanagawa, N. Saito and N. Shibata, *Org. Chem. Front.*, 2019, **6**, 1157–1161.
- 31 C. R. Pitts, D. Bornemann, P. Liebing, N. Santschi and A. Togni, *Angew. Chemie - Int. Ed.*, 2019, **58**, 1950–1954.
- 32 J. M. W. Chan, *J. Mater. Chem. C*, 2019, **7**, 12822–12834.
- 33 J. D. Knight, S. J. Sauer and D. M. Coltart, *Org. Lett.*, 2011, **13**, 3118–3121.
- 34 P. Wipf, T. Mo, S. J. Geib, D. Caridha, G. S. Dow, L. Gerena, N. Roncal and E. E. Milner, *Org. Biomol. Chem.*, 2009, **7**, 4163.
- 35 T. Mo, X. Mi, E. E. Milner, G. S. Dow and P. Wipf, *Tetrahedron Lett.*, 2010, **51**, 5137–5140.
- 36 J. T. Welch and D. S. Lim, *Bioorganic Med. Chem.*, 2007, **15**, 6659–6666.
- 37 L. Stach and P. S. Freemont, *Biochem. J.*, 2017, **474**, 2953–2976.
- 38 C. Alvarez, M. R. Arkin, S. L. Bulfer, R. Colombo, M. Kovaliov, M. G. Laporte, C. Lim, M. Liang, W. J. Moore, R. Jeffrey Neitz, Y. Yan, Z. Yue, D. M. Huryn and P. Wipf, *ACS Med. Chem. Lett.*, 2015, **6**, 1225–1230.
- 39 J. M. Coteron, M. Marco, J. Esquivias, X. Deng, K. L. White, J. White, M. Koltun, || Farah, E. Mazouni, S. Kokkonda, K. Katneni, R. Bhamidipati, D. M. Shackleford, || I~ Nigo Angulo-Barturen, S. B. Ferrer, M. Bel, J. Enez-Díaz, F.-J. Gamo, E. J. Goldsmith, W. N. Charman, I. Bathurst, D. Floyd, D. Matthews, J. N. Burrows, P. K. Rathod, S. A. Charman and M. A. Phillips, *J. Med. Chem.*, 2011, **54**, 5540–5561.
- 40 S. H. Loh, B. Sun and R. D. Vaughan-Jones, *Br. J. Pharmacol.*, 1996, **118**, 1905–1912.

- 41 M. Bassetto, S. Ferla and F. Pertusati, *Future Med. Chem.*, 2015, **7**, 527–546.
- 42 J. Spencer, R. P. Rathnam, A. L. Harvey, C. J. Clements, R. L. Clark, M. P. Barrett, P. E. Wong, L. Male, S. J. Coles and S. P. MacKay, *Bioorganic Med. Chem.*, 2011, **19**, 1802–1815.
- 43 M. Beig, F. Oellien, L. Garoff, S. Noack, R. Luise Krauth-Siegel and P. M. Selzer, *PLoS Negl. Trop. Dis.*, DOI:10.1371/journal.pntd.0003773.
- 44 B. Stump, C. Eberle, W. B. Schweizer, M. Kaiser, R. Brun, R. L. Krauth-Siegel, D. Lentz and F. Diederich, *ChemBioChem*, 2009, **10**, 79–83.
- 45 P. Kirsch, M. Bremer, M. Heckmeier and K. Tarumi, *Angew. Chem., Int. Ed.*, 1999, **38**, 1989.
- 46 D. Sung LIM, J. Sup CHOI, C. Siek PAK and J. T. Welch, *J. Pestic. Sci.*, 2007, **32**, 255–259.
- 47 D. Kumar Pradhan, T. S. Dharamrajan, M. Ranjan Mishra and A. Mishra, *Int. J. Res. Dev. Pharm. Life Sci.*, 2012, **1**, 44–50.
- 48 M. Taylor, B. Atri and S. Minhas, Developments in microwave, [https://www.rsc.org/images/evaluserve\\_tcm18-16758.pdf](https://www.rsc.org/images/evaluserve_tcm18-16758.pdf), (accessed 20 April 2021).
- 49 R. Gedye, F. Smith, K. Westaway, H. Ali, L. Baldisera, L. Laberge and J. Rousell, *Tetrahedron Lett.*, 1986, **27**, 279–282.
- 50 K. K. Rana and S. Rana, *OALib*, 2014, **01**, 1–20.
- 51 C. O. Kappe, *Microwave-Assisted Chemistry*, Elsevier, 2007.
- 52 C. Gabriel, S. Gabriel, E. H. Grant, B. S. J. Halstead, D. Michael and P. Mingos, *Chem. Soc. Rev.*, 1998, **27**, 213.
- 53 C. O. Kappe, *Angew. Chemie Int. Ed.*, 2004, **43**, 6250–6284.
- 54 J.-S. Schanche, *Mol. Divers.*, 2003, **7**, 291–298.
- 55 N. E. Leadbeater and M. Marco, *Org. Lett.*, 2002, **4**, 2973–2976.
- 56 J. L. Howard, Q. Cao and D. L. Browne, *Chem. Sci.*, 2018, **9**, 3080–3094.
- 57 T. K. Achar, A. Bose and P. Mal, *Beilstein J. Org. Chem.*, 2017, **13**, 1907–1931.
- 58 Mixer Mill MM 400 - RETSCH - powerful grinding by impact and friction, <https://www.retsch.com/products/milling/ball-mills/mixer-mill-mm-400/function-features/>, (accessed 21 April 2021).
- 59 Retsch PM 100 Planetary Ball Mill | Asa Global Medical, <https://asaglobalmedical.com/product/retsch-pm-100/>, (accessed 21 April 2021).
- 60 D. V. Glyzdova, N. S. Smirnova, D. A. Shlyapin and P. G. Tsyryl'nikov, *Russ. J. Gen. Chem.*, 2020, **90**, 1120–1140.
- 61 D. Wang and D. Astruc, *Chem. Rev.*, 2015, **115**, 6621–6686.
- 62 Y. Sawama, T. Kawajiri, M. Niikawa, R. Goto, Y. Yabe, T. Takahashi, T. Marumoto, M. Itoh, Y. Kimura, Y. Monguchi, S. I. Kondo and H. Sajiki, *ChemSusChem*, 2015, **8**, 3773–3776.
- 63 M. Löffler, J. Jöckel, G. Schuster and C. Becker, *Mol. Cell. Biochem.*, 1997, **174**, 125–129.

- 64 G. K. H. Zupanc and I. Horschke, *Comp. Biochem. Physiol. - B Biochem. Mol. Biol.*, 1996, **114**, 269–274.
- 65 L. R. Engelking, in *Textbook of Veterinary Physiological Chemistry*, Academic Press, 3rd edn., 2015, pp. 83–87.
- 66 M. Ellen Jones, *Ann. Rev. Biochem.*, 1980, **49**, 253–79.
- 67 S. Yin, T. Kabashima, Q. Zhu, T. Shibata and M. Kai, *Sci. Rep.*, 2017, **7**, 1–7.
- 68 W. Hoffman, F. G. Lakkis and G. Chalasani, *Clin. J. Am. Soc. Nephrol.*, 2016, **11**, 137–154.
- 69 G. Martine Ffrench, J.-P. Revillard and L. Laurence Quéméneur, *J Immunol Ref.*, 2020, **170**, 4986–4995.
- 70 A. Papadopoulou, L. Kappos and T. Sprenger, *Expert Opin. Drug Saf.*, 2015, **14**, 749–759.
- 71 E. K. Li, L. S. Tam and B. Tomlinson, *Clin. Ther.*, 2004, **26**, 447–459.
- 72 V. Hinesand and M. Johnston, *Biochemistry*, 1989, **28**, 1222–1226.
- 73 S. Liu, E. A. Neidhardt, T. H. Grossman, T. Ocain and J. Clardy, *Structure*, 2000, **8**, 25–33.
- 74 H. Kellner, K. Bornholdt and G. Hein, *Clin. Rheumatol.*, 2010, **29**, 913–920.
- 75 V. Strand, S. Cohen, M. Schiff, A. Weaver, R. Fleischmann, G. Cannon, R. Fox, L. Moreland, N. Olsen, D. Furst, J. Caldwell, J. Kaine, J. Sharp, F. Hurley and I. Loew-Friedrich, *Arch. Intern. Med.*, 1999, **159**, 2542–2550.
- 76 B. C. Kieseier and M. Benamor, *Neurol. Ther.*, 2014, **3**, 133–138.
- 77 H.-Y. Yap, S. Tee, M. Wong, S.-K. Chow, S.-C. Peh and S.-Y. Teow, *Cells*, 2018, **7**, 161.
- 78 P. B. B. Jones and D. H. N. White, *Open Access Rheumatol. Res. Rev.*, 2010, **2**, 53–71.
- 79 D. Cowen, P. Bedingfield, G. A. McConkey, C. W. G. Fishwick and A. P. Johnson, *Bioorganic Med. Chem. Lett.*, 2010, **20**, 1284–1287.
- 80 N. Hail, P. Chen, J. J. Kepa, L. R. Bushman and C. Shearn, *Free Radic. Biol. Med.*, 2010, **49**, 109–116.
- 81 X. Ji and Z. Li, *Med. Res. Rev.*, 2020, 1–39.
- 82 A. E. Gorbalenya, S. C. Baker, R. S. Baric, R. J. de Groot, C. Drosten, A. A. Gulyaeva, B. L. Haagmans, C. Lauber, A. M. Leontovich, B. W. Neuman, D. Penzar, S. Perlman, L. L. M. Poon, D. V. Samborskiy, I. A. Sidorov, I. Sola and J. Ziebuhr, *Nat. Microbiol.*, 2020, **5**, 536–544.
- 83 L. Zhang, D. Lin, X. Sun, U. Curth, C. Drosten, L. Sauerhering, S. Becker, K. Rox and R. Hilgenfeld, *Science (80-. )*, 2020, **368**, 409–412.
- 84 L. Zhang, D. Lin, Y. Kusov, Y. Nian, Q. Ma, J. Wang, A. Von Brunn, P. Leyssen, K. Lanko, J. Neyts, A. De Wilde, E. J. Snijder, H. Liu and R. Hilgenfeld, *J. Med. Chem.*, 2020, **63**, 4562–4578.
- 85 T. Pillaiyar, M. Manickam, V. Namasivayam, Y. Hayashi and S. H. Jung, *J. Med. Chem.*, 2016, **59**, 6595–6628.
- 86 R. Liang, L. Wang, N. Zhang, X. Deng, M. Su, Y. Su, L. Hu, C. He, T. Ying, S. Jiang and F.

- Yu, *Viruses*, 2018, **10**, 1–25.
- 87 Z. Jin, X. Du, Y. Xu, Y. Deng, M. Liu, Y. Zhao, B. Zhang, X. Li, L. Zhang, C. Peng, Y. Duan, J. Yu, L. Wang, K. Yang, F. Liu, R. Jiang, X. Yang, T. You, X. Liu, X. Yang, F. Bai, H. Liu, X. Liu, L. W. Guddat, W. Xu, G. Xiao, C. Qin, Z. Shi, H. Jiang, Z. Rao and H. Yang, *Nature*, 2020, **582**, 289–293.
- 88 S. Ullrich and C. Nitsche, *Bioorganic Med. Chem. Lett.*, , DOI:10.1016/j.bmcl.2020.127377.
- 89 C. A. Devaux, J. M. Rolain and D. Raoult, *J. Microbiol. Immunol. Infect.*, 2020, **53**, 425–435.
- 90 J. Lan, J. Ge, J. Yu, S. Shan, H. Zhou, S. Fan, Q. Zhang, X. Shi, Q. Wang, L. Zhang and X. Wang, *Nature*, 2020, **581**, 215–220.
- 91 E. G. Favalli, F. Ingegnoli, O. De Lucia, G. Cincinelli, R. Cimaz and R. Caporali, *Autoimmun. Rev.*, 2020, **19**, 102523.
- 92 R. Xiong, L. Zhang, S. Li, Y. Sun, M. Ding, Y. Wang, Y. Zhao, Y. Wu, W. Shang, X. Jiang, J. Shan, Z. Shen, Y. Tong, L. Xu, Y. Chen, Y. Liu, G. Zou, D. Lavillete, Z. Zhao, R. Wang, L. Zhu, G. Xiao, K. Lan, H. Li and K. Xu, *bioRxiv*, 2020, 2020.03.11.983056.
- 93 Y. Xu and H. Jiang, *Protein Cell*, 2020, **11**, 699–702.
- 94 K. Hu, M. Wang, Y. Zhao, Y. Zhang, T. Wang, Z. Zheng, X. Li, S. Zeng, D. Zhao, H. Li, K. Xu and K. Lan, *Virol. Sin.*, , DOI:10.1007/s12250-020-00258-7.
- 95 W. Li, Y. Y. Su, S. S. Zhi, J. Huang, C. L. Zhuang, W. Z. Bai, Y. Wan, X. R. Meng, L. Zhang, Y. B. Zhou, Y. Y. Luo, S. X. Ge, Y. K. Chen and Y. Ma, *Clin. Microbiol. Infect.*, 2020, **26**, 1556.e1-1556.e6.
- 96 K. Gibbert, J. F. Schlaak, D. Yang and U. Dittmer, *Br. J. Pharmacol.*, 2013, **168**, 1048–1058.
- 97 R. Asmana Ningrum, *Scientifica (Cairo)*, 2014, **2014**, 1–8.
- 98 M. Wang, Y. Zhao, W. Hu, D. Zhao, Y. Zhang, T. Wang, Z. Zheng, X. Li, S. Zeng, Z. Liu, L. Lu, Z. Wan and K. Hu, *Clin. Infect. Dis.*, , DOI:10.1093/cid/ciaa1417.
- 99 B. Berber and D. Osman, *ChemRxiv*, 2020, **22**, 1023–1037.
- 100 PostEra | COVID-19, <https://covid.postera.ai/covid>, (accessed 30 November 2020).
- 101 The COVID Moonshot Consortium, H. Achdout, A. Aimon, E. Bar-David, H. Barr, A. Ben-Shmuel, J. Bennett, M. L. Bobby, J. Brun, B. Sarma, M. Calmiano, A. Carbery, E. Cattermole, J. D. Chodera, A. Clyde, J. E. Coffland, G. Cohen, J. Cole, A. Contini, L. Cox, M. Cvitkovic, A. Dias, A. Douangamath, S. Duberstein, T. Dudgeon, L. Dunnett, P. K. Eastman, N. Erez, M. Fairhead, D. Fearon, O. Fedorov, M. Ferla, H. Foster, R. Foster, R. Gabizon, P. Gehertz, C. Gileadi, C. Giroud, W. G. Glass, R. Glen, I. Glinert, M. Gorichko, T. Gorrie-Stone, E. J. Griffen, J. Heer, M. Hill, S. Horrell, M. F. D. Hurley, T. Israely, A. Jajack, E. Jnoff, T. John, A. L. Kantsadi, P. W. Kenny, J. L. Kiappes, L. Koekemoer, B. Kovar, T. Krojer, A. A. Lee, B. A. Lefker, H. Levy, N. London, P. Lukacik, H. B.

- Macdonald, B. MacLean, T. R. Malla, T. Matviiuk, W. McCorkindale, S. Melamed, O. Michurin, H. Mikolajek, A. Morris, G. M. Morris, M. J. Morwitzer, D. Moustakas, J. B. Neto, V. Oleinikovas, G. J. Overheul, D. Owen, R. Pai, J. Pan, N. Paran, B. Perry, M. Pingle, J. Pinjari, B. Politi, A. Powell, V. Psenak, R. Puni, V. L. Rangel, R. N. Reddi, S. P. Reid, E. Resnick, M. C. Robinson, R. P. Robinson, D. Rufa, C. Schofield, A. Shaikh, J. Shi, K. Shurrush, A. Sittner, R. Skyner, A. Smalley, M. D. Smilova, J. Spencer, C. Strain-Damerell, V. Swamy, H. Tamir, R. Tennant, A. Thompson, W. Thompson, S. Tomasio, A. Tumber, I. Vakonakis, R. P. van Rij, F. S. Varghese, M. Vaschetto, E. B. Vitner, V. Voelz, A. von Delft, F. von Delft, M. Walsh, W. Ward, C. Weatherall, S. Weiss, C. F. Wild, M. Wittmann, N. Wright, Y. Yahalom-Ronen, D. Zaidmann, H. Zidane and N. Zitzmann, *bioRxiv*, DOI:10.1101/2020.10.29.339317.
- 102 G. Schrödinger, LLC, N. York and NY, 2020.
- 103 R. A. Friesner, J. L. Banks, R. B. Murphy, T. A. Halgren, J. J. Klicic, D. T. Mainz, M. P. Repasky, E. H. Knoll, M. Shelley, J. K. Perry, D. E. Shaw, P. Francis and P. S. Shenkin, *J. Med. Chem.*, 2004, **47**, 1739–1749.
- 104 K. Raha and K. M. Merz, *Annu. Rep. Comput. Chem.*, 2005, **1**, 113–130.
- 105 M. D. Eldridge, C. W. Murray, T. R. Auton, G. V. Paolini and R. P. Mee, *J. Comput. Aided. Mol. Des.*, 1997, **11**, 425–445.
- 106 D. S. Goodsell and A. J. Olson, *Proteins Struct. Funct. Genet.*, 1990, **8**, 195–202.
- 107 J. Leban, W. Saeb, G. Garcia, R. Baumgartner and B. Kramer, *Bioorganic Med. Chem. Lett.*, 2004, **14**, 55–58.
- 108 M. Davies, T. Heikkilä, G. A. McConkey, C. W. G. Fishwick, M. R. Parsons and A. P. Johnson, *J. Med. Chem.*, 2009, **52**, 2683–2693.
- 109 M. Erra, I. Moreno, J. Sanahuja, M. Andrés, R. F. Reinoso, E. Lozoya, P. Pizcueta, N. Godessart and J. C. Castro-Palomino, *Bioorganic Med. Chem. Lett.*, 2011, **21**, 7268–7272.
- 110 M. E. Sitzmann, *J. Fluor. Chem.*, 1995, **70**, 31–38.
- 111 M. F. Sowaileh, R. A. Hazlitt and D. A. Colby, *ChemMedChem*, 2017, **12**, 1481–1490.
- 112 US2017073304A1, 2017.
- 113 C. Schotten, *J. Inorg. Chem.*, 1886, **19**, 3218.
- 114 B. S. Jursic and D. Neumann, *Synth. Commun.*, 2001, **31**, 555–564.
- 115 Apollo Scientific, <https://store.apolloscientific.co.uk/product/5-methylisoxazole-4-carbonyl-chloride>, (accessed 12 July 2020).
- 116 Sigma-Aldrich,  
<https://www.sigmaaldrich.com/catalog/product/aldrich/633771?lang=en&region=GB>,  
(accessed 10 November 2020).
- 117 I. ADACHI and H. KANO, *Chem. Pharm. Bull. (Tokyo)*, 1969, **17**, 2201–2208.
- 118 J. Kujawski, M. K. Bernard, E. Jodłowska, K. Czaja and B. Drabińska, *J. Mol. Model.*, 2015,

- 21, 105.
- 119 A. Alex, D. S. Millan, M. Perez, F. Wakenhut and G. A. Whitlock, *Medchemcomm*, 2011, **2**, 669–674.
- 120 P. V. Desai, T. J. Raub and M. J. Blanco, *Bioorganic Med. Chem. Lett.*, 2012, **22**, 6540–6548.
- 121 B. Kuhn, P. Mohr and M. Stahl, *J. Med. Chem.*, 2010, **53**, 2601–2611.
- 122 S. Christian, C. Merz, L. Evans, S. Gradl, H. Seidel, A. Friberg, A. Eheim, P. Lejeune, K. Brzezinka, K. Zimmermann, S. Ferrara, H. Meyer, R. Lesche, D. Stoeckigt, M. Bauser, A. Haegerbarth, D. B. Sykes, D. T. Scadden, J. A. Losman and A. Janzer, *Leukemia*, 2019, **33**, 2403–2415.
- 123 Reaction Biology, [https://www.reactionbiology.com/services/in-vivo-pharmacology?gclid=CjwKCAiAzNj9BRBDEiwAPsL0dzqvZvJ2R2zzWqZpJoLGtnUDZV-U3J5aMtF8JxRjeoZrS45i7OIdDdxoC96wQAvD\\_BwE](https://www.reactionbiology.com/services/in-vivo-pharmacology?gclid=CjwKCAiAzNj9BRBDEiwAPsL0dzqvZvJ2R2zzWqZpJoLGtnUDZV-U3J5aMtF8JxRjeoZrS45i7OIdDdxoC96wQAvD_BwE), (accessed 19 November 2020).
- 124 B. R. Stockwell, *Nature*, 2004, **432**, 846–854.
- 125 J. Clayden, *Nature*, 2019, **573**, 37–38.
- 126 D. G. Brown and J. Boström, *J. Med. Chem.*, 2016, **59**, 4443–4458.
- 127 S. Kumari, A. V Carmona, A. K. Tiwari and P. C. Trippier, *Cite This J. Med. Chem*, 2020, **63**, 12290–12358.
- 128 M. L. Brown, W. Aaron, R. J. Austin, A. Chong, T. Huang, B. Jiang, J. A. Kaizerman, G. Lee, B. S. Lucas, D. L. McMinn, J. Orf, M. Rong, M. M. Toteva, G. Xu, Q. Ye, W. Zhong, M. R. Degraffenreid, D. Wickramasinghe, J. P. Powers, R. Hungate and M. G. Johnson, *Bioorganic Med. Chem. Lett.*, 2011, **21**, 5206–5209.
- 129 S. D. Roughley and A. M. Jordan, *J. Med. Chem.*, 2011, **54**, 3451–3479.
- 130 P. Patil, R. Madhavachary, K. Kurpiewska, J. Kalinowska-Thus and A. Do, *Org. Lett.*, 2017, **19**, 642–645.
- 131 P. Goel, O. Alam, M. J. Naim, F. Nawaz, M. Iqbal and M. I. Alam, *Eur. J. Med. Chem.*, 2018, **157**, 480–502.
- 132 M. Baumann and I. R. Baxendale, *Beilstein J. Org. Chem.*, 2013, **9**, 2265–2319.
- 133 Y. Gao, L. Yan, Y. Huang, F. Liu, Y. Zhao, L. Cao, T. Wang, Q. Sun, Z. Ming, L. Zhang, J. Ge, L. Zheng, Y. Zhang, H. Wang, Y. Zhu, C. Zhu, T. Hu, T. Hua, B. Zhang, X. Yang, J. Li, H. Yang, Z. Liu, W. Xu, L. W. Guddat, Q. Wang, Z. Lou and Z. Rao, *Science (80-. )*, 2020, **368**, 779–782.
- 134 A. Frediansyah, F. Nainu, K. Dhama, M. Mudatsir and H. Harapan, *Clin. Epidemiol. Glob. Heal.*, 2021, **9**, 123–127.
- 135 H. L. Nguyen, N. Q. Thai, D. T. Truong and M. S. Li, *J. Phys. Chem. B*, 2020, **124**, 11337–11348.
- 136 P. Reszka, K. Methling, M. Lalk, Z. Xiao, K. Weisz and P. J. Bednarski, *Tetrahedron*

- Asymmetry*, 2008, **19**, 49–59.
- 137 L. A. Carpino, P. Henklein, B. M. Foxman, I. Abdelmoty, B. Costisella, V. Wray, T. Domke, A. Ayman El-Faham and C. Mügge, 2001, **66**, 5245–5247.
- 138 J. Eames and M. Watkinson, *European J. Org. Chem.*, 2001, **2001**, 1213–1224.
- 139 P. G. Steel, L. J. Oates and A. Chesney, *Encycl. Reagents Org. Synth.*, 2003, 1–4.
- 140 T. Bosanac and C. S. Wilcox, *J. Am. Chem. Soc.*, 2002, **124**, 4194–4195.
- 141 A. R. Nekoei and M. Vatanparast, *Phys. Chem. Chem. Phys.*, 2019, **21**, 623–630.
- 142 Activity Data, [https://covid.postera.ai/covid/activity\\_data](https://covid.postera.ai/covid/activity_data), (accessed 4 August 2021).
- 143 S. Ravi Suman Rudrangi, V. Kumar Bontha, V. Reddy Manda and S. Bethi, *Asian J. Research. Chem.*, 2011, **4**, 335–338.
- 144 M. Kaur, M. Singh, N. Chadha and O. Silakari, *Eur. J. Med. Chem.*, 2016, **123**, 858–894.
- 145 F. Ardito, M. Giuliani, D. Perrone, G. Troiano and L. Lo Muzio, *Int. J. Mol. Med.*, 2017, **40**, 271–280.
- 146 D. S. Metibemu, O. A. Akinloye, A. J. Akamo, D. A. Ojo, O. T. Okeowo and I. O. Omotuyi, *Egypt. J. Med. Hum. Genet.*, 2019, **20**, 1–16.
- 147 P. A. Schwartz and B. W. Murray, *Bioorg. Chem.*, 2011, **39**, 192–210.
- 148 N. Dhanasekaran and E. Premkumar Reddy, *Oncogene*, 1998, **17**, 1447–1455.
- 149 Q. Liu, Y. Sabnis, Z. Zhao, T. Zhang, S. J. Buhrlage, L. H. Jones and N. S. Gray, *Chem. Biol.*, 2013, **20**, 146–159.
- 150 F. A. Al-Obeidi and K. S. Lam, *Oncogene*, 2000, **19**, 5690–5701.
- 151 A. Luxenburger, D. Schmidt, C. Ianes, C. Pichlo, M. Krüger, T. von Drathen, E. Brunstein, G. J. Gainsford, U. Baumann, U. Knippschild and C. Peifer, *Molecules*, , DOI:10.3390/molecules24050873.
- 152 A. Östman and F. D. Böhmer, *Trends Cell Biol.*, 2001, **11**, 258–266.
- 153 J. Grassot, G. Mouchiroud and G. Perrière, *Nucleic Acids Res.*, 2003, **31**, 353–358.
- 154 J. Schlessinger and M. A. Lemmon, *Sci. Signal.*, 2003, **2003**, re12.
- 155 Z. Du and C. M. Lovly, *Mol. Cancer*, 2018, **17**, 1–13.
- 156 G. Chen, Q. Weng, L. Fu, Z. Wang, P. Yu, Z. Liu, X. Li, H. Zhang and G. Liang, *Bioorganic Med. Chem.*, 2014, **22**, 6953–6960.
- 157 T. H. Adair and J.-P. Montani, *Overview of Angiogenesis*, Morgan & Claypool Life Sciences, San Rafael, 2010.
- 158 S. Patan, *Cancer Treat. Res.*, 2004, **117**, 3–32.
- 159 S. Sansook, C. A. Ocasio, I. J. Day, G. J. Tizzard, S. J. Coles, O. Fedorov, J. M. Bennett, J. M. Elkins and J. Spencer, *Org. Biomol. Chem.*, 2017, **15**, 8655.
- 160 Y. H. Jhan, T. W. Kang and J. C. Hsieh, *Tetrahedron Lett.*, 2013, **54**, 1155–1159.
- 161 T. L. Pavlovska, R. G. Redkin, V. V. Lipson and D. V. Atamanuk, *Mol. Divers.*, 2016, **20**, 299–344.



- 162 E. Chupakhin, O. Babich, A. Prosekov, L. Asyakina and M. Krasavin, *Molecules*, 2019, **24**, 4165.
- 163 Y. Xu, X. J. Zhang, W. B. Li, X. R. Wang, S. Wang, X. P. Qiao and S. W. Chen, *Eur. J. Med. Chem.*, 2020, **208**, 112780.
- 164 L. Sun, N. Tran, F. Tang, H. App, P. Hirth, G. McMahon and C. Tang, *J. Med. Chem.*, 1998, **41**, 2588–2603.
- 165 M. H. Ngai, C. L. So, M. B. Sullivan, H. K. Ho and C. L. L. Chai, *ChemMedChem*, 2016, **11**, 72–80.
- 166 S. Raziullah Hussaini, A. Kuta, A. Pal, Z. Wang, M. A. Eastman and R. Duran, *ACS Omega*, 2020, **5**, 24848–24853.
- 167 H. Ishitani, Y. Saito, Y. Nakamura, W. J. Yoo and S. Kobayashi, *Asian J. Org. Chem.*, 2018, **7**, 2061–2064.
- 168 C. Xu, S. De, A. M. Balu, M. Ojeda and R. Luque, *Chem. Commun.*, 2015, **51**, 6698–6713.
- 169 S. Haferkamp, A. Paul, A. A. L. Michalchuk and F. Emmerling, *Beilstein J. Org. Chem.*, 2019, **15**, 1141–1148.
- 170 S. Haferkamp, F. Fischer, W. Kraus and F. Emmerling, *Beilstein J. Org. Chem.*, 2017, **13**, 2010–2014.
- 171 O. Eguagie, J. S. Vyle, P. F. Conlon, M. A. Gilea and Y. Liang, *Beilstein J. Org. Chem.*, 2018, **14**, 955–970.
- 172 Ceramic Grinding and Milling Media,  
<https://zircoa.com/product.fine.grain/grinding.media.html>, (accessed 7 January 2021).
- 173 K. Keating and R. Knight, *Geophysics*, 2007, **72**, E27–E32.
- 174 E. V. Dalessandro, H. P. Collin, L. G. L. Guimarães, M. S. Valle and J. R. Pliego, *J. Phys. Chem. B*, 2017, **121**, 5300–5307.
- 175 D. Hasa, G. Schneider Rauber, D. Voinovich and W. Jones, *Angew. Chemie*, 2015, **127**, 7479–7483.
- 176 G. Iakobson, M. Pošta and P. Beier, *Synlett*, 2013, **24**, 855–859.
- 177 WO 2014/060411 A1, 2014.
- 178 T. A. T. Fong, L. K. Shawver, L. Sun, C. Tang, H. App, T. J. Powell, Y. H. Kim, R. Schreck, X. Wang, W. Risau, A. Ullrich, K. P. Hirth and G. McMahon, *Cancer Res.*, 1999, **59**, 99–106.
- 179 H. P. Goodkin and J. Kapur, *Epilepsia*, 2009, **50**, 2011–2018.
- 180 M. Lader, *Br. J. Clin. Pharmacol.*, 2014, **77**, 295–301.
- 181 M. Olfson, M. King and M. Schoenbaum, *JAMA Psychiatry*, 2015, **72**, 136–142.
- 182 L. N. Ravindran and M. B. Stein, *Brain Res.*, 2009, **1293**, 24–39.
- 183 S. Mohamed and R. A. Rosenheck, *J. Clin. Psychiatry*, 2008, **69**, 959–965.
- 184 J. Guina and B. Merrill, *J. Clin. Med.*, 2018, **7**, 17.

- 185 N. E. Calcaterra and J. C. Barrow, *ACS Chem. Neurosci.*, 2014, **5**, 253–260.
- 186 A. Sachdeva, M. Choudhary and M. Chandra, *J. Clin. DIAGNOSTIC Res.*, 2015, **9**, VE01.
- 187 M. F. Mayo-Smith, *J. Am. Med. Assoc.*, 1997, **278**, 144–151.
- 188 C. Wu and D. Sun, *Metab. Brain Dis.*, 2015, **30**, 367–379.
- 189 C. E. Griffin, A. M. Kaye, F. R. Bueno, A. D. Kaye and A. D. Kaye, *Ochsner J.*, 2013, **13**, 214–23.
- 190 E. Sigel and A. Buhr, *Trends Pharmacol. Sci.*, 1997, **18**, 425–429.
- 191 J. Bormann, *Trends Pharmacol. Sci.*, 2000, **21**, 16–19.
- 192 E. Batlle, E. Lizano, M. Viñas and M. Dolors Pujol, in *Medicinal Chemistry*, IntechOpen, 2019, pp. 63–90.
- 193 S. Masiulis, R. Desai, T. Uchański, I. Serna Martin, D. Laverty, D. Karia, T. Malinauskas, J. Zivanov, E. Pardon, A. Kotecha, J. Steyaert, K. W. Miller and A. R. Aricescu, *Nature*, 2019, **565**, 454–459.
- 194 E. A. Barnard, P. Skolnick, R. W. Olsen, H. Mohler, W. Sieghart, G. Biggio, C. Braestrup, A. N. Bateson and S. Z. Langer, *Pharmacol. Rev.*, 1998, **50**, 291–313.
- 195 M. D. Kelly, A. Smith, G. Banks, P. Wingrove, P. W. Whiting, J. Atack, G. R. Seabrook and K. A. Maubach, *Br. J. Pharmacol.*, 2002, **135**, 248–256.
- 196 P. Howard, R. Twycross, J. Shuster, M. Mihalyo and A. Wilcock, *J. Pain Symptom Manage.*, 2014, **47**, 955–964.
- 197 R. Nussinov and C.-J. Tsai, *Curr. Pharm. Des.*, 2012, **18**, 1311–1316.
- 198 A. F. Abdel-Magid, *ACS Med. Chem. Lett.*, 2015, **6**, 104–107.
- 199 J. Herrington and B. J. Arey, in *Biased Signaling in Physiology, Pharmacology and Therapeutics*, ed. B. J. Arey, Elsevier Inc., 2014, pp. 173–207.
- 200 D. J. Nutt and A. L. Malizia, *Br. J. Psychiatry*, 2001, **179**, 390–396.
- 201 J. G. Richards and H. Möhler, *Neuropharmacology*, 1984, **23**, 233–242.
- 202 I. Khan and B. Singh, *Sci. Revs. Chem. Commun*, 2015, **5**, 13–20.
- 203 D. J. Maddalena and G. A. R. Johnston, *J. Med. Chem.*, 1995, **38**, 715–724.
- 204 L. H. Sternbach, *Angew. Chemie Int. Ed. English*, 1971, **10**, 34–43.
- 205 Q. Wang, Y. Han and H. Xue, *CNS Drug Rev.*, 2006, **5**, 125–144.
- 206 S. G. Smith, R. Sanchez and M.-M. Zhou, *Chem. Biol.*, 2014, **21**, 573–583.
- 207 M. Altenkämper, B. Bechem, J. Perruchon, S. Heinrich, A. Mädler, R. Ortmann, H. M. Dahse, E. Freunsch, Y. Wang, J. Rath, A. Stich, M. Hitzler, P. Chiba, M. Lanzer and M. Schlitzer, *Bioorganic Med. Chem.*, 2009, **17**, 7690–7697.
- 208 A. R. Massah, S. Gharaghani, H. A. Lordejani and N. Asakere, *Med. Chem. Res.*, 2016, **25**, 1538–1550.
- 209 N. Kaur and D. Kishore, *Synth. Commun.*, 2014, **44**, 1375–1413.
- 210 A. Liu, H. Zhou, G. Su, W. Zhang and B. Yan, *J. Comb. Chem.*, 2009, **11**, 1083–1093.

- 211 P. R. Savoie and J. T. Welch, *Chem. Rev.*, 2015, **115**, 1130–1190.
- 212 L. H. Sternbach and E. Reeder, *J. Org. Chem.*, 1961, **26**, 1111–1118.
- 213 L. H. Sternbach, *J. Med. Chem.*, 1979, **22**, 1–7.
- 214 L. H. Sternbach, I. Fryer, W. Metlesics, E. Reeder, G. Sach, G. Saucy and A. Stempel, *J. Org. Chem.*, 1962, **27**, 3788–3796.
- 215 L. H. Sternbach, in *Jucker E. (eds) Progress in Drug Research*, Birkhäuser Basel, 1978, pp. 229–230.
- 216 Hoffmann-La Roche Inc., 1976, US3996209A.
- 217 G. Mwande-Maguene, J. Jakhlal, J. B. Lekana-Douki, E. Mouray, T. Bousquet, S. Pellegrini, P. Grellier, F. S. T. Ndouo, J. Lebibi and L. Pelinski, *New J. Chem.*, 2011, **35**, 2412–2415.
- 218 M. Panunzio, E. Campana, G. Martelli, P. Vicennati and E. Tamanini, *Mater. Res. Innov.*, 2004, **8**, 27–31.
- 219 J. Spencer, D. P. Sharratt, J. Dupont, A. L. Monteiro, V. I. Reis, M. P. Stracke, F. Rominger and I. M. McDonald, *Organometallics*, 2005, **24**, 5665–5672.
- 220 Y. Sumii, K. Sasaki, S. Tsuzuki and N. Shibata, *Molecules*, 2019, **24**, 3610.
- 221 M. J. Taghizadeh, G. reza malakpouri and A. Javidan, *J. Iran. Chem. Soc.*, 2019, **16**, 785–794.
- 222 P. Cheng, Q. Zhang, Y. B. Ma, Z. Y. Jiang, X. M. Zhang, F. X. Zhang and J. J. Chen, *Bioorganic Med. Chem. Lett.*, 2008, **18**, 3787–3789.
- 223 N. Blažević, D. Kolbah, B. Belin, V. Šunjić and F. Kajfež, *Synth.*, 1979, **1979**, 161–176.
- 224 G. M. Clarke and J. B. Lee, *J. Chem. Research*, 1980, 4773–4781.
- 225 R. Khan, R. Felix, P. D. Kemmitt, S. J. Coles, I. J. Day, G. J. Tizzard and J. Spencer, *Adv. Synth. Catal.*, , DOI:10.1002/adsc.201501009.
- 226 R. Khan, S. Boonseng, P. D. Kemmitt, R. Felix, S. J. Coles, G. J. Tizzard, G. Williams, O. Simmonds, J.-L. Harvey, J. Attack, H. Cox and J. Spencer, *Adv. Synth. Catal.*, 2017, **359**, 3261–3269.
- 227 R. Khan, R. Felix, P. D. Kemmitt, S. J. Coles, G. J. Tizzard and J. Spencer, *Synlett*, 2018, **29**, 193–198.
- 228 Maestro, Schrodinger, LLC and NY, 2021.
- 229 J. D. Yesselman, S. Horowitz, C. L. Brooks and R. C. Trievel, *Proteins Struct. Funct. Bioinforma.*, 2015, **83**, 403–410.
- 230 G. Cavallo, P. Metrangolo, R. Milani, T. Pilati, A. Priimagi, G. Resnati and G. Terraneo, *Chem. Rev.*, 2016, **116**, 2478–2601.
- 231 M. Mortensen, U. Kristiansen, B. Ebert, B. Frølund, P. Krogsgaard-Larsen and T. G. Smart, *J. Physiol.*, 2004, **557**, 389–413.
- 232 M. R. Bauer, R. N. Jones, M. G. J. Baud, R. Wilcken, F. M. Boeckler, A. R. Fersht, A. C. Joerger and J. Spencer, *ACS Chem. Biol.*, 2016, **11**, 2265–2274.

- 233 E. P. Gillis, K. J. Eastman, M. D. Hill, D. J. Donnelly and N. A. Meanwell, *J. Med. Chem.*, 2015, **58**, 8315–8359.
- 234 E. Pujol, N. Blanco-Cabra, E. Julián, R. Leiva, E. Torrents and S. Vázquez, *Molecules*, 2018, **23**, 1–17.
- 235 M. S. Owaileh, R. A. Hazlitt and D. A. Colby, *ChemMedChem*, 2017, **12**, 1481–1490.
- 236 A. Gilbert, P. Langowski, M. Delgado, L. Chabaud, M. Pucheault and J. F. Paquin, *Beilstein J. Org. Chem.*, 2020, **16**, 3069–3077.
- 237 MP-Trisamine, <https://www.biotage.com/mp-trisamine>, (accessed 13 May 2021).